

DEVELOPMENT OF POLYMERIC DRUG DELIVERY VEHICLES FOR
TARGETED CANCER THERAPY

BY

RONG TONG

DISSERTATION

Submitted in partial fulfillment of the requirements
for the degree of Doctor of Philosophy in Materials Science and Engineering
in the Graduate College of the
University of Illinois at Urbana-Champaign, 2010

Urbana, Illinois

Doctoral Committee:

Professor Jianjun Cheng, Chair
Professor Paul V. Braun
Professor Yi Lu
Professor Gerard C. L. Wong
Professor Steven C. Zimmerman

Abstract

The aim of my Ph. D. thesis is to generalize a method for targeted anti-cancer drug delivery. Hydrophilic polymer-drug conjugates involve complicated synthesis; drug-encapsulated polymeric nanoparticles limit the loading capability of payloads. This thesis introduces the concept of nanoconjugates to overcome difficulties in synthesis and formulation. Drugs with hydroxyl group are able to initiate polyester synthesis in a regio- and chemo- selective way, with the mediation of ligand-tunable Zinc catalyst. Herein, three anti-cancer drugs are presented to demonstrate the high efficiency and selectivity in the method (Chapter 2-4). The obtained particles are stable in salt solution, releasing drugs over weeks in controlled manner. With the conjugation of aptamer, particles are capable to target prostate cancer cells in vitro. These results open the gateway to evaluate the in vivo efficacy of nanoconjugates for target cancer therapy (Chapter 5). Mechanism study of the polymerization leads to the discovery of chemosite selective synthesis of prodrugs with acrylate functional groups. Functional copolymer-drug conjugates will expand the scope of nanoconjugates (Chapter 6). Liposome-aptamer targeting drug delivery vehicle is well studied to achieve reversible cell-specific delivery of non-hydroxyl drugs e.g. cisplatin (Chapter 7). New monomers and polymerization mechanisms are explored for polyester in order to synthesize nanoconjugates with variety on properties (Chapter 8). Initial efforts to apply this type of prodrugs will be focused on the preparation of hydrogels for stem cell research (Chapter 9).

ACKNOWLEDGEMENTS

I acknowledge with gratitude my advisor, Prof. Jianjun Cheng and his role in shaping my graduate career. He introduced me to the field of biomaterials which has a lot of scope for engineering applications. My project was to develop polymeric drug delivery system based on such potential application. Through the many twists and turns of my graduate research, both academic and non-academic, his firm backing and constant encouragement ensured that my Ph.D thesis finally saw the light of day. He was always available whenever I needed to brainstorm fundamental concepts and analyze results. His meticulous critique of my manuscripts, and the high standards he set made me work hard but on the other hand it made it easy for the eventual reviewer of those reports. My project involved active collaboration among other research groups and I learnt a lot from about fostering healthy working relationships between groups with mutually independent goals and philosophies. Through various presentations and discussions in our group, and the feedback obtained therein, he trained me to instantly connect with my audience or peers. Without his backing up and instructing, I cannot reach the achievement of my Ph.D. degree.

Special thanks to Prof. Yi Lu and Prof. Gerard Wong on collaborating in the aptamer-liposome delivery systems. Their critical comments during our collaboration group meetings were of great help. I thank our collaborator, Prof. Timothy Fan for his inputs on my results in the *in vivo* study of nanoparticles and imaging analysis. Thanks are also due to Prof. Paul Braun and Prof. Steven Zimmerman for agreeing to be in my defense committee and for their sightful suggestions.

I would like to thank Dr. Zehui Cao who was the co-author in the liposome-aptamer project. The creative aspect of the reversible aptamer-liposome delivery was a

useful pointer to my work. Thanks to Dr. Yunxiang Xu as well for providing great help on the OCA monomer synthesis. I would like to thank Juliana Chan and Dr Omid Farokhzad at MIT on the collaboration of PtxI nanoconjugates for cardiovascular disease. I would like to thank Prof. Steve Boppart on the collaboration of the imaging work; also Prof. Fei Wang and Prof. Jennifer Lewis on the stem cell cultivation project.

I also thank various members of my research group: Hua Lu, Li Tang (who helps a lot on the nanoconjugates project), Dr Nate Gabrilson, Yugang Bai, George Li, Dr Xueyun Gao.

The experimental component of my research utilized the resources of Center for Microanalysis of Materials. Special thanks to Dr. Wenjian Guo and Dr. Changhui Lei. The chemical analysis extensively used the resource of Mass Spectrometer Center. Great thanks to Dr. Haijun Yao and Dr. Furong Sun. Grateful thanks to Prof. Martin Burke and Prof. Jeff Moore for providing anhydrous solvents, and Prof. Dan Pack for allowing using his light scattering facilities.

I would also thank my friends Wenjun Cai, Xindi Yu, Shengquan Zhou and Yang Liu for their support and sincere friendship. Especially I would like to thank Wenjun for her emotional support through these years.

Lastly but not the least, my parents Jianwei Tong and Liping Wan, whose continuous encouragement and emotional support always kept my sights firmly set on my goal.

TABLE OF CONTENTS

CHAPTER 1	INTRODUCTION.....	1
1.	Background.....	1
2.	Scope and Organization	6
3.	References	10
CHAPTER 2	NANOCONJUGATES: INCORPORATING CAMPTOTHECIN	13
1.	Introduction	13
2.	Materials and Methods	16
3.	Results and Discussion	22
4.	Conclusions.....	42
5.	References	43
CHAPTER 3	NANOCONJUGATES: INCORPORATING PACLITAXEL.....	45
1.	Introduction	45
2.	Materials and Methods	45
3.	Results and Discussion	54
4.	Conclusions	74
5.	References	75
CHAPTER 4	NANOCONJUGATES: INCORPORATING DOXORUBICIN	77
1.	Introduction	77
2.	Materials and Methods	79
3.	Results and Discussion	85
4.	Conclusions	107
5.	References	108
CHAPTER 5	NANOCONJUGATES: FORMULATION AND PRELIMINARY <i>IN VIVO</i> STUDY	110
1.	Introduction.....	110
2.	Materials and Methods	113
3.	Results and Discussion	121
4.	Conclusions	155
5.	References	155
CHAPTER 6	EFFICIENT REGIOSELECTIVE <i>O</i> -ACYLATION OF THERAPEUTIC AGENTS BY β -DIIMINATE ZINC CATALYST	158
1.	Introduction	158
2.	Materials and Methods	161
3.	Results and Discussion	173
4.	Conclusions	191
5.	References	193

CHAPTER 7	REVERSIBLE CELL-SPECIFIC DELIVERY OF CISPLATIN USING APTAMER-FUNCTIONALIZED LIPOSOMES	195
1.	Introduction	195
2.	Materials and Methods	199
3.	Results and Discussion	202
4.	Conclusions	214
5.	References	215
CHAPTER 8	POLYMERIZATION OF <i>O</i> -CARBOXYANHYDRIDES	218
1.	Introduction	218
2.	Materials and Methods	219
3.	Results and Discussion	219
4.	Conclusions	229
5.	References	230
CHAPTER 9	INITIAL EFFORTS FOR STEM CELL CULTIVATION	231
1.	Introduction	231
2.	Materials and Methods	234
3.	Results and Discussion	238
4.	Conclusions	246
5.	References	247

CHAPTER 1

INTRODUCTION

1. Background

1.1 *Nanomedicine and cancer therapy*

Small molecule chemotherapeutics often have undesired physiochemical and pharmacological properties, such as low solubility and narrow therapeutic index.^[1] These drawbacks limit their applications for clinical cancer treatments. Two strategies have emerged over the past 2-3 decades to address these intrinsic drawbacks of chemotherapeutics.^[2] One approach is to design and develop new derivatives of chemotherapeutics with improved physiochemical and pharmacological properties so that they can be used to precisely and specifically modulate the molecular processes and pathways associated with tumor progression.^[3] The other widely used approach is to modify the existing chemotherapeutic agents using drug delivery technologies.^[4]

Most drug delivery vehicles of chemotherapeutics have particles size below 200nm and usually contain many therapeutic agents per vehicle. Nowadays these new anticancer modalities were often also termed nanomedicine. The first generation of anticancer nanomedicine has been focused on the preparation of delivery vehicles using well-developed biomaterials and methodologies, and on targeting and treating primary tumors based mainly on the Enhanced Permeation and Retention effect (EPR effect).^[5] The EPR effect refers to the accumulation of nanoparticles (NPs) in tumor facilitated by the highly permeable nature of the tumor vasculature and poor lymphatic drainage of the interstitial fluid surrounding a tumor. Nanocarriers based on passive targeting mechanism have been evaluated in clinic since the mid-1980s; the first sets were approved for

clinical use in the mid-1990s.^[6] The second generation of nanomedicine, however, placed a greater emphasis on novel strategies, such as bypassing biological barriers at the systemic, tissue, and cellular levels, and targeting metastatic lesions (active targeting).^[4c] Recent development of new chemistry (e.g. click chemistry^[7]) and fabrication technologies^[8] is expected to allow for unprecedented, precise control of nanomedicine formulation, making it possible to evaluate nanomedicine with the variation of one parameter (e.g. size, surface property, and shape) at a time.^[9]

In the construction of nanomedicine, lipid and polymer-based systems are amongst most extensively explored, accounting for more than half of the nanomedicines approved for clinical disease treatment. I mainly focus on polymeric nanomedicine, especially those with the use of poly(lactide) (PLA) based polyesters and their copolymers.

1.2 Development of polyester

Since 1970s, much effort has been focused on developing different polymers for drug delivery to improve therapeutic efficacy. The main criteria of the eligibility of polymers used in drug delivery involve bioavailability, biocompatibility, straightforward production, sustained release of drug and degradation rate.^[10] Polyester, alone or in combination with other polymers have been widely adapted for the formulation of NPs. Poly (lactic acid) (PLA) and poly(lactic-co-glycolic acids) are among the most well known choices due to their highly biocompatibility and biodegrade property. These aliphatic polyesters have been used for surgical sutures since its first file as resorbable suture in 1967 (Schmitt, E. E.; Polistina, R. A. In U.S. Patent, 1967). Drug delivery research using PLGA and PLA polymers first confined in low molecular weight steroids

for contraception and small peptides such as LHRH analogues in 1970-80s. This area of research for slow release of small peptides showed the clinical impact. In 1989, the U.S. Food and Drug Administration (FDA) approved the first PLGA system to slowly release a peptide^[11]. These PLGA matrix slowly release luteinizing hormone releasing hormone (LHRH) analogues, which are of about 1200 Da molecular weight. This later becomes the most widely used system for treating advanced prostate cancer, endometriosis, and precocious puberty. Meanwhile, serious delivery problems for the emerging of large-molecular-weight drugs (e.g. recombinant proteins) required a sustained dosage system to continuously release drugs in unaltered form. PLGA was first investigated by Langer group to delivery high molecular weight proteins in 1990^[12]. PLGA microspheres with diameters of 55-95 μm can encapsulate more than 90% of proteins and slowly release them over 100 days *in vitro*. Later in 1994, Langer group sophisticatedly apply PLA-PEG copolymer system for small molecule drug delivery with control release and long circulation profiles within simply formulation step and nanometer sizes^[13]. The inclusion of PEG into the copolymer aims to reduce non-specific effects of protein adsorption and colloidal aggregation, and further facilitate circulation. The molecular origins of these phenomena are still under investigation ^[14]. Rapidly growing area to apply PLA and PLGA and their combination with other copolymers microparticles and NPs for biomedical therapeutics delivery, including small molecules^[15], proteins^[16] and genes^[17]. The delivery routes have also been substantially expanded, from injection^[13] to pulmonary^[18], oral^[19], and recently targeting delivery strategy^[20]. Progress in the nanotechnology and microfabrication ^[21] produced many advanced nanodevices based on PLGA and PLA with PEG copolymer for smart drug delivery ^[22]. Additionally, the morphology of nanocarriers is beyond spherical shapes due to the development of

microscale technology. In 2005, DeSimone and coworkers^[23] prepared polymeric NPs (including PLA copolymer) of various shapes (e.g. cylinder and cube) using the PRINT technique and demonstrated in vitro that shape greatly impacted the cellular uptake of NPs. In 2009, Mitragotri and coworkers engineered an intriguing type of nanoparticles based on PLGA mimicking the nature shape and size of red blood cells^[24]. These new particles, similar to their nature counterpart, possess the ability to carry oxygen and flow through capillaries smaller than their own diameters. Another area under intense investigation is to study the self-assemble of amphiphilic copolymers. The increasing understanding in this area eventually creates new delivery vehicles such as polymersomes^[25] (polymer based liposome) and filamicelles^[26]. The flexible cylinder-shaped filomicelles (20-60 nm in cross-sectional diameter and a few micrometers in length) in rodents could persist in the circulation up to one week after intravenous injection, which is about ten-times longer than their spherical counterparts. One trend is to dedicate PLA and PLGA in novel biomedical area, such as emerging stem cell areas and siRNA regarded as promising therapy. In 2002, human embryonic stem cells could be cultured onto supportive 3D PLGA scaffolds, and could be induced to early differentiation^[27]. In 2009 Saltzman and coworkers apply PLGA as siRNA delivery vehicles for *in vivo* gene silencing therapy^[28]. A single dose of high amount siRNA-loaded NPs to the mouse female reproductive tract caused efficient and sustained gene silencing. Another intriguing work published in 2009 by Cheng group showed that PLA-mPEG micelle can effectively repair traumatically injured spinal cord through intravenously injection. Substantial attention was recently also focused on designing smart biomaterials on the basis of simple structure of PLA and PLGA, including thermosensitive hydrogel composed of PLA and PLGA^[29], and PLA/polyurethane^[30] possessing with shape

memory as its similar aliphatic ester PCL^[31]. It witness the extensive investigation of PLA/PLGA polymers and rapidly growth of their biomedical application, largely influenced by the concurrent development in technology and understanding of chemistry, biology, and materials science. As one of the most important and materials for nanomedicine, PLA was selected as the basis of my research. The exploration of the chemistry, properties, application of PLA leads me to understand the nanomedicine field, to synthesize new materials for various applications, and to design new biomaterials and chemistries to contribute for the biomedicine society.

1.3 Cancer targeting

To achieve tumor targeting, nanocarriers must first overcome systemic barriers, especially clearance via phagocytic uptake and hepatic filtration. Then they are expected to extravasate the tumor vasculature and penetrate the tumor microenvironment so that even cancer cells situated distal to the tumor vessel can be exposed to the anticancer agent at high enough concentrations.

The first examples of targeted NPs were reported in 1980, and despite nearly three decades of research, targeted NPs have made a limited impact on human health. This, in part, is because the optimal bio-physicochemical properties of NPs, including the choice of a suitable targeting ligand, have remained elusive. Aptamers (Apts) or single-stranded DNA or RNA that can fold into unique conformations capable of binding to specific targets with high affinity and specificity recently emerged as a new class of targeting ligands that showed some unique abilities unattainable from antibodies or small molecules. Apts are non-immunogenic and exhibit remarkable stability in a wide range of pH (4–9), temperature, and organic solvents without the loss of activities. The synthesis

of Apts is an entirely chemical process that can decrease batch-to-batch variability.^[32] These advantages of Apts are superior to immunogenic or labile antibodies, which have significant batch-to-batch variability due to the dependence on biological systems. Farokhzad, et al. demonstrated for the first time that intratumorally administered polymeric NPs with surface-coated aptamers specific for prostate-specific membrane antigen (PSMA) could successfully recognize and target PSMA-positive lymph node carcinoma of prostate (LNCaP) cells and eradicate the tumor more effectively than the NPs without aptamers.^[33] When injected systemically, the nanoparticle-aptamer conjugates could target subcutaneously implanted LNCaP tumor.^[20] One of the ultimate research goals for my projects is to fabricate delivery vehicles which can efficiently target tumors, eventually, *in vivo*.

2. Scope and Organization

The aim of my thesis work is to develop potential polymeric drug delivery vehicles for the treatment of cancers (e.g. prostate and breast cancers). Although polymeric nanoparticles are attractive vehicles for the delivery of anticancer drugs to solid tumors by selective penetration through leaky tumor vessels, many current nanoparticle formulations exhibit low drug loading and encapsulation efficiency, bimodal particle distributions, and undesirable drug “burst” release kinetics. Our new developed technology, described in Chapter 2 to Chapter 5, is expected to overcome the above limitations and permit the clinical translation of nanoparticles for polymeric targeted cancer therapy.

The nanoconjugation technique I developed that allows for the efficient preparation of PLA-drug conjugated nanoparticles, termed nanoconjugates (NCs). These

nanoconjugates are 100 nm or less in size, have exceptionally high drug loading (up to 37%), 100% drug loading efficiency and controlled release profiles without the so-called “burst” effect. The comprehensive development of nanoconjugation chemistry are documented in Chapter 2, 3, 4, organized by the increased complexity of the drug structures from camptothecin to paclitaxel and doxorubicin. Chapter 2 described this simple, unique chemistry that allows for one-step conjugation of camptothecin to the terminus PLA by the nanoconjugation technique. The tertiary less reactive hydroxyl group on the CPT was activated for LA polymerization by the selection of asymmetric β -diiminate Zinc (BDI-Zn) catalysts, overcoming conventional tedious coupling chemistry. These findings are also reported in one published paper.

Chapter 3 showed the efforts to incorporate paclitaxel, a significant potent drug for cancer therapy with multi hydroxyls, on PLA. We demonstrated, for the first time, anticancer drugs like paclitaxel can be incorporated into polymers in a regioselective manner via a well-controlled living polymerization process. The most reactive 2'-OH group in paclitaxel can readily initiate the living polymerization of PLA mediated by BDI-Zn catalyst. The paper published on 2008 on the development of PLA-paclitaxel conjugates set up the basis for our NCs projects. This chapter also includes the work to use various cyclic lactones and carbonates as the monomers for living polymerization initiated by the combination of paclitaxel/BDI-Zn, expanding the scope of nanoconjugates synthesis.

Additionally, doxorubicin, another cancer therapeutic agent which containing one amine and three hydroxyl groups, can be incorporated into polymers in a regio- and chemo-selective manner via the well-controlled living polymerization process. The comprehensive study on the preparation of PLA-doxorubicin NCs, described in Chapter 4,

was also reported in the published paper. Therefore, a handful of complicated chemotherapeutics with hydroxyl groups widely used in clinical settings have been readily incorporated into the biodegradable NCs.

Successively, Chapter 5 showed the initial efforts to address the translational barriers for NCs. We first addressed the formulation issues of NCs. A unique method was developed to store NCs in solid form for potential clinical translation. NCs with targeting ligands for bone tumor and prostate tumors, respectively, are developed. Preliminary *in vivo* radiolabeling imaging study showed the potential for tumor targeting. Pre-clinical *in vivo* trials for tumor prevention using PLA-paclitaxel NCs further confirmed the potential application of NCs. We published two papers on this topic, nevertheless, to date the understanding and improvement of our NCs systems for clinical translation are still undergoing.

Inspired by our new chemistry on the PLA polymerization with regioselective initiation on drugs (in Chapter 3 and 4), in 2009, I explored the *O*-acylation chemistry for drugs/ anhydride reaction, catalyzed by the BDI-Zn catalyst. The objective of this project is to introducing functional groups in regioselective manner for further modification. Chapter 6 concluded the initial efforts for this project. In addition to many drugs we studied before, rapamycin, one of the most significant drugs for both immunotherapy and cancer treatment, was found to react with various anhydrides with regioselectivity using the developed methods. This intriguing reaction is expected to provide another elegant facile strategy to synthesize new prodrugs for both medicinal chemistry and bioconjugation.

Current cancer targeting strategies use antibodies to recognize specific markers on tumor cell surfaces. However, the resulting antibody-drug delivery systems are often

ineffective *in vivo* as they suffer from inconsistent binding affinity for cancer cells and can be potentially immunogenic. The collaborative work (with Dr. Yi Lu and Dr. Gerard Wong group) on liposome –aptamer for targeting delivery of cisplatin to breast cancer was documented in Chapter 7. We incorporated aptamers with liposome-based delivery systems and successfully delivered cisplatin, an important chemotherapeutic agent, to breast cancer cells without significant damage to regular cells. Furthermore, because each patient responds to chemotherapeutics differently, over-dosage of drugs can lead to severe consequences. We showed for the first time that a complementary DNA of the aptamer can function as “antidote” to prohibit or even disrupt aptamer-mediated targeted drug delivery, and one paper was published based on these encouraging findings. The results described in Chapter 7 suggested that aptamer-mediated cancer-targeting strategy can be highly specific in terms of targeting and dosage modulation.

Aforementioned six chapters are comprised as the main focus in my graduate research.

It is also demanding to expand the scope of the monomer for polyester not only for biomedical use, such as drug conjugates, but also for the plastic engineering. In 2010 we adapted the monomer *O*-carboxyanhydride, with the mediation of BDI-Zn catalysts and additional co-catalyst (HMDS) to achieve controlled living polymerization of new polyesters. Chapter 8 reported the undergoing research of this direction. We expect drugs can be potentially incorporated the new polyesters, in order to modulate nanoconjugates properties for further biomedical applications.

Chapter 9 briefly summarized the initial efforts to utilize biomaterials for stem cell engineering on regenerative medicine in past one year, through the collaboration with Dr. Jennifer Lewis group and Dr. Fei Wang group. The ultimate goal for this project is to

delivery biological active cues in controlled manner for regulate stem cell fate. The preliminary is involved with the protein delivery and fabrication of scaffolds for cultivation stem cells.

3. References

- [1] R. Langer, *Nature* **1998**, 392, 5.
- [2] C. Li, S. Wallace, *Adv. Drug Delivery Rev.* **2008**, 60, 886.
- [3] I. Collins, P. Workman, *Nat. Chem. Biol.* **2006**, 2, 689.
- [4] (a) R. Duncan, *Nat. Rev. Cancer* **2006**, 6, 688; (b) M. Ferrari, *Nat. Rev. Cancer* **2005**, 5, 161; (c) D. Peer, J. M. Karp, S. Hong, O. C. FaroKhazad, R. Margalit, R. Langer, *Nat. Nanotechnol.* **2007**, 2, 751.
- [5] H. Maeda, J. Wu, T. Sawa, Y. Matsumura, K. Hori, *J. Controlled Release* **2000**, 65, 271.
- [6] R. Duncan, *Anti-Cancer Drugs* **1992**, 3, 175.
- [7] (a) H. C. Kolb, M. G. Finn, K. B. Sharpless, *Angew. Chem. Int. Ed.* **2001**, 40, 2004; (b) S. T. Laughlin, J. M. Baskin, S. L. Amacher, C. R. Bertozzi, *Science* **2008**, 320, 664; (c) K. L. Killos, L. M. Campos, C. J. Hawker, *J Am Chem Soc* **2008**, 130, 5062.
- [8] (a) J. A. Champion, Y. K. Katare, S. Mitragotri, *Proc. Natl. Acad. Sci. U. S. A.* **2007**, 104, 11901; (b) R. S. Kane, *Angew. Chem. Int. Ed.* **2008**, 47, 1368; (c) D. Dendukuri, D. C. Pregibon, J. Collins, T. A. Hatton, P. S. Doyle, *Nat. Mater.* **2006**, 5, 365; (d) G. M. Gratson, M. J. Xu, J. A. Lewis, *Nature* **2004**, 428, 386.
- [9] J. R. Heath, M. E. Davis, *Annu Rev Med* **2008**, 59, 251.
- [10] J. Panyam, V. Labhasetwar, *Adv Drug Deliver Rev* **2003**, 55, 329.
- [11] Y. Ogawa, M. Yamamoto, H. Okada, T. Yashiki, T. Shimamoto, *Chem. Pharm. Bull.* **1988**, 36, 1095.
- [12] (a) S. Cohen, T. Yoshioka, M. Lucarelli, L. H. Hwang, R. Langer, *Pharm. Res.* **1991**, 8, 713; (b) T. G. Park, S. Cohen, R. Langer, *Pharm. Res.* **1992**, 9, 37.
- [13] R. Gref, Y. Minamitake, M. T. Peracchia, V. Trubetskoy, V. Torchilin, R. Langer, *Science* **1994**, 263, 1600.
- [14] Y. Y. Wang, S. K. Lai, J. S. Suk, A. Pace, R. Cone, J. Hanes, *Angew. Chem. Int. Ed.* **2008**, 47, 9726.
- [15] R. Tong, J. J. Cheng, *Polym. Rev.* **2007**, 47, 345.
- [16] S. D. Putney, P. A. Burke, *Nat. Biotechnol.* **1998**, 16, 153.

- [17] (a) D. Luo, K. Woodrow-Mumford, N. Belcheva, W. M. Saltzman, *Pharm. Res.* **1999**, *16*, 1300; (b) D. Luo, W. M. Saltzman, *Nat. Biotechnol.* **2000**, *18*, 33.
- [18] D. A. Edwards, J. Hanes, G. Caponetti, J. Hrkach, A. BenJebria, M. L. Eskew, J. Mintzes, D. Deaver, N. Lotan, R. Langer, *Science* **1997**, *276*, 1868.
- [19] O. Benny, O. Fainaru, A. Adini, F. Cassiola, L. Bazinet, I. Adini, E. Pravda, Y. Nahmias, S. Koirala, G. Corfas, R. J. D'Amato, J. Folkman, *Nat. Biotechnol.* **2008**, *26*, 799.
- [20] O. C. Farokhzad, J. J. Cheng, B. A. Teply, I. Sherifi, S. Jon, P. W. Kantoff, J. P. Richie, R. Langer, *Proc. Natl. Acad. Sci. U. S. A.* **2006**, *103*, 6315.
- [21] A. Khademhosseini, R. Langer, J. Borenstein, J. P. Vacanti, *Proc. Natl. Acad. Sci. U. S. A.* **2006**, *103*, 2480.
- [22] A. C. R. Grayson, M. J. Cima, R. Langer, *Biomaterials* **2005**, *26*, 2137.
- [23] (a) S. E. A. Gratton, S. S. Williams, M. E. Napier, P. D. Pohlhaus, Z. L. Zhou, K. B. Wiles, B. W. Maynor, C. Shen, T. Olafsen, E. T. Samulski, J. M. Desimone, *Acc. Chem. Res.* **2008**, *41*, 1685; (b) S. E. A. Gratton, P. A. Ropp, P. D. Pohlhaus, J. C. Luft, V. J. Madden, M. E. Napier, J. M. DeSimone, *Proc. Natl. Acad. Sci. U. S. A.* **2008**, *105*, 11613; (c) J. P. Rolland, B. W. Maynor, L. E. Euliss, A. E. Exner, G. M. Denison, J. M. DeSimone, *J. Am. Chem. Soc.* **2005**, *127*, 10096.
- [24] N. Doshi, A. S. Zahr, S. Bhaskar, J. Lahann, S. Mitragotri, *Proc Natl Acad Sci U S A* **2009**.
- [25] (a) D. E. Discher, F. Ahmed, *Annu. Rev. Biomed. Eng.* **2006**, *8*, 323; (b) B. M. Discher, Y. Y. Won, D. S. Ege, J. C. M. Lee, F. S. Bates, D. E. Discher, D. A. Hammer, *Science* **1999**, *284*, 1143.
- [26] Y. Geng, P. Dalhaimer, S. S. Cai, R. Tsai, M. Tewari, T. Minko, D. E. Discher, *Nat. Nanotechnol.* **2007**, *2*, 249.
- [27] (a) S. Levenberg, J. S. Golub, M. Amit, J. Itskovitz-Eldor, R. Langer, *Proc. Natl. Acad. Sci. U. S. A.* **2002**, *99*, 4391; (b) S. Levenberg, N. F. Huang, E. Lavik, A. B. Rogers, J. Itskovitz-Eldor, R. Langer, *Proc. Natl. Acad. Sci. U. S. A.* **2003**, *100*, 12741.
- [28] K. A. Woodrow, Y. Cu, C. J. Booth, J. K. Saucier-Sawyer, M. J. Wood, W. M. Saltzman, *Nat. Mater.* **2009**, *8*, 526.
- [29] (a) B. Jeong, Y. H. Bae, D. S. Lee, S. W. Kim, *Nature* **1997**, *388*, 860; (b) L. Yu, J. D. Ding, *Chem. Soc. Rev.* **2008**, *37*, 1473.
- [30] W. S. Wang, P. Ping, X. S. Chen, X. B. Jing, *Eur. Polym. J.* **2006**, *42*, 1240.

- [31] (a) M. Behl, A. Lendlein, *Mater Today* **2007**, *10*, 20; (b) A. Lendlein, A. M. Schmidt, R. Langer, *P Natl Acad Sci USA* **2001**, *98*, 842; (c) A. Lendlein, R. Langer, *Science* **2002**, *296*, 1673.
- [32] (a) S. M. Nimjee, C. P. Rusconi, B. A. Sullenger, *Annu. Rev. Med.* **2005**, *56*, 555; (b) C. Wilson, J. W. Szostak, *Chem. Biol.* **1998**, *5*, 609.
- [33] O. C. Farokhzad, S. Y. Jon, A. Khadelmhosseini, T. N. T. Tran, D. A. LaVan, R. Langer, *Cancer Res.* **2004**, *64*, 7668.

CHAPTER 2

NANOCONJUGATES: INCORPORATING CAMPTOTHECIN

1. Introduction

1.1 General consideration of polymer-drug conjugates

Polymeric nanomedicine, an emerging field that involves the use of drug-containing polymeric nanoparticles (NPs) for cancer treatment, is expected to alter the landscape of oncology. Although the nomenclature of nanomedicine emerged only a few years ago, the practice of applying nanotechnology to cancer drug delivery dates back to the 1970s. Through numerous efforts, a handful of polymeric NPs have been developed and evaluated in various preclinical or clinical studies, some of which have been approved for clinical cancer treatment.

The application of nanotechnology to conventional chemotherapy has obvious benefits. In general, the incorporation of chemotherapeutic agents in NP delivery vehicles has improved water solubility, reduced clearance, reduced drug resistance and enhanced therapeutic effectiveness. However, the drawbacks of the incorporation of chemotherapeutic agents in delivery NPs are also obvious. Compared to conventional chemotherapy, where all therapeutic agents have identical structures and molecular weights, polymeric NPs are heterogeneous in their composition, structure and size.

The heterogeneities of polymer-drug conjugates, a class of well-known polymeric NP delivery vehicles, may result from (1) the polydispersity of the polymer; (2) the lack of control over the site on the polymer backbone to which the drug is conjugated; and (3)

the lack of control over the regio- and chemoselective conjugation of the therapeutic agents containing multiple conjugation-amenable functional groups. These heterogeneities are not easily addressable and may present bottlenecks to the clinical translation of polymeric NPs. Without eliminating the heterogeneities inherent in polymeric-drug conjugates, it will be difficult, if not entirely impossible, to achieve advanced drug delivery for targeted or even personalized cancer therapy. In the past several decades, there have been numerous efforts to reduce these heterogeneities by developing polymers with low polydispersities, conjugating therapeutic agents to the termini of polymers or to specific sites along polymer backbones and blocking the undesirable conjugation of competing functional groups on therapeutic agents through the use of protection and deprotection chemistries.

Ring-opening polymerization (ROP) for the preparation of polyesters, such as polylactide (PLA), which is used in this study, has been investigated extensively. This polymerization typically involves lactide (LA) ring opening by a metal-alkoxide (RO-M) to form a RO-terminated LA-metal alkoxide ($\text{ROOCCH}(\text{CH}_3)\text{O-M}$), followed by chain propagation to form RO-terminated PLA. The RO is connected to the PLA terminus through an ester bond. This process is well understood and has been used extensively for the incorporation of hydroxyl-containing small molecules, macromolecules and NPs to the termini of PLA. We hypothesize with judicious choices of the metal catalyst, it is likely we can incorporate drugs containing hydroxyl group onto the terminus of PLA by hydroxyl initiated ROP. Here we first used the drug containing one hydroxyl group to demonstrate the concept.

1.2 *Incorporation of camptothecin*

20(S)-Camptothecin (CPT), a topoisomerase II inhibitor isolated from the Chinese tree *Camptotheca acuminata* in the 1960s, exhibits a broad range of anticancer activity in various animal models. CPT has low aqueous solubility in its therapeutically active lactone form. Once placed in an aqueous solution at physiological pH, the lactone form of CPT is quickly transformed to its carboxylate form, which is highly toxic and therapeutically inactive. Serum albumin preferentially binds to the carboxylate form of CPT and serves as the driving force of shifting the lactone-carboxylate equilibrium (shown in Scheme 2.1) toward the formation of the carboxylate. These pharmacological properties of CPT result in rapid deactivation and fast clearance of CPT from the circulation after it is intravenously administered. To overcome these drawbacks, CPT has been conjugated to various polymeric carriers for improved solubility, enhanced stability of its lactone form and reduced renal clearance.

Polymer-CPT conjugates prepared with conventional coupling chemistry have various heterogeneities that may impact their pharmacological and pharmacokinetic properties *in vivo*. For instance, various polymers used for the conjugation of CPT were prepared via condensation reaction with molecular weight distributions (MWDs) over a range of 1.5 to 2.5. It is also difficult to control the site of CPT conjugation to polymers with pendant functional groups. Furthermore, the direct conjugation of CPT through its C20-hydroxyl groups is difficult multistep reaction; the CPT must first be converted to a CPT-amino ester and then conjugated to a polymer that contains carboxylate groups via the amine end group of the CPT-amino ester.

Here, we report a simple, unique chemistry that allows for one-step conjugation of CPT to the terminal carboxylate group of polylactide (PLA). Instead of using coupling chemistry, we developed a ring-opening polymerization method to facilitate the

incorporation of CPT to PLA. Through a living polymerization, both the initiation (drug incorporation) and the chain propagation proceed in a well-controlled manner and result in materials with pre-defined drug loadings and MWDs as narrow as 1.02. The resulting CPT-PLA conjugate was nanoprecipitated to form CPT-PLA conjugate nanoparticles, termed nanoconjugates (NCs), around 100 nm in size with narrow polydispersities and controlled antitumor toxicities.

2. Materials and Methods

2.1 General

D,L-Lactide (LA) was purchased from TCI America (Portland, OR), recrystallized three times in toluene and stored at -30°C in a glove box prior to use. The BDI ligands and the corresponding metal catalysts ((BDI)Mn(TMS)₂, M = Mg, Zn) were prepared by following the published procedures and stored at -30°C in a glove box prior to use. All anhydrous solvents were purified by being passing through dry alumina columns and were kept anhydrous by using molecular sieves. Doxo·HCl was purchased from Bosche Scientific (New Brunswick, NJ) and used as received. Removal of HCl of Doxo·HCl was achieved by following the procedure reported in the literature. Docetaxel (Dtxl) was purchased from LC Laboratories (Woburn, MA) and used as received. Cy5 was synthesized according to the published procedure. All other chemicals were purchased from Sigma-Aldrich (St Louis, MO) and used as received, unless otherwise specified. The MWs of PLA and Doxo-PLA were determined by a size-exclusion chromatography instrument (SEC) equipped with an isocratic pump (Model 1100, Agilent Technology, Santa Clara, CA), a DAWN HELEOS 18-angle laser light scattering detector (Wyatt

Technology, Santa Barbara, CA) and an Optilab rEX refractive index detector (Wyatt Technology, Santa Barbara, CA). The wavelength of the HELEOS detector was set at 658 nm. The size exclusion columns used for the separation of PLA and Doxo-PLA conjugates were serially connected to a SEC (Phenogel columns 100 Å, 500 Å, 10³ Å and 10⁴ Å, 5 µm, 300 × 7.8 mm, Phenomenex, Torrance, CA) equipped with a 126P solvent module and a System Gold 128 UV detector (Beckman Coulter, Fullerton, CA). THF (HPLC grade) was used as the mobile phase of SEC with a 1-mL/min flow rate. The low resolution electrospray ionization mass spectrometry (LR-ESI-MS) experiments were performed on a Waters Quattro II Mass Spectrometer. The high resolution electrospray ionization mass spectrometry (HR-ESI MS) experiments were performed on a Micromass Q-TOF Ultima system. Matrix assisted laser desorption/ionization-time of flight mass spectrometry (MALDI-TOF MS) spectra were collected on an Applied Biosystems Voyager-DETM STR system. HPLC analyses were performed on a System Gold system (Beckman Coulter, Fullerton, CA) equipped with a 126P solvent module, a System Gold 128 UV detector and an analytical pentafluorophenyl column (Curosil-PFP, 250 × 4.6 mm, 5 µm, Phenomenex, Torrance, CA) or an analytical C18 column (Luna C18, 250 × 4.6 mm, 5 µm, Phenomenex, Torrance, CA). The UV wavelength for detecting Pyr-OH or Pyr-NH₂ was set at 300 nm. The UV wavelength for detecting Doxo was set at 450 nm or 500 nm, depending on the signal-to-noise ratio in corresponding studies. The NMR experiments were conducted on a Varian U500, a VXR500 or a UI500NB (500 MHz) NMR spectrometer. The sizes and particle polydispersities of the PLA-drug (dye) NCs were determined on a ZetaPlus Dynamic Light Scattering (DLS) detector (15-mW laser, incident beam = 676 nm, Brookhaven Instruments, Holtsville, NY). The PC-3 cells (ATCC, Manassas, VA) used in the MTT assay were cultured in Ham's F12K medium

containing 10% fetal bovine serum, 1000 units/mL aqueous penicillin G and 100 µg/mL streptomycin.

2.2 Synthesis and characterization of CPT-PLA nanoconjugates

2.2.1 General Procedures for the Preparation of CPT-PLA Conjugate via CPT-Mediated Ring-Opening Polymerization of LA

(BDI-3)ZnN(TMS)₂ (5.5 mg, 8.9 µmol) was dissolved in anhydrous THF (300 µL). The solution was added to a vial containing CPT (3.0 mg, 8.6 mmol) and the mixture was stirred for 15 min until the CPT was completely dissolved in THF. LA (124 mg, 0.86 mmol) was dissolved in a vial containing THF (940 µL) and the resulting solution was added to the mixture of CPT/(BDI-3)ZnN(TMS)₂ ([LA]₀ = 0.69 M). FT-IR was used to follow the conversion of the LA in the polymerization solution by monitoring the intensity of the lactone band at 1772 cm⁻¹. After the LA was completely consumed, the polymerization was quenched with ice-cold methanol (10 mL). The precipitate (CPT-PLA) was collected by centrifugation and then dried under vacuum. The resulting CPT-PLA conjugate was denoted as CPT-LA_n where *n* is the monomer/initiator (LA/CPT) molar ratio.

2.2.2 Reaction of CPT with Succinic Anhydride (SA) Mediated by Zn or Mg Catalysts.

In a glove box, (BDI-3)ZnN(TMS)₂ (6.2 mg, 0.01 mmol) was dissolved in anhydrous THF (200 µL). The solution was added to a clean vial containing CPT (3.5 mg, 0.01 mmol) and THF (300 µL) and stirred for 15 min until the CPT was completely dissolved. SA (1.1 mg, 0.011 mmol) in THF (600 µL) was added and the vial was tightly

sealed. It was then immediately taken out of the glove box and stirred for 4h at 40°C. The reaction was quenched with ice-cold methanol (1 mL). An aliquot of this solution was analyzed by HPLC equipped with an analytical C18 column (Luna C18(2), 250 × 4.6 mm, 5 μ, Phenomenex, Torrance, CA). The mobile phase for the HPLC analysis was a solvent mixture containing equal volume of acetonitrile and water (0.1% TFA). All HPLC spectra were recorded and analyzed by a UV detector at 370 nm. The areas of the HPLC peaks of CPT and the CPT-SA were integrated and used for the quantification of their concentrations as compared to corresponding standard curves. An aliquot of the reaction mixture was also used for the MS analysis.

The CPT-SA used for NMR analysis was collected by preparative thin layer chromatography (prep-TLC, silica gel with a fluorescent indicator (254 nm), 1.5 mm thickness, Aldrich) and developed by ethyl acetate/methanol (v/v = 10/1). The R_f values of CPT and CPT-SA were 0.7 and 0.1, respectively. The silica gel was removed from the glass plate and the CPT-SA was extracted with methanol (2 × 30 mL). The methanol solution was then removed under vacuum; the resulting CPT-SA was analyzed by ^1H -NMR. ^1H -NMR (CD_3OD , 500 MHz): δ 8.63 (s, 1H, 7-H), 8.21 (d, $J = 8.5$ Hz, 1H, 12-H), 8.07 (d, $J = 8.0$ Hz, 1H, 9-H), 7.87 (td, $J_t = 8.5$ Hz, $J_d = 1.5$ Hz, 1H, 11-H), 7.71 (td, $J_t = 8.0$ Hz, $J_d = 1.0$ Hz, 1H, 10-H), 7.43 (s, 1H, 14-H), 5.57, 5.44 (AB, $J_{AB} = 17.0$ Hz, 2H, 17-H), 5.35 (s, 1H, 5-H), 2.81 (t, $J = 7.5$ Hz, 2H, $-\text{CH}_2\text{-COOH}$), 2.55 (t, $J = 7.5$ Hz, 2H, $-\text{CH}_2\text{-CH}_2\text{-COOH}$), 2.24 (m, 2H, 18-H), 0.99 (t, $J = 8.0$ Hz, 19-H). MS (LR-ESI, positive mode): calculated for $\text{C}_{24}\text{H}_{20}\text{N}_2\text{O}_7$ $[\text{M} + \text{H}]^+$ m/z 449.1; found m/z 449.1. MS (HR-ESI, positive mode): calculated for $\text{C}_{24}\text{H}_{20}\text{N}_2\text{O}_7$ $[\text{M} + \text{H}]^+$ m/z 449.1349; found m/z 449.1355.

2.2.3 General Procedure for the Formation and Characterization CPT-PLA Nanoconjugates (NCs)

A DMF solution containing the CPT-LA₁₀ conjugate (100 μ L, 5 mg/mL) was added dropwise to nanopure water (4 mL). The resulting CPT-LA₁₀ NCs were collected by ultrafiltration (15 min, 3000 \times g, Ultracel membrane with 10,000 NMWL, Millipore, Billerica, MA) and were characterized by DLS and SEM for particle sizes and by HPLC for drug loading and release kinetics.

2.2.4 Hydrolysis of CPT-LA₁₀ NCs

The CPT-LA₁₀ NC in water (1 mL, 1 mg/mL) was treated with a NaOH solution (1M, 1 mL) for 12 h. The solution was then tuned to pH 2 by phosphoric acid addition, which resulted in a yellow solution. The solvent was removed by rotary evaporation. The resulting residue was then dissolved in acetonitrile/water (0.1% TFA) (v/v = 1/1) and injected into a semi-prep HPLC column (Jupitor Proteo 90 A, 250 \times 21.20 mm, 10 μ , Phenomenex, Torrance, CA). The fraction that had the identical elution time as the authentic CPT was collected. After the solvent was removed by vacuum, the resulting yellow oily residue was dissolved in phosphoric acid/methanol at a volume ratio of 1:1. The solution was tuned to pH 3-4 by 0.1 M NaOH and then extracted with chloroform (5 \times 100 mL). The organic phase was combined and dried with MgSO₄. After the MgSO₄ was removed by filtration and the solvent was removed under vacuum, the resulting pale yellow solid was analyzed by ¹H-NMR. The ¹H-NMR spectrum of the CPT released from CPT-PLA NCs was identical to that of the authentic CPT (see Figure 2.6) ^[1].

2.2.5 Release Kinetics of the CPT-LA_n NCs and the CPT/PLA Nanoparticle (NP)

CPT/PLA NPs were prepared through nanoprecipitation of CPT and PLA (MW = 1.5×10^4 g/mol) by following the procedures reported in literature [2]. The CPT-LA₁₀ NCs were prepared with CPT-LA₁₀ conjugate by following the standard nanoprecipitation procedure described above. The NCs (or NPs) were collected and washed three times with nanopure water by ultrafiltration (Ultracel membrane 10,000 NMWL, Millipore, Billerica, MA). The NCs (or NPs) collected from the ultrafiltration device were dispersed in 1× PBS solution (1 mg/mL) and incubated at 37°C. At selected time intervals, an aliquot of NCs (or NPs) (≈ 1 mL) was taken out of the incubator and centrifuged at 10,000 rpm for 10 min. The supernatant (500 μ L) was carefully transferred to an Eppendorf tube using micropipette without disturbing the precipitates (NCs or NPs). The solution was tuned to pH 2 by phosphoric acid (85%) and the resulting solution was directly injected into HPLC equipped with an analytical pentafluorophenyl RP-column (Curosil-PFP, 250 \times 4.6 mm, 5 μ , Phenomenex, Torrance, CA). A mixture of acetonitrile and water (containing 0.1% TFA) at a volume ratio of 1:1 was used as the mobile phase. The flow rate was set at 1 mL/min. The area of the HPLC peak of the released CPT was intergraded for the quantification of CPT as compared to the standard curve for this drug.

2.2.6 Determination of the Cytotoxicity of CPT-LA_n NCs

PC-3 cells were placed in a 96-well plate for 24 h (10,000 cells per well). Cells were washed with 100 μ L of pre-warmed PBS. Freshly prepared CPT-LA₁₀, CPT-LA₂₅ and CPT-LA₅₀ NCs (prepared in 1× PBS, 100 μ L) were added to the cells. CPT was used as a positive control. Untreated cells were used as a negative control. PLA NPs

without CPT being conjugated or encapsulated were prepared via the nanoprecipitation of the PLA with a MW of 14 kDa ^[2-3] and were subsequently used as a negative control in the MTT study. The PLA-NPs were applied to PC-3 cells at a concentration up to 0.5 µg/mL. The cells were incubated for 72 h in a 5% CO₂ incubator at 37°C. The standard MTT assay protocols were followed thereafter ^[4].

3. Results and Discussion

3.1 Synthesis of CPT-PLA nanoconjugates

3.1.1 (BDI)Mn(TMS)₂/CPT (M=Zn, Mg)-Mediated Polymerization of Lactide

We first tested the feasibility of forming CPT-metal complex. (BDI-1)MgN(TMS)₂, was dissolved in THF. A colorless solution was obtained. We then added this solution to a vial containing CPT powder (1 equivalent relative to (BDI-1)MgN(TMS)₂). After the mixture was stirred for 20 min, it was noted that CPT was completely dissolved and the solution color gradually became orange. In the absence of (BDI-1)MgN(TMS)₂, however, CPT remained insoluble in THF and the solution stayed colorless. The sharp contrast of the solubility of CPT in the presence versus in the absence of (BDI-1)MgN(TMS)₂ as well as the color change after CPT was mixed with (BDI-1)MgN(TMS)₂ suggest possibly a coordination reaction between CPT and the (BDI-1)MgN(TMS)₂. (BDI-1)Mg-CPT alkoxide through the C20-OH of CPT is presumably the complex formed *in situ* via the coordination of (BDI-1)MgN(TMS)₂ and CPT (Figure 2.1).

We next examined if the mixture of (BDI-1)MgN(TMS)₂/CPT could initiate LA polymerization. After LA (100 equiv.) in THF was added dropwise to the (BDI-

1)MgN(TMS)₂/CPT mixture, the polymerization proceeded rapidly and completed within 10 h with 100% LA conversion; the monomer conversion was followed by monitoring the intensity of the lactone band of LA at 1772 cm⁻¹ on a FT-IR. One interesting observation was that the orange color of the polymerization solution gradually faded away during the course of polymerization, which indicated the segregation of the (BDI-1)Mg from CPT. This observation was in good agreement with the proposed reaction mechanism as shown in Figure 2.1a. After 100% LA conversion was achieved, the polymerization solution was analyzed by HPLC, which showed that CPT was completely incorporated to PLA with no detectable free CPT in the polymerization solution (data not shown). This observation was similar to what we observed in paclitaxel- and doxorubicin-initiated LA polymerization, both of which gave 100% drug incorporation efficiency in corresponding drug-initiated polymerization^[5]. The M_n of the resulting CPT-PLA conjugate was 1.13×10^4 g/mol, which was in good agreement with the expected M_n (1.47×10^4 g/mol) (entry 1, Table 2.1). The molecular weight distribution (MWD) of the CPT-PLA conjugate, however, was relatively broad ($M_w/M_n = 1.31$) due in part to the chain transfer during polymerization^[6]. In our previous studies of paclitaxel and doxorubicin initiated LA polymerization, only the primary or the secondary hydroxyl groups of these drugs could efficiently initiate the polymerizations of LA^[5]. The present study demonstrated for the first time that the C20-OH of CPT, a tertiary hydroxyl group, could also be activated by (BDI-1)MgN(TMS)₂ to initiate LA polymerization.

In order to achieve better controlled polymerization, we next tested (BDI-1)ZnN(TMS)₂, a Zn analogue of (BDI-1)MgN(TMS)₂. As reported by Coates and coworkers, Zn catalysts in general outperform Mg catalysts for LA polymerization^[6].

After (BDI-1)ZnN(TMS)₂ and CPT were mixed and stirred for 20 min, a light yellow solution was obtained. This (BDI-1)ZnN(TMS)₂/CPT complex mediated LA polymerization at a M/I ratio of 100 and gave CPT-PLA conjugate with a very narrow MWD ($M_w/M_n = 1.07$, entry 2, Table 2.1). However, the CPT incorporation efficiency was only 61% based on the HPLC analysis, indicating the poor efficiency of forming Zn-CPT complex during the initiation step. The actual M/I ratio in this reaction was 163 (calculated based on the LA/CPT ratio of 100:0.61). It was therefore not surprising that the obtained M_n (2.83×10^4 g/mol) was substantially higher than the M_n calculated based on the LA/CPT ratio of 100:1 (expected $M_n = 1.47 \times 10^4$ g/mol, entry 2, Table 2.1). The poor efficiency for the coordination of CPT with (BDI-1)ZnN(TMS)₂ was due in part to the relatively low activity of Zn as compared to Mg as well as the steric bulk of BDI-1 ligand surrounding the coordination site (Figure 2.1b). We next studied whether enhanced incorporation efficiency of CPT could be achieved by using a Zn catalyst with a BDI ligand with reduced steric bulk and/or altered electronic property.

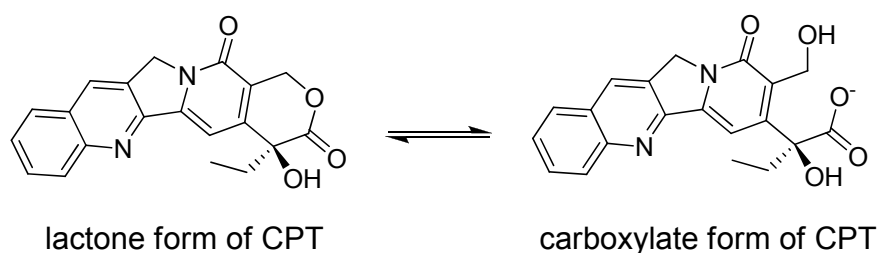
It has been reported that subtle change of BDI ligands can significantly affect the activity of (BDI)ZnN(TMS)₂ and its capability of controlling the polymerizations of cyclic esters or carbonates^[7]. Specifically, the 2, 6-substituents of the aryl groups (at the R^1 and R^2 positions) and the substitute at the R^3 position were found to have profound effects on the activities of the catalysts (Figure 2.1b)^[8]. We synthesized a series of zinc catalysts containing BDI ligands with variable 2, 6-aryl substituents and R^3 group (Figure 2.1b) and then used these catalysts in CPT-initiated LA polymerizations. We first checked the effect of the steric bulk of BDI on the LA polymerization. BDI-2 is an analogue of BDI-1 whose isopropyl (iPr) groups at both R^1 and R^2 position were replaced by ethyl (Et) groups; while BDI-3 is an analogue of BDI-1 whose iPr groups were

replaced by Et groups only at both R^1 position. Both ligands were synthesized and used to prepare the corresponding (BDI)ZnN(TMS)₂ catalysts. As expected, the steric bulk of the BDI at its R^1 and R^2 positions had profound effect on the capability of the Zn catalysts to form coordination complexes with CPT during the initiation step. As compared to the 61% of incorporation efficiency observed with the use of (BDI-1)ZnN(TMS)₂, 100% incorporation efficiencies were observed in both (BDI-2)ZnN(TMS)₂/CPT and (BDI-3)ZnN(TMS)₂/CPT mediated polymerizations. The corresponding M_n 's (2.01×10^4 g/mol and 1.73×10^4 g/mol, entries 3 and 4, Table 2.1) were much closer to the expected M_n than that of the PLA-CPT obtained from the (BDI-1)ZnN(TMS)₂/CPT mediated LA polymerization (entry 2, Table 2.1). Narrow MWDs ($M_w/M_n < 1.2$) were obtained for the CPT-PLA conjugates derived from (BDI-2)ZnN(TMS)₂/CPT and (BDI-3)ZnN(TMS)₂/CPT mediated polymerizations (entries 3 and 4, Table 2.1). BDI-4, an analogue of BDI-3 with a cyano group at the R^3 position (Figure 2.1b), was also prepared and studied. However, CPT remained insoluble in THF containing 1 equiv. (BDI-4)ZnN(TMS)₂, indicating the poor efficiency of forming (BDI-4)ZnN(TMS)₂/CPT coordination complex at room temperature. Thus, it was not surprising that the mixture of CPT and (BDI-4)ZnN(TMS)₂ could not initiate LA polymerization at room temperature (entry 5, Table 2.1). When this mixture of CPT and (BDI-4)ZnN(TMS)₂ was incubated at 40°C for 20-30 min, CPT was completely dissolved, suggesting the formation of (BDI-4)ZnN(TMS)₂/CPT coordination complex requires higher temperature. The CPT-PLA conjugate derived from (BDI-4)ZnN(TMS)₂/CPT-mediated LA polymerization had a high loading efficiency (98%) and a M_n very close to the expected molecular weight (entry 6, Table 2.1), but its MWD ($M_w/M_n = 1.32$, Table 2.1) was broader than the CPT-PLA conjugate derived from the (BDI-3)ZnN(TMS)₂/CPT-

mediated polymerizations. Based on these preliminary studies, (BDI-3)ZnN(TMS)₂ was found to be the overall best catalyst with respect to control over CPT incorporation and polymerization. (BDI-3)ZnN(TMS)₂ was therefore selected for further investigation for its capability of controlling polymerization of LA at various LA/CPT ratios.

Excellent controlled polymerizations were observed over a broad range of LA/CPT ratios from 75 to 400 when the LA polymerizations were mediated by (BDI-3)ZnN(TMS)₂/CPT (Table 2.2). Quantitative CPT incorporation efficiencies and very narrow MWDs ($M_w/M_n = 1.02-1.18$) were observed in all experiments performed. The obtained MWs of the CPT-PLA conjugates were in excellent agreement with the expected MWs (Table 2.2), which followed a linear correlation with the LA/CPT ratios (Figure 2.2a). Monomodal GPC MW distribution curves were observed in all CPT-PLA conjugates prepared with various LA/CPT ratios (Figure 2.2b). The well-controlled polymerization mediated by (BDI-3)ZnN(TMS)₂ likely proceeded through the conventional insertion-coordination mechanism (Scheme 2.2a).

Scheme 2.1 Equilibrium of CPT Lactone and Carboxylate Forms



Scheme 2.2 Suggested Insertion–Coordination Mechanism of (BDI)Zn-OR Mediated Ring Opening of (a) LA and (b) SA.

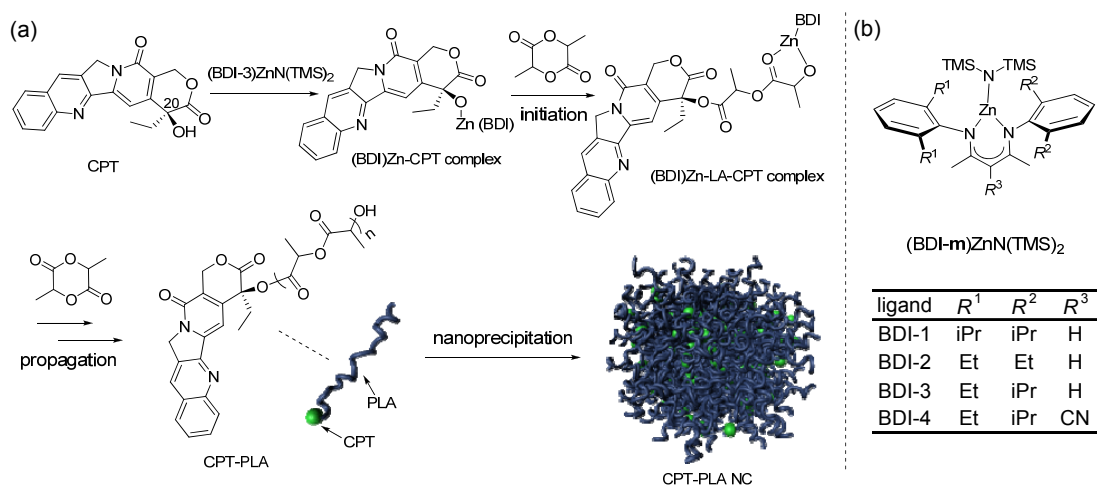
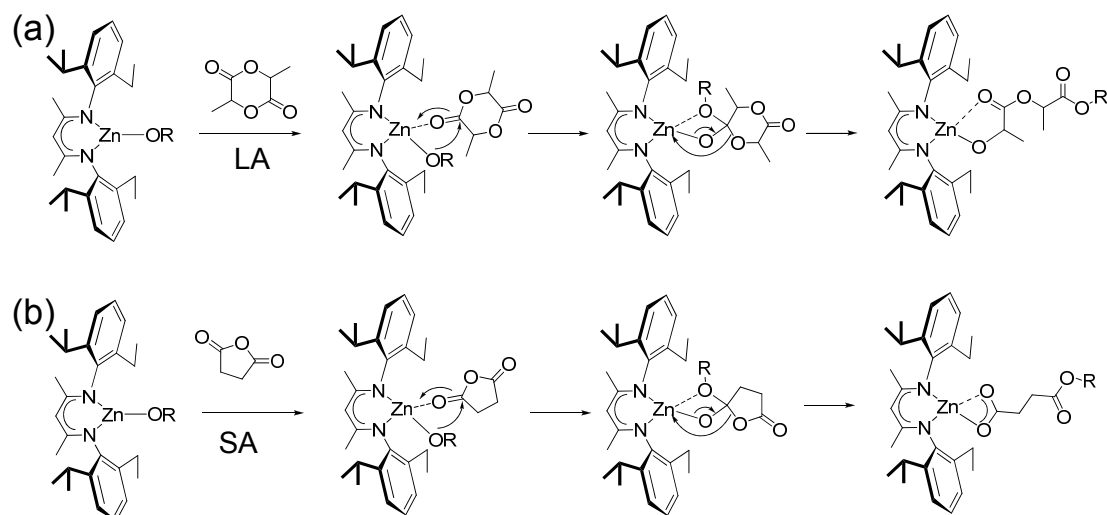


Figure 2.1 (a) Schematic illustration of (BDI-3)ZnN(TMS)₂/CPT mediated ring-opening polymerization of LA to make CPT-PLA conjugates followed by nanoprecipitation of the resulting CPT-PLA conjugates for the preparation of CPT-PLA nanoconjugates; (b) The structure of (BDI-m)ZnN(TMS)₂ (m = 1-4).

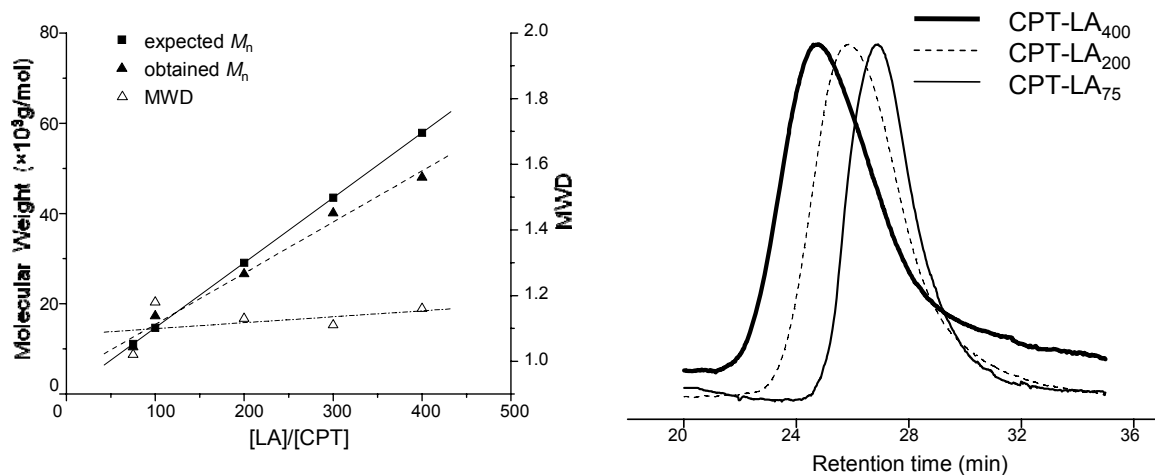


Figure 2.2 (a) (BDI-3)ZnN(TMS)₂/CPT mediated ring-opening polymerization of LA at various LA/CPT ratios; (b) Overlay of the GPC trace of CPT-LA₇₅, CPT-LA₂₀₀ and CPT-LA₄₀₀ prepared by (BDI-3)ZnN(TMS)₂/CPT mediated LA polymerizations.

Table 2.1 CPT/(BDI)MN(TMS)₂ Mediated LA Polymerization (M = Zn or Mg).^a

entry	catalyst	temp.	IE (%) ^b	CV (%) ^c	$M_n (\times 10^4 \text{ g/mol})$	MWD (M_w/M_n)
1	(BDI-1)MgN(TMS) ₂	r.t.	>99	>99	1.13	1.31
2	(BDI-1)ZnN(TMS) ₂	r.t.	61	>99	2.83	1.07
3	(BDI-2)ZnN(TMS) ₂	r.t.	>99	>99	2.01	1.20
4	(BDI-3)ZnN(TMS) ₂	r.t.	>99	>99	1.73	1.18
5	(BDI-4)ZnN(TMS) ₂	r.t.	0	0	ND	N.D
6	(BDI-4)ZnN(TMS) ₂	40 °C	>98	>98	1.12	1.32

^aAll reactions were performed at a LA/CPT/catalyst ratio of 100:1:1.01 in anhydrous THF for 12 h ($[LA]_0 = 0.69 \text{ M}$). The expected M_n of CPT-PLA conjugate = $1.47 \times 10^4 \text{ g/mol}$. Abbreviation: LA = lactide; CPT = camptothecin; temp. = temperature; IE = incorporation efficiency; CV = conversion of LA; ND = not determined. ^bDetermined by the HPLC measurement of the unreacted CPT in the polymerization solution. ^cDetermined by monitoring the IR band of the LA lactone at 1772 cm^{-1} .

Table 2.2 CPT/(BDI-3)ZnN(TMS)₂ Mediated LA Polymerization at Various LA/CPT Ratios.^a

entry	[LA]/[CPT]	IE (%) ^b	CV (%) ^c	$M_{n \text{ Cal}}$ ($\times 10^3$ g/mol)	M_n ($\times 10^3$ g/mol)	MWD (M_w/M_n)
1	75	>99	>99	11.1	10.4	1.02
2	100	>99	>99	14.7	17.3	1.18
3	200	>99	>99	29.1	26.6	1.13
4	300	>99	>99	43.5	40.1	1.11
5	400	>99	>99	57.9	48.0	1.16

^aAll reactions were performed in anhydrous THF for 12 h at room temperature ([LA]₀ = 0.69 M). Abbreviation: LA = lactide; CPT = camptothecin; IE = incorporation efficiency; CV = conversion of LA; ^bDetermined by the HPLC measurement of the unreacted CPT in the polymerization solution. ^cDetermined by monitoring IR band of LA lactone at 1772 cm⁻¹.

3.1.2 Control of Initiation by (BDI)ZnN(TMS)₂ Catalysts

As mentioned earlier, the lactone ring of CPT should be preserved in order to maintain the antitumor activity of CPT. However, it is known that the lactone ring of CPT is unstable and subject to ring opening in the presence of a nucleophile. We next studied how the initiation could be specifically controlled at the C20-OH of CPT with negligible CPT lactone ring opening during (BDI)ZnN(TMS)₂/CPT initiated LA polymerizations.

In the initiation step, LA first reacts with (BDI)Zn-CPT alkoxide and then is inserted between the CPT and Zn to generate (BDI)Zn-lactide-CPT alkoxide, the new chain-propagating end group (Scheme 2.2a). CPT does not involve the subsequent chain propagation. Apparently, the most critical step determining whether the lactone ring of CPT is opened or remains closed is the initiation step. As LA is subject to rapid polymerization and the resulting CPT-PLA conjugate is difficult to be precisely characterized, we used succinic anhydride (SA) as the model monomer to study

(BDI)ZnN(TMS)₂/CPT-mediated initiation. Such a reaction led to the formation of CPT-succinic acid (CPT-SA), a small molecule instead of a polymer, whose structure can be easily determined by routine characterization methods.

When just CPT and SA were mixed without addition of other reagents, no reaction occurred (entry 1, Table 2.3). Triethylamine (TEA), a non-nucleophilic base, has been used previously to facilitate the ring opening of SA by an alcohol ^[9]. When TEA was added to the mixture of CPT and SA, the reaction was very slow and generated CPT-SA with a yield of 10.6% after the reaction mixture was incubated at 40°C for 12 h (peak z, Figure 2.3a-i; entry 2, Table 2.3). A substantial amount of CPT in its carboxylate form was also detected (peak x, Figure 2.3a-i), indicating that the lactone ring of CPT was unstable in the presence of TEA. In a control study, when naphthalene ethanol, an alcohol with a primary -OH group that is supposed be more reactive for nucleophilic reaction than the tertiary C20-OH of CPT, was used for the conjugation with SA in the presence of TEA, the yield of naphthalene-SA was 86.8% (data not shown).

N-(3-dimethylaminopropyl)-N'-ethylcarbodiimide (EDC), in conjunction with 4-(dimethylamino)-pyridine (DMAP), has been used previously for the conjugation of CPT with SA ^[10]. When the reaction of CPT and SA was performed in the presence of EDC and DMAP at 40°C for 12 h, the yield of CPT-SA was only 12.8% (entry 3, Table 2.3), which was in good agreement with the previously reported result ^[10] and further confirmed the low activity of the tertiary C20-OH group of CPT.

We next studied the ring opening of SA by CPT in the presence of Mg or Zn catalysts. (BDI-1)MgN(TMS)₂-mediated conjugation of CPT and SA resulted in CPT-SA conjugates (Scheme 2.2b) with 59.5% yield when the reaction was carried out at 40°C for 4 h (entry 4, Table 2.3). CPT in carboxylate form was also detected (peak x, Figure

2.3a-ii), indicating the CPT lactone ring was opened in the presence of (BDI-1)MgN(TMS)₂ and that it may function not only as a ROP catalyst but also as a strong base. The mechanism of ring opening remains elusive. When such a reaction was mediated by (BDI-1)ZnN(TMS)₂, a weaker base and a less reactive ROP catalyst compared to its Mg analogue, CPT-SA in 18.8% yield was obtained (entry 5, Table 2.3). Formation of small amount of CPT in its carboxylate form was also detected (peak x, Figure 2.3a-iii).

As shown in the polymerization study mentioned above (Table 2.1), the chelating BDI ligands have a significant impact on the activities of the BDI-metal complexes for LA polymerization. We tested (BDI-3)ZnN(TMS)₂, which was previously identified to be the best catalyst for CPT initiated LA polymerization, in this CPT/SA conjugation reaction. CPT-SA in 89.1% yield was obtained when the reaction of CPT and SA was carried out at 40°C for 4 h in the presence of (BDI-3)ZnN(TMS)₂ (entry 6, Table 2.3). The substantially increased yield of CPT-SA in this experiment indicated that (BDI-3)ZnN(TMS)₂ activated the tertiary C20-OH group of CPT very effectively to allow for facile nucleophilic ring opening of SA. Very interestingly, CPT-SA was the only product formed; no carboxylate form of CPT was detected (Figure 2.4a-iv). Excellently controlled ring opening of SA by CPT with no detectable CPT carboxylate was also observed with the use of (BDI-4)ZnN(TMS)₂ (Figure 2.3a-v), although the yield of the CPT-SA (71.7%, entry 7, Table 2.3) was not as high as that derived from the (BDI-3)ZnN(TMS)₂-mediated reaction (entry 6, Table 2.3).

The CPT-SA (peak z, Figure 2.3a-iv) was collected by preparative thin layer chromatography and analyzed by MS (Figure 2.3c) and ¹H NMR (Figure 2.3d-e). The high resolution MS analysis showed that the CPT-SA has a [M + H]⁺ *m/z* = 449.1355,

which was in excellent agreement with the expected $[M + H]^+$ $m/z = 449.1349$. To determine whether the SA ring was opened by the C17-OH (formed after the opening of the lactone ring of CPT) or by the C20-OH (Figure 2.3b), we compared the ^1H -NMR spectra of CPT-SA and CPT (Figure 2.3e). If the C17-OH mediated the ring opening of SA, the chemical shift of the C17-H of CPT-SA should change to some extent. However, as shown in Figure 3e, the chemical shift of the C17-H of CPT-SA was nearly identical to that of the authentic CPT (with a change of less than 0.03 ppm, Figure 2.3e), indicating that the lactone ring of CPT is well preserved in CPT-SA. In fact, the only major change of the chemical shifts among all the protons of CPT was the C18-H, which was shifted downfield from 1.97 ppm for CPT to 2.23 ppm for CPT-SA (Figure 2.3e). The only possible explanation is that the SA ring was opened by the C20-OH by CPT (Figure 2.3b). The high yield of CPT-SA obtained in this experiment indicated that $(\text{BDI-3})\text{ZnN}(\text{TMS})_2$ was capable of efficiently activating the C20-OH of CPT to facilitate the ring-opening reaction with SA. The CPT/SA ring-opening conjugation mediated by BDI-Zn catalyst appeared to be a versatile method for converting the C20-hydroxyl group of CPT to a carboxylic acid end group with a degradable ester linker, which can be further used for conjugation to various drug delivery vehicles through the conventional carboxylate-amine coupling chemistry.

Table 2.3 Ring Opening of Succinic Anhydride (SA) by CPT in the Presence of TEA, EDC/DMAP or (BDI)Mn(TMS)₂ (M = Mg or Zn).^a

entry	temp. (°C)	catalyst	solvent	time (h)	yield (%) ^c
1	r.t	/	THF	24	0
2	40	TEA	THF	12	10.6
3	40	EDC/DMAP ^b	pyridine	12	12.8
4	40	(BDI-1)MgN(TMS) ₂	THF	4	59.5
5	40	(BDI-1)ZnN(TMS) ₂	THF	4	18.8
6	40	(BDI-3)ZnN(TMS) ₂	THF	4	89.1
7	40	(BDI-4)ZnN(TMS) ₂	THF	4	71.7

^aAll reactions were performed at a SA/CPT/catalyst ratio of 1.1:1:1 ([SA]₀ = 0.01 M). Abbreviation: SA = succinic anhydride; CPT = camptothecin; TEA = triethylamine; temp. = temperature; EDC = N-(3-dimethylaminopropyl)-N'-ethylcarbodiimide; DMAP = 4-dimethylaminopyridine; ^b[EDC]/[DMAP]=4/1. ^cDetermined by the HPLC measurement of the CPT-succinic ester (CPT-SA) generated in the reaction solution.

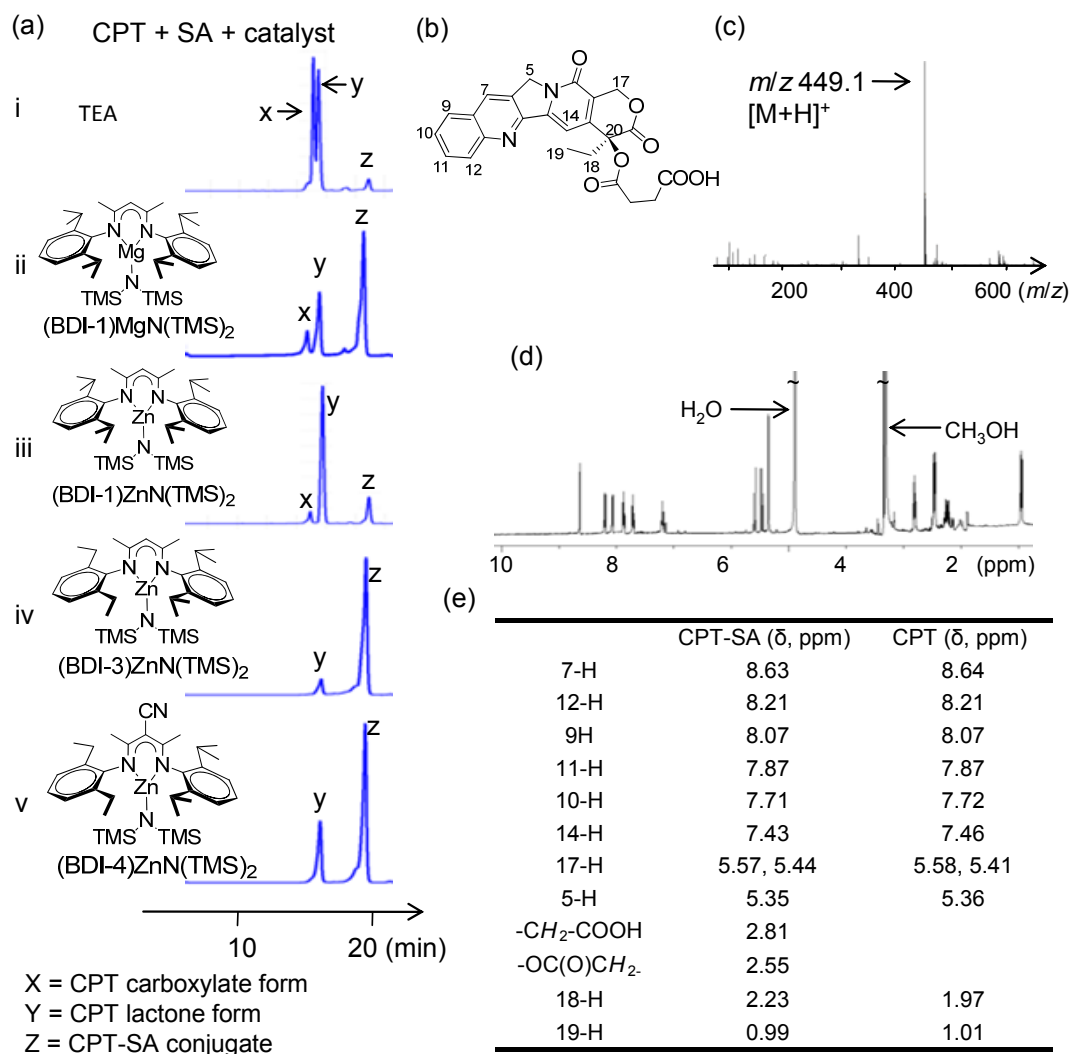


Figure 2.3 (a) HPLC analysis of the reaction of SA and CPT in the presence of (i) TEA, (ii) (BDI-1)MgNTMS₂, (iii) (BDI-1)ZnNTMS₂, (iv) (BDI-3)ZnNTMS₂ or (v) (BDI-4)ZnNTMS₂; (b) Structure and H-assignment of CPT-SA. (c) ESI-MS of CPT-SA (positive mode). $[M+H]^+$: m/z 449.1. High resolution ESI-MS for $[M+H]^+$ obtained: m/z 449.1355; calculated: m/z 449.1349; (d) ¹H NMR of CPT-SA (CD₃OD, 500 MHz). (e) The chemical shift values of CPT and CPT-SA derived from the corresponding ¹H-NMR spectra

3.1.3 *Controlled Formation of CPT-PLA Nanoconjugates and Their in vitro Evaluation*

CPT-PLA conjugated nanoparticles, termed nanoconjugates (NCs) in this study to differentiate them from the NPs prepared by co-precipitating drugs and polymers, were readily prepared through the nanoprecipitation of CPT-PLA conjugates (Figure 2.1a) after the metal and the BDI ligand were removed by solvent extraction. NCs less than 100 nm in size with narrow, monomodal particle distributions were readily obtained (Table 2.4 and Figure 2.4). The narrow size distributions of NCs were in sharp contrast to the multimodal particle distributions frequently observed in the NPs prepared by the co-precipitation of polymers and drugs ^[2-3]. It is not clear why NCs derived from the nanoprecipitation of PLA-CPT conjugates have such narrow size distributions (Figure 2.4a). As the multimodal particle distributions in conventional NPs were attributed in part to the self-aggregation of the non-encapsulated drugs ^[2], the unimolecular structure of polymer-drug conjugates with reduced heterogeneities (low polymer polydispersities, controlled site of conjugation on CPT and PLA, absence of free CPT) may contribute to the formation of NCs with low particle polydispersity.

Because both monomer conversion and drug incorporation were quantitative (Table 2.4), the drug loadings of CPT-PLA NCs can be pre-determined by adjusting LA/CPT feeding ratios. At a low M/I ratio of 10, the drug loading of CPT-PLA NC can be as high as 19.5 % (CPT-LA₁₀, Table 2.4). To our knowledge, this CPT-PLA NC has by far one of the highest loadings of CPT ever reported. Even at this high drug loading, sustained release of CPT from CPT-LA₁₀ NC was observed through the hydrolysis of the ester linker that connects the CPT and the PLA (Figure 2.5a). No burst release of CPT was observed in the CPT-LA₁₀ NC (Figure 2.5a). This observation was in sharp contrast to the burst release of PLA/CPT NP that was prepared by the co-precipitation of CPT and

PLA. In the latter system, the release of CPT depends entirely on diffusion of the drug from polymer matrices; as much as 97.1% of the encapsulated CPT was released from CPT/PLA NP when the NP was incubated in PBS for 24 h at 37°C (Figure 2.5a). The released CPT (in PBS) has an HPLC elution time identical to the authentic CPT (Figure 2.6a) and was confirmed to have the identical molecular structure as the authentic CPT after it was isolated and characterized by ¹H NMR (Figure 2.6b).

The *in vitro* toxicities of CPT-PLA NCs were determined by MTT assays in PC-3 cells (Figure 2.5b). The IC₅₀'s of CPT-LA₁₀, CPT-LA₂₅ and CPT-LA₅₀ NCs with similar sizes (50-100 nm) were 389, 730, and 908 nM, respectively. The MTT studies revealed that the toxicity of the CPT-PLA NC, which was directly related to the release kinetics of CPT, could be tuned by the CPT loading in the NCs (Figure 2.5b). In general, NCs with higher drug loadings released drug more rapidly ^[5] and therefore showed higher toxicities (Figure 2.5b). This observation was presumably due to the fact that the NCs derived from the nanoprecipitation of the higher loading (lower MW) CPT-PLA conjugates have more loosely packed structures, as compared to the NCs derived from the lower loading (higher MW) CPT-PLA conjugates. Therefore, the ester linkers between CPT and PLA in the NCs with higher drug loadings were more accessible to the aqueous phase and were subject to faster hydrolysis. PLA NPs without CPT were used as a negative control and were found to show negligible toxicity to the PC-3 cells. The cell viability was 0.956 ± 0.003 when the PC-3 cells were incubated with the PLA NPs at a concentration of 0.5 µg/mL for 72 h at 37°C.

Conventional polymeric NPs prepared via co-precipitation of polymers and drugs have several formulation challenges that remain to be addressed ^[11]. NPs typically exhibit a “burst” drug release in aqueous solution; as much as 80-90% of the

encapsulated drugs are rapidly released during the first few to tens of hours^[12]. The rapid dose dumping may cause severe systemic toxicities^[13]. In addition, drug loadings in conventional NPs can be very low, typically in a range of 1-5% in most NPs studied^[12, 14]. Drug loading of a delivery vehicle has been a critical measure of its utility in clinical settings^[15]. At lower drug loadings, a larger amount of delivery vehicles are needed. Due to the limited body weight and blood volume of animals, the administered volumes are usually fixed. For instance, the volume of a solution intravenously administered to mice with 20- to 30-g body weights should be controlled to below 100 μ L^[16]. Intravenous administration of NPs with 1 wt% drug loading in a 100 μ L solution at a dose of 50 mg/kg to a nude mouse with 20-g body weight requires the formulation of a concentrated, 1 g/mL NP solution, which is too viscous to formulate and inject intravenously. The third major challenge presented by NPs prepared via the encapsulation approach is the lack of a general strategy to achieve quantitative drug encapsulation. Depending on the amount of drug used, the hydrophobicity and hydrophilicity of the drug and the compatibility of the drug and polymer, the encapsulation efficiencies vary drastically over a range of 10 to 90%^[12, 17]. Non-encapsulated drugs may self-aggregate^[12] and can be very difficult to remove from the NPs. These formulation challenges significantly impact the process ability and clinical translation of NP delivery vehicles prepared by drug/polymer co-precipitations.

PLA/CPT NPs prepared by the co-precipitation method have been previously reported to give low drug loading (0.1-1.5%), low loading efficiency (2.8-38.3%) and poorly controlled release kinetics^[18]. Depending on the formulation method, 20-90% of the encapsulated CPT was released within 1 h after the NP was exposed to the PBS solution. The ring-opening polymerization method that we developed allows for the

incorporation of CPT to PLA with a tunable drug loading as high as 20 % and 100% loading efficiency (Table 2.4). The unique conjugation technique allows for formation of CPT-containing PLA NCs with superbly controlled formulation parameters, which makes PLA-CPT NCs potentially useful agents for sustained treatment of cancer *in vivo*.

Table 2.4 Preparation and Characterization of CPT-PLA NCs.^a

NC	[LA]/[CPT]	LD (%)	CV (%)	IE (%)	NC sizes \pm SD (nm)	PD \pm SD
CPT-LA ₁₀₀	100	2.36	>99	>99	80.6 \pm 0.8	0.083 \pm 0.016
CPT-LA ₅₀	50	4.61	>99	>99	70.7 \pm 0.7	0.096 \pm 0.007
CPT-LA ₂₅	25	8.82	>99	>99	76.6 \pm 0.9	0.092 \pm 0.006
CPT-LA ₁₀	10	19.48	>99	>99	72.5 \pm 0.7	0.056 \pm 0.015

^a Abbreviations: NC = nanoconjugates; LD = CPT loading in wt%; CV = conversion of LA; IE = incorporation efficiency; PD = polydispersity of NCs; STD = standard deviation.

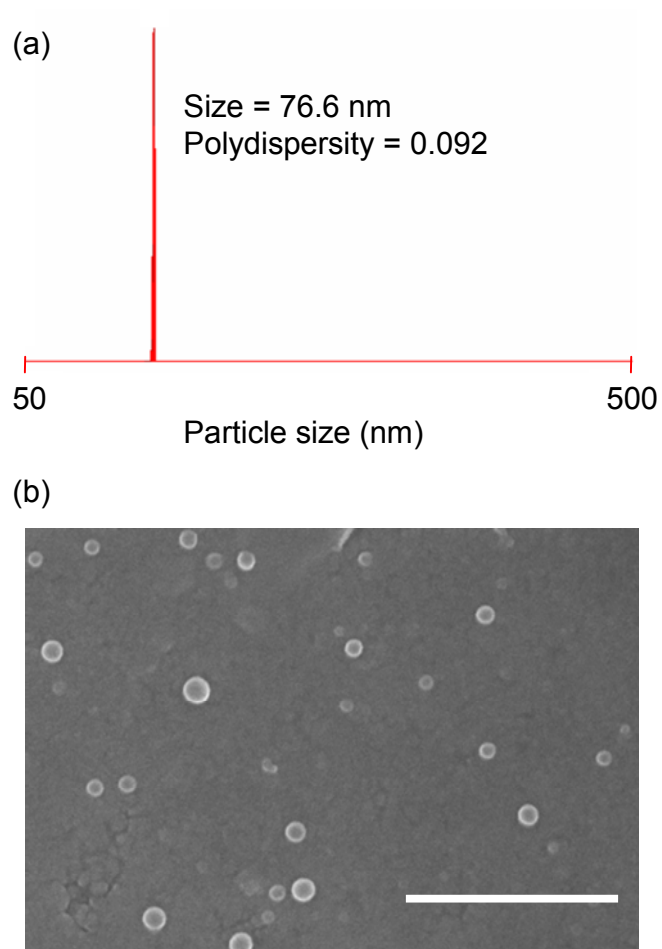


Figure 2.4 (a) Analysis of the particle size and size distribution of CPT-LA₂₅ NC by DLS. (b) Scanning electron microscope (SEM) image of CPT-LA₂₅ NC. Scale bar = 1.0 μ m

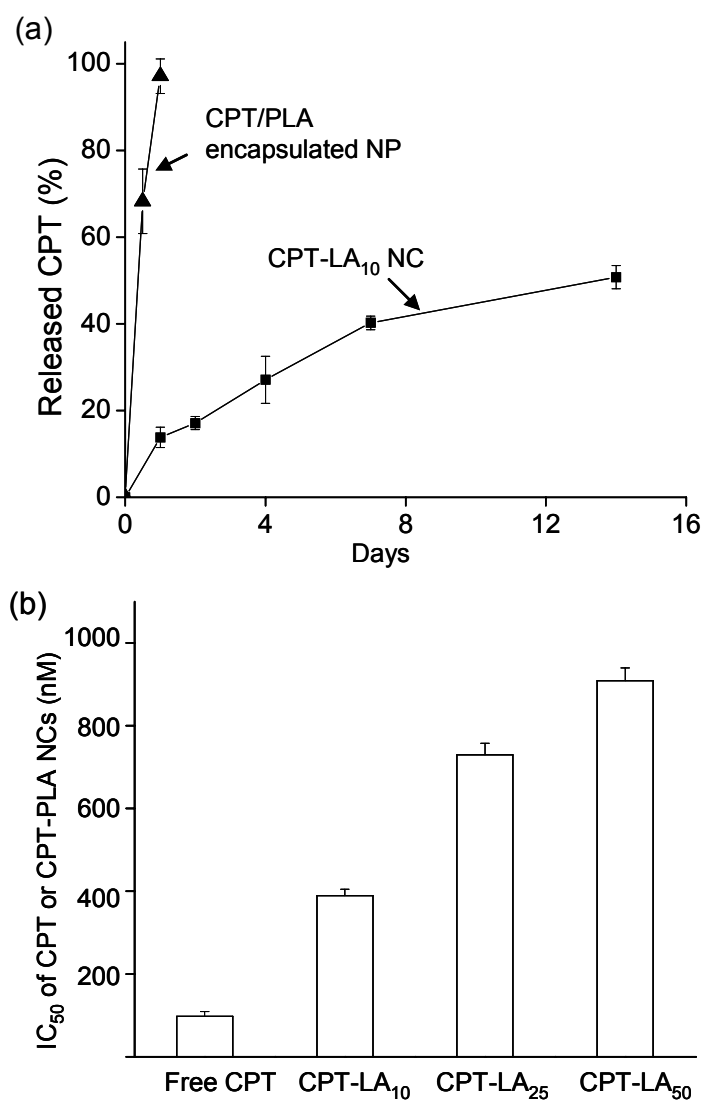


Figure 2.5 (a) Release of CPT from the CPT-LA₁₀ NC (■) and the CPT/PLA NP prepared by encapsulation (▲, CPT/PLA = 5/95 (wt/wt)); (b) MTT assay to evaluate the cytotoxicity of CPT-LA₁₀, CPT-LA₂₅, CPT-LA₅₀ NCs and CPT in PC-3 cell (37°C, 72 h).

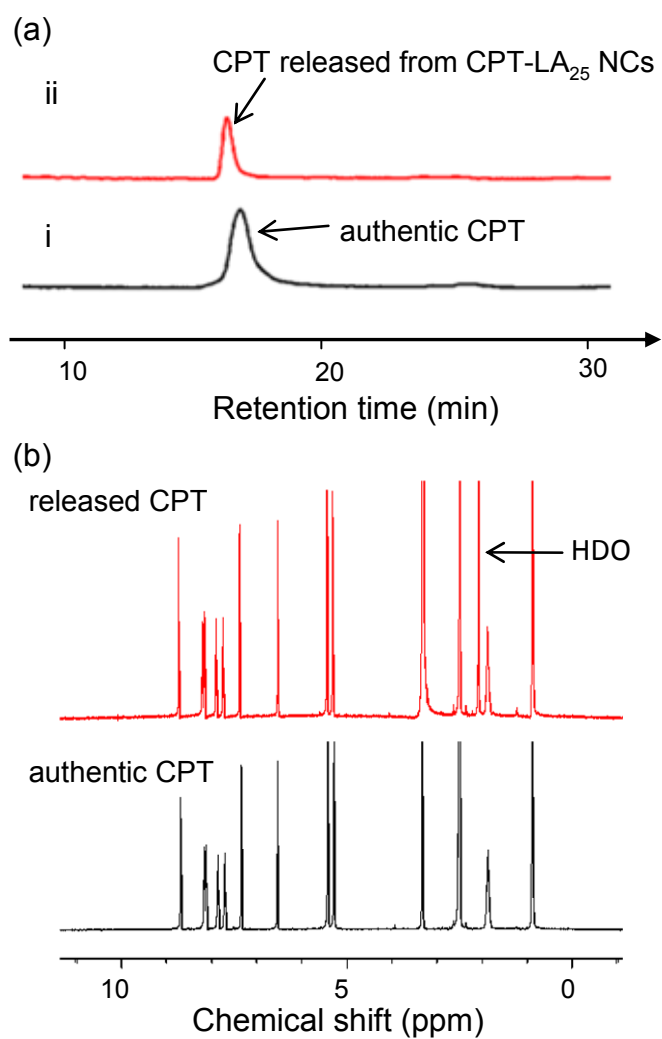


Figure 2.6. (a) Overlay of the HPLC spectrum of (a) authentic CPT and (b) CPT released from CPT-LA₂₅ NC (incubated in PBS for 2 days at 37°C). (b) ¹H NMR spectrum (DMSO-d₆) of the CPT released from CPT-LA₂₅ and collected on a preparative RP HPLC, and compared with the ¹H NMR spectrum of the authentic CPT.

4. Conclusions

Preparation of PLA-drug conjugates with controlled drug loading and release profiles have been previously reported using conventional coupling chemistry ^[19]. In this study we report a unique conjugation method that allows for CPT conjugation to PLA via CPT-initiated ROP of LA. This method allows for facile incorporation of CPT to PLA and forms PLA-CPT conjugates with low polydispersities, pre-determined drug loadings (as high as 20%) and 100% loading efficiencies. By controlling the metal and the chelating ligands of the catalysts, the initiation of LA polymerization can be specifically controlled at the C20-OH of CPT with negligible lactone ring opening in CPT. CPT conjugated to PLA should maintain its lactone form (the therapeutically active form). The BDI-metal chelating complexes do not have deleterious effects on CPT and can be easily removed by solvent extraction. Because both Zn and Mg ions are biocompatible (as key elements in our dietary mineral supplements), there should not be significant safety concerns regarding the use of these two metal catalysts for the ROP and formulation of NCs for potential clinical applications. Multi-gram scale of PLA-CPT conjugates can be readily prepared within hours using this one-pot polymerization approach. Because CPT molecules are covalently conjugated to PLA, the post-reaction formulation process (nanoprecipitation, purification, sterilization, lyophilization, shipping and handling, transporting, etc.) can be much more readily handled with a minimum change of sample property, in contrast to drug/polymer NPs prepared via encapsulation methods that struggle to prevent drug release during the formulation process. Given that the lack of a controlled formulation for nanoparticulate drug delivery vehicles presents bottlenecks to their clinical translation, this unique, ROP-mediated conjugation

methodology may contribute to the development of clinically applicable, CPT and CPT-analogue based nanomedicines.

5. References

- [1] C. D. Conover, R. B. Greenwald, A. Pendri, K. L. Shum, *Anti-Cancer Drug Design* 1999, *14*, 499.
- [2] J. Cheng, B. A. Teply, I. Sherifi, J. Sung, G. Luther, F. X. Gu, E. Levy-Nissenbaum, A. F. Radovic-Moreno, R. Langer, O. C. Farokhzad, *Biomaterials* 2007, *28*, 869.
- [3] O. C. Farokhzad, J. Cheng, B. A. Teply, I. Sherifi, S. Jon, P. W. Kantoff, J. P. Richie, R. Langer, *Proc. Natl. Acad. Sci. U. S. A.* 2006, *103*, 6315.
- [4] I. Martin-Kleiner, I. Svoboda-Beusan, J. Gabrilovac, *Immunopharma. Immunotox.* 2006, *28*, 411.
- [5] (a) R. Tong, J. Cheng, *Angew. Chem., Int. Ed.* 2008, *47*, 4830; (b) R. Tong, J. J. Cheng, *J. Am. Chem. Soc.* 2009, *131*, 4744.
- [6] B. M. Chamberlain, M. Cheng, D. R. Moore, T. M. Ovitt, E. B. Lobkovsky, G. W. Coates, *J. Am. Chem. Soc.* 2001, *123*, 3229.
- [7] (a) S. D. Allen, D. R. Moore, E. B. Lobkovsky, G. W. Coates, *J. Am. Chem. Soc.* 2002, *124*, 14284; (b) D. R. Moore, M. Cheng, E. B. Lobkovsky, G. W. Coates, *J. Am. Chem. Soc.* 2003, *125*, 11911; (c) G. W. Coates, D. R. Moore, *Angew. Chem., Int. Ed.* 2004, *43*, 6618; (d) L. R. Rieth, D. R. Moore, E. B. Lobkovsky, G. W. Coates, *J. Am. Chem. Soc.* 2002, *124*, 15239; (e) J. M. Rowley, E. B. Lobkovsky, G. W. Coates, *J. Am. Chem. Soc.* 2007, *129*, 4948; (f) D. R. Moore, M. Cheng, E. B. Lobkovsky, G. W. Coates, *Angew. Chem., Int. Ed.* 2002, *41*, 2599.
- [8] R. C. Jeske, A. M. DiCiccio, G. W. Coates, *J. Am. Chem. Soc.* 2007, *129*, 11330.
- [9] A. C. Spivey, B. I. Andrews, *Angew. Chem., Int. Ed.* 2001, *40*, 3131.
- [10] H. Lu, H. X. Lin, Y. Jiang, X. G. Zhou, B. L. Wu, J. M. Chen, *Lett. Drug Des. Discov.* 2006, *3*, 83.
- [11] (a) R. Tong, J. Cheng, *Polymer Reviews* 2007, *47*, 345; (b) R. Tong, D. A. Christian, L. Tang, H. Cabral, J. R. Baker, K. Kataoka, D. E. Discher, J. J. Cheng, *MRS Bulletin* 2009, *34*, 422; (c) B. A. Teply, R. Tong, S. Y. Jeong, G. Luther, I. Sherifi, C. H. Yim, A. Khadernhosseini, O. C. Farokhzad, R. S. Langer, J. Cheng, *Biomaterials* 2008, *29*, 1216;

- (d) J. J. Cheng, B. A. Teply, S. Y. Jeong, C. H. Yim, D. Ho, I. Sherifi, S. Jon, O. C. Farokhzad, A. Khademhosseini, R. S. Langer, *Pharm. Res.* 2006, *23*, 557.
- [12] T. Musumeci, C. A. Ventura, I. Giannone, B. Ruozzi, L. Montenegro, R. Pignatello, G. Puglisi, *Int. J. Pharm.* 2006, *325*, 172.
- [13] Y. Matsumura, T. Hamaguchi, T. Ura, K. Muro, Y. Yamada, Y. Shimada, K. Shirao, T. Okusaka, H. Ueno, M. Ikeda, N. Watanabe, *Br. J. Cancer* 2004, *91*, 1775.
- [14] (a) L. Mu, S. S. Feng, *J. Controlled Release* 2003, *86*, 33; (b) K. Avgoustakis, *Curr. Drug Delivery* 2004, *1*, 321.
- [15] (a) K. J. Hamblett, P. D. Senter, D. F. Chace, M. M. C. Sun, J. Lenox, C. G. Cerveney, K. M. Kissler, S. X. Bernhardt, A. K. Kopcha, R. F. Zabinski, D. L. Meyer, J. A. Francisco, *Clin. Cancer Res.* 2004, *10*, 7063; (b) Y. Barenholz, *J. Liposome Res.* 2003, *13*, 1.
- [16] J. Cheng, K. T. Khin, M. E. Davis, *Mol. Pharm.* 2004, *1*, 183.
- [17] D. Missirlis, R. Kawamura, N. Tirelli, J. A. Hubbell, *Eur. J. Pharm. Sci.* 2006, *29*, 120.
- [18] R. Kunii, H. Onishi, Y. Machida, *Eur. J. Pharm. Biopharm.* 2007, *67*, 9.
- [19] (a) C. C. Lee, E. R. Gillies, M. E. Fox, S. J. Guillaudeu, J. M. J. Frechet, E. E. Dy, F. C. Szoka, *Proc. Natl. Acad. Sci. U. S. A.* 2006, *103*, 16649; (b) H. S. Yoo, K. H. Lee, J. E. Oh, T. G. Park, *J. Controlled Release* 2000, *68*, 419; (c) M. Yokoyama, M. Miyauchi, N. Yamada, T. Okano, Y. Sakurai, K. Kataoka, S. Inoue, *J. Controlled Release* 1990, *11*, 269; (d) S. Sengupta, D. Eavarone, I. Capila, G. L. Zhao, N. Watson, T. Kiziltepe, R. Sasisekharan, *Nature* 2005, *436*, 568; (e) Z. P. Zhang, S. S. Feng, *Biomaterials* 2006, *27*, 262.

CHAPTER 3

NANOCONJUGATES: INCORPORATING PACLITAXEL

1. Introduction

Paclitaxel (Ptxl) is a potent chemotherapeutic agent. However, clinical application of Ptxl is often accompanied with severe, undesirable side-effects.^[1] To reduce the side-effects of Ptxl, various nanoparticulate delivery vehicles have been developed and investigated in the past 2-3 decades.^[2] Of various nanoparticles (NPs) being studied, polymeric nanoencapsulates (NEs), NPs prepared by co-precipitating hydrophobic polymers and drugs, hold particular promise because of their ease of formulation and potential control of drug release through the degradation of polymers.^[3] However, current NEs typically have low drug loadings, uncontrolled encapsulation efficiencies, and significant drug burst release effects when used in vivo.^[4] These formulation challenges significantly limit their potential clinical applications. In this chapter, I report the use of living polymerization to address these formulation challenges and facilitate controlled preparation of Ptxl-poly(lactide) (PLA) conjugated NPs with pre-defined drug loadings, nearly quantitative loading efficiencies and controlled release kinetics without burst release effects. In addition, the application of different lactone and carbonate monomers for nanoconjugates synthesis are also discussed due to the emerging problems in the synthesis process.

2. Materials and Methods

2.1 General

D,L-Lactide (LA) was purchased from TCI America (Portland, OR, USA). It was recrystallized three times in toluene and stored at -30°C in a glove box. The BDI ligands and the corresponding metal catalysts $(\text{BDI})\text{Mn}(\text{TMS})_2$ ($\text{M} = \text{Mg}, \text{Zn}$) were prepared by following the published procedure^[5] and stored at -30°C in a glove box. All anhydrous solvents were purified through alumina columns and kept anhydrous by molecular sieves. Paclitaxel (Ptxl) and docetaxel (Dtxl) were purchased from the LC Laboratories (Woburn, MA, USA), and used as received. All other chemicals were purchased from Sigma-Aldrich (St Louis, MO, USA) and used as received unless otherwise noted. The molecular weights of PLA or drug-PLA were determined on a gel permeation chromatography (GPC) equipped with an isocratic pump (Model 1100, Agilent Technology, Santa Clara, CA, USA), a DAWN HELEOS 18-angle laser light scattering detector (MALLS) and an Optilab rEX refractive index detector (Wyatt Technology, Santa Barbara, CA, USA). The wavelength of HELEOS detector was set at 658 nm. Size exclusion columns used for the separation of PLA or drug-PLA conjugates were series connected on the GPC (Phenogel columns 100 Å, 500 Å, 10^3 Å and 10^4 Å, 5 µm, 300×7.8 mm, Phenomenex, Torrance, CA, USA). THF (HPLC grade) was used as mobile phase for GPC. The low resolution electrospray ionization mass spectrometry (LR-ESI-MS) experiments were conducted on a Waters Quattro II mass spectrometer. HPLC analysis was performed on a System Gold system (Beckman Coulter, Fullerton, CA, USA) equipped with a 126P solvent module, a System Gold 128 UV detector and an analytical pentafluorophenyl column (Curosil-PFP, 250×4.6 mm, 5 µm, Phenomenex, Torrance, CA, USA). The UV wavelengths for Ptxl, Dtxl and CPT were set at 227, 237 and 350 nm, respectively. NMR analyses were conducted on a Varian U500, VXR500 or UI500NB (500 MHz). The sizes and polydispersities of NCs were determined on a

ZetaPALS dynamic light-scattering (DLS) detector (15 mW laser, incident beam = 676 nm, Brookhaven Instruments, Holtsville, NY, USA). The SEM analysis of nanoparticles is performed on a Hitachi-S4700 high resolution scanning electron microscopy. PC-3 cells (ATCC, Manassas, VA, USA) used for MTT assays were cultured in Ham's F12K medium containing 10% FBS (Fetal Bovine Serum), 1000 units/mL aqueous Penicillin G and 100 μ g/mL streptomycin.

2.2 Synthesis and characterization of Ptxl-PLA nanoconjugates

2.2.1 General procedure for the preparation of Ptxl-LA₁₀₀ and Ptxl-LA₁₀₀ NCs

In a glove box, Ptxl (8.5 mg, 0.01 mmol) was dissolved in anhydrous THF (2 mL). (BDI)MgN(TMS)₂^[5] (6.2 mg, 0.01 mmol) was added and allowed to react with Ptxl for 15-20 min. LA (144.0 mg, 1.0 mmol) in THF (1 mL) was added dropwise to the mixture of Ptxl and (BDI)MgN(TMS)₂ under vigorous stirring. The polymerization was monitored using FT-IR by following the lactone band at 1772 cm⁻¹ or using ¹H-NMR by checking the methine (-CH-) peak of LA around 5.2-5.0 ppm. After the polymerization was complete, an aliquot of the polymerization solution was analyzed using HPLC to quantify the unreacted Ptxl in order to determine the incorporation efficiency of Ptxl in Ptxl-PLA. One drop of water was added to the polymerization solution to hydrolyze the Mg-Ptxl oxide. The resulting Ptxl-LA₁₀₀ was precipitated with ethyl ether (10 mL), washed with ether and toluene to remove BDI ligand, dried under vacuum and characterized by GPC. Complete removal of BDI from Ptxl-PLA was verified by TLC.

The Ptxl-LA₁₀₀ conjugate in DMF (100 μ L, 10 mg/mL) (or in other water-miscible solvent such as THF, acetone, etc.) was dropwise added to nanopure water (2

mL). The resulting NCs were collected by ultrafiltration (15 min, $3000 \times g$, Ultracel membrane with 10,000 NMWL, Millipore, Billerica, MA, USA) and characterized by DLS or SEM.

2.2.2 Formation and characterization of Ptxl-LA₂₅/PLGA-mPEG core-shell nanostructure

The Ptxl-LA₂₅ conjugate (5 mg/mL in DMF, 100 μ L) was dropwise added to 2 mL nanopure water to give the Ptxl-LA₂₅ NCs. PLGA-mPEG^[3b] (MW of the PLGA block = 13kDa, MW of the mPEG block = 5 kDa, 5 mg/mL in DMF, 100 μ L) or mPEG (MW of PEG = 5 kDa, 5 mg/mL in DMF, 100 μ L) was dropwise added to Ptxl-LA₂₅ NC.

The particle sizes were analyzed by DLS. PBS (245 μ L, 10 \times) was added slowly to the mixture. The size of Ptxl-LA₂₅ NC coated with PLGA-mPEG was monitored for 30 mins by DLS or by SEM. The resulting NCs were purified by ultrafiltration; their *in vitro* toxicities were then evaluated using MTT assay in PC-3 cells (24 hr incubation at 37°C). To determine the release kinetics of Ptxl-PLA, a PBS solution of NCs was equally divided into several portions and then incubated at 37°C. At scheduled time, the release study was terminated. DMF solution was added to dissolve all precipitation. All the samples were then dried, re-dissolved in DCM and reacted with Bu₄NBH₄ for 1.5 hours. A drop of acetic acid was added into the solution. The solution was stirred for 20 min before the solvent was evaporated. The residual solid was reconstituted in acetonitrile for RP HPLC analysis (Curosil, 250 \times 4.6mm, 5 μ ; Phenomenex, Torrance, CA, USA). The release kinetics of Ptxl from Ptxl-LA₂₅ was determined by quantifying PDB.

2.2.3 Reductive degradation of Ptxl and Ptxl-PLA using Bu_4NBH_4

The reductive degradation of Ptxl at its 13-position was achieved by following the literature reported procedure.^[6] Ptxl (5 mg, 5.8 mmol) in anhydrous dichloromethane (1 mL) was allowed to react with Bu_4NBH_4 (2.5 mg, 10 mmol) for one and a half hours in a glove box. Acetic acid ($\approx 100 \mu\text{L}$) was added to the reaction mixture to terminate the reaction. The reaction solution was stirred for 20 mins followed by complete removal of the solvent. The residual solid was re-dissolved in acetonitrile. An aliquot of such solution was analyzed on a HPLC equipped with a Curosil RP column ($250 \times 4.6\text{mm}$, 5μ ; Phenomenex, Torrance, CA, USA). The desired fractions were collected and analyzed by for LR-ESI-MS. The Ptxl-PLA conjugate was reductively degraded and analyzed similarly.

2.2.4 Synthesis of Ptxl-SA

In the glove box, 8.5 mg Ptxl was pre-weighed in a clean vial. 6.5 mg (BDI-1) $ZnN(TMS)_2$ was dissolved in $200 \mu\text{L}$ THF and mixed with Ptxl. $300 \mu\text{L}$ THF was added and the resulted solution was kept stirring over 15 min until all of Ptxl powder was well dissolved in solutions. 1.1 mg SA in $600 \mu\text{L}$ THF was further added into the solution. ($[SA]=0.01\text{M}$) The reaction vial was tightly sealed and immediately moved out from box and heated at 40°C . The reaction was kept for 4 hours and quenched by 1 ml ice-cold methanol. The resulted solution was immediately injected into HPLC for analysis. HPLC condition: analytical Luna C18(2) column ($250 \times 4.6 \text{ mm}$, 5μ , Phenomenex, CA, USA) ; flow rate: 1ml/min ; mobile phase: acetonitrile / water with 0.1% TFA from 50/50 to 80/20 in 40 min. All spectrums were recorded and analyzed at 227 nm. Ptxl-SA and Dtxl-SA mixture were analyzed by low resolution electrospray ionization mass spectrometry

(LR-ESI-MS) experiments, which were conducted on a Waters Quattro II mass spectrometer.

Pure Ptxl-2'-SA and Dtxl-2'-SA for NMR analysis were separated by preparative thin layer chromatography (prep TLC silica gel matrix with UV254, 1500 μm thickness, Sigma Aldrich), developed by Silica gels containing Ptxl-SA part were scratched out from the glass plate. Ptxl-2'-SA was extracted from gel by methanol solution (30 ml, 2X). The resulted methanol solution was evaporated and dried by vacuum line for NMR analysis.

^1H -NMR (500 MHz, CDCl_3); δ = 8.13 (d, J = 7.28 Hz, 2H), 7.77 (d, J = 7.36 Hz, 2H), 7.61-7.36 (m, 15H), 7.26-7.24 (m, 6H), 7.03 (d, J = 9.16 Hz, 1H), 6.25 (s, 1H), 6.22 (d, J = 8.9 Hz, 1H), 5.97, 5.95 (dd, J = 2.84 Hz, 2.76 Hz, 1H), 5.67 (d, J = 7.08 Hz, 1H), 5.56 (d, 1H), 5.47 (d, J = 2.96 Hz, 1H), 4.96 (d, J = 9.36 Hz, 1H), 4.85-4.79 (m, 3H), 4.65 (d, J = 11.9 Hz, 1H), 4.41 (s, 1H), 4.31-4.27 (m, 2H), 4.19 (d, J = 8.44 Hz, 1H), 3.99 (t, J = 9.20 Hz, 1H), 3.81-3.73 (m, 3H), 3.64 (t, J = 9.20 Hz, 1H), 3.31 (s, 3H), 2.72-2.51 (m, 6H), 2.42 (s, 3H), 2.40-2.30 (m, 1H), 2.21 (s, 3H), 1.89 (s, 3H), 1.66 (s, 6H), 1.64 (s, 3H), 1.23 (s, 3H), 1.20 (s, 3H), 1.11 (s, 3H)

^{13}C -NMR (125 MHz, CDCl_3); δ = 203.8, 171.5, 171.2, 171.1, 169.8, 167.9, 167.3, 167.0, 142.6, 138.4, 137.2, 136.9, 133.7, 133.6, 132.8, 132.0, 130.2, 129.2, 129.1, 129.0, 128.7, 128.5, 128.3, 127.7, 127.6, 127.2, 126.6, 126.0, 101.4, 97.5, 84.4, 82.1, 81.0, 79.0, 76.4, 75.6, 75.1, 74.3, 73.1, 72.1, 71.9, 58.5, 52.8, 49.1, 45.6, 43.2, 35.6, 33.9, 29.7, 29.0, 28.9, 26.8, 25.6, 24.9, 22.7, 22.1, 20.8, 14.8, 9.6

2.3 *Synthesis of nanoconjugates composed with various monomers*

2.3.1 General procedure for synthesis of Ptxl-BL_n polymer mediated by (BDI-4)ZnN(TMS)₂

In the glove box, 8.6mg Ptxl (0.010 mmol, 1 equiv) was weighed in a small vial. 6.9 mg (BDI-4)ZnN(TMS)₂ (1.02 equiv) was dissolved in 300 μ L THF and added to Ptxl, immediately forming cloudy solution. The mixture stirred over 20 min until solution became clear. 164 μ L BBL (172 mg, 2.0 mmol, 200 equiv) in 300 μ L toluene was added into the mixture. The vial was tightly sealed, moved out from the glove box, and heated at 50 degree for 10 hours. The reaction was monitored by FTIR, by observing 1829 cm⁻¹ peak (lactone bond in BBL) shifting to 1740 cm⁻¹ (ester bond in poly(3-hydroxybutyrate) (PHB)). The reaction solution was quenched by 2 ml ice-cold methanol. The conversion of BL was calculated by comparing the relative magnitude peaks corresponding to hydrogen of BBL (δ : 3.74 ppm) and PHB (δ : 5.26-5.20ppm). The resulted solution was dried by vacuum line, reconstituted in HPLC grade of THF at 20 mg/ml for GPC analysis.

¹H-NMR (500 MHz, CDCl₃) δ : 5.27-5.20 (m, 1H, -CH-CH₃-), 2.63-2.48, 2.47-2.42 (m, 2H, -CH(CH₃)-CH₂-) 1.25 (m, 3H, -CH₃)

¹³C-NMR (125 MHz, CDCl₃); δ : 169.1(-C(=O)O-), 67.6(-CH-), 40.7(-CH₂-), 19.7(-CH₃)

2.3.2 Kinetic study of Ptxl-BL₂₀₀ polymer mediated by (BDI-4)ZnN(TMS)₂

In the glove box, 8.6mg Ptxl (0.010 mmol, 1 equiv) was weighed in a small vial. 6.9 mg (BDI-4)ZnN(TMS)₂ (1.02 equiv) was dissolved in 300 μ L THF and added to Ptxl, immediately forming cloudy solution. The mixture stirred over 20 min until solution became clear. The solution was further stirred for 10 min and dried in the glove box. 164 μ L BBL (172 mg, 2.0 mmol, 200 equiv) in 1000 μ L toluene-*d*8 was added into the

mixture. The solution was immediately divided into 5 equal volume fractions in 5 vials. All vials were tightly sealed, moved out from the glove box, and heated at 50 degree. At certain time, 100 μ L reaction solution was immediately injected into NMR tube with 600 μ L toluene-*d*8 under nitrogen atmosphere. The tube was immediately analyzed by NMR. The conversion of BL was calculated by comparing the relative magnitude peaks corresponding to hydrogen of BBL (δ : 3.74 ppm) and PHB (δ : 5.26-5.20ppm). The results were plotted over the time.

2.3.3 General procedure for synthesis of Ptxl-CL_n polymer mediated by (BDI-1)ZnN(TMS)₂

In the glove box, 8.6mg Ptxl (0.010 mmol, 1 equiv) was weighed in a small vial. 6.6 mg (BDI-1)ZnN(TMS)₂ (1.02 equiv) was dissolved in 300 μ L THF and added to Ptxl. The mixture stirred over 20 min and 221 μ L ϵ -caprolactone (CL, 228mg, 2.0 mmol, 200 equiv) was added into the mixture. The polymerization was monitored by FTIR, by observing 1736 cm^{-1} peak (lactone bond in CL) shifting to 1726 cm^{-1} (ester bond in poly (ϵ -caprolactone) (PCL)). The reaction solution was quenched by 5 ml ice-cold methanol. The conversion of CL was calculated by comparing the relative magnitude peaks corresponding to the hydrogens of -C(=O)OCH₂- signals of PCL (δ : 4.04 ppm) and CL (δ : 4.19 ppm). The resulted solution was dried by vacuum line, reconstituted in HPLC grade of THF at 20 mg/ml for GPC analysis.

¹H-NMR (500 MHz, CDCl₃) δ : 4.04(t, 2H, -C(=O)OCH₂-), 2.29 (t, 2H, -CH₂C(=O)O-), 1.64 (m, 4H, CH₂CH₂CH₂), 1.38 ppm (m, 2H, CH₂CH₂CH₂).

¹³C-NMR (125 MHz, CDCl₃); δ : 173.7, 64.3, 34.3, 28.5, 25.7, 24.8 ppm

2.3.4 General procedure for synthesis of Ptxl-VL_n polymer mediated by (BDI-1)ZnN(TMS)₂

In the glove box, 8.6mg Ptxl (0.010 mmol, 1 equiv) was weighed in a small vial. 6.6 mg (BDI-1)ZnN(TMS)₂ (1.02 equiv) was dissolved in 300 μ L THF and added to Ptxl. The mixture stirred over 20 min and 92.6 μ L δ -valerolactone (VL, 100 mg, 1.0 mmol, 100 equiv) in 100 μ L THF was added into the mixture. The polymerization was monitored by FTIR, by observing 1739 cm^{-1} peak (lactone bond in VL) shifting to 1728 cm^{-1} (ester bond in poly (δ -valerolactone) (PVL)). The reaction solution was quenched by 5 ml ice-cold methanol. The conversion of CL was calculated by comparing the relative magnitude peaks corresponding to the hydrogens of -C(=O)OCH₂- signals of PVL (δ : 4.08 ppm) and VL (δ : 4.30 ppm). The resulted solution was dried by vacuum line, reconstituted in HPLC grade of THF at 20 mg/ml for GPC analysis.

¹H-NMR (500 MHz, CDCl₃) δ : 4.08(t, 2H, -C(=O)OCH₂-), 2.34 (t, 2H, -CH₂C(=O)O-), 1.70 ppm (m, 4H, CH₂CH₂).

¹³C-NMR (125 MHz, CDCl₃); δ : 173.5, 64.1, 33.9, 28.3, 21.6 ppm.

2.3.5 General procedure for synthesis of Ptxl-TMC_n polymer mediated by (BDI-1)ZnN(TMS)₂

In the glove box, 8.6mg Ptxl (0.010 mmol, 1 equiv) was weighed in a small vial. 6.6 mg (BDI-1)ZnN(TMS)₂ (1.02 equiv) was dissolved in 300 μ L THF and added to Ptxl. The mixture stirred over 20 min and 102 mg TMC (1.0 mmol, 100 equiv) in 300 μ L toluene was added into the mixture. The vial was tightly sealed, moved out from the

glove box, and heated at 50 degree for 5 hours. The reaction solution was quenched by 5 ml ice-cold methanol. The conversion of TMC was calculated by comparing the relative magnitude peaks corresponding to the hydrogens of $-CH_2OC(=O)-$ of PTMC (δ : 4.23 ppm) and TMC (δ : 4.42 ppm). The resulted solution was dried by vacuum line, reconstituted in HPLC grade of THF at 20 mg/ml for GPC analysis.

3. Results and Discussion

3.1 Synthesis of Ptxl-PLA nanoconjugates

3.1.1 $(BDI)MN(TMS)_2/Ptxl$ ($M=Zn, Mg$)-Mediated Polymerization of Lactide

Since Ptxl has multiple hydroxyl groups, we postulated that Ptxl may be incorporated to polyesters through metal-Ptxl alkoxide mediated polymerization of LA (Figure 3.1). Drug loadings can thus be precisely controlled by adjusting LA to Ptxl ratios. The incorporation efficiency of Ptxl to the resulting PLA should be 100% as the formation of metal-OR is usually quantitative. After polymerization, Ptxl molecules are covalently linked to the terminals of PLA through a hydrolysable ester linker and are subject to sustained release upon hydrolysis. Followed by nanoprecipitation (Figure 3.1), polymeric NPs containing covalently linked Ptxl should be readily obtained.

We utilized $(BDI)MgN(TMS)_2$, an active catalyst developed by Coates and coworkers for the polymerization of LA.^[5] After Ptxl was mixed with 1 eq. $(BDI)MgN(TMS)_2$, the in situ formed $(BDI)Mg$ -Ptxl complex (structure uncharacterized; tentatively illustrated as a monomeric Mg -Ptxl alkoxide) initiated and completed the polymerization of LA within hours at room temperature with nearly quantitative incorporation of Ptxl to the resulting PLA (entries 1-4, Table 3.1). The incorporated Ptxl

was released to its original form and other degradation species after the Ptxl-PLA was treated with 1 M NaOH (Figure 3.2), which demonstrated that Ptxl was linked to PLA through a ester bond. Nanoprecipitation of the Ptxl-PLA conjugates resulted in sub-100 nm NPs (Table 3.1). To differentiate from NEs, these NPs derived from nanoprecipitation of Ptxl-PLA conjugates are called nanoconjugates (NCs) with PLA being denoted as LA_n where n is the LA/Ptxl ratio.

Ptxl has three hydroxyl groups at its C-2', C-1 and C-7 positions, respectively (Figure 3.1). All these three hydroxyl groups can potentially initiate LA polymerizations, resulting in Ptxl-PLA conjugates with 1 to 3 PLA chains attached to Ptxl. To reduce the heterogeneity of Ptxl-PLA, we explored if the initiation can be controlled at a specific hydroxyl group of Ptxl to make a Ptxl-PLA conjugate containing a single PLA chain (as illustrated in Figure 3.1).

The three hydroxyl groups of Ptxl differ in steric hindrance in the order of 2'-OH < 7-OH < 1-OH. The tertiary 1-OH is least accessible and typically inactive.^[7] The 7-OH, however, could potentially compete with 2'-OH,^[8] the most accessible and active hydroxyl group of Ptxl, for coordination with metal catalyst. We postulated that a metal catalyst with a bulky chelating ligand may differentiate the 2'-OH from the 7-OH, and thus preferentially or even specifically form Ptxl-metal complex through the 2'-OH for site-specific LA polymerization.

Magri et al^[6] reported that tetrabutylammonium borohydride (Bu₄NBH₄) could selectively and quantitatively reduce the 13-ester bond of Ptxl into Baccatin III (BAC) and (1*S*,2*R*)-*N*-1-(1-phenyl-2,3-dihydroxypropyl)benzamide (PDB) (Figure 3.3). We attempted to use this reduction reaction to disassemble Ptxl-LA₅ derived from metal/Ptxl mediated polymerization and then to analyze whether PLA is attached to these fragments

(Figure 3.3 and 3.4). It was anticipated that $\text{Mg}(\text{N}(\text{TMS})_2)_2$, a catalyst without chelating ligand, would initiate polymerization non-preferentially at both the 2'-OH and the 7-OH. As expected, both PDB-PLA and BAC-PLA were obtained after the resulting Ptxl-LA₅ was treated with Bu_4NBH_4 (iv, Figure 3.3b). When $(\text{BDI})\text{MgN}(\text{TMS})_2$ rather than $\text{Mg}(\text{N}(\text{TMS})_2)_2$ was used, the amount of BAC-PLA derived was significantly reduced (v, 3.3b), indicating polymerization of LA was preferentially initiated at the 2'-OH of Ptxl by Mg catalysts with a proper chelating ligand.

Although $(\text{BDI})\text{MgN}(\text{TMS})_2$ gave significantly improved site-specific control in the metal/Ptxl initiated polymerization, the resulting Ptxl-PLAs typically have fairly broad molecular weight distribution (MWD) (e.g., Ptxl-LA₂₀₀ $M_w/M_n = 1.47$). This observation is attributed to fast propagation relative to initiation for the polymerization initiated by Mg catalysts.^[5] To reduce the propagation rate and transesterification side reactions, we tested $(\text{BDI})\text{ZnN}(\text{TMS})_2$, a zinc analogue of $(\text{BDI})\text{MgN}(\text{TMS})_2$ that gives more controlled LA polymerization.^[5] As expected, Ptxl-PLAs with projected MWs and narrow MWDs were readily prepared *via* LA polymerization mediated by the in situ formed $(\text{BDI})\text{Zn-Ptxl}$. For instance, Ptxl-LA₂₀₀ with a M_n of 28,100 Da (expected 29,700 Da) and a MWD of 1.02 were obtained in the $(\text{BDI})\text{ZnN-Ptxl}$ mediated LA polymerization (200 eq.). HPLC analysis of the Ptxl-LA₅ prepared with $(\text{BDI})\text{ZnN}(\text{TMS})_2$ and then treated with Bu_4NBH_4 showed that initiation and polymerization were exclusively at the 2'-OH of Ptxl (vi, Figure 3.3b). Various studies suggests that the polymerization process does not lead to deleterious effect on Ptxl (Figure 3.5)

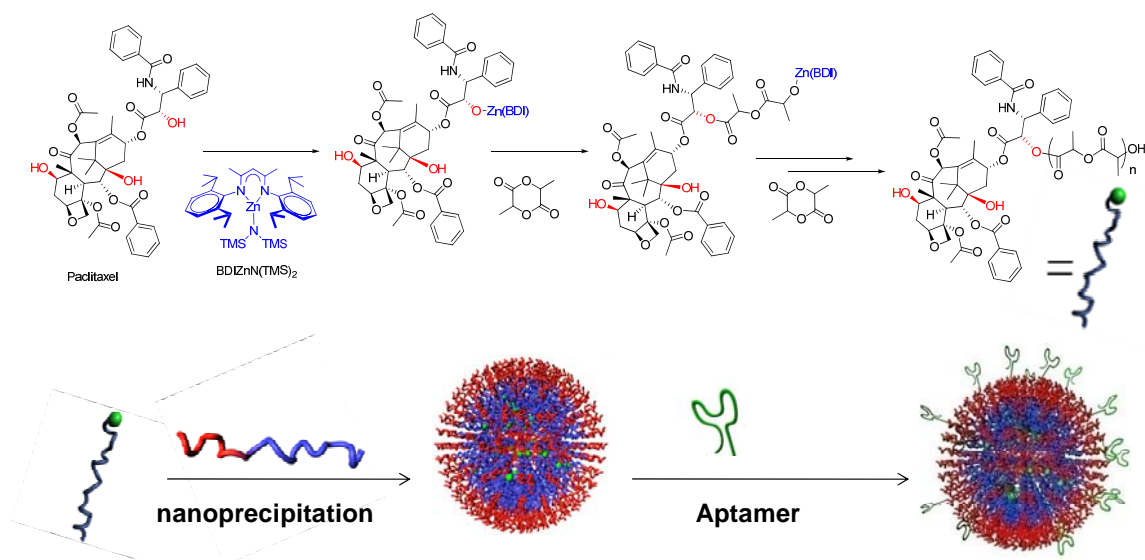


Figure 3.1 Preparation of PEGylated Ptxl-PLA NCs *via* Ptxl-initiated LA polymerization in the presence of (BDI)ZnN(TMS)₂, followed by nanoprecipitation and non-covalent surface modification with PLGA-mPEG (or for further modification with aptamer).

Table 3.1 Formation of drug-PLA nanoconjugates with high loadings, high incorporation efficiencies, small particle sizes and low particle distributions^[a]

Entry	NC ^[b]	M/I	Loading (wt%)	LA Conv. (%) ^[c]	Incorp. Eff. (%) ^[d]	NC Size ±SD (nm)	PDI
1	Ptxl-LA ₁₀₀	100	5.6	>99	>99	95.1 ± 2.7	0.04 ± 0.01
2	Ptxl-LA ₅₀	50	10.6	>99	>99	80.6 ± 0.2	0.05 ± 0.01
3	Ptxl-LA ₂₅	25	19.2	>99	97	55.6 ± 0.5	0.04 ± 0.01
4	Ptxl-LA ₁₅	15	28.3	>99	95	85.5 ± 1.4	0.09 ± 0.03
5	Dtxl-LA ₁₀	10	35.9	>99	95	77.9 ± 1.5	0.06 ± 0.02
6	CPT-LA ₁₀	10	19.5	>99	96	72.5 ± 0.7	0.06 ± 0.02

[a] Abbreviations: M/I = monomer/initiator ratio, NC = nanoconjugates, LA Conv. = lactide conversion, Incorp. Eff. = incorporation efficiency, SD = standard deviation, PDI = polydispersity derived from particles sizing using dynamic light scattering technique, Ptxl = paclitaxel, Dtxl = docetaxel, CPT = camptothecin. [b] NCs are named as drug-LA_{M/I ratio}. [c] Determined by

(Table 3.1 continued) analyzing the unreacted lactide using FT-IR (1771 cm^{-1}) or using $^1\text{H-NMR}$;
[d] Based on Reverse phase-HPLC analysis of unincorporated drug.

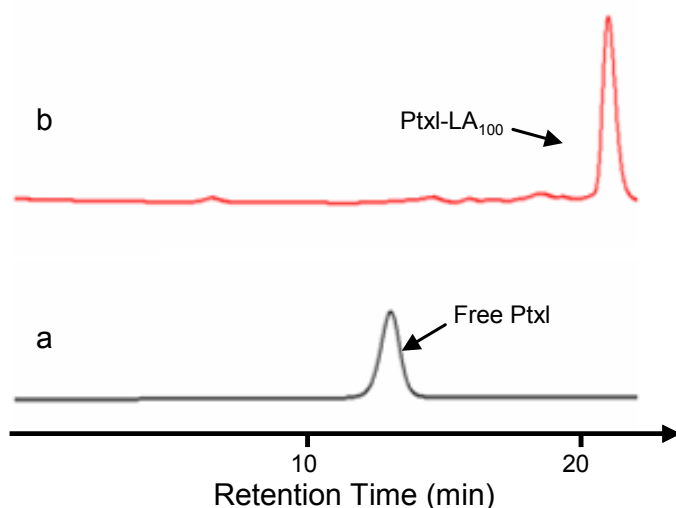


Figure 3.2 HPLC spectrum of (a) free Ptxl and (b) the solution of Ptxl / (BDI)ZnN(TMS)₂-mediated LA polymerization at a LA/Ptxl ratio of 100. An aliquot (30-50 μL) of polymerization solution was injected into HPLC equipped with analytical RP-HPLC column (Curosil-PFP, $4.6 \times 250\text{ mm}$, 5μ , Phenomenex, Torrance, CA). Mobile phase was acetonitrile/water with 0.1% TFA (50/50 (v/v)); the flow rate was set at 1.0 mL/min.

Table 3.2 Ptxl-LA_n polymerization mediated by (BDI-1)ZnN(TMS)₂

Entry	[M]/[I]	Conv. (%) ^b	M_{cal} (kg/mol)	M_n (kg/mol) ^c	PDI (M_w/M_n) ^c
1	50	>99%	8.1	7.8	1.04
2	75	>99%	11.7	9.6	1.09
3	100	>99%	15.3	12.7	1.03
4	200	>99%	29.7	28.1	1.02
5	300	>99%	44.1	35.2	1.03

^a All reactions were performed in anhydrous THF with [LA]= 0.69 M at room temperature for 12 hours. Abbreviation: LA: lactide; Ptxl: paclitaxel; Conv. %:

(Table 3.2 continued) conversion of LA %; M_{cal} : calculated molecular weight; M_n : number average molecular weight; PDI: polydispersity index. ^b The conversion of LA was measured by FT-IR, monitoring the disappearance of LA peak at 1772 cm^{-1} . ^c Determined by gel permeation chromatography (GPC).

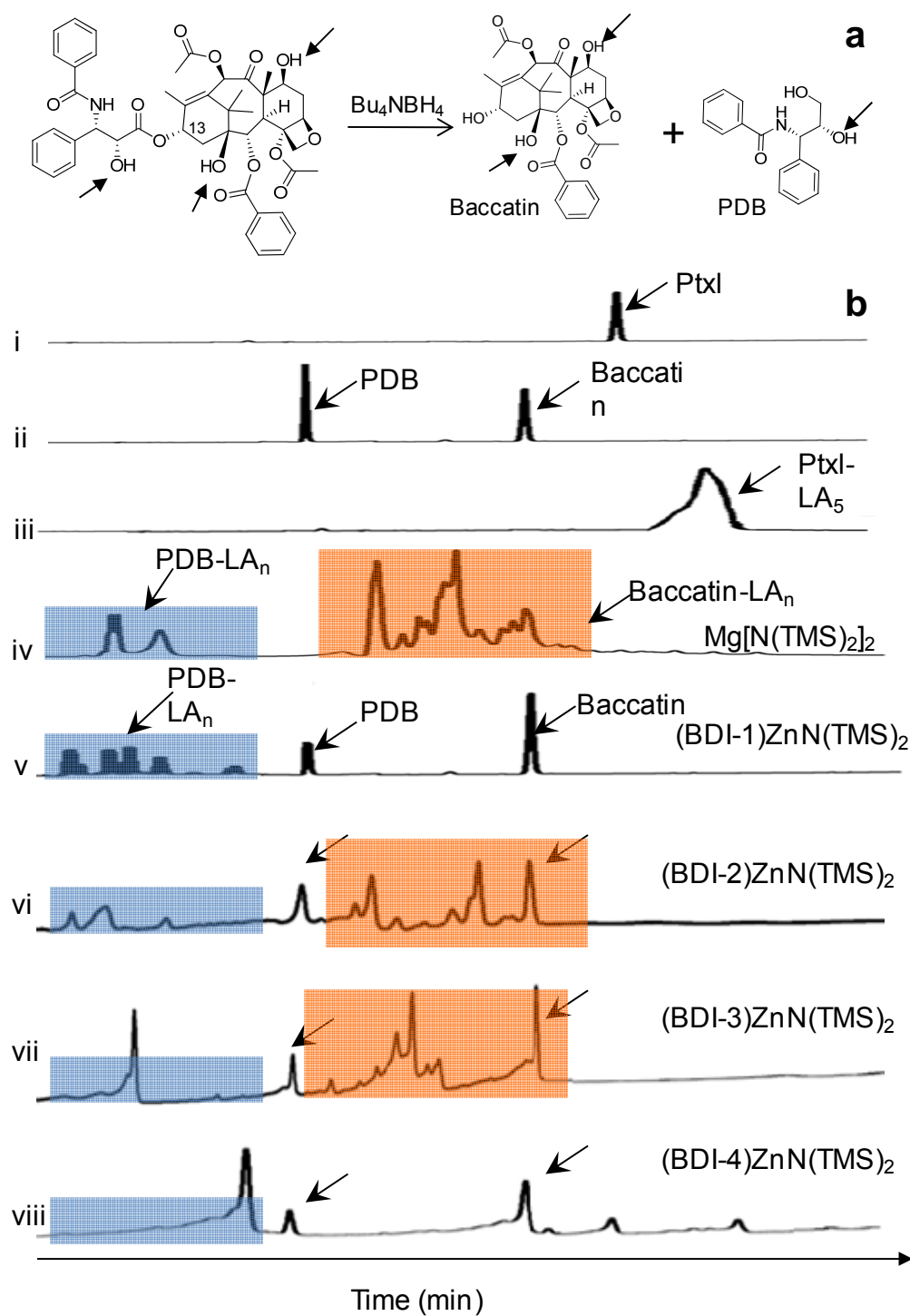


Figure 3.3 (a) Bu_4NBH_4 induced site-specific degradation of Ptxl for the formation of PDB and Baccatin (BAC). (b) Reductive degradation of 13-ester of Ptxl-PLA; HPLC analysis of (i) Ptxl, (ii) Ptxl treated with Bu_4NBH_4 , (iii) Ptxl-LA₅ (iv) Ptxl-LA₅ prepared using $\text{Mg}[\text{N}(\text{TMS})_2]_2$ followed by treatment with Bu_4NBH_4 , (v-viii) same as (iv) except that various

(Figure 3.3 continued) (BDI-m)ZnN(TMS)₂ were used. *The PDB and partial BAC detected in v-viii were from the free Ptxl that was not completely consumed during the polymerization at a very low M/I (M/I = 5). Separation of Ptxl was not attempted. Comparing BAC and PDB pattern in vi and ii, it is clear that the BAC in vi was partially from degradation of unreacted Ptxl and partially from the reduction of Ptxl-PLA with the PLA being attached to the 2'-OH of Ptxl.

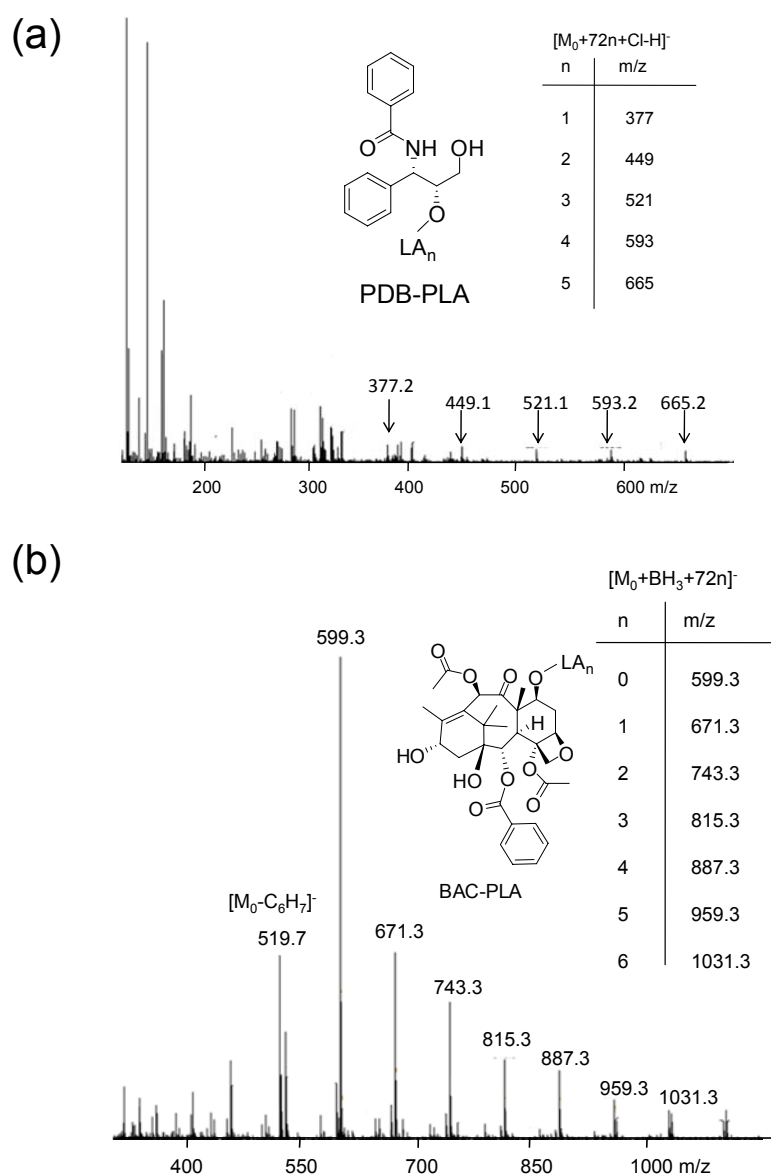


Figure 3.4. Characterization of PDB-PLA and BAC-PLA using ESI-MS. (a) ESI-MS (negative mode) analysis of Ptxl-PLA prepared by Ptxl/(BDI)ZnN(TMS)₂ (1/1 molar ratio) mediated LA (5 eq.) polymerization followed by treatment with Bu₄NBH₄ (b) ESI-MS (negative mode) analysis

(Figure 3.4 continued) of the Ptxl-PLA degradation fragments collected from prep-HPLC with elution time between PDB and BAC (see Fig 9). Ptxl-PLA was prepared through $\text{Mg}(\text{N}(\text{TMS})_2)_2$ mediated LA polymerization ($\text{Mg}/\text{Ptxl}/\text{LA} = 1/1/5$) and then treated with Bu_4NBH_4 before HPLC separation.

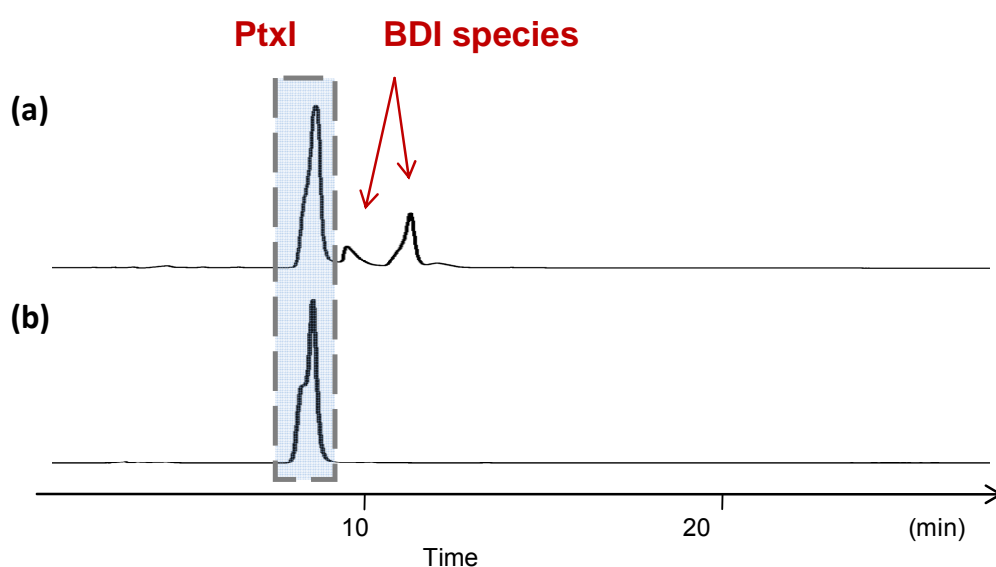


Figure 3.5. HPLC analysis of (a) Ptxl mixing with $(\text{BDI})\text{ZnN}(\text{TMS})_2$ and (b) Ptxl. The samples were analyzed by RP-HPLC equipped with Curosil column ($250 \times 4.6\text{mm}$, 5μ , Phenomenex, Torrance, CA, USA) at 227 nm. The HPLC analysis clearly showed that metal catalyst had no deleterious effect on Ptxl. Ptxl molecule remains intact during initiation and therefore should maintain its original form in Ptxl-PLA NCs, the final product.

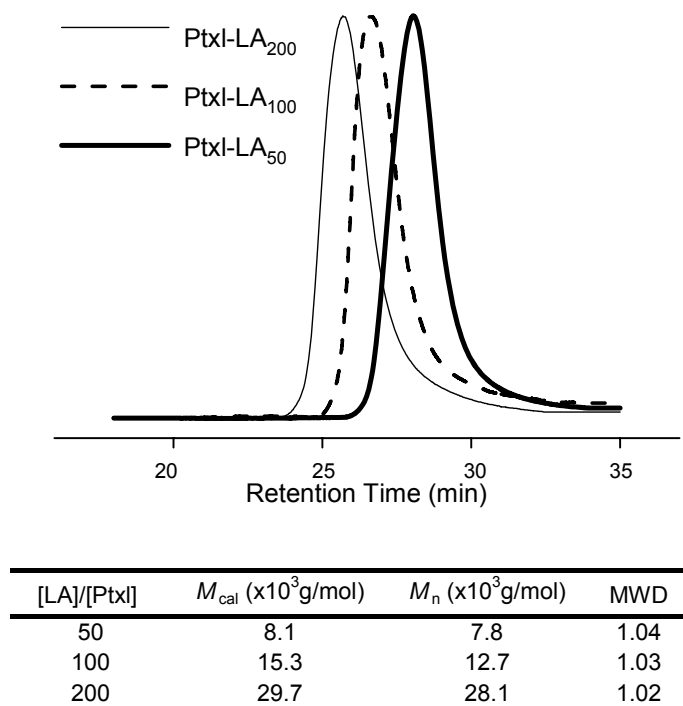


Figure 3.6 GPC analysis of Ptxl-LA₂₀₀, Ptxl-LA₁₀₀ and Ptxl-LA₅₀.

3.1.2 Controlled Formation of Ptxl-PLA Nanoconjugates and Their *in vitro* Evaluation

NEs prepared from nanoprecipitation are usually polydisperse with multimodal distributions. ^[3b, 4c] Interestingly, NCs with monomodal particle distributions and low polydispersities (entries 1-4, Table 3.1), exemplified by the Ptxl-LA₂₅ NC (Figure 3.8a), were consistently obtained through the nanoprecipitation of Ptxl-PLA conjugates. As the multimodal distribution of NEs is due in part to the aggregation of the non-encapsulated free drug,^[4c] the monomodal distribution observed with NCs is likely related to the unimolecular structures of Ptxl-PLA conjugates.

Both the solvent and the concentration of polymer have dramatic effects on the sizes of NPs prepared by nanoprecipitation. At fixed concentration of Ptxl-PLA conjugate, the sizes of NCs prepared by precipitating a DMF solution of Ptxl-PLA conjugate are typically in a range of 60-100 nm, 20-30 nm smaller than those prepared with acetone or THF as solvent.^[4c] When the nanoprecipitation was carried out using DMF as solvent at a DMF/water ratio of 1/20 (v/v), the size of Ptxl-LA₂₀₀ NCs showed a linear correlation with the concentration of Ptxl-LA₂₀₀ conjugate and can be precisely tuned from 60 nm to 100 nm by changing the concentration of Ptxl-LA₂₀₀.

Drug burst release is a long-standing formulation challenge of NEs, which causes undesirable side-effect and reduced therapeutic efficacy.^[4d] Conventional NEs typically “burst” release 60-90% of their payloads within a few to tens of hours because the release of drug is controlled solely by diffusion.^[9] Since the Ptxl release kinetics of Ptxl-PLA NCs is determined not only by diffusion but also by the hydrolysis of the Ptxl-PLA ester linker, the release kinetics of Ptxl from NCs are more controllable with significantly reduced burst release effect (Figure 3.8b). Ptxl released from Ptxl-LA₅₀ (10.6 wt%) and Ptxl-LA₂₅ (19.2 wt%) were 7.0% and 8.7% at Day 1, and 43% and 70.4% at Day 6, respectively. In comparison, 89% of Ptxl was released within 24 hrs from Ptxl/PLA NE (Figure 3.8b). The release of Ptxl from Ptxl-LA₅₀ NC was slower than that from Ptxl-LA₂₅ NC, presumably because of the higher MW of Ptxl-LA₅₀ and more compact particle aggregation.

The in vitro toxicities of NCs are correlated to the amount of Ptxl released; they show strong correlation with drug loadings (Figure 3.8c). The IC₅₀s of Ptxl-LA₁₅, Ptxl-LA₂₅ and Ptxl-LA₅₀ NCs with similar sizes (~ 100 nm), determined by MTT assays in PC-3 cells, are 111, 370 and 855 nM, respectively. The Ptxl-LA₁₅ NC has nearly identical

IC₅₀ as free Ptxl (87 nM); while the IC₅₀ of the Ptxl-LA₅₀ NC is an order of magnitude higher. As a result, the toxicity of NCs can be tuned in a wide range simply by controlling NC drug loading.

Surface modification of NPs with poly(ethylene glycol) (PEG) is widely used for prolonged systemic circulation and reduced aggregation of NPs in blood.^[10] To reduce the efforts of removing unreacted reagents and by-products, we attempted to use non-covalent approach to PEGylate NC surface instead of covalently conjugating PEG to NCs.^[2d, 3b] We used poly(glycolide-co-lactide)-*b*-methoxylated PEG (PLGA-mPEG), an amphiphilic copolymer that has a 13 kDa PLGA and a 5 kDa segment,^[11] to PEGylate NCs. It is expected that the PLGA block forms strong interaction with NCs through hydrophobic interaction to create a stable PEG shell (Figure 3.1). Similar approach has been used previously in NP surface PEGylation.^[12] Sequential addition of 0.4 to 2 equivalent (in mass) PLGA-mPEG to Ptxl-LA₂₀₀ resulted in a linear increase in particle size from 54.5 nm to 100.3 nm.

Ptxl-LA_n NCs have negative surface zeta-potential, and thus remain non-aggregated in water due to surface charge repulsion. However, aggregation of NCs occurred immediately after they were added to PBS, presumably due to salt-induced screen of the repulsive force.^[13] The PLGA-mPEG modified Ptxl-LA₂₀₀ NCs showed significantly enhanced stability in PBS as compared to the un-treated NCs or NCs treated with mPEG (Figure 3.8d), indicating the importance of the hydrophobic PLGA segment to the non-covalent interaction between PLGA-mPEG and NCs.

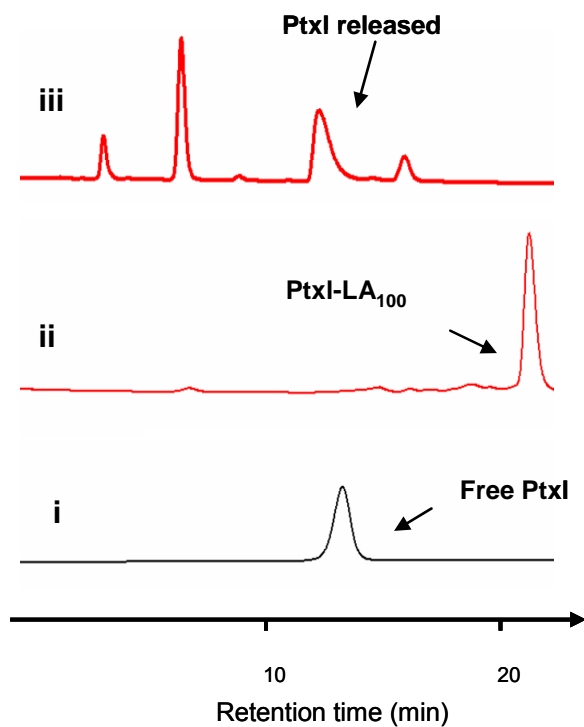


Figure 3.7 HPLC analysis of (i) Free Ptxl, (ii) Ptxl-LA₁₀₀ and (iii) released Ptxl from Ptxl-LA₁₀₀ after Ptxl-LA₁₀₀ was treated with 1N NaOH for 60 min and extracted with octanol. HPLC condition: RP-HPLC column (Curosil-PFP, 4.6 × 250 mm, 5μ, Phenomenex, Torrance, CA). Mobile phase was acetonitrile/water with 0.1% TFA (v/v = 50/50). The flow rate was 1.0 mL/min.

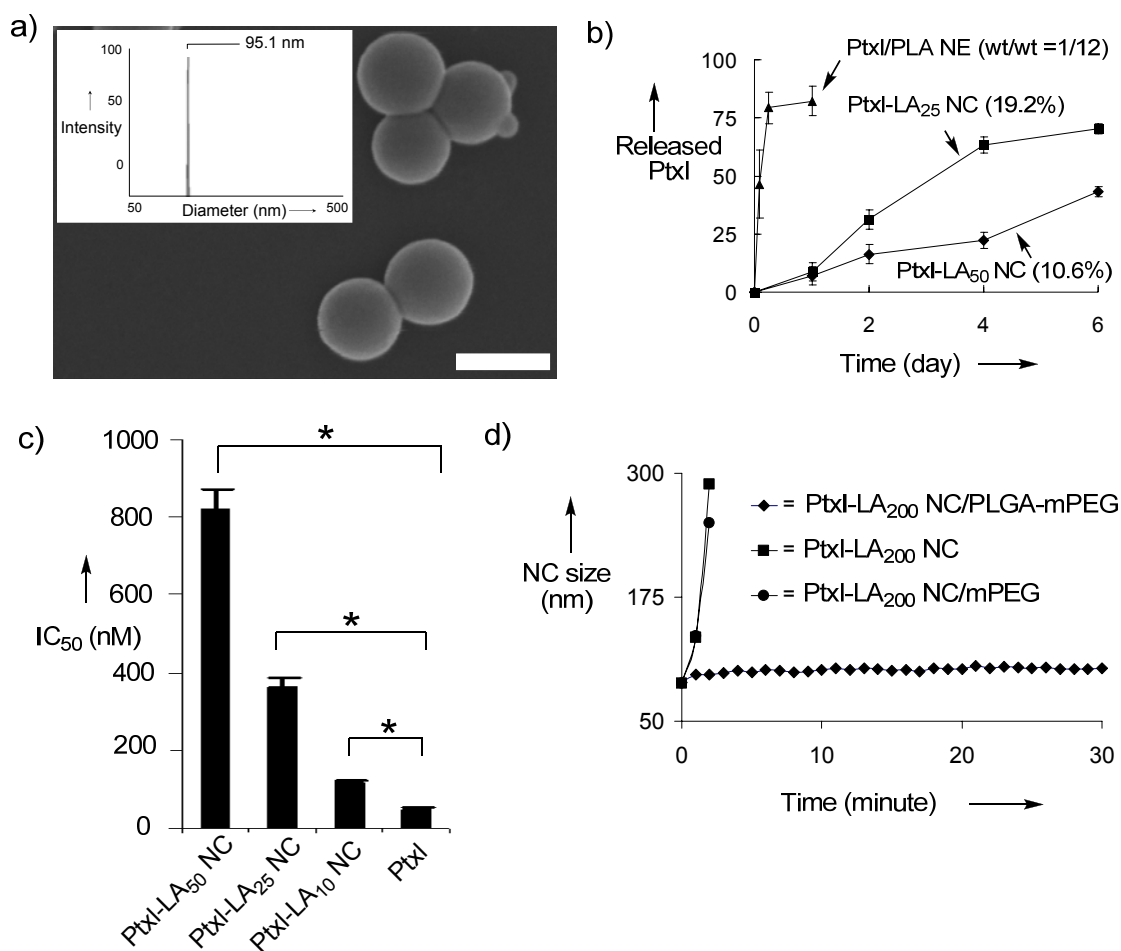


Figure 3.8 Characterization and properties of Ptxl-PLA NCs (a) Ptxl-LA₂₅ (paclitaxel-PLA NC prepared at a LA/Ptxl ratio of 25) analyzed by scanning electron microscopy (SEM) and dynamic light scattering (DLS, inset). Scale bar = 150 nm. (b) Release kinetics of Ptxl from Ptxl-PLA NCs and Ptxl/PLA NE (prepared by nanoprecipitating a mixture of Ptxl and PLA (Ptxl/PLA (wt/wt) = 1/12) at 37°C in 1× PBS. (c) Toxicity evaluation of Ptxl-LA₅₀ NC, Ptxl-LA₂₅ NC, Ptxl-LA₁₀ NC and Ptxl using MTT assay in PC-3 cells after 24 hr incubation. *Significance at 95% confidence interval. (d) Stability of Ptxl-LA₂₀₀ NC in PBS at 37°C before and after being treated with PLGA-mPEG_{5k} or mPEG_{5k}

3.2 *Nanoconjugates synthesized from other cyclic lactones*

For VL and CL, the polymerization proceeded similar to LA. At room temperature, monomer conversion was quantitative and Ptxl were successfully incorporated in the polymer. PVL had a little broad distribution than PCL polymerization. Molecular weights were both obtained in control manner, by changing the monomer/Ptxl concentration ratio. Table 3.3 also showed Dtxl could be incorporated in polymer similar to Ptxl.

It was reported that BDI-Zn complex could be used for the six-membered carbonate ring opening polymerization, through the insertion-coordination mechanism similar as LA. A pioneer study was conducted using (BDI-1)ZnN(TMS)₂ and BnOH to polymerize TMC in bulk. Previously study showed (BDI-1)ZnN(TMS)₂ had low activity towards TMC; while the (BDI-1)ZnN(TMS)₂ and BnOH complex after mixing in 20 min showed ultraproductive activity to polymerize TMC in living manner. We confirmed that during 6 hours, TMC was all consumed and formed polymer in toluene solution at 50 degree. No free Ptxl was detected after the polymerization. It suggested that all Ptxl participate in the PTMC.

PHB is an aliphatic polyester produced by many living organism e.g. bacteria in isotactic stereochemistry. It is biodegradable and biocompatible and recently has been commercially engineered to make copolymer with 3-hydroxylvalerate, which have similar properties as polypropylene. Ring opening of BBL are always extremely slow and in uncontrollable manner with few exceptions such as BDI-Zn series catalyst. In this study we used racemic BBL to form atactic PHB. Ptxl system was incorporated in PHB by similar method like LA we mentioned before. We decided to use (BDI-1)Zn and (BDI-4)ZnN(TMS)₂ as the catalyst, since site specific activation by these two catalyst

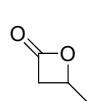
has been demonstrated. BBL is known to have strong lactone band at 1829 cm^{-1} in FTIR spectrum, and after polymerization, the ester band at 1740 cm^{-1} . FTIR was used to monitor the reaction process. We first tested the ROP reaction of BBL initiated by Ptxl with these two catalysts respectively at room temperature in THF solution. After 10 hours reaction, the conversions of BBL for both catalysts were less than 50%, which slower than other cyclic ester polymerization. We raised the reaction temperature to $50\text{ }^{\circ}\text{C}$ in order to accelerate the polymerization kinetic rates. Solvent effect for BBL polymerization was also taken in consideration. Coates previously reported BBL polymerizations of BBL in benzene and toluene were faster than in THF and DCM. We then conducted polymerization in toluene at $50\text{ }^{\circ}\text{C}$ with the ratio of $[\text{BBL}]/[\text{Ptxl}]=100/1$. In 10 hours, conversion of BBL was 98% for $(\text{BDI-1})\text{ZnN}(\text{TMS})_2$ and 97% for $(\text{BDI-4})\text{Zn}$, which is nearly quantitative. Ptxl were both successfully incorporated into polymer over 98% efficiency, measured by HPLC. The molecular weight of BBL was accessed by GPC. It was found PHB catalyzed by $(\text{BDI-1})\text{ZnN}(\text{TMS})_2$ (Table 3.3 entry 11) had broad molecular weight distribution ($\text{PDI}=3.80$) and M_n was dramatically smaller than expected ($M_n=5.4\text{ kg/mol}$, $M_{\text{cal}}=9.5\text{ kg/mol}$). PHB catalyzed by $(\text{BDI-4})\text{ZnN}(\text{TMS})_2$ (Table 3.3 entry 12) had $M_n=10.7\text{ kg/mol}$ with $\text{PDI}=1.10$, suggesting the polymerization reaction proceeded in control manner. The reduction of molecular weight and broaden of distribution was previously reported for many system, including Al aloxide and BDI-Zn series catalyst for BBL polymerization. Coates also noted $(\text{BDI-1})\text{ZnN}(\text{TMS})_2$ catalyst potentially would reduce molecular weight over long time. To investigate whether polymerization conducted with $(\text{BDI-4})\text{ZnN}(\text{TMS})_2$ was in controlled living manner, we conducted kinetic study for $[\text{BBL}]/[\text{Ptxl}]=200/1$ by NMR. k_{app} was 0.315 h^{-1} (Figure 3.9c). The linear kinetic plot suggested that the polymerization was living polymerization. It

was likely (BDI-1)ZnN(TMS)₂ have fast kinetic rates than (BDI-4)ZnN(TMS)₂. After polymerization completed the side reaction would happen immediately, resulting in broad distribution in 10 hours (Figure 3.9a).

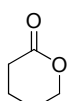
It was reported that during the reduction of PHB by metal aloxide catalyst, the cleaved chain end would form crotonic structure (Scheme 3.1). The polymer will be shortened and show wide distribution. We also investigated the NMR spectrum to see the side reaction happening or not. We confirmed that in 10 hours polymerization, no side reaction was observed. Overall, in 10 hours, the polymerization of PHB with (BDI-4)ZnN(TMS)₂ was still living polymerization to successfully provide polymer with controllable molecular weight and narrow distribution.

Table 3.3 Polymerization of various cyclic lactone/carbonate initiated by Ptxl (or Dtxl) and BDI-Zn catalyst

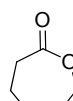
Entry ^b	initiator	monomer	[M]/[I]	catalyst	Time (h)	Temp. (°C)	Conv. (%) ^c	M _{cal} (kg/mol)	M _n (kg/mol) ^d	PDI (M _w /M _n) ^d
1	Ptxl	CL	200	(BDI-1)Zn	10	r.t.	>99	23.7	20.3	1.07
2	Ptxl	CL	200	(BDI-2)Zn	10	r.t.	>99	23.7	16.4	1.11
3	Ptxl	CL	200	(BDI-3)Zn	10	r.t.	>99	23.7	21.9	1.06
4	Ptxl	CL	200	(BDI-4)Zn	10	r.t.	>99	23.7	26.2	1.07
5	Ptxl	CL	300	(BDI-1)Zn	10	r.t.	>99	35.1	25.5	1.15
6	Dtxl	CL	100	(BDI-1)Zn	10	r.t.	>99	12.2	11.2	1.05
7	Dtxl	CL	300	(BDI-1)Zn	10	r.t.	>99	35.0	38.4	1.13
8	Ptxl	VL	100	(BDI-1)Zn	12	r.t.	>99	10.8	15.1	1.17
9	Ptxl	VL	200	(BDI-1)Zn	12	r.t.	>99	20.8	23.1	1.18
10	Ptxl	VL	300	(BDI-1)Zn	12	r.t.	>99	30.8	31.2	1.18
11	Ptxl	BL	100	(BDI-1)Zn	10	50	98	9.5	5.4	3.80
12	Ptxl	BL	100	(BDI-4)Zn	10	50	97	9.5	10.7	1.10
13	Ptxl	BL	200	(BDI-4)Zn	10	50	97	18.1	18.7	1.12
14	Ptxl	BL	300	(BDI-4)Zn	10	50	98	26.7	25.4	1.06
15	Ptxl	TMC	100	(BDI-1)Zn	6	50	>99	11.1	14.7	1.10
16	Ptxl	TMC	100	(BDI-4)Zn	6	50	>99	11.1	18.1	1.10
17	Ptxl	TMC	200	(BDI-1)Zn	6	50	>99	21.3	27.6	1.21
18	Ptxl	TMC	300	(BDI-1)Zn	6	50	>99	31.5	49.2	1.21



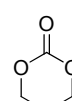
BL



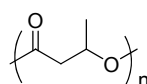
VL



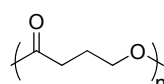
CL



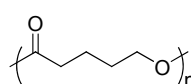
TMC



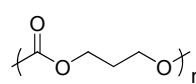
PHB



PVL



PCL



PTMC

^aPolymerization procedures see experimental sections. For all monomers initial concentrations: [CL]=3.84M; [BL]=2.62M; [VL]=2.03M; [TMC]=1.67M. Abbreviation: Temp: temperature. r.t.: room temperature. Conv. %: conversion % of monomer. M_{cal}: theoretical calculation of molecular weight. M_n: number average molecular weight; M_w: weight average molecular weight. PDI: polydispersity index. ^bEntry 1-10 were performed in THF solution at room temperature. Entry 11-18 were performed in toluene. All reactions had over 98% Ptxl (or Dtxl) incorporation efficiency, determined by HPLC. ^c Conversion was measured by NMR. ^dDetermined by gel permeation chromatography (GPC).

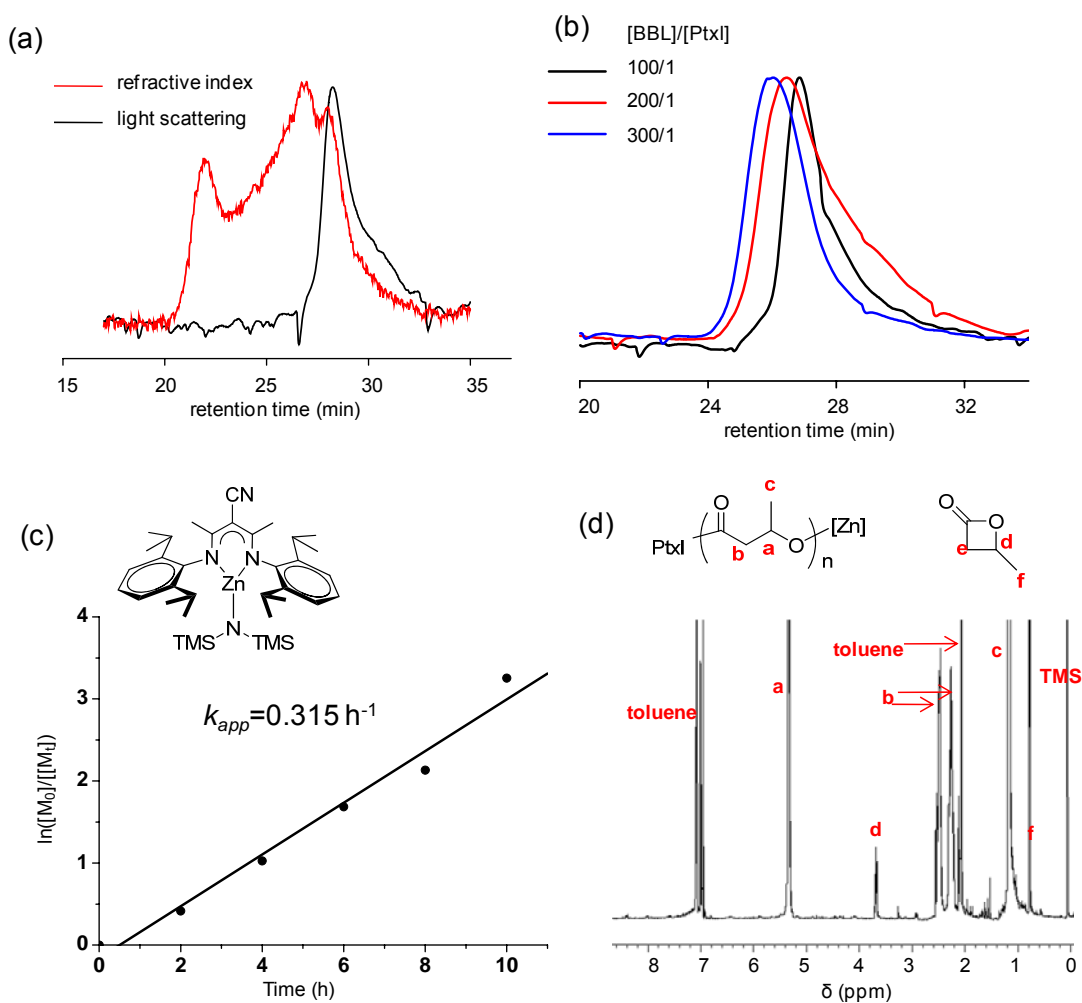


Figure 3.9 (a) PHB was prepared according to the feeding ratio: [BBL]/[Ptxl]/[(BDI-1)Zn]=100/1/1. GPC overlay of polymer curves measured by refractive index detector (red) and light scattering detector (black). (b) PHB was prepared according to various [BBL]/[Ptxl] feeding ratio and catalyzed by (BDI-4)Zn at 50 degree in toluene over 10 hours. (c) kinetic study of BBL in toluene-d8. [BBL]/[Ptxl]/[(BDI-4)Zn]=200/1/1. [BBL]=1.72M. (d) $^1\text{H-NMR}$ spectrum of 8 hour of kinetic study (c) of PHB and BBL mixture in toluene-d8. No crotonic peak around 7-5 ppm was found in the spectrum

Scheme 3.1 Polymerization of BBL and side reaction of molecular weight reduction and broaden of distribution

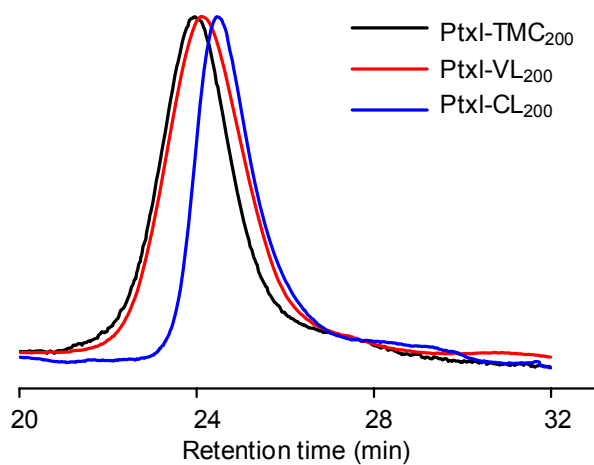
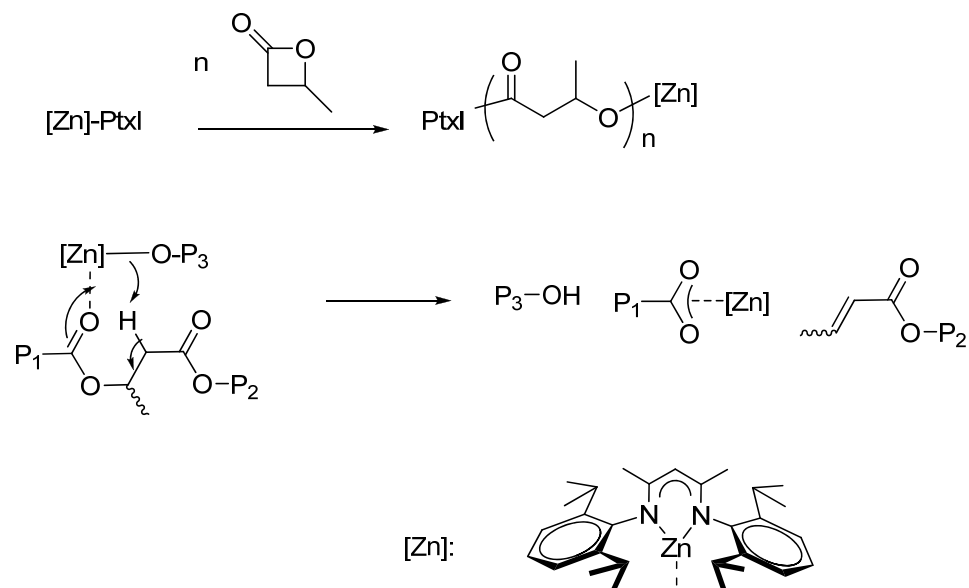


Figure 3.10 GPC curve of PtxI-CL₂₀₀, PtxI-VL₂₀₀, and PtxI-TMC₂₀₀. All polymers were catalyzed by (BDI-1)ZnN(TMS)₂

4. Conclusions

Nanotechnology is making a significant impact on cancer drug delivery. In conjunction with the development of lipid based drug delivery, the advancement of modern polyester chemistry make it possible for the preparation of a large variety of synthetic PLA/PLGA materials with structures tailored to accommodate the specific needs of systemic drug delivery. It is anticipated that synergistic integration of the efforts of chemists, materials scientists, chemical and biomedical engineers and physicians will facilitate the design and development of polymeric nanomedicine at an unprecedented pace, and eventually allow for cancer therapy in a time-, tissue-, or even patient-specific manner. We developed a new formulation method for preparing polymeric nanoconjugates using drug-initiated, controlled, living polymerization of cyclic esters. This unprecedented strategy is alternative to the coupling chemistry-mediated polyester-drug conjugation,^[14] and allows preparation of polymer-drug nanoconjugates with very high drug loadings, nearly quantitative loading efficiencies, controlled release profiles without burst release effects, and narrow particle distributions. It usually takes only a few hours to prepare gram- or larger-scale, salt-stable NCs. The drug release profiles can potentially be further modified by using different cyclic esters other than LA. This formulation method can potentially be broadly used for the nano-formulation of numerous hydroxyl-containing therapeutic agents to achieve excellent control over drug loading and release. The catalyst structure-activity relationship still significantly imposed on the regioselectivity and yield of final conjugates, as shown in previous chapter. Some regioselective *O*-acylation study in this chapter is eventually expanded and further discussed in Chapter 6. Last but not least, because of the scalable preparation of the Ptxl-

PLA conjugates, they are the model polymer for formulation and preclinical *in vivo* study, which are reported in chapter 5.

5. References

- [1] E. K. Rowinsky, R. C. Donehower, *N. Engl. J. Med.* **1995**, 332, 1004.
- [2] (a) C. Li, *Cancer Res.* **1998**, 58, 2404; (b) J. W. Singer, *J Control Release* **2005**, 109, 120; (c) C. Fonseca, S. Simoes, R. Gaspar, *J. Controlled Release* **2002**, 83, 273; (d) R. Gref, Y. Minamitake, M. Peracchia, V. S. Trubetskoy, V. P. Torchilin, R. Langer, *Science* **1994**, 263, 1600.
- [3] (a) O. C. Farokhzad, J. M. Karp, R. Langer, *Expert Opin Drug Deliv* **2006**, 3, 311; (b) O. C. Farokhzad, J. Cheng, B. A. Teply, I. Sherifi, S. Jon, P. W. Kantoff, J. P. Richie, R. Langer, *Proc. Natl. Acad. Sci. U. S. A.* **2006**, 103, 6315.
- [4] (a) J. Panyam, V. Labhasetwar, *Adv. Drug Delivery Rev.* **2003**, 55, 329; (b) R. Tong, J. J. Cheng, *Polymer Reviews* **2007**, 47, 345; (c) J. Cheng, B. A. Teply, I. Sherifi, J. Sung, G. Luther, F. X. Gu, E. Levy-Nissenbaum, A. F. Radovic-Moreno, R. Langer, O. C. Farokhzad, *Biomaterials* **2007**, 28, 869; (d) K. S. Soppimath, T. M. Aminabhavi, A. R. Kulkarni, W. E. Rudzinski, *J. Controlled Release* **2001**, 70, 1.
- [5] B. M. Chamberlain, M. Cheng, D. R. Moore, T. M. Ovitt, E. B. Lobkovsky, G. W. Coates, *J. Am. Chem. Soc.* **2001**, 123, 3229.
- [6] N. F. Magri, D. G. I. Kingston, C. Jitrangsri, T. Piccariello, *J. Org. Chem.* **1986**, 51, 3239.
- [7] D. Mastropaolo, A. Camerman, Y. G. Luo, G. D. Brayer, N. Camerman, *Proc. Natl. Acad. Sci. U. S. A.* **1995**, 92, 6920.
- [8] A. E. Mathew, M. R. Mejillano, J. P. Nath, R. H. Himes, V. J. Stella, *J. Med. Chem.* **1992**, 35, 145.
- [9] T. Musumeci, C. A. Ventura, I. Giannone, B. Ruozi, L. Montenegro, R. Pignatello, G. Puglisi, *Int. J. Pharm.* **2006**, 325, 172.
- [10] P. Caliceti, F. M. Veronese, *Advanced Drug Delivery Reviews* **2003**, 55, 1261.
- [11] E. Pierri, K. Avgoustakis, *J. Biomed. Mater. Res. Part A* **2005**, 75A, 639.
- [12] X. H. Gao, Y. Y. Cui, R. M. Levenson, L. W. K. Chung, S. M. Nie, *Nat. Biotechnol.* **2004**, 22, 969.

- [13] A. L. Kjoniksen, F. Joabsson, K. Thuresson, B. Nystrom, *J. Phys. Chem. B* **1999**, *103*, 9818.
- [14] (a) Z. Xie, H. L. Guan, X. Chen, C. Lu, L. Chen, X. Hu, Q. Shi, X. Jing, *J. Controlled Release* **2007**, *117*, 210; (b) Z. G. Xie, T. C. Lu, X. S. Chen, C. H. Lu, Y. H. Zheng, X. B. Jing, *J. Appl. Polym. Sci.* **2007**, *105*, 2271; (c) X. F. Zhang, Y. X. Li, X. S. Chen, X. H. Wang, X. Y. Xu, Q. Z. Liang, J. L. Hu, X. B. Jing, *Biomaterials* **2005**, *26*, 2121; (d) H. S. Yoo, J. E. Oh, K. H. Lee, T. G. Park, *Pharm. Res.* **1999**, *16*, 1114; (e) H. S. Yoo, K. H. Lee, J. E. Oh, T. G. Park, *J. Controlled Release* **2000**, *68*, 419.

CHAPTER 4

NANOCONJUGATES: INCORPORATING DOXORUBICIN

1. Introduction

In this chapter, I report the use of doxorubicin (Doxo), a therapeutic agent that contains multiple types of conjugation-amenable groups (three hydroxyl groups, one amine group and one ketone group), as an initiator for the ROP of LA.

In general, the coupling of the terminal carboxylate of PLA with Doxo, a molecule bearing both amine and hydroxyl groups, predominately formed Doxo-PLA conjugates through the 3'-NH₂ of Doxo by creating an amide bond.^[1,2] Such Doxo-PLA conjugates, however, cannot release Doxo in its original form by hydrolysis. Instead, Doxo-3'-lactamide, a prodrug of Doxo, is formed. In poly(ethylene glycol)-*b*-poly(aspartic acid) (PEG-*b*-PAsp) copolymer micelles in which Doxo was conjugated via its 3'-NH₂ to the pendant carboxylate groups of the PAsp block, Doxo may not be readily released from PEG-*b*-PAsp(Doxo) micelles to exhibit therapeutic effectiveness.

In order for Doxo to be released in its original form, the hydroxyl groups of Doxo should be used for conjugation with the terminal carboxylate group of PLA to form an ester linker between Doxo and PLA. To facilitate such a reaction, protection and deprotection of the Doxo amine group before and after the conjugation, respectively, are thereby required. Although these protection and deprotection chemistries are possible, the manipulation of such chemistries on a multifunctional, unstable drug is difficult and may result in degradation of Doxo. Due to these challenges, efforts have been devoted mainly to the conjugation between the 13-ketone group of Doxo and hydrazine groups of

polymeric carriers by forming an acid-labile hydrazone bond.^[3-6] Some promising preclinical results of polymer-Doxo delivery vehicles with hydrazone linkers have been reported.^[7,8] However, clinical studies of immunoconjugates with Doxo connected to monoclonal antibodies with hydrazone linkers gave unsatisfactory antitumor effects, which led to the termination of the clinical development of such immunoconjugates.^[9] Acylation of Doxo with its hydroxyl groups was achieved through a Subtilisin Carlsberg (a serine endopeptidase)-mediated reaction with vinyl butyrate.^[10] Nevertheless, it is unlikely that this method can be used for the conjugation of Doxo to polymers. Diatos S. A. Laboratories recently reported the synthesis of Vectocell peptide-Doxo conjugates in which Doxo was linked to a peptide with an ester bond through its 14-OH group.^[11] However, the synthesis was not achieved through the coupling of Doxo and the peptide. Multistep reactions starting from daunorubicin, rather than doxorubicin, were involved in the synthesis of the final product. To our knowledge, there has been no report of effective acylation of Doxo via its hydroxyl groups for the formulation of polymer-Doxo conjugates.

In numerous previous studies involving the use of metal catalysts for LA polymerization, ring openings of LA proceeded predominately by metal-alkoxides (M-ORs) rather than by metal-amides (M-NHRs). Although there are only limited reports that describe the differences in the polymerization activities between these two classes of initiators, M-OR complexes typically have higher activities for LA ring opening to form ester bonds than their amine analogues in a similar ring-opening reaction to form amide bonds. For instance, Coates and co-workers reported that (BDI)ZnOCH(CH₃)₂ initiated and completed a LA polymerization within 20 min at a monomer/initiator (M/I) ratio of 200, while a similar polymerization mediated by (BDI)ZnN(TMS)₂ required 10 h to

complete. Based on this finding, we studied whether it was possible to use Zn catalysts for controlling Doxo conjugation to PLA preferentially with the hydroxyl groups of Doxo. Our approach allows for one-pot synthesis of Doxo-PLA conjugate and concurrently addresses all three of the heterogeneities observed in polymer-drug conjugates. This study demonstrated, for the first time, that Doxo can be incorporated into PLA in a regio- and chemoselective manner via a well-controlled polymerization process. Quantitative incorporation of Doxo and controlled polymerization (polydispersity (PDI) of Doxo-PLA as low as 1.02) were achieved simultaneously. Doxo was conjugated to the terminus of PLA through its 14-hydroxyl group specifically, without the need to protect its 3'-amine or 4'- and 9-hydroxyl groups. The nanoprecipitation of Doxo-PLA conjugates allowed for the formation of Doxo-PLA conjugate NPs, which are also called nanoconjugates (NCs) to differentiate them from NPs prepared by co-precipitating drugs and polymers, with narrow particle size distributions and controlled release kinetics. We demonstrated that this unique, polymerization-mediated drug conjugation method can be applied to the formulation of PLA NCs with a variety of hydroxyl-containing molecules.

2. Materials and Methods

2.1 General

D,L-Lactide (LA) was purchased from TCI America (Portland, OR), recrystallized three times in toluene and stored at -30°C in a glove box prior to use. The BDI ligands and the corresponding metal catalysts ((BDI)Mn(TMS)₂, M = Mg, Zn) were prepared by following the published procedures and stored at -30°C in a glove box prior to use. All

anhydrous solvents were purified by being passing through dry alumina columns and were kept anhydrous by using molecular sieves. Doxo·HCl was purchased from Bosche Scientific (New Brunswick, NJ) and used as received. Removal of HCl of Doxo·HCl was achieved by following the procedure reported in the literature. Docetaxel (Dtxl) was purchased from LC Laboratories (Woburn, MA) and used as received. Cy5 was synthesized according to the published procedure. All other chemicals were purchased from Sigma-Aldrich (St Louis, MO) and used as received, unless otherwise specified. The MWs of PLA and Doxo-PLA were determined by a size-exclusion chromatography instrument (SEC) equipped with an isocratic pump (Model 1100, Agilent Technology, Santa Clara, CA), a DAWN HELEOS 18-angle laser light scattering detector (Wyatt Technology, Santa Barbara, CA) and an Optilab rEX refractive index detector (Wyatt Technology, Santa Barbara, CA). The wavelength of the HELEOS detector was set at 658 nm. The size exclusion columns used for the separation of PLA and Doxo-PLA conjugates were serially connected to a SEC (Phenogel columns 100 Å, 500 Å, 10³ Å and 10⁴ Å, 5 µm, 300 × 7.8 mm, Phenomenex, Torrance, CA) equipped with a 126P solvent module and a System Gold 128 UV detector (Beckman Coulter, Fullerton, CA). THF (HPLC grade) was used as the mobile phase of SEC with a 1-mL/min flow rate. The low resolution electrospray ionization mass spectrometry (LR-ESI-MS) experiments were performed on a Waters Quattro II Mass Spectrometer. The high resolution electrospray ionization mass spectrometry (HR-ESI MS) experiments were performed on a Micromass Q-TOF Ultima system. Matrix assisted laser desorption/ionization-time of flight mass spectrometry (MALDI-TOF MS) spectra were collected on an Applied Biosystems Voyager-DETM STR system. HPLC analyses were performed on a System Gold system (Beckman Coulter, Fullerton, CA) equipped with a 126P solvent module, a System Gold

128 UV detector and an analytical pentafluorophenyl column (Curosil-PFP, 250 × 4.6 mm, 5 μ , Phenomenex, Torrance, CA) or an analytical C18 column (Luna C18, 250 × 4.6 mm, 5 μ , Phenomenex, Torrance, CA). The UV wavelength for detecting Pyr-OH or Pyr-NH₂ was set at 300 nm. The UV wavelength for detecting Doxo was set at 450 nm or 500 nm, depending on the signal-to-noise ratio in corresponding studies. The NMR experiments were conducted on a Varian U500, a VXR500 or a UI500NB (500 MHz) NMR spectrometer. The sizes and particle polydispersities of the PLA-drug (dye) NCs were determined on a ZetaPlus Dynamic Light Scattering (DLS) detector (15-mW laser, incident beam = 676 nm, Brookhaven Instruments, Holtsville, NY). The PC-3 cells (ATCC, Manassas, VA) used in the MTT assay were cultured in Ham's F12K medium containing 10% fetal bovine serum, 1000 units/mL aqueous penicillin G and 100 μ g/mL streptomycin.

2.2 Synthesis and characterization of Doxo-PLA nanoconjugates

2.2.1. 1-Pyrenemethylamine/(BDI)ZnN(TMS)₂ and 1-pyrenemethanol / (BDI)ZnN(TMS)₂-mediated LA polymerization

In a glove box, 1-pyrenemethylamine (Pyr-NH₂) (2.3 mg, 10 μ mol) was dissolved in chloroform (0.5 mL). The solution was mixed with a THF solution (0.5 mL) of (BDI)ZnN(TMS)₂ (6.3 mg, 0.01 μ mol). A THF solution (400 μ L) of LA (36 mg, 0.25 μ mol) was added to a vigorously stirred mixture of Pyr-NH₂ and (BDI)ZnN(TMS)₂. The mixture was stirred for 3 h at room temperature. An aliquot of the reaction mixture (100 μ L) was taken out of the glove box for HPLC analysis. Pyr-OH (2.1 mg, 0.009 μ mol) in

300 μ L of chloroform was added to the polymerization solution. The reaction solution was stirred for an additional 3 h and analyzed by HPLC.

2.2.2 Preparation of Doxo-LA₁₀₀ NCs

In a glove box, Doxo (5.5 mg, 0.01 mmol) was dissolved in anhydrous THF (1 mL). (BDI)ZnN(TMS)₂ (18.3 mg, 0.03 mmol) was added to the Doxo solution. The mixture was stirred for 15-20 min at room temperature. LA (144 mg, 1.0 mmol) in DMF (1 mL) was added dropwise to a vigorously stirred mixture of Doxo and (BDI)ZnN(TMS)₂. The polymerization was monitored by following the lactone band at 1772 cm^{-1} using FTIR or by checking the methine (-CH-) peak of LA using ¹H NMR. After the polymerization was complete (usually within 12 h), an aliquot of the polymerization solution was injected to HPLC to quantify the unreacted Doxo, in order to determine the incorporation efficiency of Doxo to the Doxo-PLA conjugate. One drop of water was added to the polymerization solution to hydrolyze the Zn-Doxo alkoxide and thus terminate the polymerization. The resulting Doxo-LA₁₀₀ was precipitated with ethyl ether (10 mL), washed with ether and methanol/acetic acid (v/v = 100/1, 10mL) to remove BDI ligand and metal catalyst and dried under vacuum. Complete removal of BDI was confirmed by NMR, HPLC and TLC. After the organic solvent was evaporated, the residue was dissolved in HPLC-grade THF (10 mg/mL) and analyzed by SEC to determine the MWs and polydispersities. Doxo-PLA conjugates prepared at various M/I ratios were also analyzed by a SEC equipped with a UV detector.

2.2.3 Doxo/(BDI)ZnN(TMS)₂-mediated ring opening of succinic anhydride

In a glove box, Doxo·HCl (2.0 mg, 0.0035 mmol) was mixed with (BDI)ZnN(TMS)₂ (2.4 mg, 0.0042 mmol, 1.2 eq.) ((BDI')ZnN(TMS)₂ 1.2 equiv., Zn(N(TMS)₂)₂, 1.2 equiv. or (BDI)MgN(TMS)₂ 1.2 equiv.) in THF (200 μL) for 30 min, followed by removal of the solvent under vacuum. Freshly crystallized succinic anhydride (SA) (0.41 mg, 0.0042 mmol, 1.2 equiv.) in THF (42 μL) was added dropwise to the mixture of Doxo·HCl and (BDI)ZnN(TMS)₂. The reaction mixture was diluted with 200 μL of THF and stirred for an additional 60-90 min. The solvent was removed under vacuum. The residue was then dissolved using a mixture of acetic acid and methanol (v/v = 1/1, 300 μL). An aliquot of this solution was used for ESI-MS analysis.

2.2.4 Formation, characterization and evaluation of Doxo-LA₁₀₀ nanoconjugate

A Doxo-LA₁₀₀ conjugate in DMF (100 μL, 10 mg/mL) was added dropwise to nanopure water (2 mL). The resulting Doxo-LA₁₀₀ NC was collected by ultrafiltration (15 min, 3000 × g, Ultracel membrane with 10,000 NMWL, Millipore, Billerica, MA) and was used for the characterization of particle size by DLS, drug loading by HPLC and release kinetics by HPLC.

2.2.5 Determination of release kinetics

The Doxo/PLA NPs were prepared through nanoprecipitation of PLA (1.5 × 10⁴ g/mol) and Doxo by following the procedure reported in the literature.⁴⁶ Doxo-LA₁₀ and Doxo-LA₅₀ NCs were prepared by following the standard nanoprecipitation procedure described above using Doxo-LA₁₀ and Doxo-LA₅₀ conjugates, respectively. The NPs and NCs were collected and washed three times with water by ultrafiltration, using a 10,000

MWCO Amicon Ultra membrane (Ultracel YM-10, Millipore Inc., Billerica, MA), in order to completely remove DMF. The NCs (or NPs) collected from the ultrafiltration device were dispersed in 5 mL 1× PBS solution; the PBS solution containing NCs (or NPs) was then divided into equal portions, added to five separate eppendorf tubes (1 mL per tube) and incubated at 37°C. At selected time intervals, the corresponding eppendorf tubes were taken out of the incubator and centrifuged at 4,000 rpm for 5 min. The supernatant (500 µL) was carefully transferred, using a micropipette, to a separate eppendorf tube without disturbing the precipitated NCs (or NPs). The supernatant was injected into HPLC to quantify the released Doxo from PLA/Doxo NP, Doxo-LA₁₀ NC and Doxo-LA₅₀ NC. An analytical RP-HPLC column (Luna C18, 250 × 4.6 mm, 5 µ, Phenomenex, Torrance, CA) was used for the quantification of the released Doxo. The area of the released Doxo peak was integrated and compared to a standard curve. To confirm that Doxo was released in its original form from Doxo-PLA NCs, we collected the fraction that had an elution time identical to that of the authentic Doxo on HPLC and analyzed it with high resolution ESI-MS. The MS (HR-ESI) was calculated for C₂₇H₃₀NO₁₁ [M + H]⁺ to be *m/z* 544.1819, and we found *m/z* 544.1827.

2.2.6 Determination of the cytotoxicity of Doxo-PLA NCs

PC-3 cells were plated in a 96-well plate for 24 h (10,000 cells per well) before the addition of NCs. The cells were washed with pre-warmed PBS. Freshly prepared Doxo-LA₁₀, Doxo-LA₂₅ and Doxo-LA₅₀ NCs (prepared in 1× PBS, 100 µL) were added to the cells. The cells were incubated for 72 h in a 5% CO₂ incubator at 37°C. Doxo was used as a positive control. Untreated cells were used as a negative control. After

incubation for 72 h, the medium was removed from the cells. Standard MTT (3-(4,5-dimethylthiazol-2-yl)-2,5-diphenyltetrazolium bromide) assay protocols were followed thereafter.

3. Results and Discussion

3.1 Synthesis and characterization of Doxo-PLA nanoconjugates

3.1.1 Metal-amide- and metal-alkoxide-initiated LA polymerization

To evaluate metal-amide- and metal-alkoxide-initiated LA polymerization, we utilized 1-pyrenemethanol (Pyr-OH) and 1-pyrenemethylamine (Pyr-NH₂) as the corresponding model hydroxyl and amine initiators. Pyrene is UV-active and thus can be easily characterized by a UV detector equipped with a HPLC. (BDI)ZnN(TMS)₂, the Coates catalyst mentioned above, was chosen for our initial study. Instead of preparing and isolating (BDI)ZnOPyr and (BDI)ZnNHPyr, we tested whether these complexes could be formed *in situ* and subsequently initiate LA polymerization. In the LA polymerization initiated by an equal molar mixture of Pyr-OH and (BDI)ZnN(TMS)₂, 100% consumption of LA was observed. Pyr-OH was not detectable in the polymerization solution after the reaction was complete. In contrast, a similar LA polymerization initiated by an equal molar mixture of Pyr-NH₂ and (BDI)ZnN(TMS)₂ produced no reaction; Pyr-NH₂ remained intact in the reaction solution (ii, Figure 4.1). To further verify the observed chemoselectivity, we used an equal molar mixture of Pyr-NH₂ and Pyr-OH with 1 equiv. (BDI)ZnN(TMS)₂ to initiate a LA polymerization. The polymerization was initiated exclusively by Pyr-OH, whereas Pyr-NH₂ remained intact in the polymerization solution (i, Figure 4.1). This study demonstrated that the (BDI)ZnN(TMS)₂ catalyst had remarkable chemoselectivity and could specifically

coordinate with hydroxyl groups to initiate LA polymerization, regardless the presence or absence of amine groups (Figure 4.1). It also should be noted that Pyr-NH_3^+ , the protonated form of Pyr-NH_2 , behaved similarly to Pyr-NH_2 in this polymerization (data not shown). Pyr-OH can be quantitatively recovered from the Pyr-PLA conjugate, the product of the $\text{Pyr-OH}/(\text{BDI})\text{ZnN}(\text{TMS})_2$ -mediated LA polymerization, by treating Pyr-PLA with NaOH (0.1-1 M) overnight (data not shown). This study suggests that Pyr-OH molecules were linked to PLA termini through ester linkers that were subject to base-induced rapid hydrolysis (Figure 4.1).

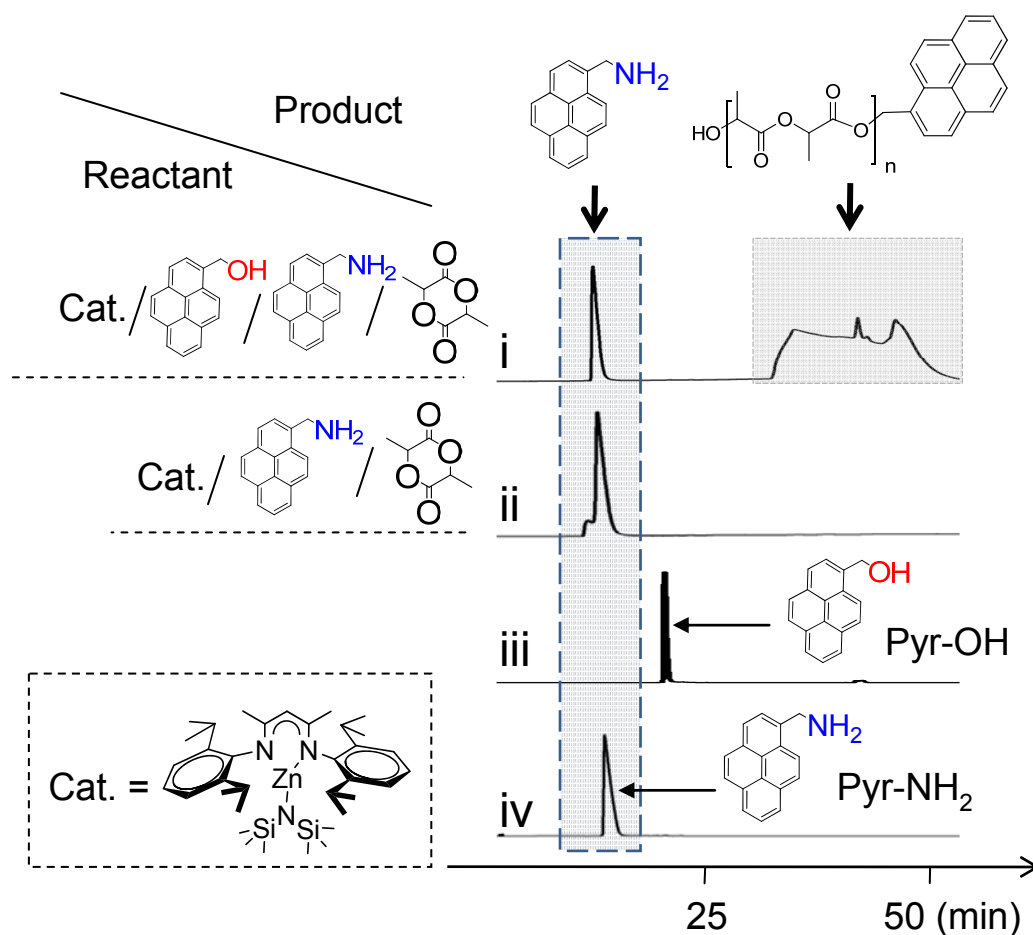


Figure 4.1 Reverse-Phase (RP) HPLC analysis of (i) the mixture of $\text{Pyr-NH}_2/\text{Pyr-OH}$ (1:1 molar ratio), $(\text{BDI})\text{ZnN}(\text{TMS})_2$ (1 equiv.) and LA (25 equiv.); (ii) the mixture of Pyr-NH_2 ,

(Figure 4.1 continued) (BDI)ZnN(TMS)₂ (1 equiv.) and LA (25 equiv.); (iii) Pyr-OH; (iv) Pyr-NH₂. Note: The ill-defined peak of Pyr-PLA in (i) is largely due to the use of the reverse-phase HPLC column that is not suitable for the separation of Pyr-PLA. Substantially improved elution peak was obtained when SEC columns were used for the analysis of Doxo-PLA conjugates.

3.1.2 Chemoselective conjugation of Doxo to PLA

We first studied whether the metal catalyst would decompose Doxo during the initiation step and evaluated the coordination of (BDI)ZnN(TMS)₂ and Doxo without adding LA monomers. From the HPLC and MS analyses, it was evident that Doxo remained in its original form in the presence of the metal catalyst (Figure 4.2). It was thus very unlikely that Doxo would be deleteriously affected during Doxo/(BDI)ZnN(TMS)₂-mediated LA polymerization.

We next used Doxo as the initiator in (BDI)ZnN(TMS)₂-mediated LA polymerization. When 100 equiv. LA was added to a mixture of (BDI)ZnN(TMS)₂ and Doxo, the polymerization was complete within 12 h, with 100% Doxo incorporation efficiency (Figure 4.3a-ii) and 100% LA conversion. After Doxo-LA₁₀₀, the Doxo-PLA conjugate prepared with a LA/Doxo ratio of 100, was treated with 0.1 M NaOH, 88-92% of Doxo was recovered in its original form (Figure 4.3a-iii). Doxo is known to be unstable in NaOH; therefore, it is not surprising that Doxo cannot be recovered quantitatively. This study suggests that Doxo molecules were likely linked to PLA through its hydroxyl group(s) by forming ester linker(s) with PLA and were subject to base-induced rapid hydrolysis. To demonstrate that Doxo was conjugated to PLA, we prepared Doxo-LA₁₀ using Doxo/(BDI)ZnN(TMS)₂-mediated LA polymerization at a

LA/Doxo ratio of 10 and analyzed its end group using MALDI-TOF MS. The MS analysis clearly showed that Doxo was covalently conjugated to PLA (Figure 4.4).

To evaluate whether Doxo can be released from Doxo-PLA in physiological conditions in its original form, we incubated Doxo-LA₁₀ in PBS solution at 30°C for 10 days and then analyzed the solution using HPLC. As shown in Figure 4.3b-ii, a peak with an elution time identical to that of the original Doxo was observed, along with other peaks that were presumed to represent the Doxo-PLA oligomers. The fragment with the same elution time as Doxo was isolated and confirmed to be Doxo by high resolution ESI-MS (Figure 4.3b-iii) and UV spectrometry (Figure 4.5).

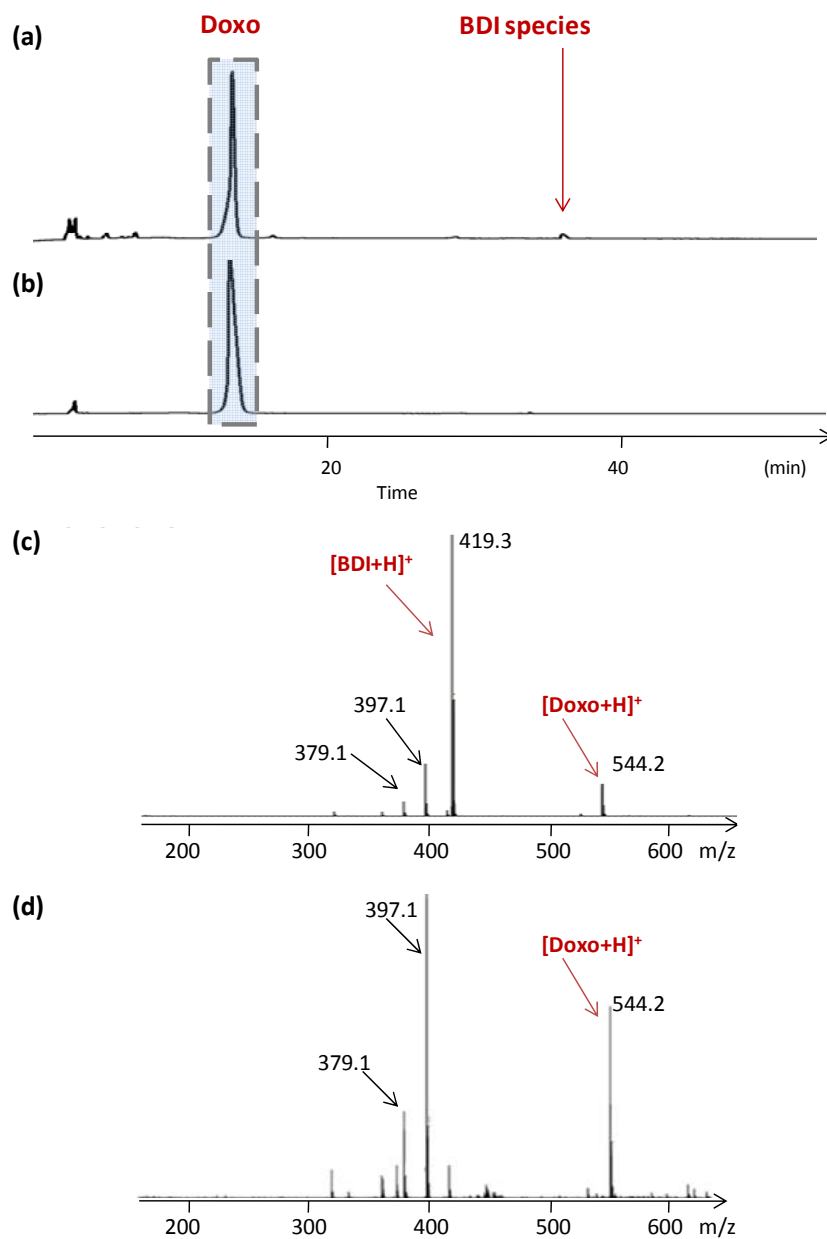


Figure 4.2 HPLC analysis of (a) Doxo treated with (BDI)ZnN(TMS)₂ and (b) Doxo treated without (BDI)ZnN(TMS)₂. ESI-MS analysis of Doxo treated (c) with (BDI)ZnN(TMS)₂ and (d) without (BDI)ZnN(TMS)₂. For (c) Doxo treated with (BDI)ZnN(TMS)₂, MS (HR-ESI): calcd. for C₂₇H₃₀NO₁₁ [M + H]⁺ *m/z* 544.1819, found *m/z* 544.1832. For (d) the Doxo control (Doxo treated without (BDI)ZnN(TMS)₂), MS (HR-ESI): calcd. for C₂₇H₃₀NO₁₁ [M + H]⁺ *m/z* 544.1819, found *m/z* 544.1829.

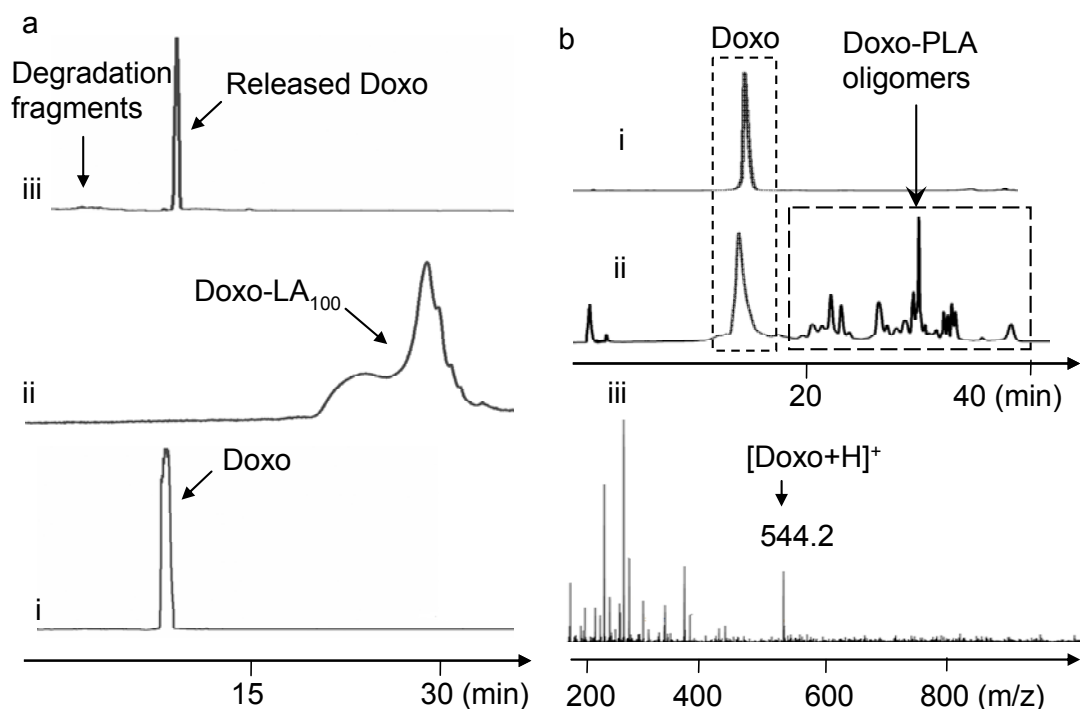


Figure 4.3 (a) RP-HPLC analysis of (i) Doxo, (ii) the polymerization solution of Doxo/(BDI)ZnN(TMS)₂ (1/3 molar ratio) mediated LA polymerization (LA/Doxo = 100), and (iii) Doxo-LA₁₀₀ treated with 1 N NaOH overnight followed by Doxo extraction with chloroform. HPLC analysis was mediated by an analytical pentafluorophenyl column (Curosil-PFP, 250 × 4.6 mm, 5 μ, Phenomenex, Torrance, CA) with acetonitrile/water (0.1% TFA) (50/50) at a flow rate of 1 mL/min. Note: the ill-defined peak of Doxo-LA₁₀₀ in ii is largely due to the use of the reverse-phase HPLC column that is not suitable for the separation of Doxo-LA₁₀₀. Substantially improved elution peak of Doxo-LA₁₀₀ was obtained when SEC columns were used for the analysis of this polymer-drug conjugate. (b) RP-HPLC analysis of (i) free Doxo incubated at 37°C in 1× PBS for 72 h and (ii) Doxo-LA₁₀ incubated in 1× PBS at 37°C for 10 days. (iii) High resolution ESI (HR-ESI) MS analysis of the fraction in (Figure 4.3b-ii) that has the identical elution time as the authentic Doxo and was isolated using RP-HPLC. HPLC analysis and Doxo separation were mediated by an analytical RP-HPLC column (Luna C18, 250 × 4.6 mm, 5 μ, Phenomenex, Torrance, CA) with acetonitrile/water (0.1% TFA) (50/50) at a flow rate of 1 mL/min. MS (HR-ESI): calcd. C₂₇H₃₀NO₁₁ [M + H]⁺ *m/z* 544.1819, found *m/z* 544.1827.

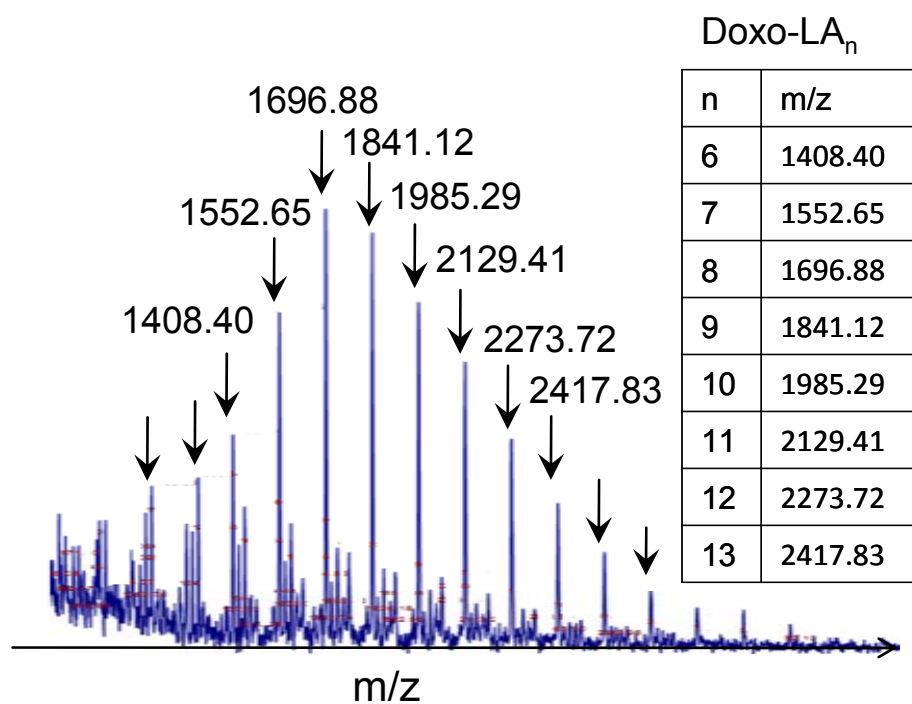


Figure 4.4 MALDI-TOF MS analysis of Doxo-LA₁₀. The obtained m/z is identical to the calculated m/z of Doxo-LA_n ($543.52 + 144.13 \times n$). $M_w = 2.0 \times 10^3$ g/mol, $M_n = 1.7 \times 10^3$ g/mol, PDI = 1.17 (determined by MALDI-TOF MS)

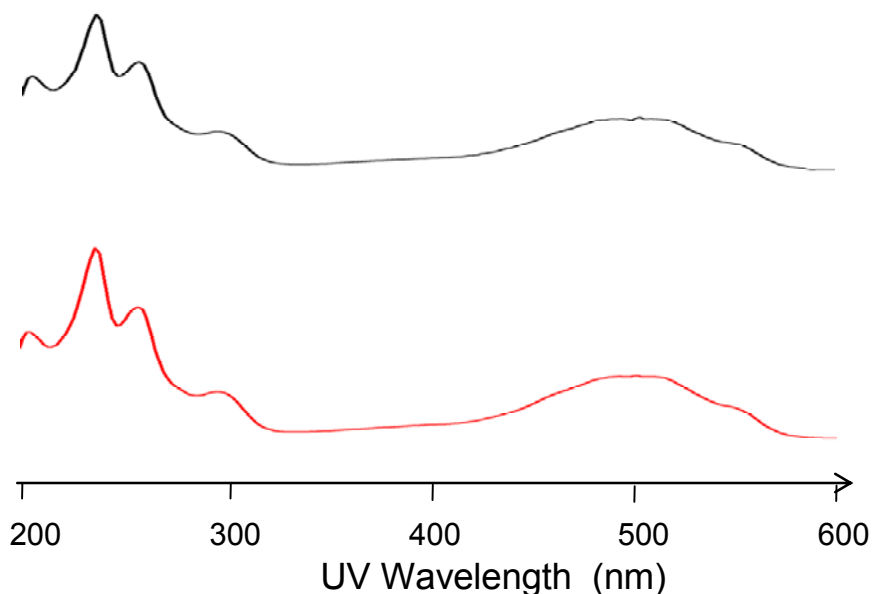


Figure 4.5 HPLC analysis of the authentic Doxo (red trace) and the Doxo released from Doxo-LA₁₀ after incubation in 1× PBS at 37°C for 10 days (black trace). The spectra were recorded on a System Gold 128 UV detector between 200 and 600 nm (Beckman Coulter, Fullerton, CA).

3.1.3 *Effects of metals and ligands on regioselective conjugation of Doxo to PLA*

Doxo has three hydroxyl groups at its C4', C9 and C14 positions. Theoretically, LA polymerization can be initiated by any or all of these hydroxyl groups of Doxo. In the latter case, a lack of control over regioselective initiation will result in Doxo-PLA conjugates with heterogeneous structures. We next studied whether the initiation could be specifically controlled at one of the three hydroxyl groups of Doxo. Previous studies have indicated that the C14-OH of Doxo is most sterically accessible.⁷³ Due to the steric bulk of BDI, the catalyst likely forms an alkoxide complex with Doxo preferentially with its C14-OH, rather than with the more sterically hindered C4'- or the most sterically hindered C9-OH, to facilitate regioselective initiation and polymerization.

To evaluate the initiation regioselectivity, we mixed Doxo/(BDI)ZnN(TMS)₂ with succinic anhydride (SA) to mimic the initiation step of the Doxo/(BDI)ZnN(TMS)₂-mediated LA polymerization and characterized the reaction mixture by MS (Figure 4.6) and NMR (Figure 4.7). As expected, Doxo-14-succinic ester (Doxo-SE) was the predominate product (Figure 4.6a and Figure 4.7). The chemical signal of the C14-H (peak g, Figure 4.7b and 4.7c) was shifted downfield by 0.69 ppm (from 4.59 ppm to 5.28 ppm), while the peaks corresponding to the C4'-H and C3'-H remained nearly unchanged (peak i and e, respectively, Figure 4.7b and 4.7c). It was thus evident that the SA ring was opened by the C14-OH of Doxo rather than by the C4'-OH or C3'-NH₂ of Doxo. C9-OH is the most sterically hindered and is thus unlikely to initiate polymerization. When (BDI)ZnN(TMS)₂ was replaced by (BDI')ZnN(TMS)₂, a catalyst with a structure similar to (BDI)ZnN(TMS)₂ but having a less bulky diimine ligand (Figure 4.6b), the formation of Doxo-4', 14-bissuccinic ester (Doxo-2SE) was identified in conjunction with Doxo-SE (Figure 4.6b). When (BDI)ZnN(TMS)₂ was replaced by Zn(N(TMS)₂)₂, a Zn catalyst without ligands, the initiation regioselectivity completely disappeared. Doxo-4', 14-bissuccinic ester (Doxo-2SE) and Doxo-4', 9, 14-trisuccinic ester (Doxo-3SE) were the predominant products (Figure 4.6c). Interestingly, the metal activity also had a profound effect on regioselectivity. When (BDI)MgN(TMS)₂ (which is more active than its Zn analogue) was used in a similar reaction, the formation of Doxo-2SE was also identified in conjunction with Doxo-SE (Figure 4.6d). Thus, by rationally designing ROP metal catalysts, Doxo-PLA conjugates with highly controlled regio- and chemoselectivity are achievable within one step without the need to protect the C3'-NH₂ and other competing hydroxyl groups of Doxo.

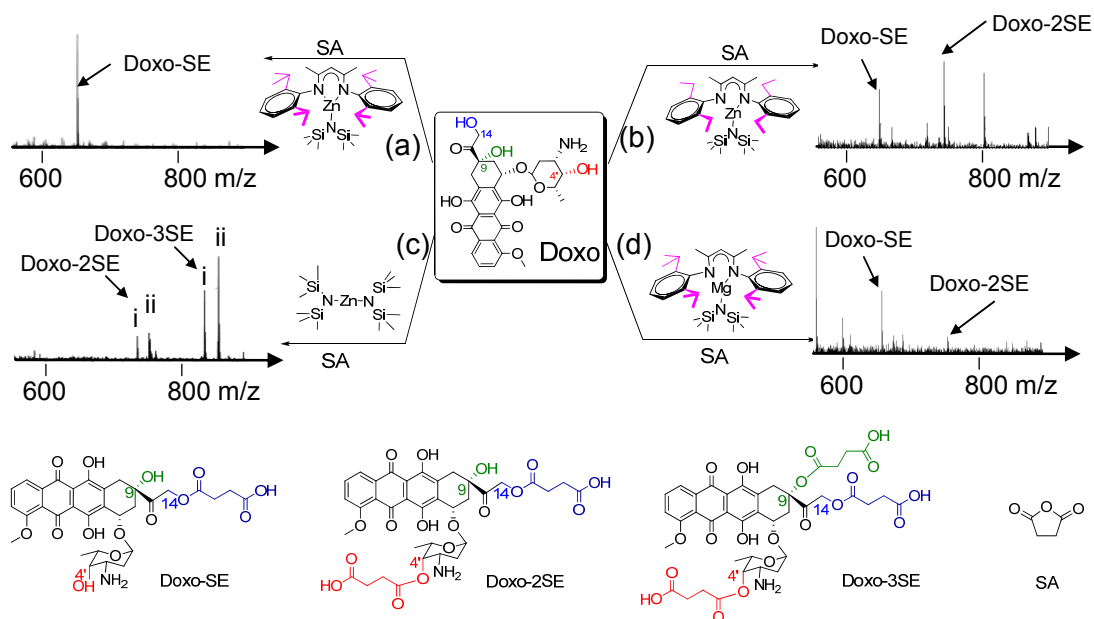
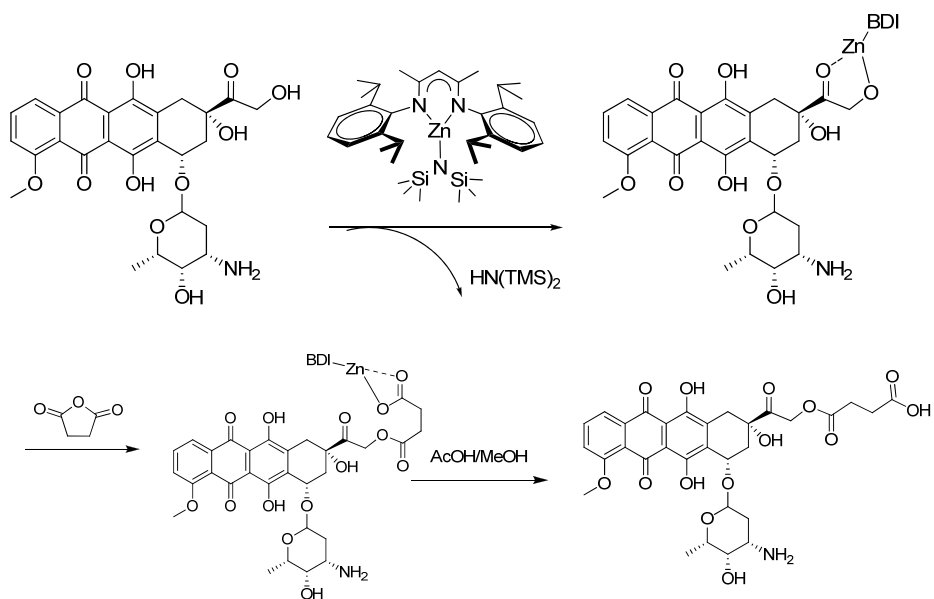
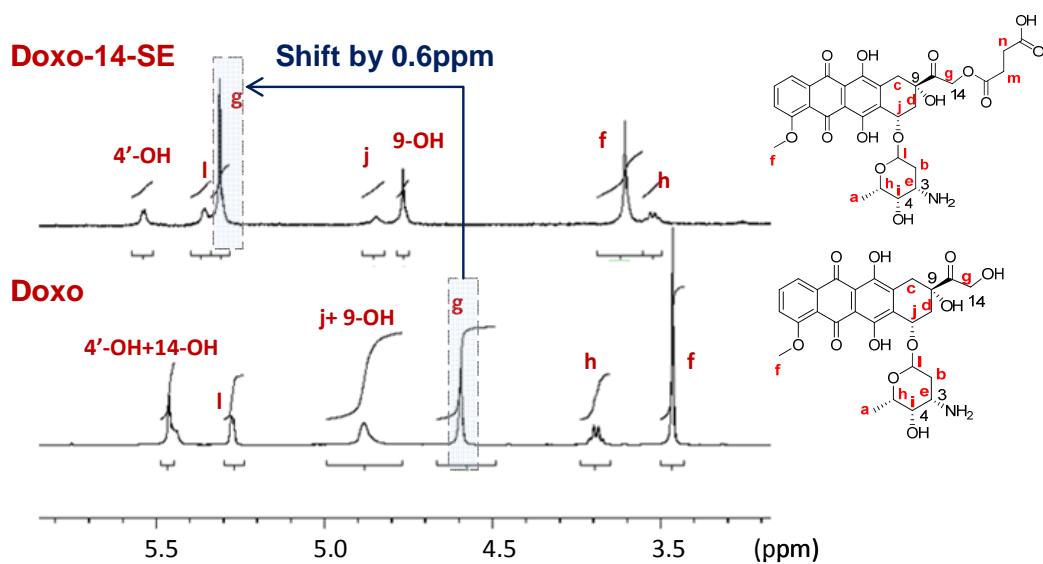


Figure 4.6 MS analysis of the mixture of (a) Doxo, 1 eq. (BDI)ZnN(TMS)₂ and 3 equiv. SA, (b) Doxo, 1 equiv. (BDI')ZnN(TMS)₂ and 3 equiv. SA, (c) Doxo, 1 eq. Zn(N(TMS)₂)₂ and 3 equiv. SA, and (d) Doxo, 1 eq. (BDI)MgN(TMS)₂ and 3 eq. SA. Peak assignment: (a) Doxo-SE: ($M_{\text{Doxo-SE}} + \text{H}$) 644.3; (b) Doxo-SE: ($M_{\text{Doxo-SE}} + \text{H}$) 644.3; Doxo-2SE: ($M_{\text{Doxo-2SE}} + \text{H}$) 744.2; (c) Doxo-2SE: (i = ($M_{\text{Doxo-2SE}} + \text{H}$) 744.3, ii = ($M_{\text{Doxo-2SE}} + \text{NH}_4$) 759.7; Doxo-3SE: (i = ($M_{\text{Doxo-3SE}} + \text{H}$) 842.3, ii = ($M_{\text{Doxo-3SE}} + \text{Na}$) 863.3); (d) Doxo-SE: ($M_{\text{Doxo-SE}} + \text{H}$) 644.3; Doxo-2SE: ($M_{\text{Doxo-2SE}} + \text{H}$) 744.3.

a)



b)



(c) Chemical Shift

δ	a	b	c	d	e	f	g	h	i	j	m	n
Doxo	1.16	1.68, 1.90	2.82, 2.95	2.08, 2.18	3.34	3.96	4.59	4.19	3.61	4.88	/	/
Doxo-14-SE	1.1	1.80-2.10	2.90, 3.05	2.00-2.20	3.38	4.11	5.28	4.09	3.49	4.76	2.35	2.62

(Figure 4.7, continue on page 96)

(Figure 4.7 continued)

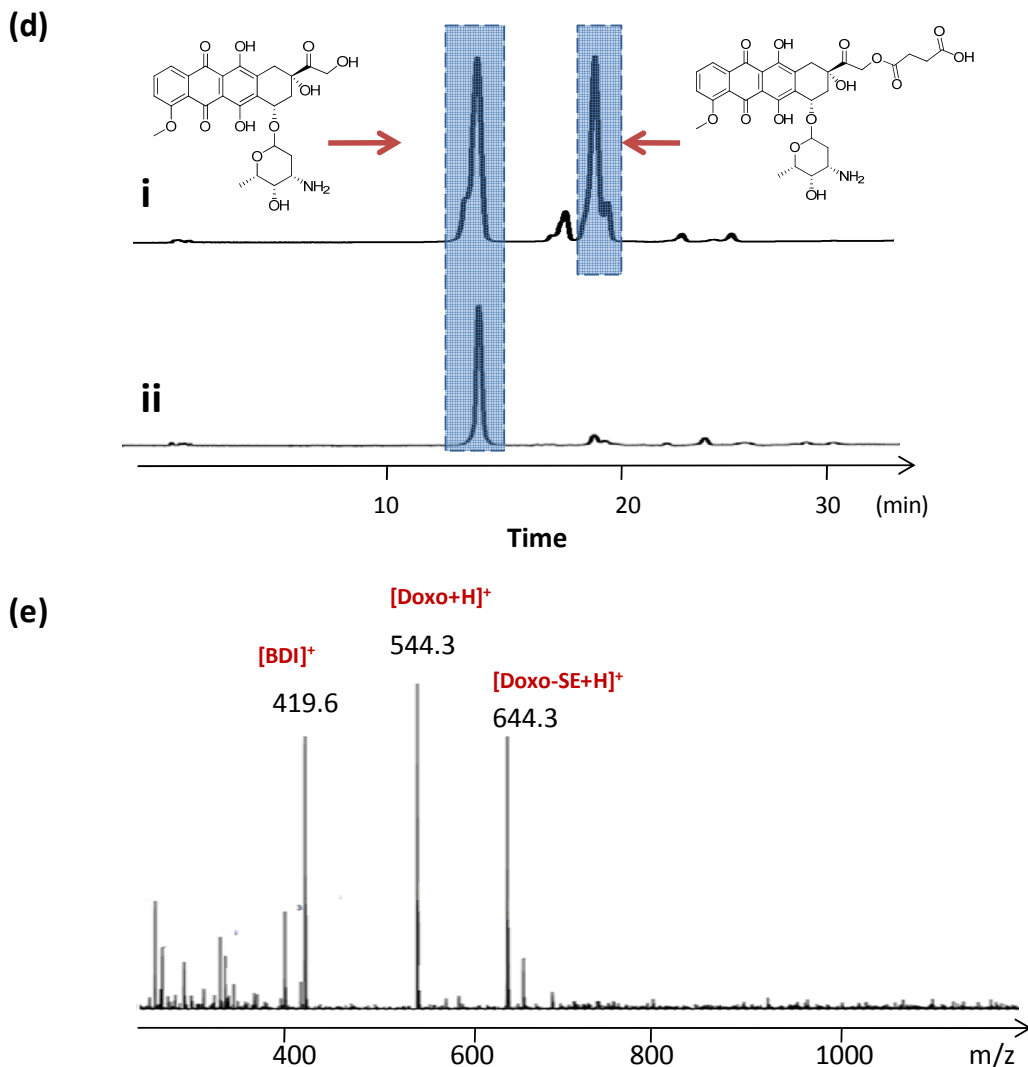


Figure 4.7 (a) Schematic illustration of the anticipated ring opening of succinic anhydride (SA) by the C14-OH of Doxo when SA was treated with Doxo/(BDI)ZnN(TMS)₂. (b) ¹H NMR analysis (DMSO-d₆) of Doxo and Doxo-succinic ester (Doxo-SE) to confirm the attachment of SE to the C14-OH of Doxo and formation of Doxo-SE. (c) ¹H NMR chemical shifts of Doxo and Doxo-SE. (d) HPLC analysis of (i) the reaction mixture of SA (1 equiv.) and Doxo/(BDI)ZnN(TMS)₂ (1/1.2 molar ratio) and (ii) Doxo-SE incubated in 1× PBS solution at 37°C for 48 h. (e) ESI-MS analysis of the compound derived from the reaction of SA with Doxo/(BDI)ZnN(TMS)₂ (i). The high resolution ESI-MS analysis of Doxo-SE was performed on

a Micromass Q-TOF Ultima system. MS (HR-ES): calcd. for $C_{31}H_{34}NO_{14}$ $[M + H]^+$ m/z 644.1979; found m/z 644.1987.

3.1.4 Metal and ligand effects on Doxo-PLA molecular weight

We next studied Doxo-initiated LA polymerization in the presence of these metal catalysts. Doxo/(BDI)ZnN(TMS)₂-mediated LA polymerization resulted in Doxo-PLA with low polydispersities (M_w/M_n less than 1.2) and the expected molecular weights (MWs) by adjusting the LA/Doxo feeding ratios (Table 4.1 and Figure 4.8a). For example, Doxo/(BDI)ZnN(TMS)₂-mediated LA polymerization at a M/I ratio of 200 resulted in Doxo-LA₂₀₀ with a polydispersity as low as 1.02 (Table 4.1). The obtained M_n of Doxo-LA₂₀₀ (3.38×10^4 g/mol) was close to the expected M_n (2.93×10^4 g/mol). A similar Doxo/(BDI)MgN(TMS)₂-mediated polymerization also produced Doxo-LA₂₀₀ with well-controlled MW ($M_n = 3.12 \times 10^4$ g/mol). Nonetheless, a much higher polydispersity ($M_w/M_n = 1.50$) was observed, which was attributed presumably to the poorly controlled regioselectivity during initiation (Figure 4.8d), slow initiation relative to chain propagation and potential trans-esterification side reactions. In general, Zn-alkoxides undergo slightly slower but better controlled polymerization reactions, as compared with their Mg analogues (Figure 4.8a-b).^{61,75} (BDI')ZnN(TMS)₂, the Zn catalyst with a less bulky diimine ligand, also resulted in Doxo-LA₂₀₀ with relatively high polydispersity (Table 4.1). These observations were in good agreement with the observed initiation regioselectivity of the corresponding Doxo/catalyst complexes for the ring openings of SA (Figure 4.6).

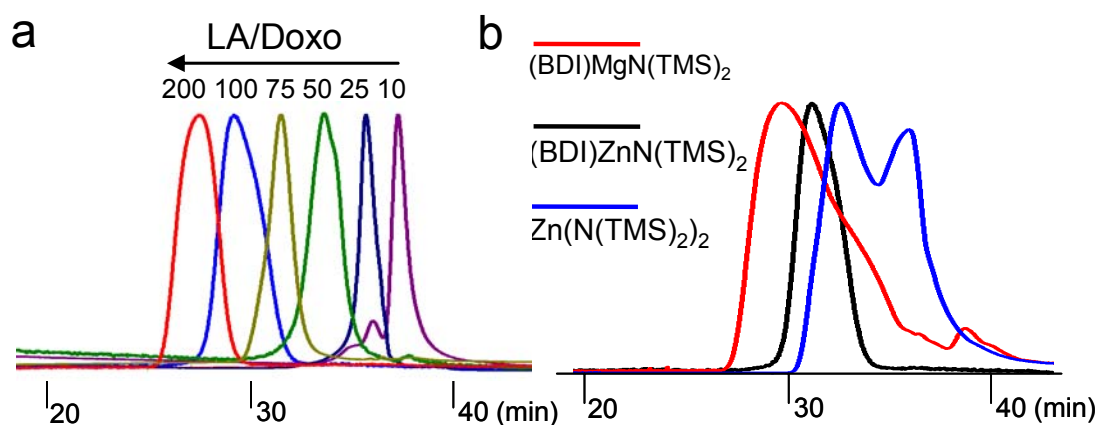
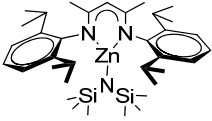
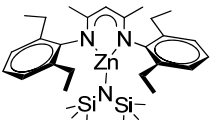
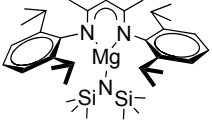


Figure 4.8. (a) SEC (equipped with a UV detector) analysis of Doxo- LA_n ($n = \text{LA/Doxo (M/I)}$) prepared through Doxo/ $(\text{BDI})\text{ZnN}(\text{TMS})_2$ mediated LA polymerizations at LA/Doxo ratios of 10, 25, 50, 75, 100 and 200, respectively; Note: Polymerizations at LA/Doxo ratio of 25, 50, 75, 100 and 200 resulted in corresponding Doxo-PLAs with monomodal SEC distribution patterns. Polymerization at a LA/Doxo ratio of 10, however, resulted in Doxo- LA_{10} with a multimodal SEC distribution pattern, which indicated that polymerization at such a low M/I ratio may not be as well controlled as similar polymerizations at higher M/I ratios. (b) SEC (equipped with a UV detector) analysis of the Doxo- LA_{100} prepared through Doxo/ $(\text{BDI})\text{ZnN}(\text{TMS})_2$, Doxo/ $(\text{BDI})\text{MgN}(\text{TMS})_2$, and Doxo/ $\text{Zn}(\text{N}(\text{TMS})_2)_2$ mediated LA polymerizations at a LA/Doxo ratio of 100.

Table 4.1 Polymerization of LA initiated by the complex of Doxo with (BDI)ZnN(TMS)₂, (BDI')ZnN(TMS)₂, or (BDI)MgN(TMS)₂

Catalyst	LA/Doxo (M/l)	Expected M_n (x 10 ³ g/mol)	Obtained M_n (x 10 ³ g/mol)	Obtained M_w (x 10 ³ g/mol)	M_w/M_n
 (BDI)ZnN(TMS) ₂	10 ^a	2.0	1.7	2.0	1.17
	25	4.1	ND	ND	ND
	50 ^b	7.7	6.3	7.4	1.18
	75 ^b	11.3	12.7	13.6	1.07
	100 ^b	14.9	18.3	19.8	1.08
	200 ^b	29.3	33.8	34.5	1.02
 (BDI')ZnN(TMS) ₂	200 ^b	29.3	25.4	33.8	1.33
 (BDI)MgN(TMS) ₂	200 ^b	29.3	31.2	46.8	1.50

^a MW determined by MALDI-TOF MS (see Figure 4.4). ^b MW determined by SEC (See Figure 4.8a). Note: The MW of Doxo-LA₂₅ was too high to be analyzed by MALDI-TOF MS and too low to be determined by SEC equipped with a multi-angle static light scattering detector. However, the SEC distribution pattern of Doxo-LA₂₅ collected on a UV detector was monomodal and very similar as those of Doxo-LA₅₀₋₂₀₀. Therefore, it is very likely that the Doxo-LA₂₅ also had the expected M_n and low polydispersity. ND = Not Determined.

3.1.5 Doxo-PLA conjugated nanoparticle

Due to the excellent control over the Doxo-PLA structure and composition, NPs derived from these materials have well-controlled formulation parameters, which could potentially impact their *in vivo* performance and clinical translation. Doxo-PLA

conjugated nanoparticles, termed nanoconjugates (NCs) in this paper to differentiate them from NPs prepared from the co-precipitation of drugs and polymers, were readily prepared through the nanoprecipitation of Doxo-PLA conjugates (Table 4.1e). NCs less than 100 nm in size with narrow, monomodal particle distributions were readily obtained (Table 4.2 and Figure 4.9), similar to the results that we reported previously for paclitaxel-PLA NCs.⁶⁵ The narrow size distributions of the NCs were in sharp contrast to the multimodal particle distributions frequently observed in conventional NPs prepared by co-precipitating polymers and drugs. It is not clear why NCs derived from nanoprecipitation have such narrow size distributions. The multimodal particle distributions in conventional NPs have been attributed in part to the self-aggregation of non-encapsulated drugs, and thus, the unimolecular structure of polymer-drug conjugates with reduced heterogeneities (low polymer polydispersities, the controlled site of conjugation on both polymer and Doxo and the absence of free Doxo) may contribute in part to the formation of NCs with low particle polydispersities (Table 4.2).

The surface compositions of Doxo-PLA NCs are unclear. Because the daunosamine sugar moiety of Doxo is hydrophilic, it is likely that Doxo molecules reside on or close to the surface of Doxo-PLA NCs and are subject to rapid release after the ester linkers between Doxo and PLA are hydrolyzed. The size of Doxo-PLA NCs can be fine-tuned within a range of 50-150 nm by adjusting the Doxo-PLA concentration in water-miscible organic solvents or by varying the types of water-miscible solvents present during nanoprecipitation. For instance, NCs prepared using DMF as solvent are typically 20-30 nm smaller than those prepared using THF or acetone as solvent, following the same trend that we observed previously in our study of docetaxel/poly(lactide-co-glycolide) nanoprecipitation. We will report a comprehensive

study of NC formulation, in particular for the control of NC sizes and formulation of NCs in solid form, in a separate paper.

Because both the monomer conversion and drug incorporation were nearly quantitative (Table 4.2), Doxo loadings in Doxo-PLA NCs could thus be predetermined by adjusting the LA/Doxo feeding ratios. At a low M/I ratio of 10, the drug loading was as high as 27.4% (Doxo-LA₁₀, Table 4.2). To our knowledge, this is by far the highest loading ever reported in Doxo-containing polymeric NPs. Even at this high drug loading, sustained release of Doxo from Doxo-LA₁₀ NC was observed through the hydrolysis of the ester linker connecting the Doxo and the PLA (Figure 4.10a). No burst release of Doxo was observed in Doxo-LA₁₀. This observation was in sharp contrast to the burst release of PLA/Doxo NP prepared by co-precipitation (Figure 4.10a), in which Doxo release depended entirely on diffusion and over 90% was released within 3 hours. The HPLC elution time and the MS spectrum of the Doxo released in PBS were identical to those of authentic Doxo, similar to the results we observed in the separate study mentioned above (Figure 4.2b). The MTT studies revealed that the toxicity of Doxo-PLA NC, which is directly related to the release kinetics of Doxo, could be tuned by adjusting the Doxo loading in the NCs (Figure 4.10b). In general, NCs with higher Doxo loadings released Doxo more rapidly (Figure 4.10a) and, therefore, showed higher toxicities (Figure 4.10b). This observation is presumably due to the fact that the NCs derived from the nanoprecipitation of higher loading (lower MW) Doxo-PLA conjugates have more loosely packed structures, as compared to NCs derived from the lower loading (higher MW) Doxo-PLA conjugates. Therefore, the ester linkers between Doxo and PLA in NCs with higher drug loadings were more accessible to the aqueous phase and were subject to faster hydrolysis.

Doxo has amine and multiple hydroxyl groups; it is therefore highly water soluble in its protonated form (10 mg/mL). Due to its high hydrophilicity, the encapsulation of Doxo in hydrophobic polymer can be very difficult. For instance, Yoo et al. reported a Doxo loading of 0.51% and a loading efficiency of 23% for micelles formed by co-precipitating Doxo and poly(DL-lactic-co-glycolic acid)-*b*-poly(ethylene glycol) (PLGA-PEG).^[2] Doxo loadings of 0.6-8.7% and loading efficiencies of 11.4-43.6% were also reported by Hubbell and co-workers in their studies of encapsulating non-protonated Doxo (which has increased hydrophobicity) into polymeric NPs using inverse emulsion polymerization.^[12] The unencapsulated Doxo has to be removed from the NPs by column separation. Burst releases of Doxo were reported in both systems.

The Doxo-initiated ring-opening polymerization method that we have developed allows for the controlled incorporation of Doxo to PLA with drug loadings as high as 30% and up to 100% loading efficiency (Table 4.2). The Doxo-PLA NCs derived from this Doxo-initiated ROP technique followed by nanoprecipitation exhibit controlled release kinetics without any burst release effects and a precisely controlled Doxo-PLA structure. This unique formulation technique allows for the formation of Doxo-containing PLA NCs with well-controlled formulation parameters.

Table 4.2 Doxo/(BDI)ZnN(TMS)₂ Initiated LA Polymerization followed by nanoprecipitation to form NC^a

M/I	LD(%)	CV(%)	IE(%)	NC ^b	NC size ± SD (nm)	PD ± SD
100	3.6	>99	>99	Doxo-LA ₁₀₀	79.1 ± 0.7	0.08 ± 0.01
50	7.1	>99	>99	Doxo-LA ₅₀	101.6 ± 0.7	0.07 ± 0.01
25	13.1	>99	98	Doxo-LA ₂₅	90.8 ± 0.9	0.09 ± 0.01
10 ^c	27.4	>99	94	Doxo-LA ₁₀	125.2 ± 2.3	0.11 ± 0.01

^aAbbreviations: M/I = LA/Doxo ratio; LD = Doxo loading in wt%; CV = conversion of LA; IE = incorporation efficiency of Doxo; SD = standard deviation; PD = polydispersity of NC. ^bNCs are denoted by Doxo-LA_{M/I ratio}. ^cPrepared with (BDI)MgN(TMS)₂

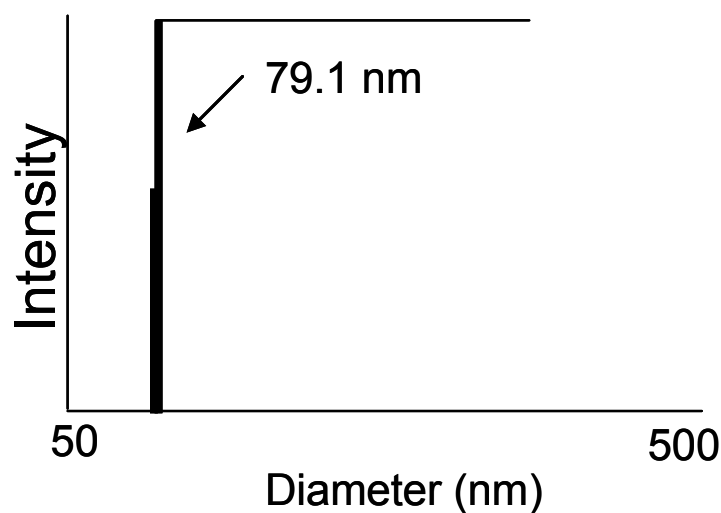


Figure 4.9 Analysis of Doxo-LA₁₀₀ NC using dynamic light scattering. Doxo-LA₁₀₀ was prepared using (BDI)ZnN(TMS)₂ by following the standard procedure as described in the experimental section.

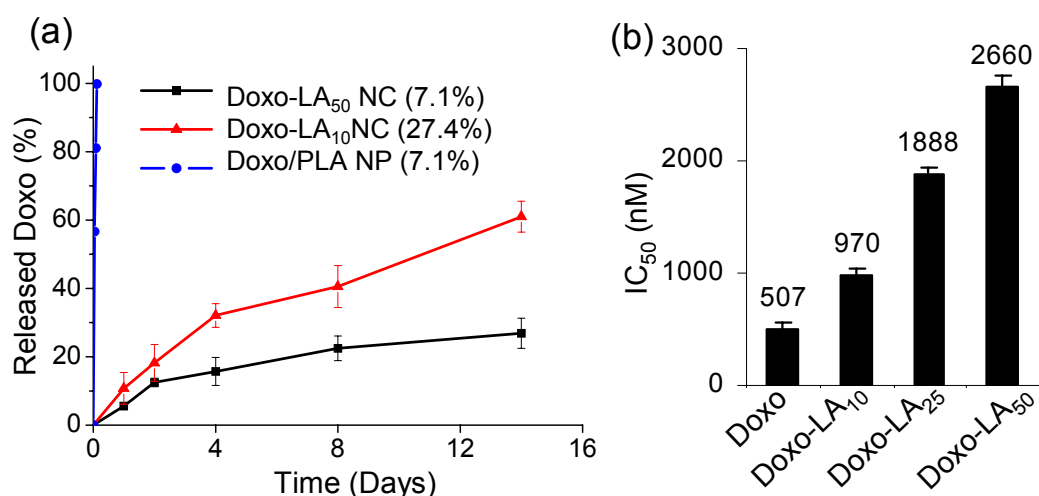


Figure 4.10 (a) Release of Doxo from Doxo-LA₅₀ NC, Doxo-LA₁₀ NC and Doxo/PLA NP ((Doxo/PLA (wt/wt) = 1/13), ~7.1 wt% theoretical drug loading) prepared by co-precipitation of Doxo and PLA (MW = 15,000 g/mol) at 37°C in 1× PBS. Doxo-LA₁₀ and Doxo-LA₅₀ were prepared using (BDI)ZnN(TMS)₂ by following the standard procedure as described in the experimental section. (b) MTT assay for the analysis of cytotoxicity of Doxo-PLA NCs in PC-3 cells.

3.2 Nanoconjugates incorporating other drugs

To demonstrate that this technique can be broadly applied to the formation of NCs with agents that contain hydroxyl groups, we tested the capabilities of Cyanine 5 (Cy5), camptothecin (CPT), docetaxel (Dtxl) and cyclopamine (Cpa) to initiate LA polymerization in the presence of Zn or Mg catalysts. All of the therapeutic (Dtxl, CPT, Cpa) and dye (Cy5) molecules tested, when mixed with (BDI)ZnN(TMS)₂, initiated LA polymerization similar to that observed with Doxo, with nearly quantitative incorporation efficiencies and 100% LA conversions (Table 4.3). NCs with adjustable loadings (achieved by controlling the LA/drug (or dye) ratio) and low polydispersities were readily

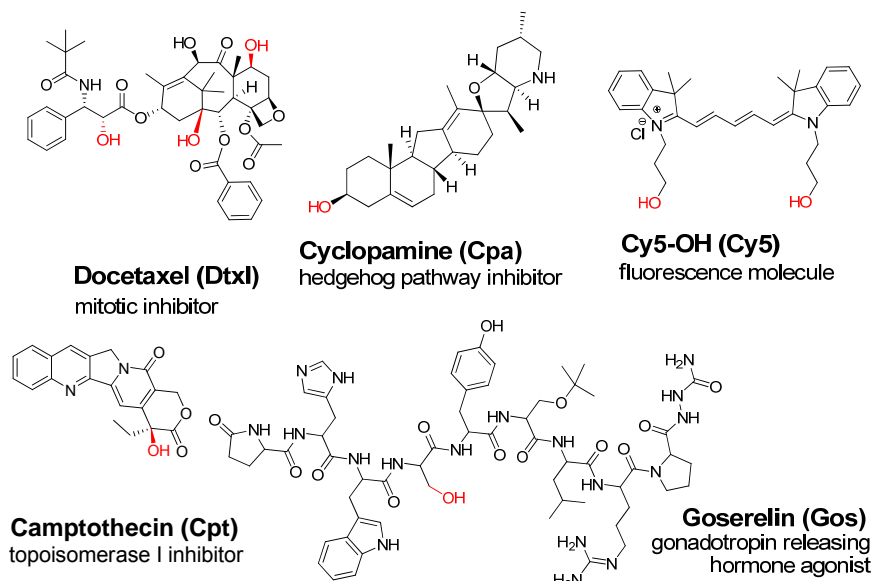
obtained (Table 4.3). Surprisingly, oligopeptides can even be used as initiators in Zn-catalyst-mediated LA polymerization. Goserelin (Gos), a luteinizing hormone-releasing hormone agonist,^[13] initiated the successful ROP of LA in DMF. The resulting Gos-PLA conjugates and corresponding NCs could be prepared with extremely high drug loadings (>50%) at low LA/Gos ratios and very low polydispersities (Table 3). Gos was recovered quantitatively through base treatment of Gos-PLA conjugates.

Table 4.3 Dtxl-LA_n polymerization mediated by (BDI-1)ZnN(TMS)₂

Entry	[M]/[I]	Conv. (%) ^b	M _{cal} (kg/mol)	M _n (kg/mol) ^c	PDI (M _w /M _n) ^c
1	75	>99%	11.6	8.9	1.05
2	100	>99%	15.2	13.6	1.04
3	200	>99%	29.6	25.2	1.03
4	300	>99%	44.0	47.1	1.04
5	400	>99%	58.4	55.3	1.13

^a All reactions were performed in anhydrous THF with [LA]= 0.69 M at room temperature for 12 hours. Abbreviation: LA: lactide; Dtxl: Docetaxel; Conv. %: conversion of LA %; M_{cal}: calculated molecular weight; M_n: number average molecular weight; PDI: polydispersity index ^b The conversion of LA was measured by FT-IR, monitoring the disappearance of LA peak at 1772 cm⁻¹. ^c Determined by gel permeation chromatography (GPC).

Table 4.4 Formulation of NCs with Hydroxyl-Containing Therapeutic and Dye Molecules



Substrate	M/I	NCs ^b	Loadin g (%)	LA Conv. (%) ^c	Incorp. Eff. (%) ^d	NC size ± SD (nm) ^e	PDI ± Sd ^e
Dtxl	25	Dtxl-LA ₂₅	18.3	>99	>99	64.5 ± 0.7	0.05 ± 0.02
Dtxl	10	Dtxl-LA ₁₀	35.9	>99	97	77.9 ± 1.5	0.06 ± 0.02
Cpa	100	Cpa-LA ₁₀₀	2.8	>99	>99	89.9 ± 1.8	0.04 ± 0.01
Cpa	50	Cpa-LA ₅₀	5.4	>99	>99	78.0 ± 2.7	0.12 ± 0.01
Cy5	100	Cy5-LA ₁₀₀	3.4	>99	98	95.1 ± 0.6	0.04 ± 0.02
Cy5	25	Cy5-LA ₂₅	12.3	>99	95	76.3 ± 3.8	0.06 ± 0.01
CPT	100	CPT-LA ₁₀₀	2.4	>99	>99	68.3 ± 0.8	0.08 ± 0.02
CPT	25	CPT-LA ₂₅	8.8	>99	96	76.6 ± 0.9	0.09 ± 0.01
Gos	100	Gos-LA ₁₀₀	8.1	>99	90	97.6 ± 2.3	0.05 ± 0.02
Gos	10	Gos-LA ₁₀	46.8	>99	81	120.6 ± 2.7	0.01 ± 0.01

^aAbbreviations: M/I = monomer/initiator ratio, NC = nanoconjugates, LA Conv. = lactide conversion, Incorp. Eff. = incorporation efficiency, SD = standard deviation, PDI = polydispersity, Dtxl = docetaxel, Cpa = cyclopamine, Cy5 = cyanine 5, CPT = camptothecin, Gos = goserelin. ^bNCs are named as drug(or dye)-LA_n where n is the ratio of [LA] to [agent] ^cDetermined by analyzing unreacted lactide using FTIR (1772 cm⁻¹); ^dBased on RP-HPLC analysis of free molecules. We use incorporation efficiency instead of encapsulation efficiency because drug molecules are conjugated to, not encapsulated in PLA. ^eDetermined by dynamic light scattering.

4. Conclusions

Preparations of Doxo-polymer conjugates with controlled loadings and release profiles have been previously reported using conventional coupling chemistry.^{17,54,55,62,86} In this paper, we report a unique conjugation method accomplished via Doxo-initiated ROPs. This ROP-mediated Doxo conjugation method allows for facile regio- and chemoselective incorporation of Doxo into PLA and allows for the formation of PLA-Doxo conjugates with low polydispersity, pre-determined drug loadings (up to $\approx 30\%$) and quantitative loading efficiencies. The BDI-metal chelating complexes do not have deleterious effects on Doxo and can be easily removed by solvent extraction. Because both Zn and Mg ions are biocompatible (as key elements in our dietary mineral supplements), there should not be significant safety concerns regarding the use of these two metal catalysts for the ROP and formulation of NCs for potential clinical applications. The multi-gram scale of PLA conjugates can be readily prepared within hours using this one-pot polymerization approach. Because drug molecules are covalently conjugated to PLA, the post-reaction formulation process (precipitation, removal of catalysts, nanoprecipitation, sterilization, lyophilization, shipping and handling, etc.) can be much more readily handled with a minimum change of sample property, as compared to drug/polymer NPs prepared via encapsulation methods. This polymerization-mediated conjugation method may be utilized for the formulation of polymer-drug conjugates, not only for drug delivery but also for other controlled release applications (scaffolds, coatings of stents, etc). Other cyclic esters (e.g., ϵ -caprolactone and β -valerolactone) are likely to replace LA and find use as monomers in such drug-initiated polymerizations. The Doxo/(BDI)ZnN(TMS)₂-initiated polymerization of these cyclic esters at room temperature has recently been achieved in our laboratory, which will

provide further tunability of the release profiles and other physicochemical properties. Given that the lack of a controlled formulation for nanoparticulate drug delivery vehicles is one of the bottlenecks to their clinical development, this unique, ROP-mediated conjugation methodology may contribute to the development of clinically applicable nanomedicines.

5. References

- [1] S. Sengupta, D. Eavarone, I. Capila, G. L. Zhao, N. Watson, T. Kiziltepe, R. Sasisekharan, *Nature* **2005**, *436* 568-572.
- [2] H. S. Yoo, K. H. Lee, J. E. Oh, T. G. Park, *J.Control.Release* **2000**, *68* 419-431.
- [3] F. Kratz, U. Beyer, M. T. Schutte, *Critical Reviews in Therapeutic Drug Carrier Systems* **1999**, *16* 245-288.
- [4] K. Ulbrich, V. Subr, *Advanced Drug Delivery Reviews* **2004**, *56* 1023-1050.
- [5] R. S. Greenfield, T. Kaneko, A. Daues, M. A. Edson, K. A. Fitzgerald, L. J. Olech, J. A. Grattan, G. L. Spitalny, G. R. Braslawsky, *Cancer Research* **1990**, *50* 6600-6607.
- [6] T. Kaneko, D. Willner, I. Monkovic, J. O. Knipe, G. R. Braslawsky, R. S. Greenfield, D. M. Vyas, *Bioconjugate Chemistry* **1991**, *2* 133-141.
- [7] C. C. Lee, E. R. Gillies, M. E. Fox, S. J. Guillaudeu, J. M. J. Frechet, E. E. Dy, F. C. Szoka, *P Natl Acad Sci USA P Natl Acad Sci USA* **2006**, *103* 16649-16654.
- [8] N. Nishiyama, Y. Morimoto, W. D. Jang, K. Kataoka, *Adv Drug Deliver Rev* **2009**, *61* 327-338.
- [9] J. C. Florent, C. Monneret, *Anthracycline Chemistry and Biology Ii: Mode of Action, Clinical Aspects and New Drugs* **2008**, *283* 99-140.
- [10] D. H. Altreuter, J. S. Dordick, D. S. Clark, *Journal of the American Chemical Society* **2002**, *124* 1871-1876.
- [11] F. Meyer-Losic, J. Quinonero, V. Dubois, B. Alluis, M. Dechambre, M. Michel, F. Cailler, A. M. Fernandez, A. Trouet, J. Kearsy, *Journal of Medicinal Chemistry* **2006**, *49* 6908-6916.
- [12] D. Missirlis, R. Kawamura, N. Tirelli, J. A. Hubbell, *Eur.J.Pharm.Sci.* **2006**, *29* 120-129.

- [13] S. S. Dharap, Y. Wang, P. Chandna, J. J. Khandare, B. Qiu, S. Gunaseelan, P. J. Sinko, S. Stein, A. Farmanfarmaian, T. Minko, *Proceedings of the National Academy of Sciences of the United States of America* **2005**, 102 12962-12967.

CHAPTER 5

NANOCONJUGATES: FORMULATION AND PRELIMINARY *IN VIVO* STUDY

1. Introduction

Polymeric nanoparticles (NPs) are attractive drug delivery vehicles ^[1]. They have been employed for the delivery of many types of chemotherapeutic agents for cancer treatment ^[2]. In these polymeric NPs, chemotherapeutic agents are either encapsulated in polymer matrices ^[3] or covalently conjugated to polymers via hydrolysable or enzymatically degradable linkages. Ideally, systemically administered NPs are able to bypass the recognition of the reticuloendothelial system (RES), extravasate at the leaky tumor vasculatures ^[2b], penetrate and homogeneously distribute in solid tumor tissues ^[4], get internalized by the target cancer cells, penetrate cellular and subcellular membranes, and then release the payload in the cytoplasm of the target cancer cells in a sustained manner.

NPs that can successfully overcome all these systemic, tissue and cellular barriers are yet to be developed. However, much information has been accumulated in the last 10-20 years for the control of the physicochemical properties of NPs and for the correlation of these properties with the *in vivo* biodistribution and antitumor efficacy of NPs ^[5]. Although the ideal physicochemical properties of NPs for drug delivery applications have not been completely elucidated, a general consensus about important parameters of NPs, such as particle size, drug loading, loading efficiency, and release kinetics, that are critical to their *in vivo* applications, have been reached ^[2b, 2c]. The sizes of NPs should typically be controlled at less than 200 nm with narrow polydispersities to

give satisfactory *in vivo* biodistribution ^[2b]. High drug loadings, quantitative loading efficiencies and controlled release profiles are also desirable for the *in vivo* applications of NPs ^[6].

Poly lactide (PLA), a biodegradable and non-cytotoxic material, has been extensively used in the formulation of particles for biotechnology and drug delivery applications ^[7]. NPs are typically prepared via nanoprecipitation of PLA and drugs ^[7c]. However, this conventional method tends to give NPs with various formulation challenges remaining to be addressed. PLA/drug NPs typically show “burst” drug release profiles in aqueous solution; as much as 80-90 % of the encapsulated drug is rapidly released during the first few to tens of hours ^[8]. The rapid drug release, also called dose dumping, may cause severe systemic toxicities [1]. In addition, drug loadings in conventional NPs can be very low, typically in a range of 1-5% for most NPs studied ^[9]. The drug loading of a delivery vehicle has been a critical measure of its utility in clinically settings ^[9]. At lower drug loadings, larger amounts of delivery vehicles are needed. Because of the limited body weight and blood volume of animals, the administration volumes are usually fixed. For instance, the volume of a solution intravenously administered to mice with 20- to 30-g body weights should be controlled around 100 to 200 μL ^[10]. Intravenous administration of NPs with 1% drug loading in a 100- μL solution at a dose of 50 mg/kg to a mouse with 20-g body weight requires the formulation of a concentrated, 1 g/mL NP solution. In practice, it is impossible to formulate such concentrated solutions and inject them intravenously. Furthermore, there is also a lack of general strategy to achieve quantitative drug encapsulation in PLA/drug NPs. Depending on the amount of drug being used, the hydrophobicity and hydrophilicity of drug, and the compatibility of drug and polymer, the encapsulation

efficiencies vary drastically in a range of 10 to 90% ^[8]. Unencapsulated drugs may self-aggregate ^[7c] and can be very difficult to be removed from the NPs. These formulation challenges significantly impact the processability and the clinical translation of PLA NP delivery vehicles for cancer therapy.

Controlled polymerization methodologies allowing preparations of polyesters ^[11], polypeptides ^[12] and hydrocarbon based synthetic polymers ^[13] with precisely controlled molecular weights and narrow polydispersities have been well established. These materials have been extensively utilized in drug delivery. However, controlled polymerization directly used in the formulation of drug delivery vehicles is rare. Since we developed the new method that allows drug molecules to be incorporated into PLA via drug-initiated, controlled ring-opening polymerization of lactide (LA) (Figure 5.1a) ^[6], quantitative incorporation of paclitaxel (Ptxl) ^[6a] and other hydroxyl-containing therapeutic molecules ^[6b] can be incorporated to PLA via ester bonds facilitated by Zn-catalysts. When bulky chelating complexes are used, the Zn-catalyst regulates the initiation and polymerization via the least sterically hindered 2'-OH of Ptxl and results in Ptxl-PLA conjugates with precisely controlled composition and molecular weights ^[6a]. At a monomer/initiator (LA/Ptxl) ratio of 10, the drug loading of Ptxl-PLA conjugates and the NPs derived from the conjugates can be as high as 40% with nearly 100% loading efficiencies ^[6a]. Ptxl can be released in a controlled manner with negligible burst from these Ptxl-PLA conjugate NPs, termed nanoconjugates (NCs) to differentiate them from the PLA/drug NPs prepared via encapsulation methods ^[6a].

Extended from these preliminary studies that were mainly focused on controlled polymerization, here we report a comprehensive study of the formulation of Ptxl-PLA NCs as well as the development of cancer targeting NCs by conjugating a cancer-specific

targeting aptamer ligand to the surface of NCs. Our study addressed various formulation challenges central to the clinical translation of polymeric NPs, such as control of particle size in salt solution, minimization of NP aggregation during lyophilization and solid formulation, and formulation of NPs in solid form with targeting property well preserved. These techniques may find widespread utility in the controlled formulation of many other polymeric nanomedicines for disease diagnosis, monitoring, and therapy.

2. Materials and Methods

2.1 General

D,L-Lactide (LA) was purchased from TCI America (Portland, OR), recrystallized three times in toluene and stored at -30°C in a glove box prior to use. β -Diimine (BDI) ligand and the corresponding metal complex (BDI)ZnN(TMS)₂ were prepared by following the published procedures ^[11a] and stored at -30°C in a glove box. All anhydrous solvents were purified by passing the solvents through alumina columns and kept anhydrous by storing them with molecular sieves. Ptxl was purchased from LC Laboratories (Woburn, MA) and stored at -30°C in a glove box prior to use. All other chemicals were purchased from Sigma-Aldrich (St Louis, MO) and used as received unless otherwise noted. The molecular weights (MWs) of PLA were determined on a gel permeation chromatography (GPC) equipped with an isocratic pump (Model 1100, Agilent Technology, Santa Clara, CA), a DAWN HELEOS 18-angle laser light scattering detector and an Optilab rEX refractive index detector (Wyatt Technology, Santa Barbara, CA). The wavelength of the HELEOS detector was set at 658 nm. Size exclusion columns (Phenogel columns 100 Å, 500 Å, 10³ Å and 10⁴ Å, 5 µm, 300 × 7.8 mm, Phenomenex, Torrance, CA) used for the separation of PLA or Ptxl-PLA conjugates were

serially connected on the GPC. THF (HPLC grade) was used as the mobile phase of GPC. HPLC analysis was performed on a System Gold system (Beckman Coulter, Fullerton, CA) equipped with a 126P solvent module, a System Gold 128 UV detector and an analytical pentafluorophenyl column (Curosil-PFP, 250×4.6 mm, 5μ , Phenomenex, Torrance, CA). The UV wavelength for Ptxl analysis was set at 227 nm. The NMR studies were performed on a Varian UI500NB system (500 MHz). The sizes and polydispersities of PLA NCs were determined on a ZetaPALS dynamic light-scattering (DLS) detector (15 mW laser, incident beam = 676 nm, Brookhaven Instruments, Holtsville, NY). The lyophilization of NCs was carried out on a benchtop lyophilizer (Freezone 2.5, Fisher Scientific, Pittsburgh, PA).

2.2 Preparation and characterization of Ptxl-LA₁₀₀

In a glove box, Ptxl (8.5 mg, 0.01 mmol) was dissolved in anhydrous THF (2 mL). (BDI)ZnN(TMS)₂ (6.4 mg, 0.01 mmol) was added and allowed to react with Ptxl for 15-20 min. LA (144.0 mg, 1.0 mmol) in THF (1.2 mL) was added dropwise to the vigorously stirred mixture of Ptxl and (BDI)ZnN(TMS)₂. The polymerization was monitored using FT-IR by following the disappearance of the lactone band of LA monomer at 1772 cm^{-1} or using ¹H-NMR by checking the methine (-CH-) peak of LA around 5.2-5.0 ppm. After the polymerization was complete, an aliquot of the polymerization solution was analyzed using HPLC to quantify the unreacted Ptxl in order to determine the incorporation efficiency of Ptxl in the Ptxl-PLA conjugates. The resulting Ptxl-PLA conjugate prepared at a LA/Ptxl ratio of 100 (Ptxl-LA₁₀₀) was precipitated with ethyl ether (10 mL), washed with ether and methanol to remove the BDI

ligand, dried under vacuum and characterized by GPC and ^1H NMR. Complete removal of BDI from Ptxl-PLA was verified by TLC.

2.3 General procedure for the preparation of Ptxl- LA_{100} NCs via nanoprecipitation

Ptxl- LA_{100} conjugate in DMF (50 μL , 10 mg/mL) (or in another water-miscible solvent such as acetone) was added dropwise to a nanopure water solution (2 mL). The resulting NCs were analyzed by DLS after nanoprecipitation, collected by ultrafiltration (5 min, $3000 \times g$, Ultracel membrane with 10,000 NMWL, Millipore, Billerica, MA), washed with water to remove DMF (or other organic solvent), and then analyzed by SEM.

2.4 Synthesis of PLA-PEG multiblock copolymer

PLA-PEG block polymers were synthesized by following the procedures as described in Section 2.2 using $(\text{BDI})\text{ZnN}(\text{TMS})_2$ as the catalyst and PEG as initiator. To prepare PLA-PEG diblock copolymer and PLA-PEG-PLA triblock copolymer (LE5 and LE5L, respectively, Table 5.1), we used $\text{mPEG}_{5k}\text{-OH}$ and $\text{HO-PEG}_{5k}\text{-OH}$ as the corresponding initiator in the presence of $(\text{BDI})\text{ZnN}(\text{TMS})_2$.

General Procedure In a glove box, $\text{mPEG}_{5k}\text{-OH}$ (50 mg, 0.01 mmol) in anhydrous dichloromethane (DCM, 300 μL) was mixed with a DCM solution of $(\text{BDI})\text{ZnN}(\text{TMS})_2$ (6.5 mg, 0.01 mmol, 50 μL). The mixture was stirred for 15 min. A DCM solution of LA (144 mg, 1 mmol, 2.88 mL) was added to the vigorously stirred $\text{mPEG}_{5k}\text{-OH}/(\text{BDI})\text{ZnN}(\text{TMS})_2$ solution. The mixture was stirred at room temperature for 16 h. The conversion of LA was determined by FT-IR by monitoring the lactone band at 1772 cm^{-1} . The resulting copolymer LE5 was precipitated with ethyl ether (10 mL), washed with ether and methanol/acetic acid (100/1 (v/v), 10 mL) to remove the BDI

ligand, and dried under vacuum. Complete removal of BDI was confirmed by NMR, HPLC and TLC. After the organic solvent was evaporated, the resulting product (LE5) was dissolved in THF (10 mg/mL) and analyzed by GPC. LE5L was prepared and characterized similarly as LE5. The MWs and molecular weight distributions (MWDs) of both LE5 and LE5L were listed in Table 5.1.

2.5 *Formation and characterization of Ptxl-LA₁₀₀/LE5 via sequential precipitation*

A DMF solution of Ptxl-LA₁₀₀ conjugate (50 μ L, 2 mg/mL) was added dropwise into a nanopure water solution (2 mL) to give the Ptxl-LA₁₀₀ NCs. LE5 ($M_n = 1.9 \times 10^4$ g/mol, 2 mg/mL, 100 μ L) or mPEG_{5k} (E5, 2 mg/mL, 100 μ L) in DMF was added dropwise to the Ptxl-LA₁₀₀ NCs. A concentrated PBS solution (10 \times , 228 μ L) was added to the nanoprecipitation solution to make the final salt concentration equivalent to 1 \times PBS. The NC sizes were measured by DLS. To determine the stability of the NCs in PBS solution, the particle sizes were followed for 30 min by DLS.

2.6 *Formation and characterization of Ptxl-LA₁₀₀/LE5 NC via co-precipitation (CPP)*

A DMF solution of Ptxl-LA₁₀₀ conjugate (12 mg/mL, 50 μ L) was mixed with a DMF solution of LE5 (12 mg/mL, 50 μ L). The mixture was then added dropwise to a vigorously stirred water solution (4 mL). The resulting NCs were analyzed by DLS.

2.7 *Formation and characterization of Ptxl-LA₁₀₀/LE5L via co-precipitation*

A DMF solution of PtxI-LA₁₀₀ (8 mg/mL, 50 μ L) was mixed with LE5L in acetone (8 mg/mL, 50 μ L). The mixture was then added dropwise to a vigorously stirred water or PBS solution (4 mL). The resulting NCs were analyzed by DLS. The stability of the NCs in the PBS solution was followed for 10-30 min by DLS.

2.8 *Lyophilization of PLGA-mPEG NPs in the presence of lyoprotectants*

An acetone solution of PLGA-mPEG (5 mg/mL, 100 μ L) was added dropwise into a vigorously stirred water solution (4 mL) to make the PLGA-mPEG NP. A lyoprotectant was added to the vigorously stirred NC solution at the selected lyoprotectant/NC mass ratio (varying from 2 to 20). The solution was then lyophilized, reconstituted with 2 mL water and stirred for 5 min. The sizes of the resulting NCs were analyzed by DLS.

2.9 *Lyophilization of PtxI-LA₁₀₀/LE5L NCs in the presence of albumin*

An acetone solution of PtxI-LA₁₀₀ (4 mg/mL, 50 μ L) was mixed with an acetone solution of LE5L (4 mg/mL, 50 μ L). The mixture was added dropwise to a vigorously stirred water solution (4 mL). The resulting NC solution was stirred for 6 h in a fume hood to evaporate the acetone; the resulting NC solution was then analyzed by DLS. An aqueous solution of bovine serum albumin (BSA) (12 mg/mL, 500 μ L) was added to the NC solution. The mixture was lyophilized for 16 h at -50°C . The resulting white powder was reconstituted with nanopure water (2 mL) and followed by addition of a concentrated PBS solution ($10\times$, 222 μ L). The solution was stirred for 5 min at room temperature. The resulting NC solution was analyzed by DLS.

2.10 Conjugation of aptamer to Cy5-LA₅₀/PLA-PEG-COOH NCs

Cy5-LA₅₀ was prepared by following the previously reported procedure^[6b]. Cy5-LA₅₀ / PLA-PEG-COOH NCs (w/w=1/1, 1 mL, 1 mg/mL in DNase RNase-free water) were incubated with an aqueous solution of 1-(3-dimethylaminopropyl)-3-ethylcarbodiimide hydrochloride (EDC) (400 mM, 200 μ L) and *N*-hydroxysuccinimide (NHS) (100 mM, 200 μ L) for 15 min at room temperature. The resulting NHS-activated NCs were reacted with 5'-NH₂-modified A10 PSMA aptamer (1 μ g/ μ L in DNase RNase-free water, 50 μ L). The resulting NC-aptamer bioconjugates were washed with ultrapure water (15 mL) by ultrafiltration (5 min, 1000 \times g, Ultracel membrane with 10,000 NMWL, Millipore, Billerica, MA, USA). The aptamer-modified NCs were re-suspended (1 mg/mL in DNase RNase-free water) and analyzed by fluorescence-activated cell sorting (FACS, BD FACScan™ Flow Cytometer) and fluorescence microscopy (Leica SP2 Laser Scanning Confocal Microscope).

2.11 Analysis of cellular uptake of Cy5-LA₅₀/PLA-PEG-COOH NC-aptamer bioconjugates by fluorescence microscope

LNCaP and PC3 cells were grown in chamber slides in RPMI medium 1640 and F-12 medium (American Type Culture Collection), respectively, supplemented with 100 units/ml aqueous penicillin G, 100 μ g/mL streptomycin, and 10% FBS at concentrations to allow 70% confluence in 24 h (i.e., 40,000 cells per cm²). On the day of experiments, the medium was replaced with Opti-MEM medium (200 μ L) containing Cy5-LA₅₀/PLA-PEG-COOH (w/w=1/1, 50 μ g) NC or Cy5-LA₅₀ /PLA-PEG-COOH NC-aptamer (NC-aptamer, 50 μ g, 5 wt% of aptamer). The cells and NCs were co-incubated for 2-6 h, after

which the cells were washed with PBS ($3 \times 200 \mu\text{L}$), fixed with 4% formaldehyde, counterstained with Alexa-Fluor 488 Phalloidin (Invitrogen, CA, USA), mounted and then analyzed on a Leica SP2 Laser Scanning Confocal Microscope at $40\times$ magnification. The images were collected along the z axis with a $0.8\text{-}\mu\text{m}$ interval and reconstructed using the provided software.

2.12 Analysis of cellular uptake of Cy5-LA₅₀/PLA-PEG-COOH NC-aptamer bioconjugates by FACS

LNCaP and PC3 cells were grown in 24-well plates in RPMI medium 1640 and F-12 medium (American Type Culture Collection), respectively, supplemented with 100 units/ml aqueous penicillin G, $100 \mu\text{g/mL}$ streptomycin, and 10% FBS at concentrations to allow 70% confluence in 24 h (i.e., $40,000 \text{ cells per cm}^2$). On the day of experiments, cells were washed with prewarmed PBS and incubated with prewarmed phenol-red reduced OptiMEM media for 30 min before the addition of the Cy5-LA₅₀/PLA-PEG-COOH ($50 \mu\text{g}$) NC or Cy5-LA₅₀/PLA-PEG-COOH NC-aptamer ($50 \mu\text{g}$, 5 wt% of aptamer). The cells were incubated for 4 h at 37°C , washed with PBS ($2 \times 500 \mu\text{L}$ per well) and subsequently treated with 0.25% trypsin with EDTA for 10 min. The cells were transferred to a 15-mL falcon centrifuge tube and centrifuged at 1200 rpm for 5 min followed by removal of the trypsin solution using a pipette. After the cells were washed with PBS ($2 \times 500 \mu\text{L/well}$), they were fixed with 4% formaldehyde for 10 min at room temperature, washed with PBS ($1 \times 500 \mu\text{L}$) and analyzed by FACS.

2.13 Preparation and formation of PLA-PEG-PAM NPs for bone tumor targeting study

A DMF solution of PLGA-mPEG/PLA-PEG-PAM conjugate (15 mL, v/v=10/1, 10 mg/mL) was added dropwise into a nanopure water solution (300 mL) to give the NPs. The solution was then concentrated using the filtration tube (Ultracel membrane with 10,000 NMWL, Millipore, Billerica, MA, USA) by centrifuge (3000 rpm) to 5 mL. The concentrated solution with 45 mL saline (sterilized) in the biohood and used within 6 hours for labeling with active ^{99m}Tc and bone tumor targeting.

2.14 Preparation and formation of Doxo-LA₂₅/PLA-PEG-PAM NPs for in vivo toxicity study

A DMF solution of Doxo-LA₂₅/PLGA-mPEG/PLA-PEG-PAM conjugate (15 mL, v/v=10/1, 10 mg/mL) was added dropwise into a nanopure water solution (300 mL) to give the NPs. The solution was then concentrated using the filtration tube (Ultracel membrane with 10,000 NMWL, Millipore, Billerica, MA, USA) by centrifuge (3000 rpm) to 5 mL for further dilution for *in vivo* cytotoxicity study. The analysis of tissues was assisted by Prof. Tim Fan (UIUC).

2.15 Formation of Ptxl-LA₂₅/PLA-mPEG NPs for Lewis Lung carcinoma (LLC) tumor prevention study

Female C57BI/6 mice were anesthetized, shaved, and prepared for implantation of the tumor cells. LLC cells were collected from culture, and 1,000,000 cells were then mixed with NPs and immediately injected subcutaneously into one flank of a mouse. Equivalent injections of cells with drug-free NPs, Ptxl solubilized with Cremophor EL /

ethanol (currently used clinically), and saline were also performed. The animals were monitored closely, and measurements of the tumor size for each animal were performed at regular intervals using calipers without knowledge of which injection each animal had received. The tumor volume for each time point was calculated according to the formula $(\text{length}) \times (\text{width}) \times (\text{height}) \times \pi/2$, where the long axis is the length, the short axis is the width, and the protrusion from the body is the height. When the tumor load reached 2000 mm³ or the animal had become moribund, the mouse was sacrificed.

2.16 *In vivo* evaluation of Cy5-PLA NPs biodistribution

3 female balb/c mice were injected each with 1 mg of PLA/Cy-5 NP (300 μ l) via lateral tail vein and then sacrificed 24 hours later. One untreated balb/c mouse was sacrificed and used as an autofluorescence background control. The *in vivo* biodistribution of PLA/Cy-5 NP within visceral organs including heart, lung, liver, spleen, and kidney was studied using a LI-COR Odyssey scanner (LI-COR Bioscience, Lincoln, NE).

3. Results and Discussion

3.1 *Synthesis of Ptxl-LA₁₀₀ nanoconjugates*

To ensure a rapid and complete polymerization of LA at room temperature using Ptxl as the initiator, we utilized (BDI)ZnN(TMS)₂, an active catalyst developed by Coates and coworkers for the polymerization of LA (Figure 5.1a) ^[11a]. We have previously reported regioselective initiation of Ptxl followed by controlled polymerization of LA when the polymerization was mediated by (BDI)ZnN(TMS)₂ ^[6a]. After Ptxl was mixed with 1 equiv. (BDI)ZnN(TMS)₂, the (BDI)Zn-Ptxl alkoxide formed *in situ* via the 2'-OH

of Ptxl (Figure 5.1a) initiated and completed the polymerization of LA within hours at room temperature, with nearly quantitative incorporation of Ptxl to the resulting PLA.

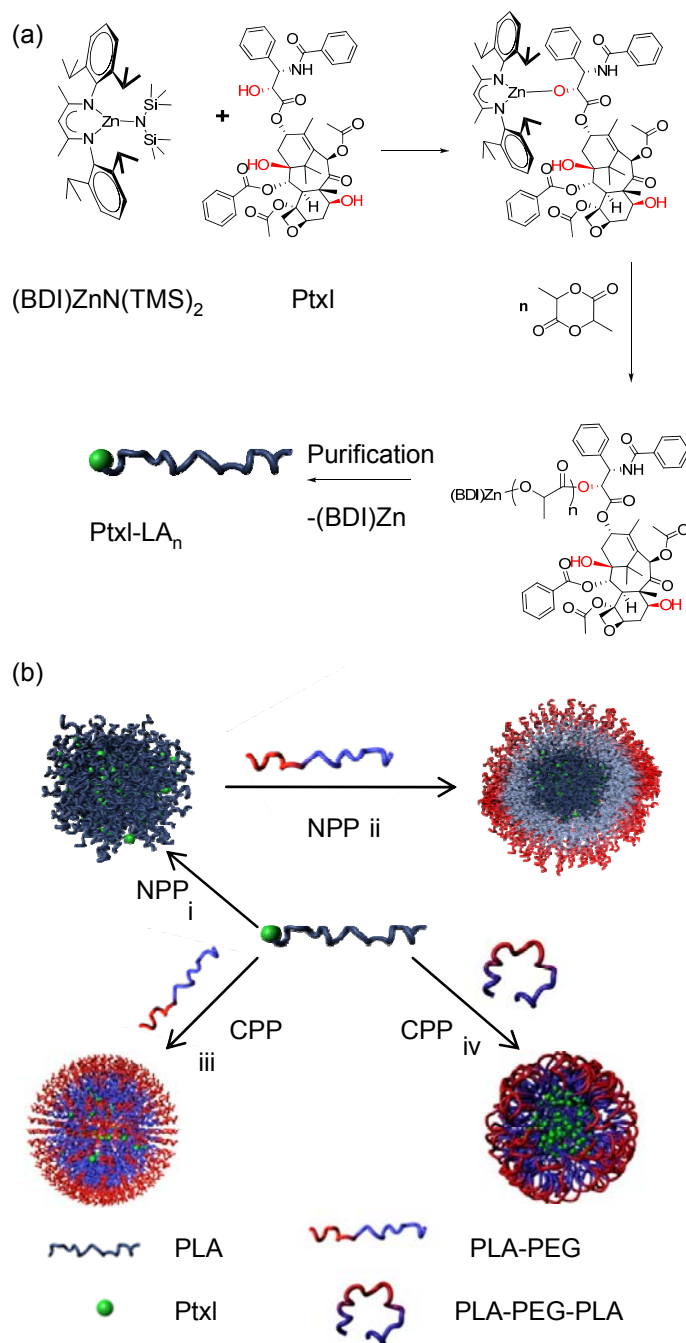


Figure 5.1 (a) Regioselective initiation and controlled LA polymerization mediated by the Ptxl/(BDI)ZnN(TMS)₂ complex to give Ptxl-PLA conjugate. (b) Formulation of Ptxl-PLA NCs

(Figure 5.1 continued) through i) nanoprecipitation of Ptxl-PLA, ii) nanoprecipitation of Ptxl-PLA followed by coating with PLA-PEG, iii) co-precipitation of Ptxl-PLA and PLA-PEG, and iv) co-precipitation of Ptxl-PLA and PLA-PEG-PLA. NPP = nanoprecipitation; CPP = co-precipitation.

3.2 *Formation of Ptxl-LA₁₀₀ nanoconjugates via nanoprecipitation (NPP)*

Nanoprecipitation (NPP) is an extensively used method for the preparation of NPs with therapeutic agents embedded in the hydrophobic polymeric matrices ^[7c, 14]. This method allows for rapid access to NPs in large quantity. Typically, a mixture of hydrophobic polymer and drug is dissolved in water-miscible organic solvent (e.g., DMF or acetone) and then added dropwise to a vigorously stirred water solution ($V_{\text{water}}/V_{\text{solvent}} = 10$ to 40). The instantaneous diffusion of the organic solvent into water results in formation of polymer/drug NPs.

The NPP of Ptxl-LA₁₀₀ resulted in sub-100 nm Ptxl-LA₁₀₀ NCs with monomodal particle size distributions and low polydispersities (Figure 5.2). In hundreds of NPP experiments that we have performed using Ptxl-PLA conjugates with various MWs, we rarely observed NCs with more than one particle size distribution based on the DLS analysis. The narrow, monomodal particle size distributions for NCs derived from NPP of the Ptxl-PLA conjugates have also been confirmed by SEM analysis in our previous study ^[6a], and are in sharp contrast to the multimodal particle size distribution typically observed with the NPs prepared by the co-precipitation (CPP) of a mixture of Ptxl and hydrophobic polymer (e.g., PLA or PLGA (poly(lactide-co-glycolide))) ^[7c]. As the multimodal distribution of NPs is due in part to the aggregation of the non-encapsulated drug molecules ^[7c], the monomodal particle size distribution pattern observed and very

low polydispersities with the Ptxl-LA₁₀₀ NCs are likely related to the unimolecular structures of the Ptxl-PLA conjugates.

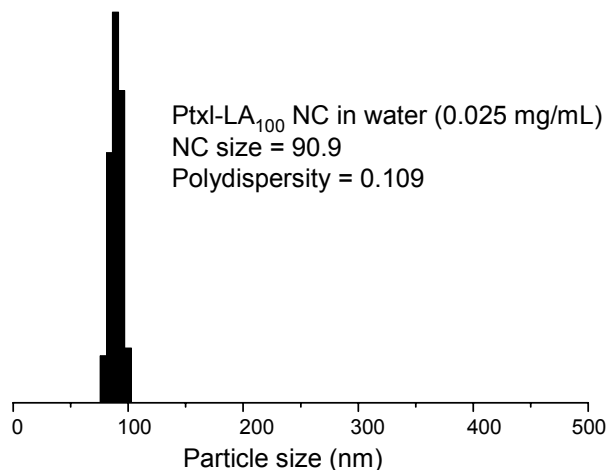


Figure 5.2. Dynamic light scattering (DLS) analysis of Ptxl-LA₁₀₀ NC in water (0.025 mg/mL).

3.3. Control of Ptxl-LA₁₀₀ NC size in the NPP process (Approach i, Figure 5.1b)

Particle size is one of the most important parameters of NPs and has significant impact on biodistribution, clearance kinetics, and *in vivo* efficacy ^[3, 15]. With respect to biodistribution, the upper limit of desirable NP size is typically around 200 nm. Particles with diameters of 200 nm or greater are more likely to induce an immune response and be taken up by the Kupffer cells than their smaller counterparts, resulting in rapid clearance of particles from circulation ^[2b]. Particles 150 nm or smaller can escape through fenestration of the vascular endothelium and be cleared from circulation, while particles smaller than 10 and 30 nm are easily cleared through the kidney or lymph nodes, respectively ^[2b]. Although it is still not entirely clear which NP size leads toward the most favorable biodistribution and highest therapeutic efficacy *in vivo* when NPs are

systemically administered, there is a general consensus that NPs should be controlled below 200 nm ^[2b]. Previous studies have revealed that NPs with diameters less than 200 nm can passively accumulate in solid tumor through the enhanced permeation retention effect (EPR) ^[16], a mechanism that has been broadly utilized to improve the residence of NPs in tumor tissues. However, NPs with sizes below 200 nm may still behave dramatically different in different size ranges in terms of their *in vivo* biodistribution, tumor targeting efficiency, tumor penetration and anticancer efficiency^[4]. One goal of this research project is to develop NCs with various size ranges as a tool to facilitate the evaluation of the correlation of the biodistribution and anticancer efficacy of NCs with NC size. Such information can be subsequently utilized for *in vivo* targeted cancer therapy. To achieve this goal, it is essential to develop methods that allow for facile formulation of NCs with precisely-controlled sizes. For this reason, we performed a series of studies using Ptxl-LA₁₀₀ as a model PLA-drug conjugate to assess how solvent, concentration of Ptxl-LA₁₀₀ and surfactant would affect the sizes of NCs and how NCs could be prepared with no or negligible aggregation in PBS solution for an extended period of time to facilitate their *in vivo* applications.

We first studied the effect of solvent on the NPP of Ptxl-LA₁₀₀ with water as the non-solvent. Previous studies by us ^[7c] and others ^[17] showed that the miscibility of the organic solvent with water can dramatically impact NP size in a given solvent/water system. As shown in Figure 5.3, the sizes of Ptxl-LA₁₀₀ NCs and the water-miscibility of the two organic solvents used in this study were well correlated; an increase of water miscibility led to a decrease in the mean NC size when all other formulation parameters were held constant. Ptxl-LA₁₀₀ NCs prepared with DMF as the solvent, a more water-miscible solvent, resulted in smaller particles. This is presumably due to more efficient

solvent diffusion and polymer dispersion into water in this DMF/water NPP system. The Ptxl-LA₁₀₀ NCs prepared with acetone, a less water-miscible solvent than DMF, were typically 20-30 nm larger than the NCs prepared with DMF as the solvent at the corresponding concentration (Figure 5.3). Acetone can be readily removed by evaporation because of its low boiling point. In contrast, DMF has to be removed by ultrafiltration followed by extensive washing. Thus, NC formulation via NPP in the acetone/water system is much easier, which is more suitable for the large-scale preparation of NCs.

We next studied the effect of the Ptxl-LA₁₀₀ concentration during NPP on the size of NCs. When the polymer concentrations were varied during the NPP of Ptxl-LA₁₀₀ at a fixed solvent:water ratio (Figure 5.3), we observed a linear correlation of NC size with the Ptxl-LA₁₀₀ concentration. The sizes of the NC increased from 90.9 nm to 195.3 nm as the polymer concentration in DMF increased from 1 mg/mL to 10 mg/mL. Similar correlation was also observed with acetone as the solvent for the NPP of Ptxl-LA₁₀₀ (Figure 5.5). In both DMF/water and acetone/water NPP systems, the polydispersities of the NCs at all concentrations remained very low, ranging 0.061-0.128 and 0.081-0.168 for NCs derived from DMF/water and acetone/water system, respectively. Because of the linear correlation of NC size with the concentration of Ptxl-PLA conjugate during NPP, NCs with any desirable sizes ranging from 80 to 250 nm can be obtained simply by adjusting precipitation concentration.

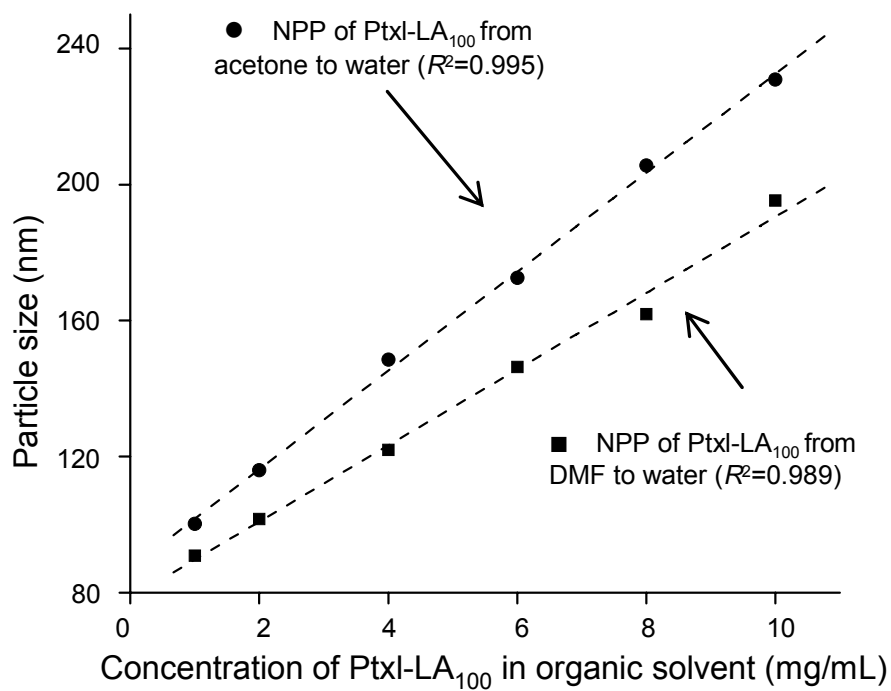


Figure 5.3 Ptxl-LA₁₀₀ NC size versus the concentration of Ptxl-LA₁₀₀ with the use of acetone (●) or DMF (■) as the solvent for nanoprecipitation. The volume ratio of organic solvent to water was fixed at 1/40. The dash line indicated the linear correlation of the NC size with the concentration of Ptxl-LA₁₀₀. R^2 is the linear correlation constant of corresponding system.

3.4. Formation of NCs via sequential precipitation of Ptxl-LA₁₀₀ and LE5 (Approach ii, Figure 5.1b)

NCs are designed specifically for *in vivo* drug delivery applications. It is desirable to have NCs with prolonged circulation to maximize their therapeutic efficacy. To achieve protracted retention in circulation with reduced recognition by reticuloendothelial system, both the size and surface properties of NCs have to be well controlled ^[2b]. Systemically administered NPs without proper surface modification are usually cleared rapidly from the circulation and localized predominately in liver and spleen ^[7c, 18]. Severe liver and spleen retention greatly diminishes the accessibility of the NPs to tumor tissues and also causes liver and spleen damage. The clearance is due to the scavenging by liver Kupffer cells and spleen macrophages ^[2b]. NP surface properties play a critical role in the blood opsonization, a process involving the deposition of protein opsonins that are recognized by phagocytic cells, thereby accelerating the clearance of NPs from blood. Opsonization of NPs can be substantially reduced when NP surface features are properly controlled ^[19]. Modification of NP surfaces with PEG, termed “PEGylation”, is a well-established approach to reduce protein binding ^[20]. Suppression of opsonization is thus achievable by PEGylation and has been utilized to enhance the circulation half-life of NPs from several minutes to several or tens of hours ^[10, 15, 21]. Since the report of long-circulating NP ^[15], surface PEGylation has been extensively used to prepare *in vivo* applicable drug delivery systems ^[20] and other biotechnology applications ^[22].

Ptxl-LA_n NCs have negative surface zeta-potential and remain non-aggregated in water due to surface charge repulsion. However, aggregation of NCs occurred in PBS, presumably due to salt-induced screening of the repulsive force (Figure 5.6a) ^[23]. The popular PEGylation strategy was thus adopted in this study to create NCs that will not

aggregate in salt solution. PEGylated NCs likely also have reduced protein binding for their *in vivo* applications.

PEG is typically covalently conjugated to the surface of NPs ^[7c, 14]. To minimize efforts involved in conjugation chemistry, we attempted a direct deposition method to coat NC with PEG. PLA-mPEG_{5k} (LE5, Table 5.1), an amphiphilic block copolymer with PLA block of 14 kDa and mPEG segment of 5 kDa, was synthesized via the ring opening polymerization of LA using a mixture of mPEG and (BDI)ZnN(TMS)₂. Dropwise addition of LE5 to the Ptxl-LA₁₀₀ NC aqueous solution resulted in rapid coating of Ptxl-LA₁₀₀, presumably via the hydrophobic interaction of PLA segment of LE5 and the hydrophobic NC surface. After treatment, the size of the Ptxl-LA₁₀₀ NC increased from 101.6 nm to 112.7 nm. The resulting NCs remained non-aggregated for at least 30 min in PBS (Figure 5.6a). To demonstrate the importance of the PLA block to the non-covalent surface PEGylation, we added mPEG5k (E5, Table 5.1) to the NC solution followed by the addition of PBS. Without the hydrophobic PLA block, E5 should not form stable interaction with NCs. As expected, Ptxl-LA₁₀₀/E5 NCs formed large aggregates almost instantaneously after PBS was added, following a very similar aggregation pattern as the parental NCs in PBS (Figure 5.4a). Furthermore, analyses of the Ptxl-LA₁₀₀ NC by DLS before and after treatment showed that particles retained their monomodal distribution pattern (Figure 5.4b). The DLS experiments indicated that LE5 favorably precipitated on the surface of Ptxl-LA₁₀₀ NCs instead of self-assembling to form micelles. The resulting PEG coated NCs form a core-shell nano-structure with hydrophobic polymer-drug conjugate being in the core and LE5 on the shell, which has been confirmed by various TEM studies.

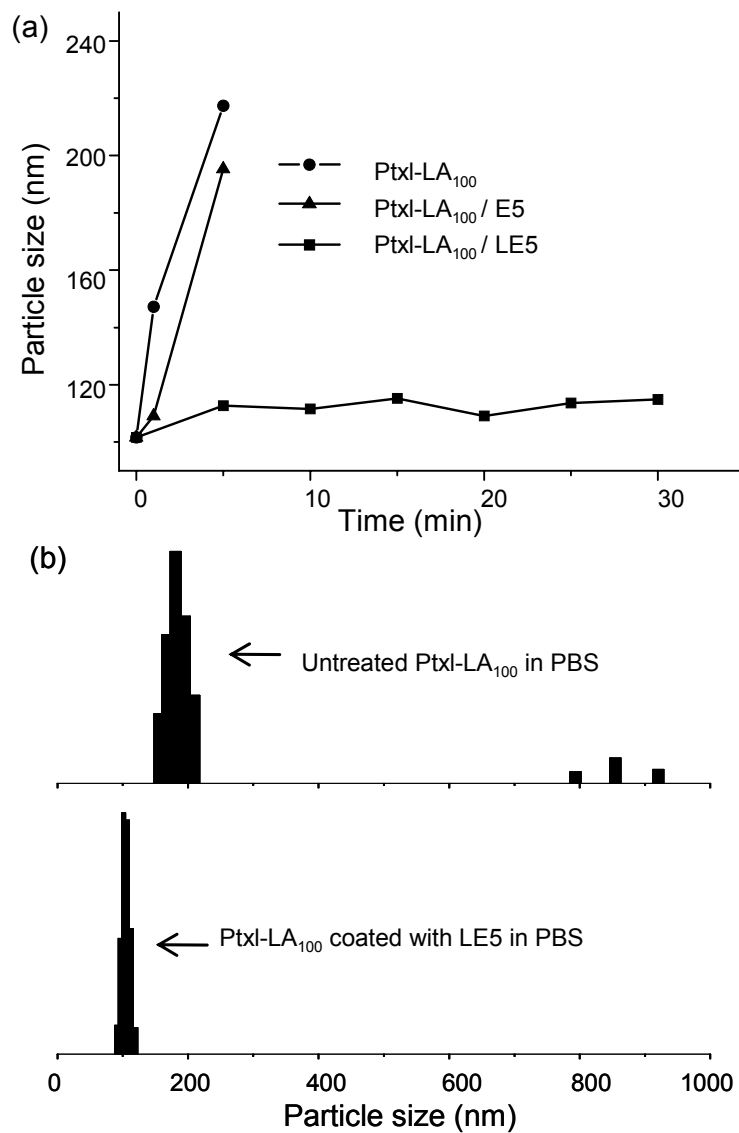


Figure 5.4 (a) Stability of Ptxl-LA₁₀₀ NCs in PBS (1×) after coated with mPEG_{5k} (E5) or with PLA-mPEG_{5k} (LE5). (b) DLS spectra of Ptxl-LA₁₀₀/LE5 NC and the untreated Ptxl-LA₁₀₀ NC. Particle sizes were determined 4 min after particles were present in PBS solution.

Table 5.1 PEG and PEG-PLA copolymers*

Abbreviation	Name	M_n ($\times 10^3$ g/mol)	MWD
E5	mPEG _{5k} -OH	5.3	1.01
LE5	PLA-mPEG _{5k}	19.3	1.09
LE5L	PLA-PEG _{5k} -PLA	34.4	1.12
	PLGA-mPEG _{5k}	18.3	1.41

* M_n = number-average molecular weight; PDI = polydispersity index. Abbreviations of chemicals: mPEG_{5k}-OH = mono-methoxy poly (ethylene glycol) with a molecular weight of 5 kDa; PLA = polylactide; PLGA = poly(lactide-*co*-glycolide) (LA/GA=50/50 molar ratio).

3.5. *Formation of NCs via co-precipitation of mixtures of Ptxl-LA₁₀₀ and LE5 (Approach iii, Figure 5.1b)*

Formation of Ptxl-LA₁₀₀/LE5 core-shell type nanostructures requires two steps to finish – the NPP of Ptxl-LA₁₀₀ to form NC core followed by coating with LE5 to form the PEG shell. Preparation of salt-stable NCs in such a step-wise manner is difficult to handle, especially for the preparation of NCs in large scale. It is desirable to formulate salt-stable Ptxl-LA_n NCs in one step. We next tested whether we could formulate salt-stable NCs by co-precipitating (CPP) a mixture of Ptxl-LA₁₀₀ and LE5.

We mixed Ptxl-LA₁₀₀ with LE5 at 1:1 mass ratio in DMF, a fixed ratio utilized throughout the studies reported in this paper, and then precipitated them in nanopure water ($V_{\text{DMF}}/V_{\text{water}} = 1/40$). Linear increase in particle size with the increase of polymer concentration was observed (Figure 5.5a), following a similar trend as the NPP of Ptxl-LA₁₀₀ previously discussed in the Figure 5.3. The sizes of NCs gradually increased from 61.4 nm to 121.0 nm when the concentration of Ptxl-LA₁₀₀ increased from 2 mg/mL to 10

mg/mL. When acetone was used as the solvent, similar linear correlation of NC sizes with the concentration of Ptxl-LA₁₀₀ was observed. The sizes of NCs increased from 79.2 to 145.9 nm when the concentration of Ptxl-LA₁₀₀ increased from 2 mg/mL to 10 mg/mL. The NCs obtained in the latter case (CPP of Ptxl-LA₁₀₀/LE5 from acetone to water) were roughly 20-25 nm larger than the NCs prepared with DMF as solvent at corresponding concentration, similar to the solvent effect described in Figure 5.5. NCs prepared in both DMF/water and acetone/water systems showed narrow-dispersed, monomodal particle size distribution, exemplified by the Ptxl-LA₁₀₀/LE5 NC prepared via the NPP with a concentration of 6 mg/mL in acetone (Figure 5.5b). We next evaluated the stability of the NCs in PBS. After precipitating a mixed DMF solution of Ptxl-LA₁₀₀ and LE5 (Ptxl-LA₁₀₀ = 4 mg/mL) in a water solution ($V_{\text{DMF}}/V_{\text{water}} = 1/40$) followed by the addition of PBS to the resulting NC solution, the particles remained non-aggregated for an extended period of time based on the DLS analyses (data not shown).

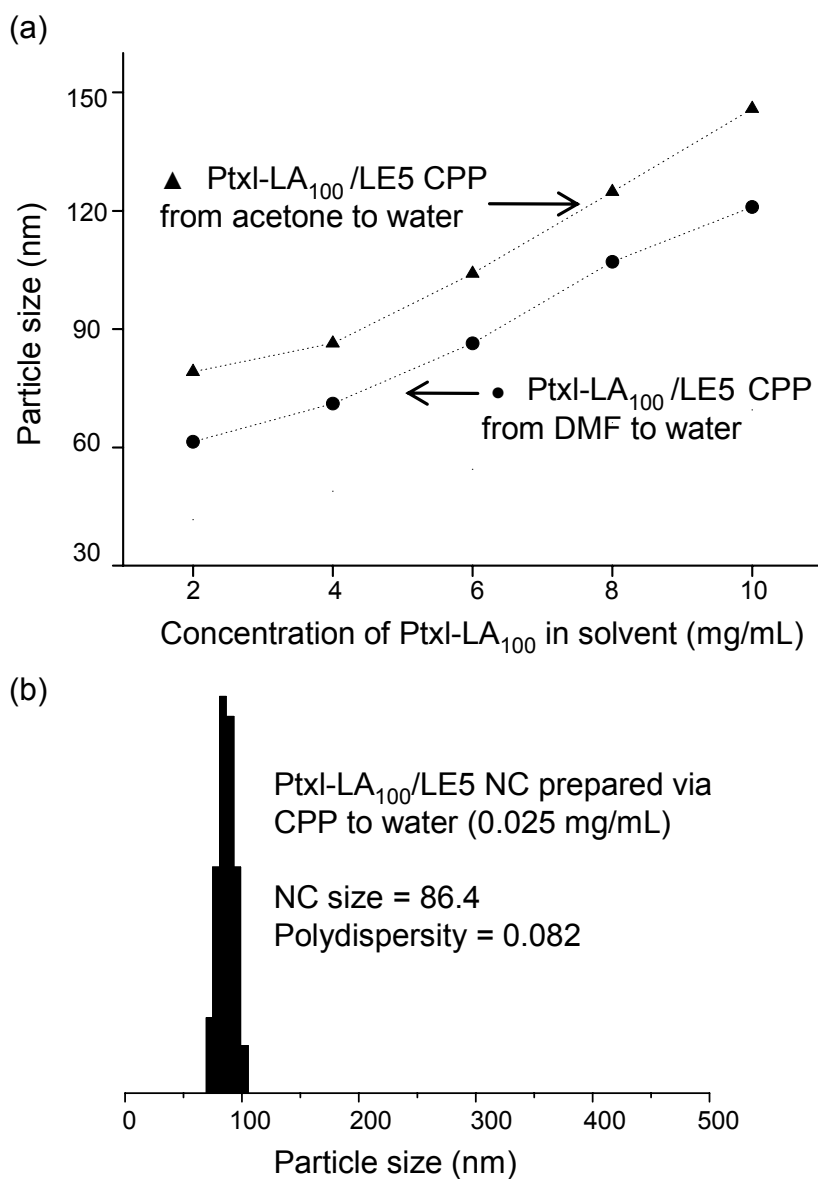


Figure 5.5 (a) Co-precipitation (CPP) of PtxI-LA₁₀₀/LE5 (wt/wt = 1/1) from DMF or acetone solution into water at various PtxI-LA₁₀₀ concentration. (DMF (or acetone)/water = 1/40 (v/v)). (b) PtxI-LA₁₀₀/LE5 NC size distribution determined by DLS. Condition: PtxI-LA₁₀₀ in DMF (50 μ L, 12 mg/mL) was mixed with a DMF solution of LE5 (50 μ L, 12 mg/mL). The mixture was added dropwise to a vigorously stirred water solution (4 mL). The resulting PtxI-LA₁₀₀/LE5 NCs was analyzed by DLS.

3.6. Formation of NCs via co-precipitation of mixtures of Ptxl-LA₁₀₀ and LE5L (Approach iv, Figure 5.1b)

To further simplify NC formulation, we explored whether it was possible to formulate stable NCs directly in PBS solution. When the mixture of Ptxl-LA₁₀₀ and LE5 was directly co-precipitated in PBS, the resulting NCs were not stable in PBS and formed large aggregates rapidly (Figure 5.6). The particle size increased from 83 nm to 197 nm within 6 min. Interestingly, when LE5L (Table 5.1), a ABA type triblock copolymer with PEG as the B block (MW = 5 kDa) and PLA as the A block (MW = 14 kDa), was mixed with Ptxl-LA₁₀₀ at 1:1 mass ratio in DMF and subsequently precipitated in PBS, the resulting Ptxl-LA₁₀₀/LE5L NCs were found to be surprisingly stable in PBS and remained non-aggregated for an extended period of time (Figure 5.6). To compare the non-solvent effect on the NC formulation, we conducted CPP of Ptxl-LA₁₀₀ / LE5L at various concentrations in both PBS and water. When water was used as the non-solvent, the size of the Ptxl-LA₁₀₀/LE5L NC gradually increased from 66.8 nm to 125.5 nm as the concentration of the mixture increased from 2 mg/mL to 10 mg/mL. CPP of the Ptxl-LA₁₀₀ and LE5L mixture in water or to PBS showed a linear correlation of Ptxl-LA₁₀₀ concentration with NC size (Figure 5.7), similar to the NPP of the Ptxl-LA₁₀₀ in water reported previously (Figure 5.3). When the CPP was performed with PBS as the non-solvent, the sizes of NCs were typically 20-40 nm larger than those derived from the NPs prepared with water as the non-solvent and followed a linear trend with the concentration of Ptxl-LA₁₀₀; the sizes of NCs increased from 99.0 to 156.5 nm when the concentration of the of Ptxl-LA₁₀₀ in the mixture increased from 2 mg/mL to 10 mg/mL (Figure 5.7). NCs prepared at various concentrations all stayed non-aggregated in PBS for an extended period of time (data not shown). It is known that triblock LE5L and diblock LE5 self-

assemble in different manners. LE5 forms star-like micelles, while LE5L, because of its ABA type of amphiphilic structure, tends to form flower-like micelles (Figure 5.1b) ^[24]. Hydrophobic polymer chains in flower-like micelles tend to have stronger interaction than those in star-like micelles, which may in part contribute to the formation of Ptxl-LA₁₀₀/LE5L NCs with stably coated PEG shell and enhanced stability in the PBS solution. The detailed mechanism of Ptxl-LA₁₀₀/LE5L and Ptxl-LA₁₀₀/LE5 NC self-assembly is yet to be determined.

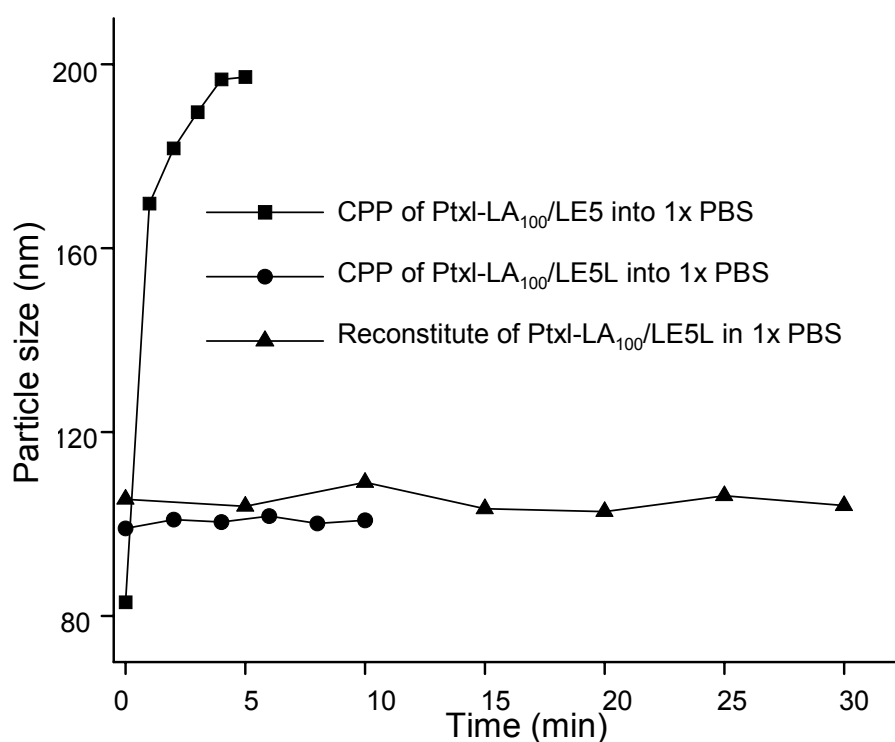


Figure 5.6 The stability of NCs in PBS solution. ■: A mixture of Ptxl-LA₁₀₀ and LE5 in DMF (w/w = 1/1, Ptxl-LA₁₀₀ = 4 mg/mL) was co-precipitated directly to 1× PBS (DMF/PBS = 1/40 (v/v)). ●: A mixture of Ptxl-LA₁₀₀ and LE5L in DMF (w/w = 1/1, Ptxl-LA₁₀₀ = 4 mg/mL) was co-precipitated directly to 1× PBS (DMF/PBS = 1/40 (v/v)). ▲: A mixture of Ptxl-LA₁₀₀ and LE5L

(Figure 5.6 continued) in acetone (w/w = 1/1, Ptxl-LA₁₀₀ = 2 mg/mL, 100 μ L) was co-precipitated to water (4 mL). The obtained NC had a diameter of 88.9 nm with a polydispersity of 0.092. The resulting NC solution was mixed with an aqueous solution of BSA (500 μ L, 12 mg/mL). The mixture was lyophilized for 16 h at -50 $^{\circ}$ C. The resulting powder was reconstituted with 2-mL water and followed by addition of a concentrated PBS solution (222 μ L, 10 \times). The mixture was stirred for 5 min at room temperature and analyzed by DLS.

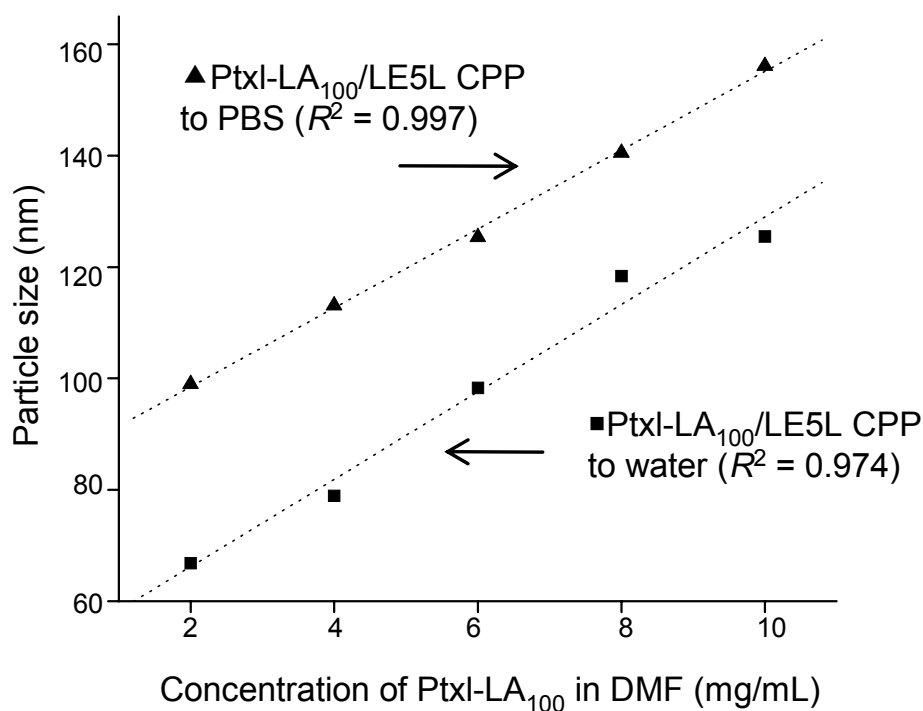


Figure 5.7 Linear correlation of Ptxl-LA₁₀₀/LE5L NC size with Ptxl-LA₁₀₀ concentration in DMF when the mixture of Ptxl-LA₁₀₀/LE5L was co-precipitated in water or in PBS

3.7. *Lyophilization and storage of Ptxl-PLA NCs*

Formulations of small-scale NPs that stay non-aggregated in PBS for *in vitro* or *in vivo* laboratory studies are relative easy to control. However, in order to facilitate their clinical translation, NPs have to be prepared in large quantity with well controlled properties, which should remain unchanged during the processes of manufacturing, storage and transport prior to their use in clinic. In Ptxl-PLA, because Ptxl is covalently conjugated to PLA through an ester bond that is subject to hydrolysis upon exposure to water, handling of NCs in aqueous solution in the abovementioned processes is undesirable. NCs have to be formulated in solid form in order for them to be used in clinic.

It is known that PLA-based NPs tend to aggregate during lyophilization. As expected, when the Ptxl-LA₁₀₀/LE5 or the Ptxl-LA₁₀₀/LE5L NCs with sub-100 nm sizes were lyophilized, reconstituted and re-analyzed by DLS, micrometer-sized, non-dispersible aggregates were observed. Administration of polymeric NPs with micron size aggregates via tail vein injection led to instantaneous mice death based on our previous experience.

There have been many studies using lyoprotectants to physically separate NP from aggregating during lyophilization. Mono- or di-saccharides, such as sucrose, dextrose, maltose, sorbitol, glucose, are frequently used as lyoprotectants because their biocompatibility and low cost ^[25]. In our previous efforts of developing aptamer-based cancer targeting and therapy, we conducted preliminary studies on the lyophilization of PLGA-mPEG_{5k} NPs with the use of sucrose as the lyoprotectant ^[7c]. Although the aggregation of PLGA-mPEG_{5k} NPs was reduced during lyophilization, formation of substantial amount of large, non-dispersible aggregates was still observed. Based on this

previous study, we screened a large number of lyoprotectants using PLGA-mPEG_{5k} based NPs and compared them with sucrose for their capabilities of preventing NP aggregation during lyophilization (Table 5.2)

PLGA-mPEG_{5k} NPs were prepared via nanoprecipitation of PLGA-mPEG_{5k} (Table 5.1) as previously described ^[7c]. Commonly used saccharide-based lyoprotectants, such as sucrose, sorbitol, maltose, dextrose and mannose, were able to reduce NP aggregation to some degree when the NPs were lyophilized along with these lyoprotectants (Table 5.2). High lyoprotectant chemical/NP mass ratio (W_c/W_{NP} , Table 5.2) was more effective in terms of reducing NP aggregation (Table 5.2). However, even at a W_c/W_{NP} ratio as high as 10, significant NP aggregations were observed in all systems (Table 5.2). DLS analyses of these NPs after lyophilization showed multimodal particle size distributions. Some large, non-dispersible aggregates precipitated from the solution and were even visible with the naked eye. Other sugars, such as galactose, could not prevent NP aggregation at all even at a lyoprotectant/NC mass ratio of 10. We also tested whether amino acid (e.g., glycine) or surfactant (e.g., SDS) could be used as the lyoprotectant and found that they were unable to prevent NP aggregation during lyophilization (Table 5.2).

Because none of the small molecules tested could effectively prevent NP aggregation during lyophilization, we next tested whether macromolecules could provide better lyoprotection during NP lyophilization. Albumin, an abundant protein in blood, has attracted much interest in drug delivery recently. Abraxane®, an albumin-paclitaxel NP, has been recently approved by the US Food and Drug Administration for cancer treatment ^[26]. We tested whether bovine serum albumin (BSA) could be used as a lyoprotectant of NPs. At a BSA/NP mass ratio of 2, the NP size increased by 8.2 times

from 62 nm before lyophilization to 512 nm after lyophilization; two particle size distributions were observed. When the BSA/NP mass ratio increased to 6 and 10, the size of the lyophilized NP became 176 nm and 114 nm, respectively. This corresponds to roughly 2.8- and 1.8-times the pre-lyophilized NPs. For the first time we were able to completely disperse the lyophilized NPs with sub-200 nm diameters with absolutely no precipitates. The reconstituted NPs showed monomodal particle size distribution as determined by DLS (data not shown).

We next tested whether albumin could be used to stabilize Ptx1-LA₁₀₀/LE5L NC. A Ptx1-LA₁₀₀/LE5L NC was first prepared by co-precipitation as described previously in Figure 5.9. The particles size and the polydispersity of the resulting NC were 88.9 nm and 0.092, respectively, as determined by DLS. After lyophilization at a BSA/NC mass ratio of 15 followed by reconstitution with 1× PBS, the NC size increased slightly to 105.9 nm (Figure 5.8) but remained non-aggregated for at least 10 min during the course of DLS analysis. Monomodal particle size distribution was verified by DLS analysis (Figure 5.10). The polydispersity of NCs remained as low as 0.112. This experiment has been repeated multiple times with consistent and highly reproducible results and no NC aggregation in each of the repeated experiments. Because of the biocompatibility of albumin, this albumin-based lyoprotection strategy may be broadly used in solid formulations for drug delivery or other translational applications.

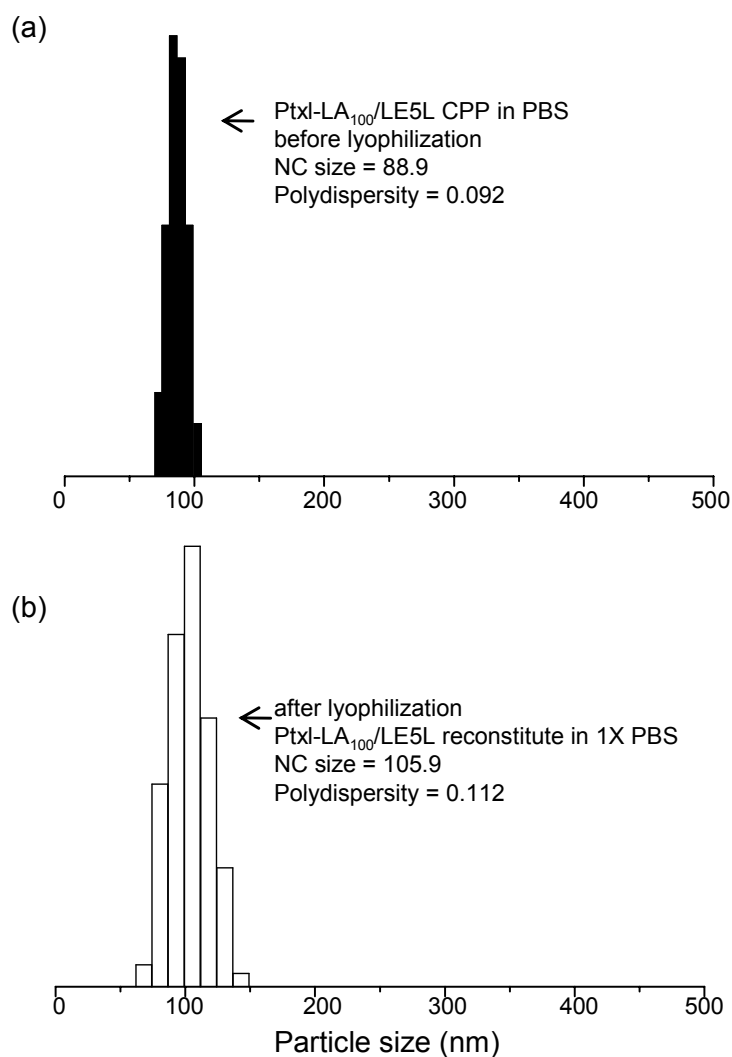


Figure 5.8 (a) DLS spectrum of NC obtained from the co-precipitation of an acetone solution of Ptxl-LA₁₀₀/LE5L (w/w = 1/1, Ptxl-LA₁₀₀ = 2 mg/ml, 100 μ L) to water (4 mL, acetone/water = 1/40 (v/v)). The obtained NC had a diameter of 88.9 nm with a polydispersity of 0.092. (b) The resulting NC solution was then mixed with an aqueous solution of BSA (500 μ L, 12 mg/mL). The mixture was lyophilized for 16 h at -50 $^{\circ}$ C. The resulting powder was reconstituted with 2-mL water and followed by addition of a concentrated PBS solution (222 μ L, 10 \times). The mixture was stirred for 5 min at room temperature and analyzed by DLS. The obtained NC had a diameter of 105.9 nm with a polydispersity of 0.112.

Table 5.2 Characterization of PLGA-mPEG NPs Lyophilized in the Presence of Various Lyoprotectant and Reconstituted by Water^a

Lyoprotectant ^b	W _C /W _{NP} ^c	Size in nm (STD) ^d	PDI (STD) ^d	Distrib. Num. ^e	S _L /S _O ^f	Aggr. ^g
Sucrose	2	245.2 (2.1)	0.227 (0.003)	2	3.93	Y
Sucrose	10	217.5 (3.0)	0.220 (0.002)	2	3.49	Y
Sorbitol	2	>1000	>1000	N.D.	N.D.	Y
Sorbitol	10	764.8 (39.2)	0.299 (0.021)	2	12.28	Y
Maltose	2	>1000	>1000	N.D.	N.D.	Y
Maltose	10	220.4 (3.2)	0.288 (0.008)	2	3.54	Y
Dextrose	2	250.4 (9.5)	0.345 (0.0120)	2	4.02	Y
Dextrose	10	79.1 (2.3)	0.075 (0.032)	2	1.26	Y
Mannose	2	>1000	>1000	N.D.	N.D.	Y
Mannose	10	245.2 (1.6)	0.254 (0.011)	2	3.93	Y
Galactose	10	>1000	>1000	N.D.	N.D.	Y
Glycine	10	>1000	>1000	N.D.	N.D.	Y
SDS	10	>1000	>1000	N.D.	N.D.	Y
BSA	2	511.8 (24.7)	0.392 (0.005)	2	8.21	Y
BSA	6	175.9 (3.3)	0.343 (0.008)	1	2.82	N
BSA	10	114.1 (1.4)	0.110 (0.002)	1	1.83	N

^aIn this study PLGA-mPEG_{5k} ($M_n = 19.4 \times 10^3$ g/mol) was used to study the efficiency of lyoprotectant. The original PLGA-mPEG NP had a diameter of 62.7 nm, which was formulated through the NPP of PLGA-mPEG to water. After the NPP was complete, the corresponding lyoprotectant was added as the selected lyoprotectant/NP mass ratio prior to lyophilization. ^bSDS = sodium dodecyl sulfate; BSA = bovine serum albumin. ^cW_C/W_{NP} = the mass ratio of lyoprotectant chemicals vs. NP. ^dPDI = polydispersity; STD = standard deviation. ^eDistrib. Num. = the number of particle size distribution. N.D. = not determined. ^fS_L/S_O = the ratio of the lyophilized NP size to pre-lyophilized NP size. ^gAggr. = visible large aggregates; Y = aggregates observed; N = no aggregates observed.

3.8. *Ptxl-PLA NCs for prostate cancer targeting*

Aptamers are either single-stranded DNA or RNA that specifically bind to a target ligand or ligands. They were selected from a library of nucleic acids with random sequences via a combinatorial process called Systematic Evolution of Ligands by

Exponential Enrichment (SELEX) ^[27]. When used for cancer targeting, aptamers are capable of binding to target antigens with extremely high affinity and specificity in a manner resembling antibody-mediated cancer targeting. Aptamers are typically non-immunogenic and exhibit remarkable stability against pH, temperature and solvent. Synthesis of aptamers is an entirely chemical process and thus shows negligible batch-to-batch inconsistency ^[28]. These unique properties of aptamers are in sharp contrast to antibodies that are typically unstable against temperature and pH change, are immunogenic, and have significant batch-to-batch variability.

An A10 aptamer with 2'-fluoro-modified ribose on all pyrimidines and a 3'-inverted deoxythymidine cap has been identified via SELEX and utilized to target extracellular prostate-specific membrane antigen (PSMA) ^[29]. It binds to the PSMA-positive LNCaP prostate cancer cells but not PSMA-negative PC3 prostate cancer cells. Previous study showed that PLGA-A10 aptamer bioconjugates were capable to target LNCaP cells *in vitro* and *in vivo* ^[14, 30].

Cy5 (a fluorescence dye with hydroxyl groups) was used to initiate LA polymerization to prepare Cy5-PLA and subsequently Cy5-PLA NCs for study of the *in vitro* cancer targeting. The amine-terminated A10 aptamer was conjugated to the PLA-PEG-COOH/Cy5-PLA NCs (particle size 132.8 nm with the polydispersity of 0.031) through the carboxylic acid-amine coupling reaction in the presence of EDC and NHS to give aptamer/PLA-PEG-COOH/Cy5-PLA NCs (aptamer-Cy5 NC) ^[30]. After purifying the aptamer-Cy5 NCs by centrifugation and washing the NPs with PBS, we found that the size of aptamer-Cy5 NCs increased slightly to 157.1 nm with a polydispersity of 0.144 after conjugation of the A10 aptamer. Freshly prepared aptamer-Cy5 NCs were then applied to the LNCaP (PSMA+) and PC-3 (PSMA-) cells, and their binding and

internalization were assessed by FACS (Figure 5.11). As shown in Figure 5.11(a), the mean fluorescence intensity of the LNCaP cells (PSMA+) incubated with aptamer-Cy5 NC for 4 h was 376.7 (arbitrary intensity unit on FACS Cy5 channel), as compared to 72.4 for PS3 cell (PSMA-) and 16.4 in the untreated LNCaP cells. The fluorescence intensity of the aptamer-Cy5 NC treated LNCaP cells was 5.2 times higher than that of PC-3 cells treated under the same condition, indicating enhanced aptamer-Cy5 NC binding to PSMA+ LNCaP cells and potentially improved NC internalization. A kinetic study for the internalization of aptamer-Cy5 NCs into LNCaP cells was then performed (Figure 5.11(b)). The LNCaP cells treated with aptamer-Cy5 NCs for 2 h revealed a mean fluorescence intensity of 136.2, as compared to 16.4 of the untreated cells. When the LNCaP cells were treated with aptamer-Cy5 NCs for 6h, the mean fluorescence intensity increased to 779.8, indicating 5.7 times more NCs were internalized into the cells. Those observations were confirmed by an uptake imaging study using confocal microscopy. As shown in Figure 5.12, the uptake of Cy5 NCs to LNCaP cells was significantly enhanced when NCs were coated with aptamer (A versus E; B versus F). Incubation of aptamer-Cy5 NCs with LNCaP cells for longer time resulted in substantially increased NC internalization (A versus B). Because PC3 cells do not express the PSMA protein, there was essentially no difference between the aptamer-Cy5 NC and the Cy5 NC without aptamer with respect to their capability of cell-binding and internalization. Incubating PC3 cells with NCs for longer time resulted in slightly increased NC uptake. The binding of aptamer-Cy5 NCs to the PC3 cells was substantially weaker than to LNCaP cells (B versus D). These *in vitro* studies demonstrated that NCs conjugated with aptamer targeting ligand can potentially be used for prostate cancer targeting.

We have previously demonstrated that NCs can be formulated into solid form when albumin is used as the lyoprotectant. We next tested whether aptamer-Cy5 NCs can be made in solid form and then reconstituted to give NCs with similar sizes and targeting capability. At a BSA/Aptamer-Cy5 NC mass ratio of 10, the size of the lyophilized and reconstituted aptamer-Cy5 NC was 212.6 nm (with a polydispersity of 0.386) as compared to NCs with 157.1 nm (with a polydispersity of 0.144) before lyophilization. DLS analysis indicated that the lyophilized and reconstituted aptamer-Cy5 NCs maintain monomodal size distribution (data not shown). The reconstituted aptamer-Cy5 NCs were then applied in cell-binding studies and analyzed by FACS; their targeting capability was found to be well preserved during the lyophilization process.

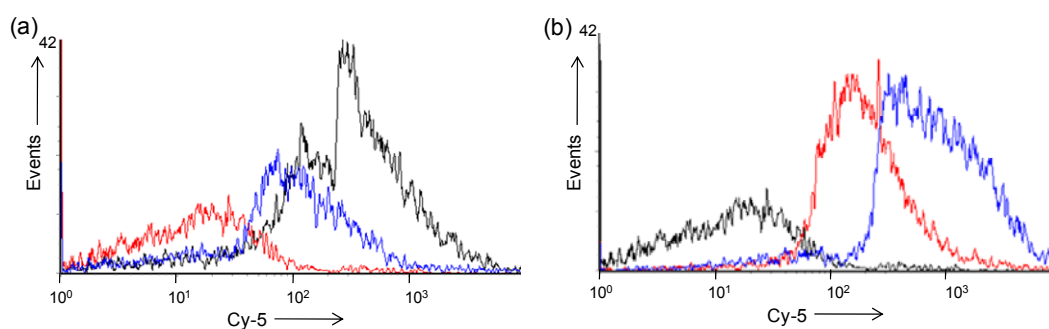


Figure 5.9 Flow cytometry analysis of NP-Apt conjugates cellular uptake. (a) Untreated LNCaP cells (red line); PC3 cells treated with NP-Apt for 4 hours (blue line); LNCaP cells treated with NP-Apt for 4 hours. (b) Untreated LNCaP cells (black line); LNCaP cells treated with NP-Apt for 2 hours (red line) and 6 hours (blue line).

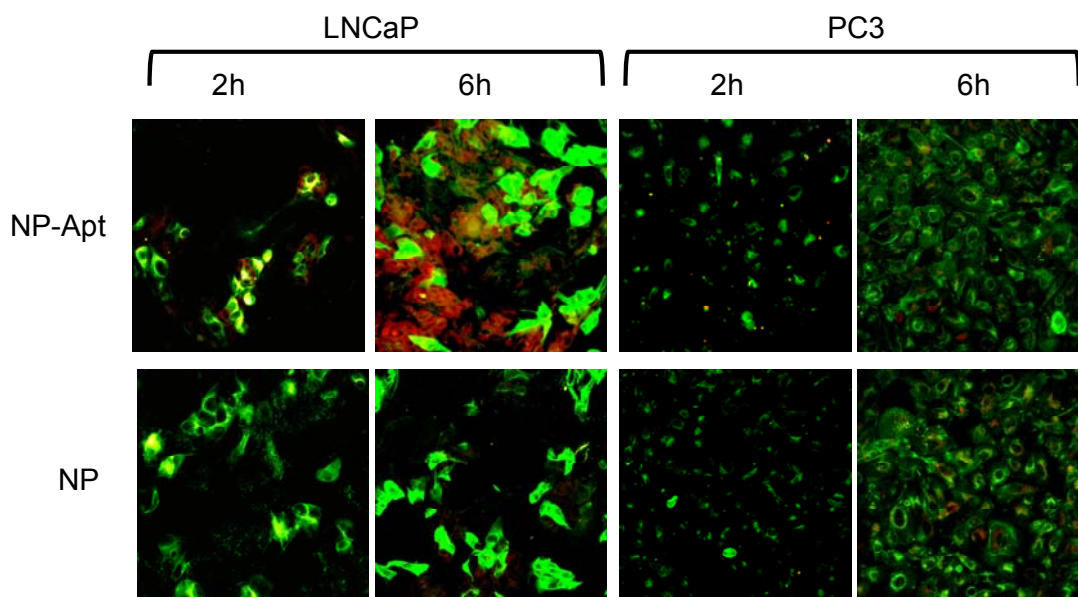


Figure 5.10 Confocal images of LNCaP (left) and PC3 (right) cells treated with aptamer-functionalized nanoparticles (NP-Apt, top) and nanoparticles without aptamer (NP, bottom). The Cy-5 incorporated NP or NP-Apt are shown in red color. The cells counterstained with Alexa-Fluor 488 Phalloidin (binding to cellular actin) are shown in green

3.9 *In vivo distribution of PLA-Cy5 NPs*

There is growing interest of developing non-invasive, whole-body animal fluorescent imaging techniques to assess the biodistribution of drug delivery systems or diagnostic agents. To ensure effective measurement of fluorescent signal *in vivo*, it is crucial to use red or near-IR dyes. Quantum dots, a class of inorganic nanocrystals with excellent fluorescent intensity and photostability, can be readily prepared to have a far-red emission band. However, there is a general consensus that quantum dots cannot be

used in human because of their severe toxicity. Small molecule organic dyes are promising probes to be coupled with imaging systems for clinical applications.

Polymeric nanoparticles (NPs) are important carriers for the delivery of chemotherapeutics or imaging materials because they can provide prolonged systemic circulation and improved tumor accumulation compared to unformulated drugs. To evaluate the biodistribution of NPs, it is particularly important to formulate NPs with stably incorporated fluorescent ligands and controlled formulation parameters (size, surface properties, etc.). Our monomodal, narrow distributed Cy5-PLA NPs with PEG on the surface has the potential as the candidate of whole body *in vivo* imaging agents.

The unique chemistry of the Cy5-PLA NP fabrication, allows for large concentrations (50 mg/kg) of Cy5-PLA NP to be safely injected into living mice without adverse or acute biologic consequences such as immediate or sudden death following intravenous delivery. To demonstrate of the potential of using Cy5-PLA NPs as a non-invasive fluorescence imaging agent, we conducted the intravenous injection via the lateral tail vein of Cy5-PLA NP to 3 female balb/c mice. After the injections, we were able to study the biodistribution of Cy5-PLA NP in balb/c mice through the use of a highly sensitive fluorescent scanner (LI-COR Odyssey scanner). Twenty-four hours following intravenous injection, Cy5-PLA NP were detected at the highest concentration within the spleen (fluorescent intensity >20-fold greater than background tissue autofluorescence). Additionally, Cy5-PLA NPs were also identified in the liver, heart, kidney, and lungs (Figure 5.11). The chemical stability of fabricated Cy5-PLA NP, in conjunction with the high detail tissue resolution (21 microns) capacity of the LI-COR Odyssey scanner, allows the possibility to study the biodistribution and biologic fate of Cy5-PLA NP when administered to living mice. The combined technologies of Cy5-

PLA NP and LI-COR Odyssey scanner will be very useful for characterizing the ability of Cy5-PLA aptamer NP to penetrate into established PSMA-expressing tumors when implanted into living mice, i.e. LNCaP xenograft studies.

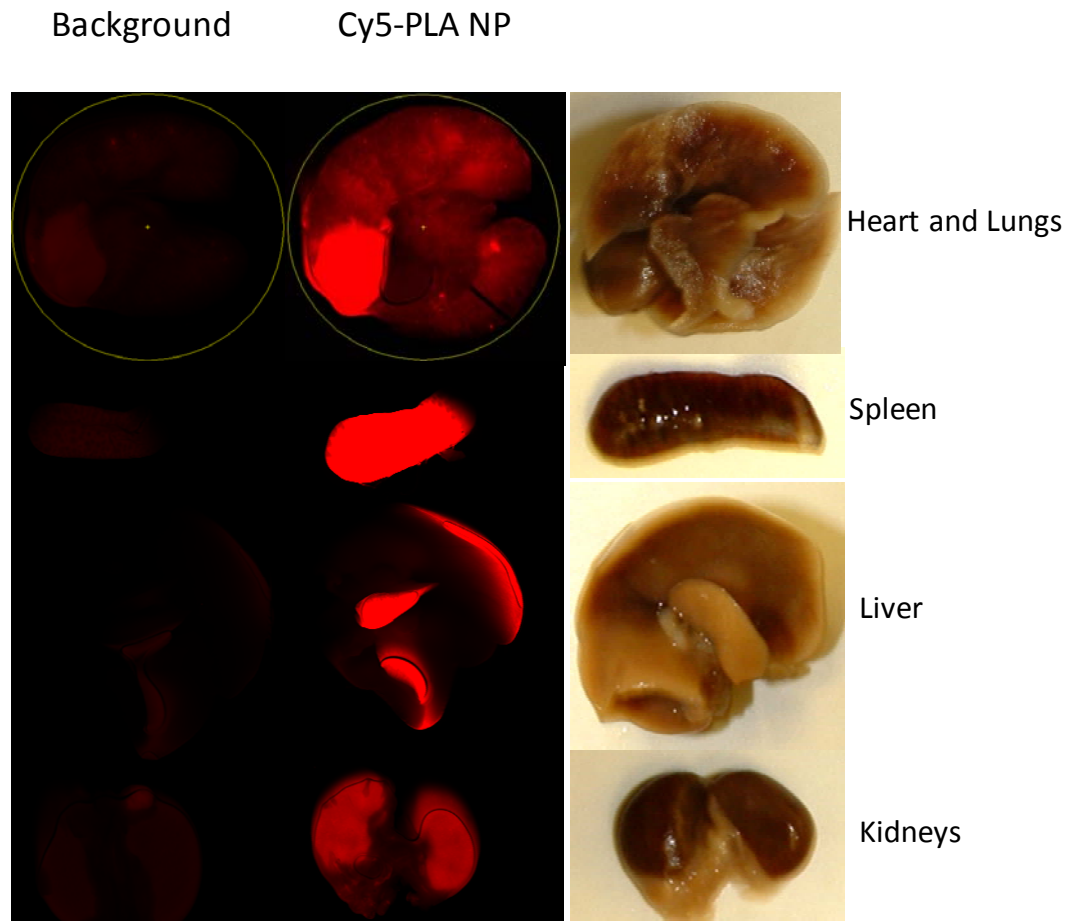


Figure 5.11 *In vivo* biodistribution of Cy5-PLA NP following intravenous administration. Visceral organ biodistribution of Cy5-PLA NP following lateral tail vein injection using the LI-COR Odyssey scanner. Accumulation of Cy5-PLA NP within visceral organs allows for greater than 10-fold increase in fluorescent intensity in comparison to background autofluorescence. Splenic accumulation of Cy5-PLA NP is the greatest for all visceral organs examined (spleen, liver, kidney, lung, and heart).

3.10 PLA NPs for Lewis Lung carcinoma tumor prevention

Of all major cancers, lung cancer has the lowest 5-year survival rate at 15.3%. Moreover, local recurrence following lobectomy for stage I lung cancer occurs in 9% of patients, with documented recurrence rates increased to 24% in patients with poor pulmonary reserve who receive more limited wedge resections. Adjuvant therapies in patients unable to tolerate lobectomy (e.g., radio frequency ablation, external radiation treatment, placement of radioactive seeds, systemic chemotherapy) result in inferior outcomes, and therefore, additional treatment strategies for improved local control of tumor growth following surgery are needed. The local delivery of antineoplastic agents to the resection site at the time of limited surgical therapies (i.e., wedge resections or ablations) is an attractive approach, as it would enhance the local efficacy of chemotherapy while minimizing detrimental systemic side effects that are common with systemic administration. Moreover, a drug delivery system capable of preventing recurrence at the tumor-tissue interface would potentially extend the benefit of surgical therapy to improve the clinical outcomes of patients previously deemed unacceptable candidates for lobectomy.

Therefore, to assess the ability of paclitaxel-loaded expansile nanoparticles to prevent establishment of lung cancer in an *in vivo* model mimicking microscopic disease that can remain when the surgical margin is close to the tumor, we evaluated Ptxl-PLA NCs in a rapidly growing subcutaneous tumor model. Specifically, we assessed the ability of Ptxl-PLA NCs to prevent establishment of rapidly growing LLC tumors in C57Bl/6 female mice compared to Ptxl alone (in clinical formulation) and controls without any drugs. In these experiments, 1,000,000 LLC tumor cells plus Ptxl-LA₂₅ / PLGA-mPEG nanoparticles containing a total dose of 5 and 50 mg/kg incorporated Ptxl

were injected subcutaneously into the flank of a mouse. Other groups received the injection of 1,000,000 LLC cells alone or LLC cells mixed with Ptxl solubilized with 1:1 Cremophor EL/ethanol as used clinically at 5mg/kg dosage. At 25 days, large tumors were noted at the site where LLC cells were coinjected with media alone, or paclitaxel alone. In contrast, sites receiving LLC cells plus paclitaxel-loaded expansile nanoparticles showed a significantly reduced incidence of tumor and tumor burden. After 30 days, rapid growing tumors were noticed at the site where LLC cells were coinjected with Ptxl-LA₂₅ NCs at 5 mg/kg; whereas tumors sizes were maintained for the group coinjected with with Ptxl-LA₂₅ NCs at 50 mg/kg (Figure 5.12). The observation that animals receiving all other treatment regimes besides the Ptxl loaded NCs (50mg/kg) rapidly developed large tumors suggests that NCs are an effective delivery vehicle for Ptxl.

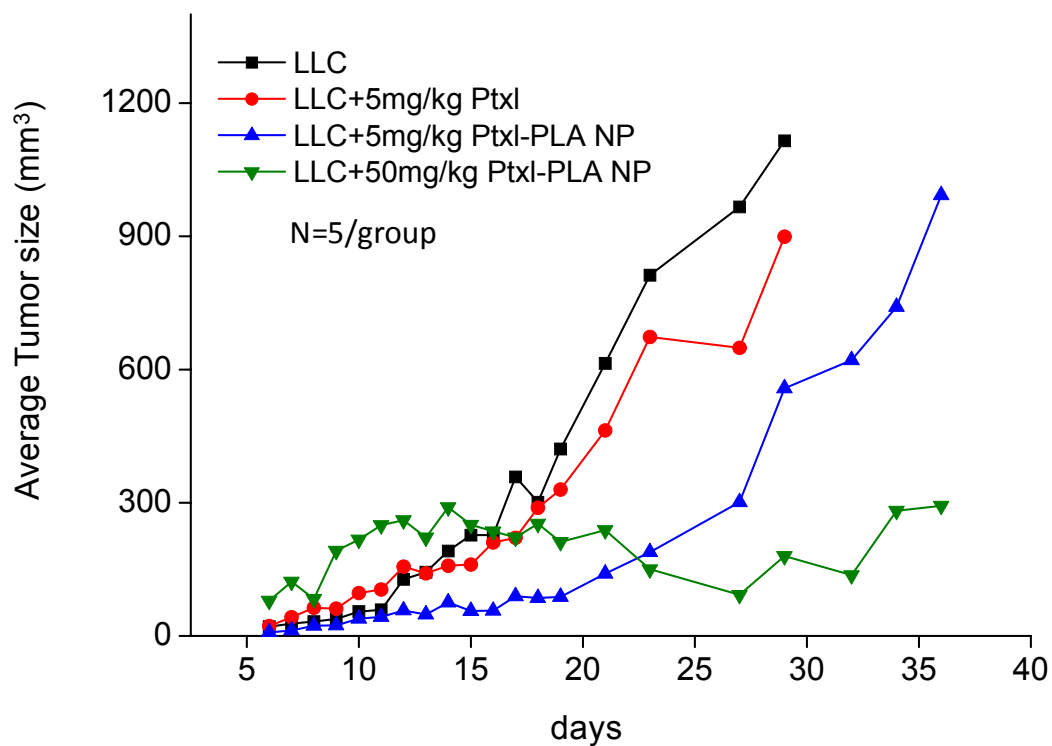
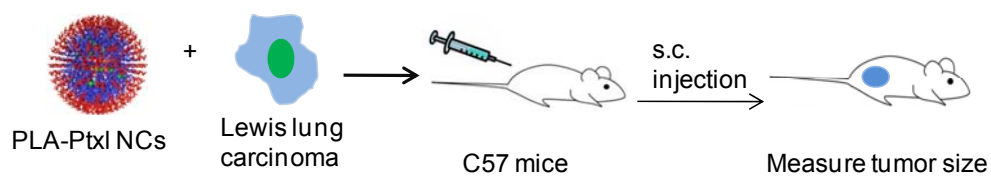


Figure 5.12 LLC tumor prevention study for C57Bl/6 mice, by mixing LLC cells (1,000,000) with Ptxl-LA₂₅/PLGA-mPEG NPs (5 and 50 mg/kg Ptxl equiv.), Ptxl in Cremophor EL / ethanol (5mg/kg Ptxl equiv.) in matrigels for s.c. injection. The data showed statistical significance after 20 days.

3.11 In vivo toxicity evaluation of PLA-Doxo NPs with pamidronate for bone tumor targeting

A treatment for osteoporosis that is gaining popularity is bisphosphonate therapy. Bisphosphonates are antiresorptive medications that bind to the mineral phase of bone and inhibit the activity of osteoclasts. Bisphosphonates have a long history with many applications including use as detergent additives in hard water treatment, in toothpaste to prevent tartar buildup, as treatment for Paget's disease, and as a diagnostic tool for bone tumor treatment. In recent years, they have been mainly studied as an osteoporosis therapy because of their ability to inhibit bone resorption. The complex mechanism of action of bisphosphonates has only recently been understood, but in general, bisphosphonate binds to hydroxyapatite, the main mineral component of bone. When osteoclasts begin to resorb the bone, bisphosphonate is taken up by the cell, which then loses its resorptive function and undergoes apoptosis. The loss in the ability of the osteoclast to resorb bone following the administration of bisphosphonates causes an increase in bone mineral density. We hence selected pamidronate (PAM), a well-known bisphosphonate drug, as the targeting ligand for bone-tumor cancer chemotherapy. PAM was conjugated to the PLA-PEG-COOH through conjugation reaction using EDC/NHS. The resulted PLA-PEG-PAM was purified by dialysis. Doxo-LA₂₅ was mixed with PLGA-mPEG/PLA-PEG-PAM in DMF and nanoprecipitation to prepare NPs with 126 nm sizes. To validate the potential of Doxo-LA₂₅/PLA-PEG-PAM NPs for bone tumor therapy, we evaluate the toxicity of NPs to tissues by histological study in balb/c mice. After staining by hematoxylin and eosin, kidney tissue damage was found in the group treated with 8 mg/kg Doxo; while no kidney tissue toxicity are found in groups received NPs with same and twice Doxo equivalent dose (8 and 16 mg/kg) and controls. In

addition PLA-PEG-PAM NPs itself did not exhibit *in vivo* toxicity in histological tissue analysis (Figure 5.13). The study demonstrated that Doxo-LA₂₅/PLA-PEG-PAM can be further applied for preclinical study for bone cancer therapy. The *in vivo* tissue toxicity was also confirmed by infusion PLA-PEG-PAM NPs (50mL saline solution, 3 mg/mL NPs) to dogs (n=5), and no severe or abnormal symptoms were observed even few days after injection.

It is noted that PAM can be labeled with ^{99m}Tc for real time *in vivo* imaging, facilitating the monitor of targeting process. The potential to employ the radionuclide technetium-99m with its optimal decay characteristics into targeting molecules has been the foremost consideration in developing diagnostic radiopharmaceuticals. ^{99m}Tc-labeled radiopharmaceuticals are preferred over other isotopes because of the ideal nuclear properties of the isotope, as well as its widespread availability from commercial generator columns. ^{99m}Tc emits a 140 keV γ -ray with 89% abundance, which is ideal for imaging with commercial γ cameras. We in situ labeled PLA-PEG-PAM NPs with sodium ^{99m}TcO₄ in saline and the reductant SnCl₂ and quickly used for *in vivo* bone tumor targeting study in dog. Bone tumors were grown in one leg of the dog and confirmed by X-ray. The accumulation of PLA-PEG-PAM NPs with ^{99m}Tc labeling was observed in γ camera images, and the amount was increased over the time even 2 hours after injection (Figure 5.14). Whole body biodistribution analysis of the dog showed NPs were not accumulated in liver and kidney over 2 hour after infusion, suggesting NPs with PAM can quickly target bone tumor *in vivo*. It is noted that intensity was also increased in the bladder site after 30 hours which was suspected the ^{99m}Tc reagents might be sheared off from NPs.

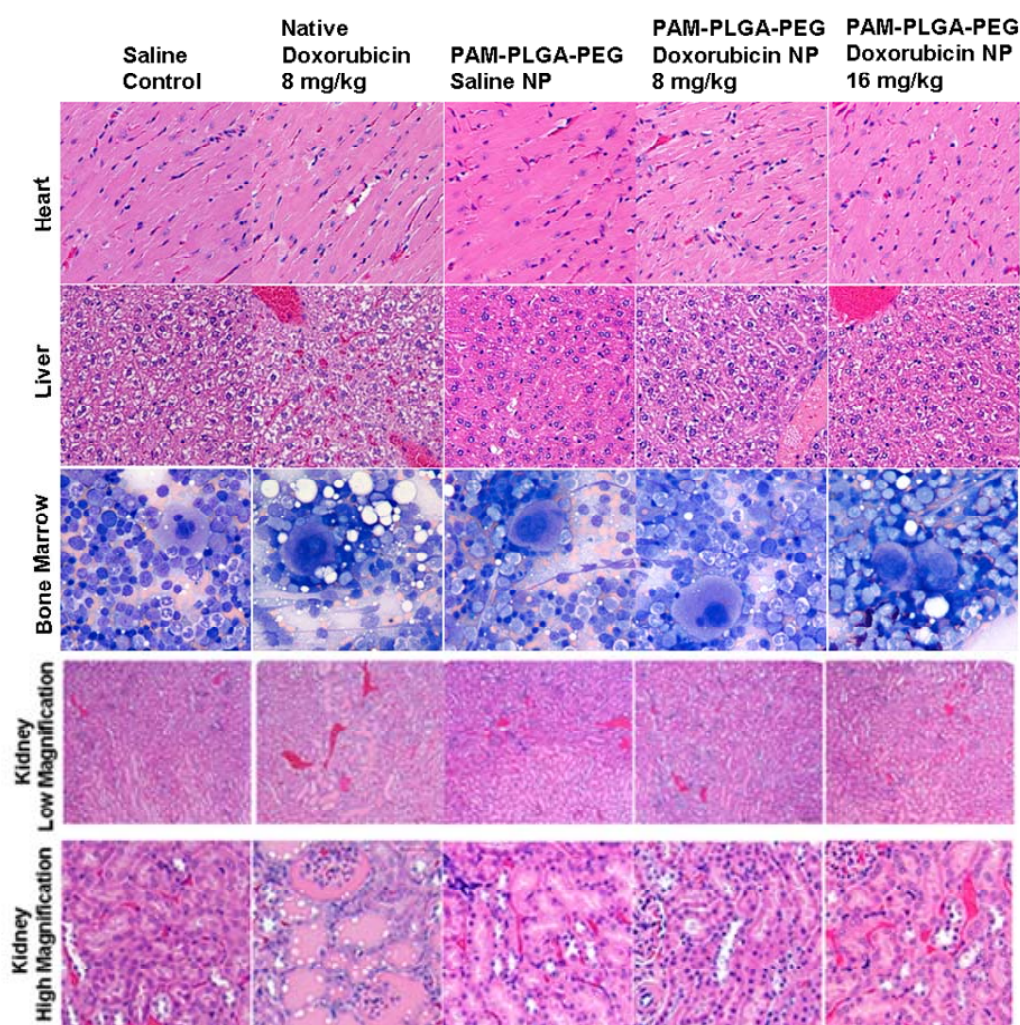


Figure 5.13 Histological analysis of balb/c mice tissue sections. The mice were dosed (i.v.) with Doxo (8 mg/kg) and PLA-PEG-PAM / Doxo-LA₂₅ (8 and 16 mg/kg), saline and blank NPs. Tissue sections from the mice kidney indicated that Doxo (8mg/kg) has severe toxicity to kidney, while NPs with 16 mg/kg Doxo equiv. did not show any toxicity to kidney tissues.

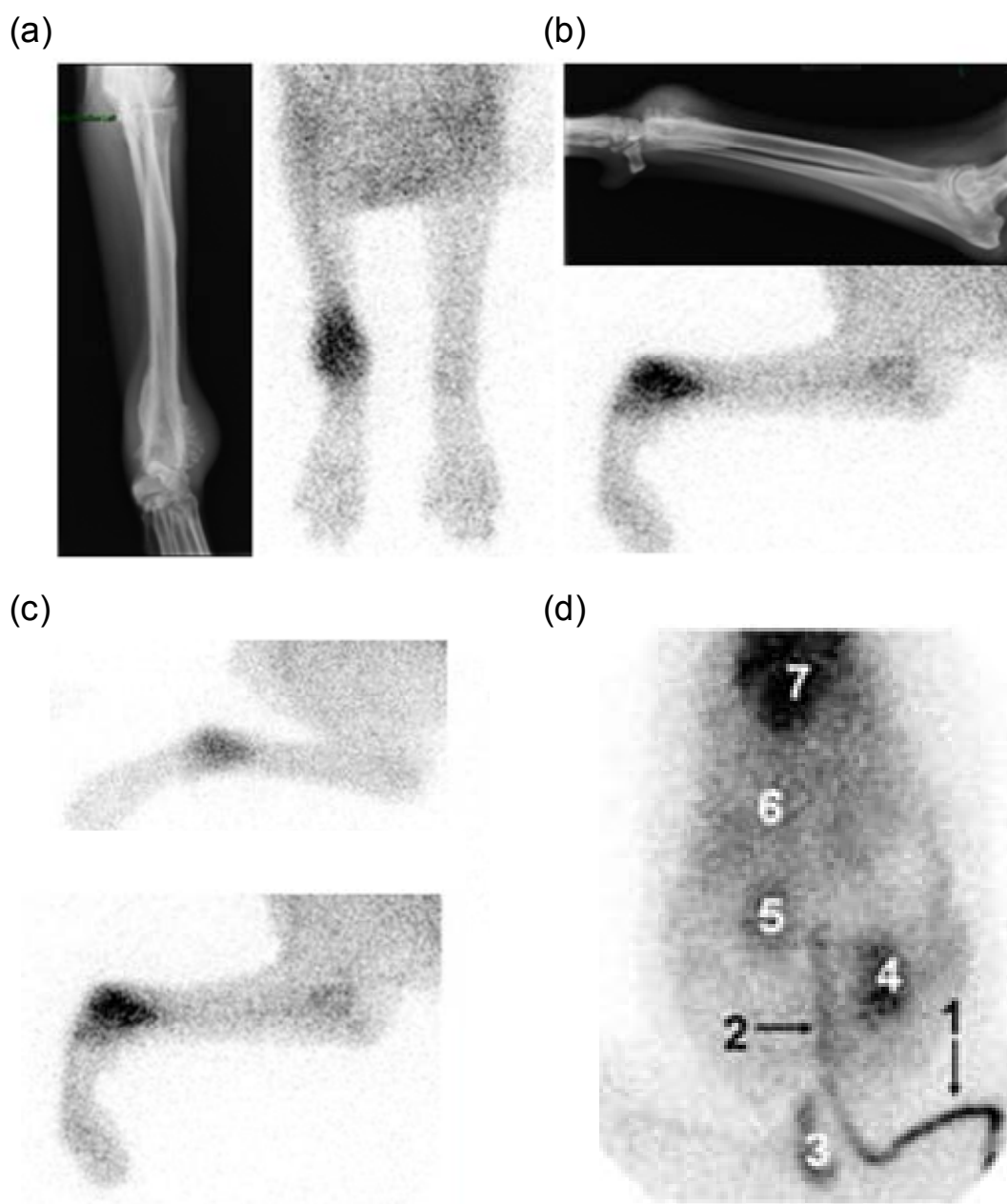


Figure 5.14 *In vivo* imaging of PLA-PEG-PAM NPs labeled with ^{99m}Tc for bone tumor in dog: X ray and ^{99m}Tc radioactive γ imagings of (a) front and (b) lateral view of dog leg with one side implanted with tumor. The intensity (black) area of ^{99m}Tc radioactive images indicated the accumulation of the NPs. (c) Kinetic study of NPs accumulation in bone tumor of 1 hour (up) and 2 hours (bottom) after injection. (d) Whole body biodistribution of NPs in dog 5 min after injection (top view). Site number: 1: lateral saphenous vein (NPs infusion site); 2: caudal vena cava; 3: urinary bladder; 4: left kidney; 5: right kidney; 6: liver; 7: heart.

4. Conclusions

In summary, we developed various techniques that allow for formulation of polymeric nanoconjugates with controlled chemo-physical and biological properties. We developed a one-step, co-precipitation method to formulate nanoconjugates that could stay non-aggregated in a salt solution with the use amphiphilic triblock copolymer as the surfactant for particle surface modification. We also discovered that albumin can function as an excellent lyoprotectant and successfully achieved the solid formulation of nanoconjugates that could be reconstituted with absolutely no particle aggregation. By incorporating the albumin-based lyoprotection technique, we demonstrated for the first time that polymer nanoparticles containing a conjugated nucleic acid targeting ligand can be prepared in solid form that can be reconstituted to well-dispersed, non-aggregated particles and well-maintained targeting capability. These new formulation strategies and findings can potentially be broadly employed for the controlled preparation of numerous nanoparticles. Preliminary *in vivo* studies showed potential application for the nanoconjugates system as the candidate for nanomedicine.

5. References

- [1] R. Tong, J. J. Cheng, *Polym. Rev.* **2007**, 47, 345.
- [2] (a) R. Tong, D. A. Christian, L. Tang, H. Cabral, J. R. Baker, K. Kataoka, D. E. Discher, J. J. Cheng, *MRS Bulletin* **2009**, 34, 422; (b) S. M. Moghimi, A. C. Hunter, J. C. Murray, *FASEB J.* **2005**, 19, 311; (c) R. Duncan, *Nat. Rev. Cancer* **2006**, 6, 688; (d) L. Zhang, F. X. Gu, J. M. Chan, A. Z. Wang, R. S. Langer, O. C. Farokhzad, *Clin. Pharmacol. Ther.* **2008**, 83, 761.
- [3] K. Avgoustakis, *Curr. Drug Deliv.* **2004**, 1, 321.
- [4] T. T. Goodman, P. L. Olive, S. H. Pun, *Int. J. Nanomedicine* **2007**, 2, 265.

- [5] F. Alexis, E. Pridgen, L. K. Molnar, O. C. Farokhzad, *Mol. Pharm.* **2008**, *5*, 505.
- [6] (a) R. Tong, J. J. Cheng, *Angew. Chem. Int. Ed.* **2008**, *47*, 4830; (b) R. Tong, J. J. Cheng, *J. Am. Chem. Soc.* **2009**, *131*, 4744.
- [7] (a) Y. Dong, S. S. Feng, *Biomaterials* **2007**, *28*, 4154; (b) B. A. Teply, R. Tong, S. Y. Jeong, G. Luther, I. Sherifi, C. H. Yim, A. Khademhosseini, O. C. Farokhzad, R. S. Langer, J. Cheng, *Biomaterials* **2008**, *29*, 1216; (c) J. Cheng, B. A. Teply, I. Sherifi, J. Sung, G. Luther, F. X. Gu, E. Levy-Nissenbaum, A. F. Radovic-Moreno, R. Langer, O. C. Farokhzad, *Biomaterials* **2007**, *28*, 869.
- [8] T. Musumeci, C. A. Ventura, I. Giannone, B. Ruozzi, L. Montenegro, R. Pignatello, G. Puglisi, *Int. J. Pharm.* **2006**, *325*, 172.
- [9] K. J. Hamblett, P. D. Senter, D. F. Chace, M. M. C. Sun, J. Lenox, C. G. Cervený, K. M. Kissler, S. X. Bernhardt, A. K. Kopcha, R. F. Zabinski, D. L. Meyer, J. A. Francisco, *Clin. Cancer Res.* **2004**, *10*, 7063.
- [10] T. Schluep, J. Hwang, J. J. Cheng, J. D. Heidel, D. W. Bartlett, B. Hollister, M. E. Davis, *Clin. Cancer Res.* **2006**, *12*, 1606.
- [11] (a) B. M. Chamberlain, M. Cheng, D. R. Moore, T. M. Ovitt, E. B. Lobkovsky, G. W. Coates, *J. Am. Chem. Soc.* **2001**, *123*, 3229; (b) B. J. O'Keefe, M. A. Hillmyer, W. B. Tolman, *J. Chem. Soc., Dalton Trans.* **2001**, 2215.
- [12] (a) J. J. Cheng, T. J. Deming, *Macromolecules* **2001**, *34*, 5169; (b) H. Lu, J. J. Cheng, *J. Am. Chem. Soc.* **2008**, *130*, 12562.
- [13] M. Ouchi, T. Terashima, M. Sawamoto, *Chem. Rev.* **2009**, *109*, 4963.
- [14] O. C. Farokhzad, J. J. Cheng, B. A. Teply, I. Sherifi, S. Jon, P. W. Kantoff, J. P. Richie, R. Langer, *Proc. Natl. Acad. Sci. U. S. A.* **2006**, *103*, 6315.
- [15] R. Gref, Y. Minamitake, M. T. Peracchia, V. Trubetskoy, V. Torchilin, R. Langer, *Science* **1994**, *263*, 1600.
- [16] H. Maeda, J. Wu, T. Sawa, Y. Matsumura, K. Hori, *J. Controlled Release* **2000**, *65*, 271.
- [17] (a) U. Bilati, E. Allemann, E. Doelker, *Eur. J. Pharm. Sci.* **2005**, *24*, 67; (b) S. Galindo-Rodriguez, E. Allemann, H. Fessi, E. Doelker, *Pharm. Res.* **2004**, *21*, 1428.
- [18] S. M. Moghimi, A. C. Hunter, J. C. Murray, *Pharmacol. Rev.* **2001**, *53*, 283.
- [19] S. M. Moghimi, I. S. Muir, L. Illum, S. S. Davis, V. Kolbbachofen, *Biochim. Biophys. Acta* **1993**, *1179*, 157.
- [20] M. J. Roberts, M. D. Bentley, J. M. Harris, *Adv. Drug Delivery Rev.* **2002**, *54*, 459.
- [21] T. Schluep, J. J. Cheng, K. T. Khin, M. E. Davis, *Cancer Chemother. Pharmacol.* **2006**, *57*, 654.

- [22] (a) J. Fukuda, A. Khademhosseini, J. Yeh, G. Eng, J. J. Cheng, O. C. Farokhzad, R. Langer, *Biomaterials* **2006**, 27, 1479; (b) J. M. Karp, J. Yeh, G. Eng, J. Fukuda, J. Blumling, K. Y. Suh, J. Cheng, A. Mahdavi, J. Borenstein, R. Langer, A. Khademhosseini, *Lab Chip* **2007**, 7, 786.
- [23] (a) A. L. Kjoniksen, F. Joabsson, K. Thuresson, B. Nystrom, *J. Phys. Chem. B* **1999**, 103, 9818; (b) S. H. Pun, F. Tack, N. C. Bellocq, J. J. Cheng, B. H. Grubbs, G. S. Jensen, M. E. Davis, M. Brewster, M. Janicot, B. Janssens, W. Floren, A. Bakker, *Cancer Biol. Ther.* **2004**, 3, 641.
- [24] Z. L. Dai, L. H. Piao, X. F. Zhang, M. X. Deng, X. S. Chen, X. B. Jing, *Colloid Polym. Sci.* **2004**, 282, 343.
- [25] T. Musumeci, L. Vicari, C. A. Ventura, M. Gulisano, R. Pignatello, G. Puglisi, *J. Nanosci. Nanotechnol.* **2006**, 6, 3118.
- [26] V. Wagner, A. Dullaart, A. K. Bock, A. Zweck, *Nat. Biotechnol.* **2006**, 24, 1211.
- [27] (a) C. Tuerk, L. Gold, *Science* **1990**, 249, 505; (b) A. D. Ellington, J. W. Szostak, *Nature* **1990**, 346, 818; (c) A. D. Ellington, J. W. Szostak, *Nature* **1992**, 355, 850.
- [28] S. M. Nimjee, C. P. Rusconi, B. A. Sullenger, *Annu. Rev. Med.* **2005**, 56, 555.
- [29] S. E. Lupold, B. J. Hicke, Y. Lin, D. S. Coffey, *Cancer Res.* **2002**, 62, 4029.
- [30] O. C. Farokhzad, S. Y. Jon, A. Khademhosseini, T. N. T. Tran, D. A. LaVan, R. Langer, *Cancer Res.* **2004**, 64, 7668.

CHAPTER 6
EFFICIENT REGIOSELECTIVE *O*-ACYLATION OF THERAPEUTIC AGENTS
BY β -DIIMINATE ZINC CATALYST

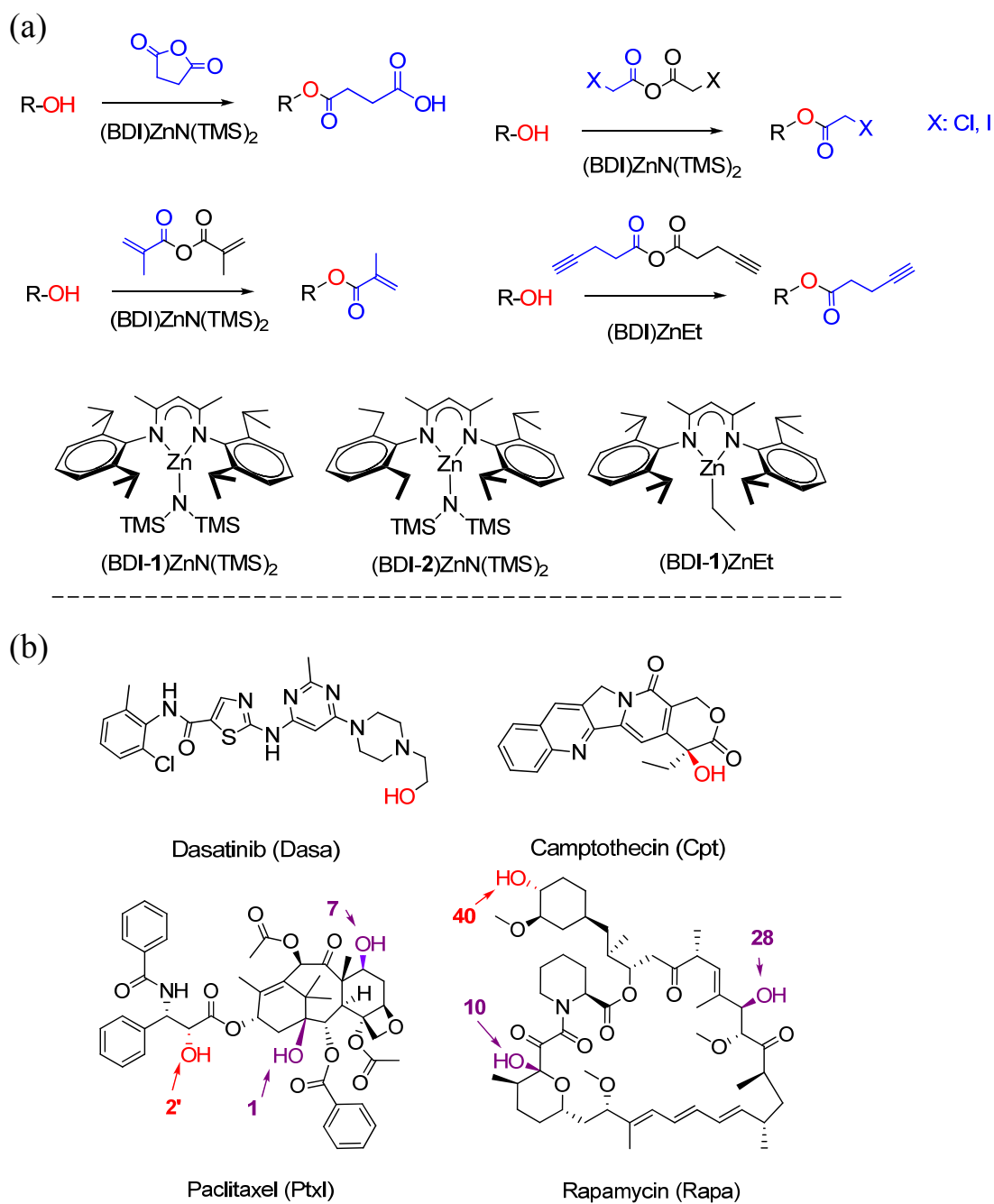
1. Introduction

The development of medicinal chemistry builds upon the efficient generation of analogs of natural products and lead drugs.^[1] Based on the statistical investigation in 1999, alcohols are the most abundant functional group in natural products (65% of pharmacophors groups in 78,318 structural entries).^[2] Standard *O*-acylation is one of the most commonly methods for direct derivatization. Besides, ester bond for linking therapeutic agents with delivery vehicles or polymeric scaffolds has been a strategy extensively employed in drug delivery and tissue engineering.^[3] Efficient acylation of the hydroxyl groups (*O*-acylation) in these hydroxyl-containing agents is expected to facilitate the generation of drug analogues and the application of conjugates in drug delivery and even bioengineering field. However, direct and precise acylation of therapeutic agents are typically challenging because of their complex structures and multifunctional nature.^[4] Enzymatic synthesis in non-aqueous solution emerged as one promising method in this context.^[5] Yet, the specificity in the reaction and the selection of enzymes leads to a limited set of natural-product analogs.^[6] Miller and coworkers recently reported an intriguing method based on the selection of oligo-peptides as acylation catalysts for the regioselective reaction of complex biologically active agents (e.g. Erythromycin A) with anhydrides.^[7] Hoveyda, Snapper and coworkers devised amino-acid based chiral catalyst to promote enantioselective silylation of alcohols.^[8] A

recent remark by the director of the National Institutes of Health pointed out: 'one interesting result of the NIH Roadmap development process came when we surveyed scientists to find out what the stumbling blocks for biological sciences were. The number one stumbling block turned out to be synthetic organic chemistry.'^[9] Given the importance and broad utility of releasable ester linkers, it is in great demand for new methodologies that allow for controlled O-acylation for many important therapeutic agents.

We previously reported drug-initiated ring-opening polymerization of lactide (LA) in the mediation of (BDI-1)ZnN(TMS)₂ catalyst^[10] (BDI= β -diiminate, the structures are shown in Scheme 6.1(a)). When (BDI-1)ZnN(TMS)₂ was mixed with hydroxyl-containing drug molecules, (BDI-1)Zn-drug alkoxides were in situ quantitatively formed. The activated hydroxyl group of the therapeutic agents allows for ring-opening of LA and gave well-controlled ROP of LA. Interestingly, in our development of drug-poly(lactide (PLA) nanoconjugates (NCs), we demonstrated that the reaction of succinic anhydride (SA) with Paclitaxel (Ptxl) or Doxorubicin (Doxo) proceeded in a highly regioselective manner in the presence of (BDI-1)ZnN(TMS)₂ and produced corresponding prodrugs with tethered carboxylic acid group.^[10] We initially investigated whether activation of the hydroxyl group of therapeutic agents by (BDI)ZnN(TMS)₂ can be used for O-acylation by reacting with acylation-amenable reagents (Scheme 6.1). Complex therapeutic agents are focused in this study due to their potential significance in the development of medicinal chemistry and bioconjugates. Finally we further explored the one pot acylation strategy, easing the protocol from more commercial available carboxylic acids instead of anhydrides.

Scheme 6.1 Regioselective O-acylation reaction mediated by BDI-Zn catalyst. (a) The O-acylation reaction scheme of SA, CIAA, MAA and PA. (b) The chemical structures of Dasa, Cpt, Ptxl and Rapa.



2. Materials and Methods

2.1 General

BDI ligands and the corresponding metal catalysts (BDI)ZnN(TMS)₂ and (BDI)ZnEt were prepared by following the published procedure^[11] and stored at -30°C in a glove box. All anhydrous solvents were purified through alumina columns and kept anhydrous by molecular sieves. Paclitaxel (Ptxl), (S)-(+)-Camptothecin (Cpt), Dasatinib (Dasa) and Rapamycin (Rapa) was purchased from the LC Laboratories (Woburn, MA, USA), and used as received. Doxorubicin HCl salt (Doxo) was purchased from Bosche Scientific (New Brunswick, NJ) and used as received. All other chemicals were purchased from Sigma-Aldrich (St Louis, MO, USA) and used as received unless otherwise noted. Triethylamine (TEA) was dried with 4 Å molecular sieves overnight, transferred by a cannula under nitrogen to a clean flask containing CaH₂, refluxed overnight, distilled and collected under nitrogen, and stored in glove box with 4 Å molecular sieves. Methacrylic anhydride (MAA) was dried with CaH₂ for 24 hours, vacuum transferred onto activated 4 Å molecular sieves, and then fractionally distilled under reduced pressure. The entire process was repeated. The fresh purified MAA was stored in the glove box fridge at -30 °C degree before use. Succinic anhydride (SA) and chloroacetic anhydride (ClAA) were recrystallized from chloroform and stored in the glove box. Pent-4-ynoic anhydride (PA) was synthesized following reference. PA was freshly distilled twice under reduced pressure and stored in the glove box fridge at -30 °C degree before use.

The low resolution electrospray ionization mass spectrometry (LR-ESI-MS) experiments were conducted on a Waters Quattro II mass spectrometer. The high

resolution electrospray ionization mass spectrometry (HR-ESI MS) experiments were performed on a Micromass Q-TOF Ultima system.

HPLC analysis was performed on a System Gold system (Beckman Coulter, Fullerton, CA) equipped with a 126P solvent module, a System Gold 128 UV detector and an analytical pentafluorophenyl column (Curosil-PFP, 250 × 4.6 mm, 5 μ , Phenomenex, Torrance, CA) or an analytical C18 column (Luna C18(2), 250 × 4.6 mm, 5 μ , Phenomenex, Torrance, CA). The UV wavelengths for analysis of Ptxl, Rapa, Cpt, Dasa, Doxo were 227, 280, 370, 400, 450 nm, respectively.

NMR analyses were conducted on a Varian U500, VXR500 or UI500NB (500 MHz). The following abbreviations are used to describe spin multiplicity: s = singlet, d = doublet, t = triplet, q = quartet, m = multiplet, b = broad, dd = doublet of doublets, dt = doublet of triplets, dq = doublet of quartets, and ddd = doublet of doublet of doublets; other combinations derive from those listed. Coupling constants (J) are reported in Hertz (Hz). Carbon-13 NMR spectra are reported as chemical shifts in ppm based on the middle peak of chloroform-d (77.0 ppm) and are recorded with complete heterodecoupling.

Analytical TLC was performed with 0.25 mm silica gel 60 plates with a 254 nm fluorescent indicator from Merck. Plates were developed in a covered chamber and visualized by UV light and by treatment with anisaldehyde stain followed by heating. Preparative thin layer chromatography (prep TLC) was conducted with silica gel plates (1500 μ m thickness, Sigma-Aldrich) with a 254 nm fluorescent indicator

PC-3 cells (ATCC, Manassas, VA, USA) were cultured in Ham's F12K medium containing 10% FBS (Fetal Bovine Serum), 1000 units/mL aqueous Penicillin G and 100 μ g/mL streptomycin.

NTera-2 cells ATCC, Manassas, VA, USA) were cultured in Dulbecco's Modified Eagle's Medium (ATCC, Catalogue 30-2002) containing 10% FBS (Fetal Bovine Serum), 1000 units/mL aqueous Penicillin G and 100 $\mu\text{g/mL}$ streptomycin. The medium were replaced every day.

2.2 *Synthesis of Naph derivatives*

In a glove box, (BDI-1)ZnN(TMS)₂ (6.4 mg, 0.01 mmol) was dissolved in anhydrous THF (200 μL). This solution was added to a clean vial containing Naph (1.7 mg, 0.01mmol). The reaction mixture was diluted with THF (300 μL) and stirred for 15 min. SA (1.1 mg, 0.011 mmol) in THF (300 μL) was added to the mixture of Naph and (BDI-1)ZnN(TMS)₂ at [SA]₀ of 0.01 M. The reaction vial was tightly sealed, immediately moved out of glove box, and put in a 40 °C oil bath. The reaction mixture was stirred for an additional of 4 h and quenched with ice-cold methanol (1 mL). An aliquot of this solution was analyzed by HPLC equipped with an analytical C18 column (Luna C18(2), 250 \times 4.6 mm, 5 μ , Phenomenex, Torrance, CA). The mobile phase for the HPLC analysis was a mixed solvent of equal volume of acetonitrile and water with 0.1% TFA. All HPLC spectra were recorded and analyzed with a UV detector at 280 nm. The areas of Naph and Naph-anhydride peaks were integrated and used for their quantification of the yield.

2.3 *Synthesis of Dasa-MAA*

Dasa (4.8 mg) was mixed with (BDI-1)ZnN(TMS)₂ at 1/1 equiv in a glove box. The mixture was stirred for 20 min. MAA was distilled freshly before using and stored in glove box fridge. 1.2 equiv MAA in THF (0.5 mL) was added into the mixture and

further stirring over 10h at room temperature. The solution was quenched by methanol, and dried. The solid was redispersed at 0.5 mL methanol solution. On 1.5 mm thick TLC plates, the concentrated solution was applied, and developed by ethyl acetate/methanol (9/1). R_f~0.3. The silica gel was scratched from plates and extracted by methanol twice (2x20ml). The solution was dried and used for NMR analysis.

MS (LR-ESI, positive mode): calculated for C₂₆H₃₀N₇O₃SCl [M + H]⁺ *m/z* 555.1, found *m/z* 555.1.

2.4 *Synthesis of Cpt-SA*

In a glove box, (BDI-2)ZnN(TMS)₂ (6.2 mg, 0.01 mmol) was dissolved in anhydrous THF (200 μL). This solution was added to a clean vial containing Cpt (3.5 mg, 0.01mmol). The reaction mixture was diluted with THF (300 μL) and stirred for 15 min until Cpt was completely dissolved. SA (1.1 mg, 0.011 mmol) in THF (600 μL) was added to the mixture of Cpt and (BDI-2)ZnN(TMS)₂ at [SA]₀ of 0.01 M. The reaction vial was tightly sealed, immediately moved out of glove box, and put in a 40 °C oil bath. The reaction mixture was stirred for an additional of 4 h and quenched with ice-cold methanol (1 mL). An aliquot of this solution was analyzed by HPLC equipped with an analytical C18 column (Luna C18(2), 250 × 4.6 mm, 5 μ, Phenomenex, Torrance, CA). The mobile phase for the HPLC analysis was a mixed solvent of equal volume of acetonitrile and water with 0.1% TFA. All HPLC spectra were recorded and analyzed with a UV detector at 370 nm. The areas of Cpt and Cpt-SA peaks were integrated and used for their quantification using the corresponding standard curves. An aliquot of reaction mixture was used for MS analysis.

Pure Cpt-SA used for NMR analysis was separated by preparative thin layer chromatography (prep TLC, silica gel matrix with UV254, 1500 μm thickness, Aldrich) and developed by ethyl acetate/methanol (10/1, v/v). The R_f values of Cpt and Cpt-SA were 0.7 and 0.1, respectively. The silica gels containing Cpt-SA were collected from the glass plate; the Cpt-SA in the gel was extracted with methanol ($2 \times 30 \text{ mL}$). The methanol solution was then removed under vacuum; the resulting Cpt-SA was analyzed by ^1H NMR. ^1H -NMR (CD_3OD , 500 MHz): δ 8.63 (s, 1H, 7-H), 8.21 (d, $J = 8.5 \text{ Hz}$, 1H, 12-H), 8.07 (d, $J = 8.0 \text{ Hz}$, 1H, 9-H), 7.87 (td, $J_t = 8.5 \text{ Hz}$, $J_d = 1.5 \text{ Hz}$, 1H, 11-H), 7.71 (td, $J_t = 8.0 \text{ Hz}$, $J_d = 1.0 \text{ Hz}$, 1H, 10-H), 7.43 (s, 1H, 14-H), 5.57, 5.44 (AB, $J_{AB} = 17.0 \text{ Hz}$, 2H, 17-H), 5.35 (s, 1H, 5-H), 2.81 (t, $J = 7.5 \text{ Hz}$, 2H, $-\text{CH}_2\text{-COOH}$), 2.55 (t, $J = 7.5 \text{ Hz}$, 2H, $-\text{CH}_2\text{-CH}_2\text{-COOH}$), 2.24 (m, 2H, 18-H), 0.99 (t, $J = 8.0 \text{ Hz}$, 19-H). MS (LR-ESI, positive mode): calculated for $\text{C}_{24}\text{H}_{20}\text{N}_2\text{O}_7$ $[\text{M} + \text{H}]^+$ m/z 449.1; found m/z 449.1. MS (HR-ESI, positive mode): calculated for $\text{C}_{24}\text{H}_{20}\text{N}_2\text{O}_7$ $[\text{M} + \text{H}]^+$ m/z 449.1349; found m/z 449.1355.

2.5 Synthesis of Cpt-MAA

In a glove box, $(\text{BDI-2})\text{ZnN}(\text{TMS})_2$ (6.2 mg, 0.01 mmol) was dissolved in anhydrous THF (200 μL). This solution was added to a clean vial containing Cpt (3.5 mg, 0.01 mmol). The reaction mixture was diluted with THF (300 μL) and stirred for 15 min until Cpt was completely dissolved. MAA (1.70 mg, 0.011 mmol) in THF (300 μL) was dropwise added to the mixture of Cpt and $(\text{BDI-2})\text{ZnN}(\text{TMS})_2$ at $[\text{MAA}]_0$ of 0.01 M. The reaction vial was tightly sealed, immediately moved out of glove box, and put in a 40 $^\circ\text{C}$ oil bath. The reaction mixture was stirred for an additional of 4 h and quenched with ice-cold methanol/acetic acid (1.1 mL, v/v=10/1). An aliquot of this solution was

analyzed by HPLC equipped with an analytical C18 column (Luna C18(2), 250 × 4.6 mm, 5 μ , Phenomenex, Torrance, CA). The mobile phase for the HPLC analysis was a mixed solvent of equal volume of acetonitrile and water with 0.1% TFA. All HPLC spectra were recorded and analyzed with a UV detector at 370 nm. The areas of Cpt and Cpt-MAA peaks were integrated and used for their quantification using the corresponding standard curves. An aliquot of reaction mixture was used for MS analysis.

Pure Cpt-MAA used for NMR analysis was separated by preparative thin layer chromatography (prep TLC, silica gel matrix with UV254, 1500 μ m thickness, Aldrich) and developed by ethyl acetate/dichloromethane/methanol (1/9/1, v/v). The R_f values of Cpt and Cpt-MAA were about 0.1 and 0.3, respectively. The silica gels containing Cpt-MAA were collected from the glass plate; the Cpt-MAA in the gel was extracted with methanol (2 × 30 mL). The methanol solution was then removed under vacuum; the resulting Cpt-MAA was analyzed by ^1H -NMR. ^1H -NMR (CD_3OD , 500 MHz): δ 8.63 (s, 1H, 7-H), 8.21 (d, J = 8.5 Hz, 1H, 12-H), 8.07 (d, J = 8.0 Hz, 1H, 9-H), 7.87 (td, J_t = 8.5 Hz, J_d = 1.5 Hz, 1H, 11-H), 7.71 (td, J_t = 8.0 Hz, J_d = 1.0 Hz, 1H, 10-H), 7.43 (s, 1H, 14-H), 6.33, 5.83 (s, $\text{C}(\text{CH}_3)=\text{CH}_2$), 5.63, 5.49 (AB, J_{AB} = 17.0 Hz, 2H, 17-H), 5.35 (s, 1H, 5-H), 2.81 (t, J = 7.5 Hz, 2H, $-\text{CH}_2-\text{COOH}$), 2.26 (m, 2H, 18-H), 1.98 (s, $\text{C}(\text{CH}_3)=\text{CH}_2$), 1.04 (t, J = 8.0 Hz, 19-H). MS (LR-ESI, positive mode): calculated for $\text{C}_{24}\text{H}_{20}\text{N}_2\text{O}_5$ [$\text{M} + \text{H}$] $^+$ m/z 417.1; found m/z 417.3.

2.6 Synthesis of Ptxl derivatives

2.6.1 General synthesis procedure

Briefly, Ptxl (8 mg, 0.0094 mmol, 1 equiv) was be mixed with (BDI-1) $\text{ZnN}(\text{TMS})_2$ (6.0mg, 0.0094 mmol) and THF (0.50mL) in a glove box. The reaction

mixture will be stirred for 20 min. Freshly distilled MAA (1.7 mg, 0.011 mmol, 1.2 equiv) in THF solution (0.20 mL) will be added into Ptxl/(BDI-1)ZnN(TMS)₂ and further stirring for certain time. The solution will be quenched by ice-cold methanol (1mL), and dried under vacuum. The solid will be redispersed in methanol solution (0.30mL). All HPLC spectra were recorded and analyzed with a UV detector at 227 nm. The areas of Ptxl and Ptxl-MAA peaks were integrated and used for their quantification of the yield. An aliquot of reaction mixture was used for MS analysis.

Pure Ptxl-MAA used for NMR analysis was obtained by prep TLC. The concentrated reaction solution will be applied on 1.5 mm thick prep-TLC plates, and developed by ethyl acetate/hexane (1/3). The product will be recovered by extraction using methanol twice (2 x 20ml). The solution will be dried under vacuum and analyzed by NMR.

2.6.2 Characterization of Ptxl derivatives

Ptxl-MAA

¹H-NMR (500MHz, CDCl₃): δ = 8.13 (d, J = 7.57 Hz, 2H), 7.72 (d, J = 7.57 Hz, 2H), 7.62 – 7.40 (m, 11H), 6.93 (d, J = 9.14 Hz, 1H), 6.29 – 6.23 (m, 2H), 6.01 (d, J = 7.14 Hz, 1H), 5.66 (d, J = 6.80 Hz, 1H), 5.55 (d, J = 2.24 Hz, 1H), 4.96 (d, J = 8.79 Hz, 1H), 4.43 (m, 1H), 4.30 (d, J = 8.29 Hz, 1H), 4.20 – 4.15 (m, 2H), 3.81 (d, J = 6.71 Hz, 1H), 2.56 – 2.34 (m, 3H), 2.45 (s, 3H), 2.21 (s, 3H), 2.19 (m, 1H), 1.95 – 1.82 (m, 3H), 1.92 s, (3H), 1.67 (s, 3H), 1.22 (s, 3H), 1.13 (s, 3H) ppm.

MS (LR-ESI, positive mode): calculated for C₅₁H₅₅NO₁₅ [M + H]⁺ m/z 922.5; found m/z 922.5.

MS (HR-ESI, positive mode): calculated for

Ptxl-2'-ClAA

^1H -NMR (500MHz, CDCl_3): δ = 8.13 (d, J = 7.57 Hz, 2H), 7.72 (d, J = 7.57 Hz, 2H), 7.62 – 7.40 (m, 11H), 6.93 (d, J = 9.14 Hz, 1H), 6.29 – 6.23 (m, 2H), 6.01 (d, J = 7.14 Hz, 1H), 5.66 (d, J = 6.80 Hz, 1H), 5.55 (d, J = 2.24 Hz, 1H), 4.96 (d, J = 8.79 Hz, 1H), 4.43 (m, 1H), 4.30 (d, J = 8.29 Hz, 1H), 4.20 – 4.15 (m, 2H), 3.81 (d, J = 6.71 Hz, 1H), 2.56 – 2.34 (m, 3H), 2.45 (s, 3H), 2.21 (s, 3H), 2.19 (m, 1H), 1.95 – 1.82 (m, 3H), 1.92 s, (3H), 1.67 (s, 3H), 1.22 (s, 3H), 1.13 (s, 3H) ppm.

^{13}C -NMR (125 MHz, CDCl_3): δ = 203.6, 171.1, 169.7, 167.3, 167.0, 166.9, 166.3, 142.3, 136.4, 133.6, 133.5, 132.9, 132.0, 130.1, 129.2, 129.1, 128.7, 128.6, 127.0, 126.5, 84.3, 81.0, 79.0, 76.3, 75.4, 75.2, 75.0, 72.2, 72.0, 58.4, 52.7, 45.5, 43.1, 40.1, 35.5, 26.7, 22.6, 22.0, 20.7, 14.7, 9.5 ppm.

MS (LR-ESI, positive mode): calculated for $\text{C}_{49}\text{H}_{53}\text{NO}_{15}\text{Cl}$ $[\text{M} + \text{H}]^+$ m/z 930.3; found m/z 930.3. MS (HR-ESI, positive mode): calculated for $\text{C}_{49}\text{H}_{53}\text{NO}_{15}\text{Cl}$ $[\text{M} + \text{H}]^+$ m/z 930.3104; found m/z 930.3094.

Ptxl-2'-PA

^1H -NMR (500MHz, CDCl_3): δ = 8.13 (d, J = 7.28 Hz, 2H), 7.77 (d, J = 7.36 Hz, 2H), 7.61-7.36 (m, 15H), 7.26-7.24 (m, 6H), 6.96 (d, J = 9.16 Hz, 1H), 6.30 (s, 1H), 6.26 (d, J = 8.9 Hz, 1H), 5.98, 5.97 (dd, J = 2.84 Hz, 2.76 Hz, 1H), 5.69 (d, J = 7.08 Hz, 1H), 5.55 (d, 1H), 4.98 (d, J = 9.36 Hz, 1H), 4.98 (m, 3H), 4.65 (d, J = 11.9 Hz, 1H), 4.32 -4.20 (m, 2H), 3.82 (t, J = 9.20 Hz, 1H), 2.72-2.51 (m, 6H), 2.46 (s, 3H), 2.40-2.30 (m, 1H), 2.23 (s, 3H), 1.94 (s, 3H), 1.66 (s, 6H), 1.69 (s, 3H), 1.24 (s, 3H), 1.14 (s, 3H)

MS (LR-ESI, positive mode): calculated for $\text{C}_{52}\text{H}_{56}\text{NO}_{15}$ $[\text{M} + \text{H}]^+$ m/z 934.3; found m/z 934.3. MS (HR-ESI, positive mode): calculated for $\text{C}_{52}\text{H}_{56}\text{NO}_{15}$ $[\text{M} + \text{H}]^+$ m/z 934.3650; found m/z 934.3638.

Ptxl-2'-SA

$^1\text{H-NMR}$ (500 MHz, CDCl_3); δ = 8.13 (d, J = 7.28 Hz, 2H), 7.77 (d, J = 7.36 Hz, 2H), 7.61-7.36 (m, 15H), 7.26-7.24 (m, 6H), 7.03 (d, J = 9.16 Hz, 1H), 6.25 (s, 1H), 6.22 (d, J = 8.9 Hz, 1H), 5.97, 5.95 (dd, J = 2.84 Hz, 2.76 Hz, 1H), 5.67 (d, J = 7.08 Hz, 1H), 5.56 (d, 1H), 5.47 (d, J = 2.96 Hz, 1H), 4.96 (d, J = 9.36 Hz, 1H), 4.85-4.79 (m, 3H), 4.65 (d, J = 11.9 Hz, 1H), 4.41 (s, 1H), 4.31-4.27 (m, 2H), 4.19 (d, J = 8.44 Hz, 1H), 3.99 (t, J = 9.20 Hz, 1H), 3.81-3.73 (m, 3H), 3.64 (t, J = 9.20 Hz, 1H), 3.31 (s, 3H), 2.72-2.51 (m, 6H), 2.42 (s, 3H), 2.40-2.30 (m, 1H), 2.21 (s, 3H), 1.89 (s, 3H), 1.66 (s, 6H), 1.64 (s, 3H), 1.23 (s, 3H), 1.20 (s, 3H), 1.11 (s, 3H)

$^{13}\text{C-NMR}$ (125 MHz, CDCl_3); δ = 203.8, 171.5, 171.2, 171.1, 169.8, 167.9, 167.3, 167.0, 142.6, 138.4, 137.2, 136.9, 133.7, 133.6, 132.8, 132.0, 130.2, 129.2, 129.1, 129.0, 128.7, 128.5, 128.3, 127.7, 127.6, 127.2, 126.6, 126.0, 101.4, 97.5, 84.4, 82.1, 81.0, 79.0, 76.4, 75.6, 75.1, 74.3, 73.1, 72.1, 71.9, 58.5, 52.8, 49.1, 45.6, 43.2, 35.6, 33.9, 29.7, 29.0, 28.9, 26.8, 25.6, 24.9, 22.7, 22.1, 20.8, 14.8, 9.6

2.7 *Synthesis of Rapa derivatives*

2.7.1 *General synthesis procedure*

Briefly, Rapa (9.1 mg, 0.01 mmol, 1 equiv) was mixed with (BDI-1) $\text{ZnN}(\text{TMS})_2$ (6.5 mg, 0.01 mmol) and THF (0.50 mL) in a glove box. The reaction mixture will be stirred for 20 min. Freshly distilled MAA (1.7 mg, 0.011 mmol, 1.2 equiv) in THF solution (0.20 mL) will be added into Rapa/(BDI-1) $\text{ZnN}(\text{TMS})_2$ and further stirring for certain time. The solution will be quenched by ice-cold methanol (1 mL), and dried under vacuum. The solid will be redispersed in methanol solution (0.30 mL). All HPLC spectra were recorded and analyzed with a UV detector at 280 nm. The areas of

Rapa and Rapa-MAA peaks were integrated and used for their quantification of the yield. An aliquot of reaction mixture was used for MS analysis.

Pure Rapa-MAA used for NMR analysis was obtained by prep TLC. The concentrated reaction solution will be applied on 1.5 mm thick prep-TLC plates, and developed by acetone/hexane. The product will be recovered by extraction using methanol twice (2 x 20ml). The solution will be dried under vacuum and analyzed by NMR.

2.7.2 Characterization of Ptxl derivatives (MS)

Rapa-40-MAA

MS (LR-ESI, positive mode): calculated for $C_{55}H_{83}NO_{14}Na$ $[M + Na]^+$ m/z 1004.9; found m/z 1004.9.

Rapa-40-PA

MS (LR-ESI, positive mode): calculated for $C_{56}H_{83}NO_{14}Na$ $[M + H]^+$ m/z 1016.5; found m/z 1016.5.

MS (HR-ESI, positive mode): calculated for $C_{56}H_{83}NO_{14}Na$ $[M + Na]^+$ m/z 1016.5711; found m/z 1016.5722.

2.8 Cytotoxicity of Ptxl prodrugs for PC-3 cells.

PC-3 cells were placed in a 96-well plate for 24 h (10,000 cells per well) before the addition of Ptxl-2'-MAA, Ptxl-2'-ClAA, Ptxl-2'-PA and Ptxl (as positive control). On the day of experiments, cells were washed with 100- μ L, pre-warmed PBS, followed by the addition of freshly prepared Ptxl prodrugs in cell medium with selected concentration. The cells for negative control were incubated with just 100- μ L medium. All cells were incubated for a total of 72 h in an incubator with 5% CO₂ at 37 °C. Standard MTT (3-

(4,5-dimethylthiazol-2-yl)-2,5-diphenyltetrazolium bromide) assay protocols was followed thereafter.

2.9 *Anti-proliferation of Rapamycin prodrugs for Ntera-2 cells.*

PC-3 cells were placed in a 24-well plate for 24 h (100,000 cells per well) before the addition of Rapa-40-MAA, and Rapa (as positive control). On the day of experiments, cells were washed with 300 μ L, pre-warmed PBS, and followed by the addition of freshly prepared Rapa and Rapa-40-MAA in cell medium (300 μ L) with selected concentration. The cells for negative control were incubated with just 300 μ L medium. All cells were incubated for a total of 72 h in an incubator with 5% CO₂ at 37 °C. Standard MTT (3-(4,5-dimethylthiazol-2-yl)-2,5-diphenyltetrazolium bromide) assay protocols was followed thereafter.

2.10 *Potential bioconjugation application exemplified by click chemistry*

2.10.1 *Materials:*

Copper(I) iodine was immobilized on the solid support, Amberlyst A-21 free base (PS-NMe₂) following the method developed by Girard etc. The loading of Cu(I)I was ~ 1.0 mmol/g. QP-TU beads (bearing thiourea) and PS-PPh₂ beads were purchased from Sigma-Aldrich.

2.10.2 *Experiment procedures of CuAAC methods using :*

The azide, 1-azido-1-deoxy- β -D-glucopyranoside tetraacetate (2.0 equiv) and Ptxl-2'-PA (1.0 equiv) were dissolved in dichloromethane solution (1.0 mL) and stirring over 3 days onto Cu(I)I immobilized Amberlyst A-21 beads (0.1 equiv.). The reaction

solution was separated from bead by filtration. The CuI beads were further washed by DCM (2.0 mL) To remove leaching copper species in the solution, 50 mg QP-TU beads was added into the solution as metal scavenging. After 30 minutes, the solution was separated from QP-TU beads by filtration. The excess azide, contaminating the desired triazole product, could be removed by flowing the reaction solution through a column of phosphine resin (PS-PPh₂), thus capturing the azide onto the solid phase as an iminophosphorane *via* a Staudinger reaction. The resulted DCM solution was concentrated for characterization. In general, all purities were assessed as being >95%, as determined by LC-ESI-MS and ¹H-NMR.

2.11 Chemoselectivity reaction of Doxo reacted with PA

Briefly, Doxo·HCl salt (5.7 mg, 0.01 mmol, 1 equiv) was be mixed with (BDI-1)ZnEt (5.1 mg, 0.01 mmol) and THF (0.50mL) in a glove box exclusive of light. The reaction mixture will be stirred for 30 min. Freshly distilled PA (1.7 mg, 0.01 mmol, 1.0 equiv) in THF solution (0.20 mL) will be added into Doxo/(BDI-1)ZnEt and further stirring for certain time. The solution will be quenched by ice-cold methanol (1mL), and analyzed by HPLC. The HPLC spectra were recorded and analyzed with a UV detector at 280 nm. The areas of Doxo and Doxo-PA peaks were integrated and used for their quantification of the yield. An aliquot of reaction mixture was used for MS analysis.

2.12 DCC/(BDI)Zn one-pot acylation

In a glove box, PhAc (27.2mg, 0.2 mmol) in DCM (0.30 mL) was mixed with DCC (20.6 mg, 0.1 mmol) at -20 °C. The mixture was stored in the fridge of glove box. After 4 hours, (BDI-1)ZnN(TMS)₂ (6.5 mg, 0.01 mmol) was mixed with Ptxl (8.5 mg,

0.01 mmol) in DCM (0.30mL) for 20 min. DCC/PhAc solution (30 μ L) was added into the (BDI-1)Zn/Ptxl solution. The mixture was stirring over 3-4 h and analyze by HPLC. QuadTU beads (Sigma-Aldrich) were added into solution to remove Zn. The solution was dried, and the final product was purified by prep TLC (EtOAc/ Hex= 2/1) for NMR and MS analysis.

3. Results and Discussion

3.1 *O*-acylation reactions of simple hydroxyl molecules

Inspired by the *O*-acylation reaction of drugs with SA in previous study, we utilized various commercially available anhydrides in the similar reaction as the activated acylation reagents. Methacrylic anhydride (MAA), chloroacetic anhydride (CIAA) and iodoacetic anhydride (IAA) were extremely reactive towards the acylation reaction with 2-naphthalene-ethanol (Naph) in the presence of (BDI-1)ZnN(TMS)₂, giving quantitative *O*-acylations products (Table 6.1). The six-membered cyclic anhydrides, e.g. diglycolic anhydride (DGA), are poor substrates for the acylation reaction (Data not shown). It was noted that cyclic SA usually requires higher temperature (40 °C) to achieve the quantatative reaction (Table 6.1, entry 1 vs 2). Additionally, pent-4-ynoic anhydride (PA) was synthesized and we found (BDI-1)ZnEt could mediate Naph/PA reaction more efficiently than (BDI-1)ZnN(TMS)₂ (Table 6.1, entry 6). The -N(TMS)₂ group was suspicious to have side effects on the acylation reaction in the presence of terminal alkyne in PA.^[12] However, replacing the leaving group with carboxylate ((BDI-1)ZnOAc) cannot initiating the acylation reaction.

Table 6.1 The reaction of Naph with various anhydrides under the mediation of BDI-Zn catalyst

Entry	Reactant	Anhydride	Catalyst	Temp. (°C)	Time (h)	Yield (%)
1	Naph	SA	(BDI-1)ZnN(TMS) ₂	25	2	73
2	Naph	SA	(BDI-1)ZnN(TMS) ₂	40	2	>98
3	Naph	MAA	(BDI-1)ZnN(TMS) ₂	25	4	>98
3	Naph	MAA	TEA	25	4	<10
4	Naph	ClAA	(BDI-1)ZnN(TMS) ₂	25	4	>98
5	Naph	IAA	(BDI-1)ZnN(TMS) ₂	25	4	>98
6	Naph	PA	(BDI-1)ZnEt	40	2	92

3.2 *O*-acylation reactions of Dasa and Cpt

We next tested whether this highly efficient reaction can be extended to other therapeutic molecules. As a prototype complex molecule for our study of acylation reaction, Dasatinib (a Bcl/Abl tyrosine kinase inhibitor) with primary hydroxyl group was chosen to subject to the reactions with MAA in the presence of (BDI-1)ZnN(TMS)₂. Significantly rapid reaction was observed to generate Dasa-MAA with the yield of 91% in 2 hours (Table 6.7, entry 1), indicating the nature of high efficiency of the zinc alkoxide intermediates. Another intriguing drug, 20(*S*)-Camptothecin (Cpt), a topoisomerase II inhibitor, was selected to examine. Cpt has inherent less active tertiary hydroxyl group, and one lactone ring which should be essentially intact to maintain its antitumor activity. The reaction between Cpt and MAA catalyzed by (BDI-1)ZnN(TMS)₂ generated the Cpt-MAA with the intact lactone ring, yet with lower yield of 26% even at 40 °C for 12 hours. Asymmetric ligand BDI-2 replacing BDI-1 for zinc catalyst strongly improved the yield of Cpt-MAA to 82% for 4 hours (Table 6.7 entry 4). These results

reinforced the drastic effect of chelating ligand architectures on the catalyst activities as reported by Coates. It is worth noting that conventional TEA or DMAP/EDC reagent failed to effectively convert 20-OH of Cpt to expected derivatives, due in part to the instability of lactone ring and low activity of 20-OH (Table 6.7 entry 2 vs 3).

Table 6.2 ^1H -NMR chemical shifts of Cpt, Cpt-MAA and Cpt-SA in CD_3OD (500MHz)

	Cpt (δ , ppm)	Cpt-SA (δ , ppm)	Cpt- MAA (δ , ppm)
7-H	8.64	8.63	8.64
12-H	8.21	8.21	8.16
9-H	8.07	8.07	8.07
11-H	7.87	7.87	7.86
10-H	7.72	7.71	7.7
14-H	7.46	7.43	7.34
17-H	5.58, 5.41	5.57, 5.44	5.63, 5.49
5-H	5 6	5.35	5.35
18-H	1.97	2.23	2.26
19-H	1.01	0.99	1.04
SA - CH ₂ COOH		2.81	
SA - OCOCH ₂		2.55	
MAA			5.83
MAA			6.33
MAA			1.98

3.3 *O*-acylation reactions of Ptxl

We then evaluated the regioselectivity using Ptxl as model drug. The site selective derivatization of polyols is demanding for the powerful catalyst to exhibit kinetic preference based on the inherent reactivity of different hydroxyl groups. We tested *O*-

acylation of Ptxl with MAA (Table 6.7 entry 5). Ptxl is a potent mitotic inhibitor and has three hydroxyl groups at its C-2', C-1 and C-7 positions, respectively (Scheme 6.1 (b)). The three hydroxyl groups of Ptxl differ in steric hindrance in the order of 2'-OH < 7-OH < 1-OH. The tertiary 1-OH is least accessible and typically inactive. The secondary 7-OH in Ptxl, however, could potentially compete with 2'-OH, the most accessible and active hydroxyl group of Ptxl. Although the reaction of Ptxl/SA mediated by Zn catalyst was slow, the reaction of Ptxl with MAA in the presence of (BDI)ZnN(TMS)₂ at a [MAA]/[Ptxl]/ [(BDI-1)ZnN(TMS)₂] ratio of 1.2:1:1 at 40 °C resulted in Ptxl-2'-MAA with >98% yield (Table 6.7 entry 5 vs 6). The ¹H- and 2D-NMR experiments confirmed that the *O*-acylation of Ptxl was mediated exclusively by its C2'-OH; wherein the chemical shift of 2'-H of Ptxl-2'-MAA noticeably shifted from 4.78 ppm to 5.50 ppm; 3'-H also from 5.78 to 5.95. Meanwhile, chemical shift of 7-H of Ptxl-2'-MAA maintained at 4.40 ppm, exactly same as Ptxl (4.40 ppm) (Table 6.4). The high *O*-acylation activity and selectivity of (BDI-1)ZnN(TMS)₂ were in sharp contrast to the low activity and poor selectivity observed with the use of triethylamine in similar reactions (the yield of Ptxl-2'-MAA was 12.7%). The acylation of Ptxl with ClAA in the presence of (BDI-1)ZnN(TMS)₂ also favoured 2'-OH acylation with the yields over 90% (Table 6.7, entry 7). Interesting, the reaction of Ptxl and PA underwent smoothly in the mediation of (BDI-1)ZnEt with the yield of 81% in 2 hours (Table 6.7, entry 8). The regio-specific tethered alkyne group on Ptxl (Ptxl-2'-PA) enable the employment of bio-orthogonal copper(I)-catalyzed azide-alkyne cycloaddition (CuAAC) to prepare diverse analogues. A small scale CuAAC reaction mixing Ptxl-2'-PA (1 equiv.) with 1-azido-1-deoxy-β-D-glucopyranoside tetraacetate (2 equiv.) catalyzed by the immobilized CuI catalyst^[13] can readily generate 1,4-disubstituted 1,2,3-triazoles over nearly quantitative yield with the

further employment using commercially copper and azide-capture beads^[14] (Figure 6.1), showing the potential broad versatility for conjugations. We also found the cytotoxicity of Ptxl-2'-site specific prodrugs were decreased for prostate cancer PC-3 cells over 72 hours. (Table 6.5)

Table 6.3 Site specific ring opening reaction on Ptxl, Dtxl with anhydride^a

Entry	initiator R	catalyst	R-2'-SA % ^b	R% ^b	Other SA form % ^b
1	Ptxl	(BDI-1)Mg	44.40	26.22	29.37
2	Ptxl	(BDI-1)Zn	39.68	60.32	0
3	Ptxl	(BDI-2)Zn	29.55	15.10	55.35
4	Ptxl	(BDI-3)Zn	45.07	41.57	13.36
5	Ptxl	(BDI-4)Zn	53.61	46.39	0
6	Ptxl	(BDI-5)Zn	5.89	54.34	39.76
7	Dtxl	(BDI-1)Zn	71.49	28.51	0

^a The reaction vial was tightly sealed and immediately moved out from box and heated at 40 °C for 4 hours and quenched by 1 ml ice-cold methanol. The resulted solution was immediately injected into HPLC for analysis.

^bHPLC condition: analytical Luna C18(2) column (250 × 4.6 mm, 5 μ, Phenomenex, CA, USA) ; flow rate: 1ml/min; mobile phase: acetonitrile / water with 0.1% TFA from 50/50 to 80/20 in 40 min. All spectrums were recorded and analyzed at 227 nm. Ptxl-SA and Dtxl-SA mixture were analyzed by low resolution electrospray ionization mass spectrometry (LR-ESI-MS) experiments, which were conducted on a Waters Quattro II mass spectrometer. Pure Ptxl-2'-SA and Dtxl-2'-SA for NMR analysis were separated by preparative thin layer chromatography

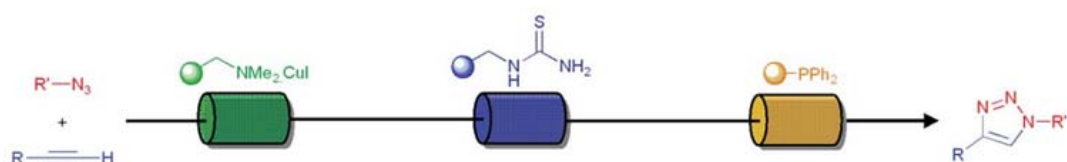
Table 6.4 ^1H -NMR chemical shifts of Ptxl and its derivatives in CDCl_3 (500MHz)

	Ptxl	Ptxl-2'-SA (δ , ppm)	Ptxl-2'- CIAA (δ , ppm)	Ptxl-2'- MAA (δ , ppm)	Ptxl-2'-PA (δ , ppm)
3'-NH	7.01	7.01	6.93	6.95	6.96
10	6.27	6.29	6.29	6.31	6.3
13	6.23	6.25	6.25	6.28	6.26
3'	5.78	6.00, 5.98	6.01	5.98, 5.96	5.98, 5.97
2	5.67	5.69	5.66	5.7	5.69
5	4.94	4.98	4.96	5	4.98
2'	4.78	5.55	5.55	5.53	5.55
7	4.4	4.44	4.43	4.47	4.45
20	4.30, 4.19	4.31, 4.20	4.3	4.34, 4.20	4.32, 4.20
3	3.79	3.81	3.81	3.83	3.82
6	2.54, 1.88	2.54, 1.89	2.54, 1.86	2.58, 1.90	2.54, 1.85
4-OAc	2.38	2.45	2.45	2.46	2.46
14	2.35, 2.28	2.37, 2.20	2.35, 2.19	2.36, 2.17	2.34, 2.17
10- OAc	2.23	2.23	2.21	2.25	2.23
18- CH ₃	1.79	1.92	1.92	1.96	1.94
19- CH ₃	1.68	1.69	1.67	1.7	1.69
17- CH ₃	1.24	1.23	1.22	1.25	1.24
16- CH ₃	1.14	1.14	1.13	1.16	1.14
other		2.56	1.95-1.82	6.18	3.57
		1.87		5.71	1.44
				1.98	2.67

Table 6.5 Evaluation of Ptxl and its derivatives anticancer effect using cytotoxic assay (MTT assay)

Drug	IC50 (nM)
Ptxl	87 ± 10
Ptxl-2'-ClAA	553 ± 12
Ptxl-2'-MAA	3477 ± 83
Ptxl-2'-PA	397 ± 11

Scheme 6.2 CuAAC reaction scheme mediated by solid bead for reaction catalyst and purification scavenger



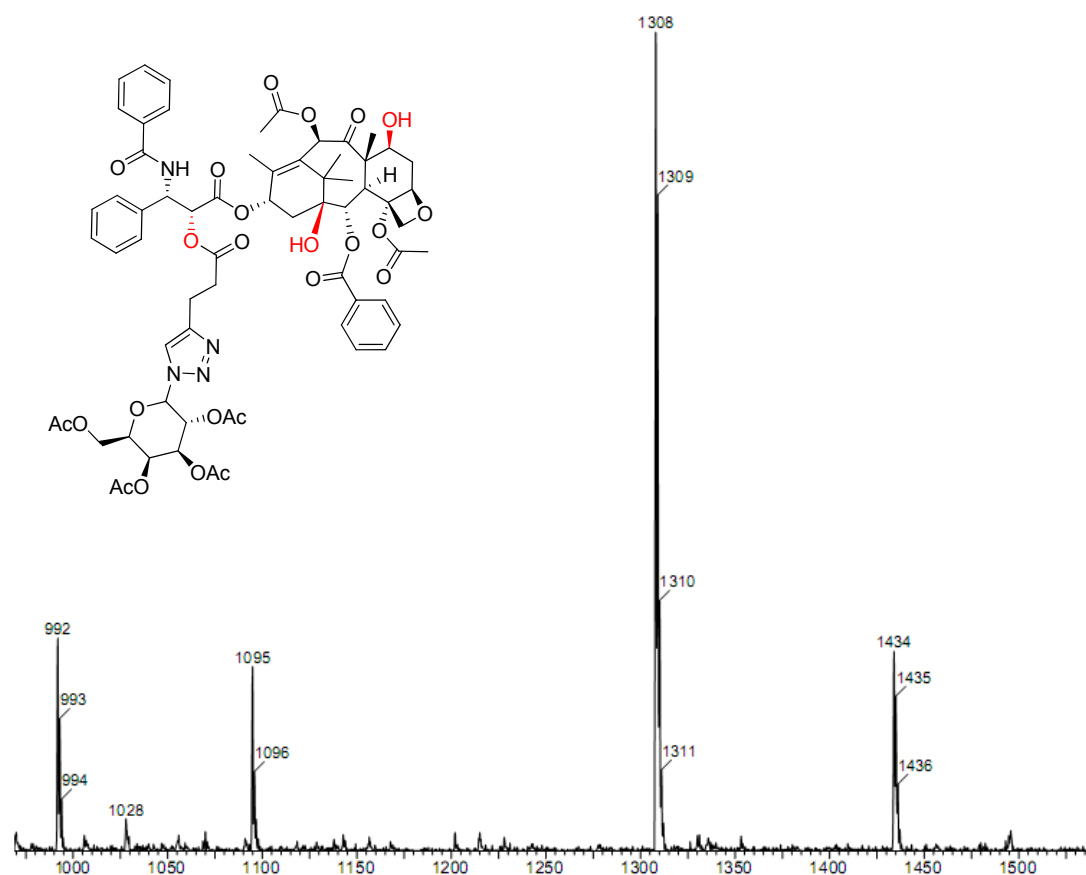


Figure 6.1 LR-ESI-MS of the solution of Ptxl-2'-PA CuAAC reaction with 1-azido-1-deoxy- β -D-glucopyranoside tetraacetate. The calculated MS of final compounds: $[M + H]^+$ $m/z=1308$, found: 1308. The Ptxl-2'-SA peak ($[M+H]^+$ $m/z=934$) was not found in the spectrum, indicating all the starting materials used up in the reaction.

3.4 O-acylation reactions of Rapa

Rapamycin (Rapa) is a macrocyclic polyketide isolated from *Streptomyces hygroscopicus* NRRL5491 as an antifungal agent and later shown as an immunosuppressive and antiproliferative agent, and currently approved for use in renal transplantation (Sirolimus, Rapamune).^[15] Recently Rapa is shown to markedly impair

the pluripotency of hESC cell lines, prevents cell proliferation, and enhances mesoderm and endoderm activities in hESCs.^[16] Rapa can also extend lifespan in old and genetically heterogeneous mice through a combination of anti-neoplastic effects.^[17] One analogue of Rapa, temsirolimus (CCI-779), is a 40-hemiester derivativ and was approved by FDA as an mTOR inhibitor for the treatment of renal cell carcinoma^[18]. Regioselective acylation of Rapa at the 40-OH has proven to be difficult, as there is another secondary hydroxyl group at C-28 (Scheme 6.1(b)). Low yields of desired 40-hemiesters are often observed due to the poor regioselectivity and the instability of Rapa in the presence of a base.^[19] A recent study using chemo-enzymatic process for Rapa exhibited excellent yields and regioselectivity for some anhydride and vinyl ester.^[5d] We explored whether our BDI-Zn/drug/anhydride system can be potentially applied to Rapa with regioselectivity. First the mixture of Rapa and (BDI)ZnN(TMS)₂ was heated at 40 °C for 4 hours and no degradation species of Rapa was detected in HPLC spectrum (Figure 6.2), suggesting the stability of Rapa in the presence of zinc catalyst. We then examined the reactions of Rapa with various anhydrides under the catalysis of (BDI)ZnN(TMS)₂ in anhydrous THF. Whereas CIAA and IAA showed no activity towards expected ester derivatives of Rapa, MAA was found, unexpectedly in HPLC spectra, to favor the regioselective acylation with the yield of 96% within 6 hours at room temperature. NMR analysis of the product after chromatographic separations exhibited the clear C-40 derivative; in ¹H NMR spectra comparison of Rapa-40-MAA with Rapa (CDCl₃), 39-H shifted from 2.9 to 3.1 ppm and 40-H from 3.4 to 4.7 ppm, whereas 28-H remained at same chemical shift (Table 8).^[20] The enzymatic reaction of MAA and Rapa in the presence of Novozym 435 in anhydrous toluene at 40 °C gave the same regioselective product with the yield of 79% after 48 hours (Table 6.7, entry 9), confirming our result using (BDI-1)ZnN(TMS)₂. Some

acylation conditions (TEA, or TEA/N-methylimidazole) replaced (BDI-1)ZnN(TMS)₂ for Rapa/MAA reaction; lack of regioselectivity and low yield were found for both conditions (Table 6.8). It is noticed that the reactions catalyzed by (BDI-1)ZnN(TMS)₂ are generally significantly faster than those promoted by lipase enzyme, and requires mild reaction condition. The regioselectivity on 40-OH of Rapa was further demonstrated through the reaction of Rapa/PA/(BDI-1)ZnEt with the yield of 67% over 4 hours (Table 6.7, entry 10). Surprisingly, Novozym 435 was inefficient to mediate the acylation reaction of Rapa/PA less than 30% conversion over 24 hours. Therefore, our BDI-Zn catalysts appeared superior to enzymes for above acylation reaction in terms of the efficiency and readily available scale. A preliminary *in vitro* study exhibited similar anti-proliferation profile between Rapa and Rapa-MAA for pluripotent human embryonal carcinoma NTERA-2 cells,^[99] suggesting the regioselective modification on 40-OH of Rapa did not affect the activity of binding sites (to mTOR and FKBP12) in Rapa (Figure 6.3).^[21]

Table 6.6 Various acylation conditions for Rapa/MAA

Entry	Reactant	Anhydride	Catalyst	Temp. (°C)	Time (h)	Yield (%)	Regioselectivity
1	Rapa	MAA	(BDI-1)ZnN(TMS) ₂	25	6	96	40-OH
2	Rapa	MAA	Novozym 435	40	48	79	40-OH
3	Rapa	MAA	TEA	40	24	<10	40 and 28-OHs
4	Rapa	MAA	TEA/NMI	25	12	20	40 and 28-OHs

Table 6.7 *O*-Acylation reaction of Dasa, Cpt, Ptxl and Rapa mediated by BDI-Zn catalyst

Entry	Reactant	Anhydride	Catalyst	Temp. (°C)	Time (h)	Yield (%)
1	Dasa	MAA	(BDI-1)ZnN(TMS) ₂	25	2	91
2	CPT	SA	TEA	40	4	<10
3	CPT	SA	(BDI-2)ZnN(TMS) ₂	40	4	89
4	CPT	MAA	(BDI-2)ZnN(TMS) ₂	40	4	82
5	Ptxl	SA	(BDI-1)ZnN(TMS) ₂	25	4	39
6	Ptxl	MAA	(BDI-1)ZnN(TMS) ₂	25	3	>98
7	Ptxl	ClAA	(BDI-1)ZnN(TMS) ₂	25	4	90
8	Ptxl	PA	(BDI-1)ZnEt	40	2	81
9	Rapa	MAA	(BDI-1)ZnN(TMS) ₂	25	6	96
10	Rapa	PA	(BDI-1)ZnEt	25	4	67

Table 6.8 ¹H-NMR chemical shifts of Rapa, Rapa-MAA and Rapa-PA in CDCl₃ (500MHz)

	Rapa (δ, ppm)	Rapa-40-MAA (δ, ppm)	Rapa-40-PA (δ, ppm)
-OH	4.83	4.80	4.77
19	6.39	6.39	6.38
20	6.32	6.32	6.29
21	6.15	6.16	6.14
18	5.97	5.97	5.98
22	5.57	5.53	5.52
30	5.42	5.43	5.32
2	5.29	5.29	5.30
34	5.17	5.18	5.16
28	4.17	4.19	4.14
14	3.86	3.87	3.92
27	3.71	3.74	3.75
16	3.66	3.67	3.68
6	3.59, 3.44	3.58, 3.44	3.57, 3.47
51 27-OCH ₃	3.40	3.40	3.40
40	3.35	4.73	4.69
50 16-OCH ₃	3.32	3.34	3.37
31	3.30	3.31	3.27
52 39-OCH ₃	3.14	3.14	3.13
39	2.91	3.22	3.16
25	2.72	2.74	
33	2.72, 2.56	2.72, 2.57	
12	1.6	1.61	
23	2.33	2.33	
38	2.10	2.10	

(Table 6.8, continue on page 185)

(Table 6.8 continued)

11		1.98	1.95	
3		1.92, 1.60	1.92, 1.60	
24		1.83, 1.68	1.83, 1.68	
4		1.78, 1.47	1.78, 1.47	
5		1.75, 1.48	1.75, 1.48	
15		1.85, 1.52	1.86, 1.52	
47	29-CH3	1.74	1.76	
44	17-CH3	1.65	1.66	
13		1.62, 1.33	1.62, 1.33	
37		1.39	1.37	
43	11-CH3	0.95	0.96	
45	23-CH3	1.05	1.06	
46	25-CH3	1.00	1.00	
48	31-CH3	1.11	1.11	
49	35-CH3	0.92	0.92	
41		1.99, 1.33	2.04, 1.34	1.98, 1.32
42		1.70, 1.00	1.74, 0.92	
36		1.22, 1.12	1.21, 1.16	
other H			6.10	
			5.56	
			1.96	

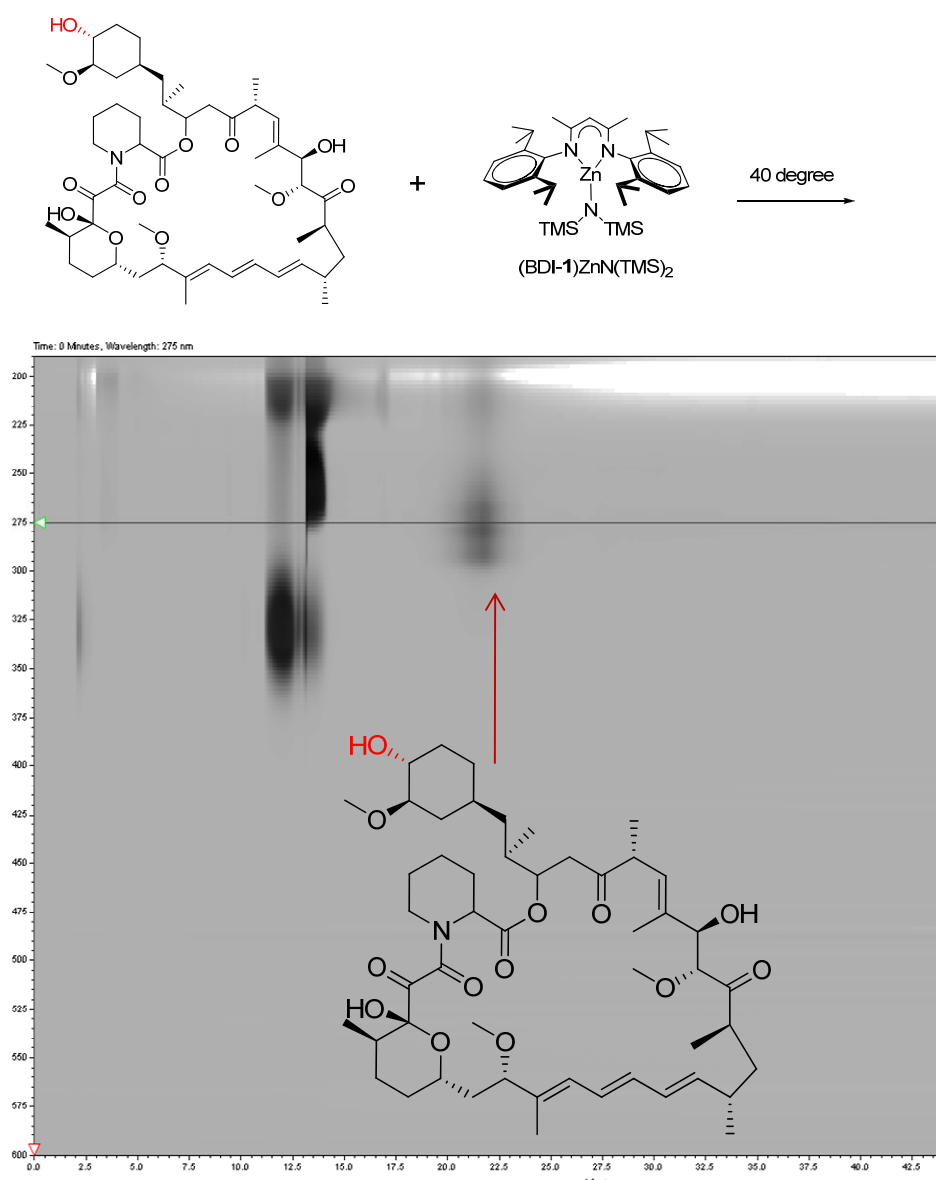


Figure 6.2 HPLC spectrum of Rapa mixed with $(\text{BDI-1})\text{ZnN}(\text{TMS})_2$ catalyst and heated at 40 degree over 30 minutes. No degradation species of Rapa was found in the HPLC spectrum. The peak at 22.5 min with highest UV absorbance at 280 nm was Rapa. The peaks around 12-14 min was BDI-Zn catalyst species.

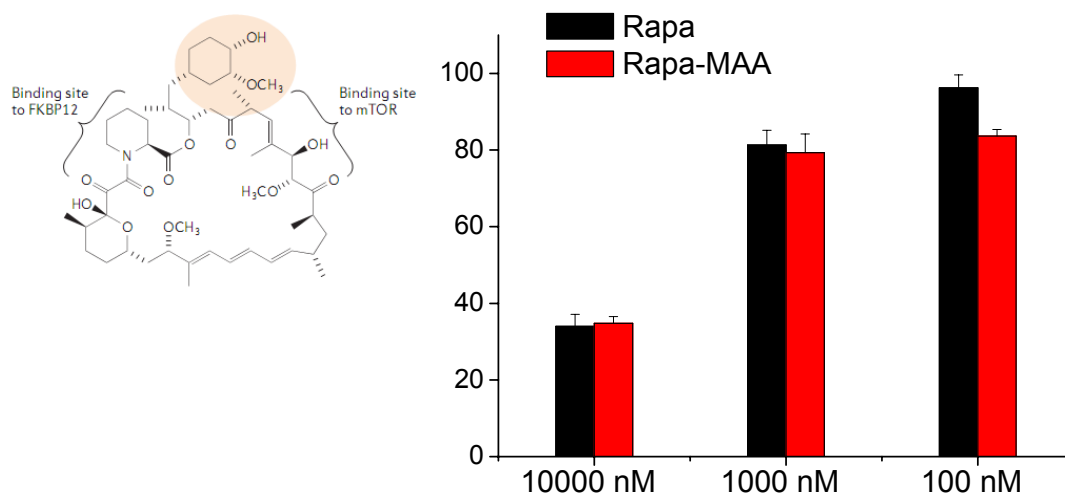


Figure 6.3 Evaluation of Rapa and Rapa-40-MAA anti-proliferation effect using cytotoxic assay (MTT assay)

3.5 *O*-acylation reactions of Doxo

Doxorubicin (Doxo) is a significant anti-cancer agent that contains multiple types of conjugation-amenable groups (three hydroxyl groups, one amine group and one ketone group). Clark and coworkers first showed that facile *O*-acylation on different OH sites of Doxo could be tuned with chemo-selectivity by the careful selection of various enzymes.^[5b] We previously demonstrated that Doxo can be incorporated into PLA in a regio- and chemo-selective manner through its C14-OH to prepare Doxo-PLA nanoconjugates.^[10a] Interestingly, Doxo-14-SA was found as the predominant product in the reaction mixture of Doxo/SA/(BDI-1)ZnN(TMS)₂. Considering MAA and CIAA have functional groups potentially reactive towards 3'-NH₂ in Doxo, PA was selected to exhibit the similar regio- and chemo-selectivity as SA for Doxo. Surprisingly, when PA

was mixed with Doxo in desalt form, *N*-acylation on 3'-NH₂ proceeded rapidly and all of PA was consumed within 60 min. Doxo HCl salt was then mixed with PA in THF to eliminate fast *N*-acylation process. In the mixture of Doxo/PA/(BDI-1)ZnEt, Doxo-PA was found as one major product (different peak from the Doxo-3'-NH-PA in HPLC spectrum), indicating the acylation was through the hydroxyl groups and most likely on 14-OH. Small amount of Doxo-2PA (<10%) was found in ESI-MS (Figure 6.4). The profound chemo-selectivity and reasonable regioselectivity will allow for generation of diverse derivatives on Doxo.

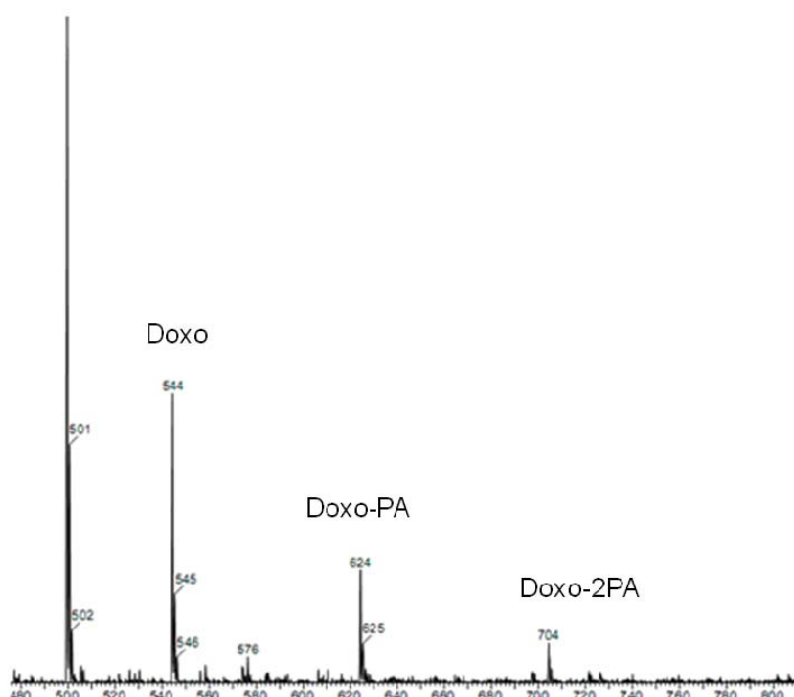


Figure 6.4 LR-ESI-MS of the solution of Doxo/PA/ (BDI-1)ZnEt reaction.

3.6 *In situ prepared anhydride for O-acylation reactions: expansion of the reaction scope*

Considering the commercial availability of anhydride compared with their precursor, carboxylic acid, an improved acylation pathway is devised to *in situ* prepare anhydride from carboxylic acid for acylation. The difficulties were overcome by the beauty of the chemistry that use of 1 equivalent of N,N'-dicyclohexylcarbodiimide (DCC) allowing almost complete conversion of 2 equivalent acid to anhydride. Since the whole process can be monitored by IR (the appearance of anhydride band around 1850-1800 cm^{-1}), we then examined the acylation method using Ptxl with phenylacetic acid (PhAc). PhAc in DCM (2 equiv.) was first mixed with DCC in glove box at -20 degree over 4 hours until quantitative acid converted to anhydride. (BDI-1)ZnN(TMS)₂ reacted with Ptxl to generate active Zn-alkoxide species before acylation (Figure 6.5). The mixture of two solution induce rapid acylation of Ptxl at room temperature in 3 hours, yielding Ptxl-2'-PhAc with over 99% yield, and no 7-position acylation product was found (Figure 6.5). The entry using Ptxl/PhAc/DCC (1/2/1, molar ratio) provided 61% yield of Ptxl-2'-PhAc over 12h, suggesting the efficiency using conventional coupling reaction condition lower than the protocols using Zinc alkoxide (Table 6.9 entry 3 vs 4). Similar satisfactory result was also found for Ptxl/4-azido phenylacetic acid reaction (Table 6.9 entry 5 vs 6, >98% over 4 hours). We further investigated the acylation of Rapa adopting this *in situ* DCC/BDI-Zn one pot strategy, tested a selection of carboxylic acid with Rapa, whose hydroxyl groups are less reactive compared to Ptxl. Table 6.9 presented the results of the yield of acylation and regioselectivity. The acylation products of Rapa have reasonable yield and specific regioselectivity on 40-OH. The outcome of the final yield might relate with the anhydride properties (stereo- and electronic-). The method is well-suited for the esterification with simple carboxylic acid ; and it may be used for the introduction of bulky protecting groups (e.g. benzyl).

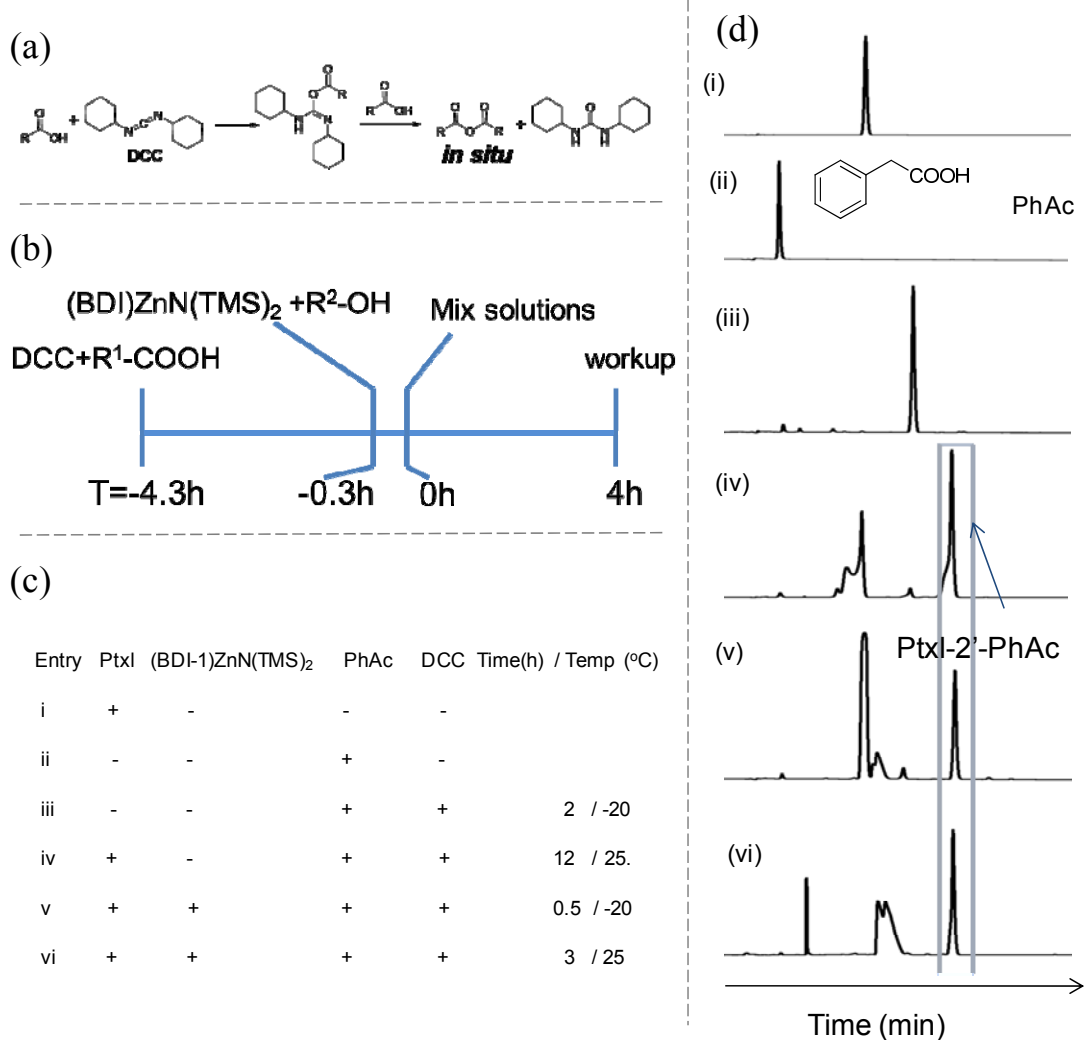


Figure 6.5 (a) Carboxylic acid reacted with DCC to *in situ* prepare corresponding anhydride; (b) Time line of DCC/BDI-Zn acylation strategy; (c) PhAc/Ptxl reactions setup condition; HPLC traces of the corresponding entry was shown in (d).

Table 6.9 In situ O-acylation of Ptxl and Rapa by carboxylic acid

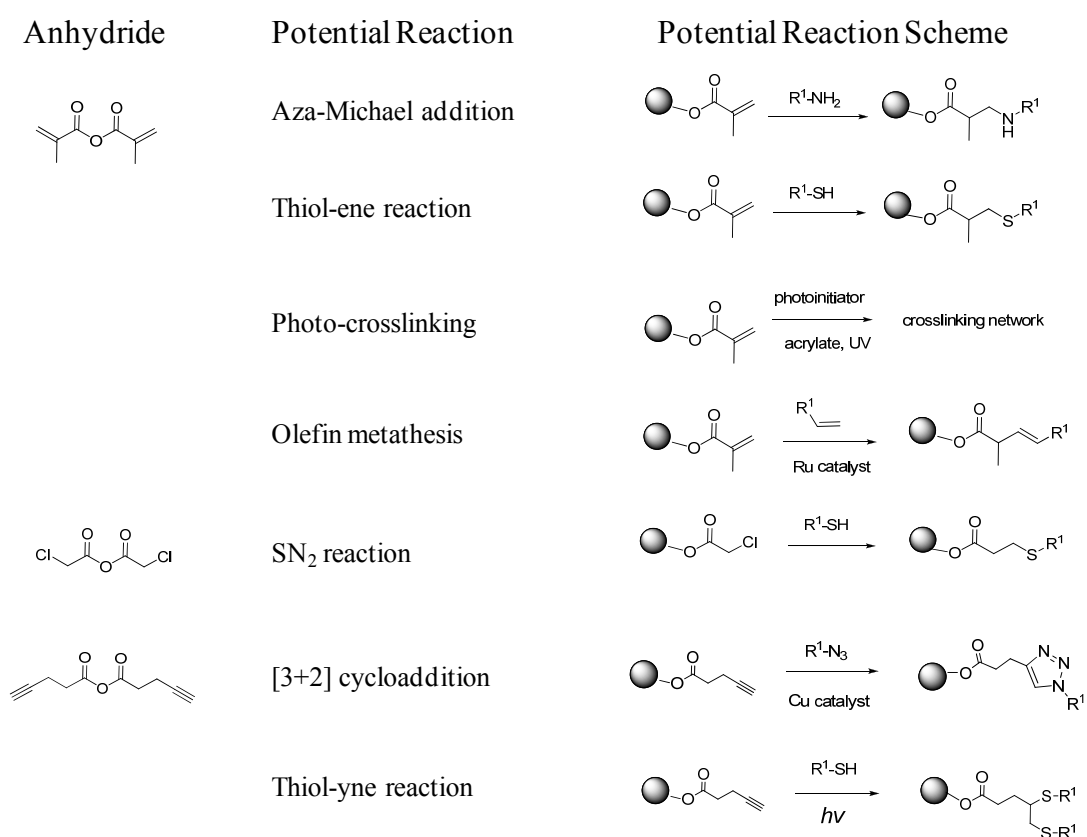
Entry	Reactant	Acid	Catalyst	Temp. (°C)	Time (h)	Yield (%)	Regioselectivity
1	Naph	PhAc	(BDI-1)ZnN(TMS) ₂	25	0.5	96	/
2	Naph	AzPhAc	(BDI-1)ZnN(TMS) ₂	25	0.5	94	/
3	Ptxl	PhAc	(BDI-1)ZnN(TMS) ₂	25	4	99	2'-OH
4	Ptxl	PhAc	DCC	25	12	61	2'-OH
5	Ptxl	AzPhAc	(BDI-1)ZnN(TMS) ₂	25	4	>98	2'-OH
6	Ptxl	AzPhAc	DCC	25	12	48	2'-OH
7	Rapa	PhAc	(BDI-1)ZnN(TMS) ₂	25	4	<15	40-OH
8	Rapa	PhAc	(BDI-1)ZnN(TMS) ₂	40	4	51	40-OH
8	Rapa	PhAc	DCC	40	12	<10	/
9	Rapa	PhAc	DCC/DMAP/TEA	40	12	<10	/
10	Rapa	PA	(BDI-1)ZnEt	40	4	82	40-OH

4. Conclusions

These findings illustrate the potential of site-selective modification of polyol natural products. In addition, the discovery of simultaneous functionalization and acylation may be of additional utility in the natural product analog generation for both medicinal chemistry and biomaterials preparation. We summarize the potential reaction of the derivatives mentioned in this paper (Scheme 6.3). In Ringsdorf model of polymer-drug conjugates, both drugs and active ligands (e.g. the targeting ligand or the imaging probe) are attached to the backbones of hydrophilic polymers. This two-step drug acylation -conjugation can potentially expand the research scope in both medicinal chemistry and biomaterials to generate intriguing therapeutic systems. Currently we are

still investigating the origin of the regioselectivity mechanism. The expansion of reaction scope and mechanism, the automation of the reaction process, and future application of the catalyst with polyfunctional substrates are underway.

Scheme 6.3 Potential bioconjugation reactions derived from drug-*O*-acylation conjugates



5. References

- [1] (a) J. Clardy, C. Walsh, *Nature* **2004**, 432, 829; (b) M. D. Burke, E. M. Berger, S. L. Schreiber, *Science* **2003**, 302, 613.
- [2] T. Henkel, R. M. Brunne, H. Muller, F. Reichel, *Angew. Chem. Int. Ed.* **1999**, 38, 643.
- [3] R. Langer, *Acc. Chem. Res.* **2000**, 33, 94.
- [4] J. Y. Ortholand, A. Ganesan, *Curr. Opin. Chem. Biol.* **2004**, 8, 271.
- [5] (a) Y. L. Khmelnitsky, C. Budde, J. M. Arnold, A. Usyatinsky, D. S. Clark, J. S. Dordick, *J. Am. Chem. Soc.* **1997**, 119, 11554; (b) D. H. Altreuter, J. S. Dordick, D. S. Clark, *J. Am. Chem. Soc.* **2002**, 124, 1871; (c) V. V. Mozhaev, C. L. Budde, J. O. Rich, A. Y. Usyatinsky, P. C. Michels, Y. L. Khmelnitsky, D. S. Clark, J. S. Dordick, *Tetrahedron* **1998**, 54, 3971; (d) J. X. Gu, M. E. Ruppen, P. Cai, *Org. Lett.* **2005**, 7, 3945.
- [6] S. Peddibhotla, Y. J. Dang, J. O. Liu, D. Romo, *J. Am. Chem. Soc.* **2007**, 129, 12222.
- [7] (a) K. W. Fiori, A. L. A. Puchlopek, S. J. Miller, *Nat Chem* **2009**, 1, 630; (b) C. A. Lewis, J. Merkel, S. J. Miller, *Bioorg. Med. Chem. Lett.* **2008**, 18, 6007; (c) C. A. Lewis, S. J. Miller, *Angew. Chem. Int. Ed.* **2006**, 45, 5616; (d) S. J. Miller, *Acc. Chem. Res.* **2004**, 37, 601.
- [8] Y. Zhao, J. Rodrigo, A. H. Hoveyda, M. L. Snapper, *Nature* **2006**, 443, 67.
- [9] S. Morrissey, *Chem. Eng. News* **2006**, 84, 12.
- [10] (a) R. Tong, J. J. Cheng, *J. Am. Chem. Soc.* **2009**, 131, 4744; (b) R. Tong, J. J. Cheng, *Angew. Chem. Int. Ed.* **2008**, 47, 4830.
- [11] B. M. Chamberlain, M. Cheng, D. R. Moore, T. M. Ovitt, E. B. Lobkovsky, G. W. Coates, *J. Am. Chem. Soc.* **2001**, 123, 3229.
- [12] A. A. Andreev, V. V. Konshin, N. V. Komarov, M. Rubin, C. Brouwer, V. Gevorgyan, *Organic Letters* **2004**, 6, 421.
- [13] C. Girard, E. Onen, M. Aufort, S. Beauviere, E. Samson, J. Herscovici, *Org. Lett.* **2006**, 8, 1689.
- [14] C. D. Smith, I. R. Baxendale, S. Lanners, J. J. Hayward, S. C. Smith, S. V. Ley, *Org. Biomol. Chem.* **2007**, 5, 1559.
- [15] (a) J. W. Choi, J. Chen, S. L. Schreiber, J. Clardy, *Science* **1996**, 273, 239; (b) R. T. Abraham, *Cell* **2002**, 111, 9.
- [16] Z. X. Jiayi, P. Su, L. Wang, J. Chen, M. Zimmermann, O. Genbacev, O. Afonja, M. C. Horne, T. Tanaka, E. Duan, S. J. Fisher, J. Y. Liao, J. Chen, F. Wang, *Proc. Natl. Acad. Sci. U. S. A.* **2009**, 106, 7840.

- [17] D. E. Harrison, R. Strong, Z. D. Sharp, J. F. Nelson, C. M. Astle, K. Flurkey, N. L. Nadon, J. E. Wilkinson, K. Frenkel, C. S. Carter, M. Pahor, M. A. Javors, E. Fernandez, R. A. Miller, *Nature* **2009**, *460*, 392.
- [18] G. Hudes, M. Carducci, P. Tomczak, J. Dutcher, R. Figlin, A. Kapoor, E. Staroslawska, J. Sosman, D. McDermott, I. Bodrogi, Z. Kovacevic, V. Lesovoy, I. G. H. Schmidt-Wolf, O. Barbarash, E. Gokmen, T. O'Toole, S. Lustgarten, L. Moore, R. J. Motzer, A. T. Global, *N. Engl. J. Med.* **2007**, *356*, 2271.
- [19] (a) M. Adamczyk, J. C. Gebler, P. G. Mattingly, *Tetrahedron Lett.* **1994**, *35*, 1019; (b) H. Kessler, R. Haessner, W. Schuler, *Helvetica Chimica Acta* **1993**, *76*, 117.
- [20] J. B. Mcalpine, S. J. Swanson, M. Jackson, D. N. Whittern, *Journal of Antibiotics* **1991**, *44*, 688.
- [21] S. Faivre, G. Kroemer, E. Raymond, *Nat. Rev. Drug Discovery* **2006**, *5*, 671.

CHAPTER 7

REVERSIBLE CELL-SPECIFIC DELIVERY OF CISPLATIN USING APTAMER-FUNCTIONALIZED LIPOSOMES

1. Introduction

Cisplatin, or *cis*-diamminedichloridoplatinum(II), is a highly potent chemotherapy drug for many different forms of cancers. It is believed that aquated form of cisplatin inside the cells readily forms adducts with various biomolecules particularly DNAs.^[1] The cisplatin-DNA adducts interfere with many DNA-mediated cellular functions including transcription, which eventually leads to cell apoptosis. Despite the excellent pharmacological efficacy of cisplatin, its application is often limited by two factors. First, cisplatin has little capability of targeting specific cells. Once in the bodily fluids, cisplatin enters cells mostly by passive diffusion.^[1a] This means that normal cells are affected by cisplatin similarly to the cancer cells. Elevated side effects are often observed accompanying cisplatin administration. Second, it is not rare that some tumor cells develop resistance to cisplatin,^[1b] which results in reduced drug potency. In theory, one way to overcome the latter problem is to increase cisplatin dosage. However, because of the poor selectivity, this approach can only lead to more serious side effects. Therefore, new strategies that facilitate delivery of drug molecules selectively to tumor cells are highly desirable. In addition, with targeted delivery, it is possible to use increased drug dosage without worrying about severe side effects.

We investigated the feasibility of using phospholipid liposomes functionalized with site-specific DNA aptamers as a nano-carrier for targeted delivery of cisplatin. Liposomes, first described in 1965,^[2] are small vesicles formed by phospholipids bilayer similar to the cellular membranes. Being able to carry large number of hydrophilic drugs inside the aqueous core and hydrophobic drugs in the lipid bilayer, liposomes are among the most attractive drug carriers for clinical applications. Since liposomes are normally made of naturally existing phospholipids, they are essentially biocompatible and safe, with minimum cytotoxicity. Other benefits of liposomes include simple preparation and formulation, and easily controllable sizes. Liposomes are particularly useful for cancer targeting because of the Enhanced Permeability and Retention (EPR) effect of tumor tissues.^[3] Generally, blood vessels around tumors exhibit more inconsistency than normal vessels and have openings ranging 100 -800 nm in diameter, allowing particles such as liposomes to penetrate and accumulate in tumor tissues. However, cancer targeting entirely based on EPR effect lacks efficiency because it usually relies on the passive diffusion of drug molecules from liposomes to cells. Slow drug release and fast drug diffusion into bodily fluids once outside the liposomes pose two major problems for efficient drug delivery. For example, Phase I and II studies of a cisplatin-containing liposome, SPI-77, showed only poor to moderate therapeutic efficacy.^[4] To overcome this problem, liposomes have been functionalized with targeting molecules on the surface to promote cell-specific binding and internalization of the vesicles. Most targeting molecules used so far are antibodies recognizing a variety of cell surface targets.^[5] The binding of antibodies to the cell membrane receptors triggers the receptor-mediated endocytosis, which is an active and site-specific internalization process and allows sub- μ m sized liposomes to enter the target cells. As a result, increased therapeutic efficacy

has been observed.^[6] However, using antibodies as targeting entities also poses some challenges. First, coupling antibodies to liposomes is not always simple. Every time an antibody is to be used on liposomes, it needs to be chemically conjugated to specialized phospholipid or polyethylene glycol (PEG) molecules.^[6] Coupling site on the antibody is usually not predictable, which could lead to reduced binding capability. Second, it is known that antibodies developed in animal hosts or cells can induce immune responses when used in human bodies. These antibodies thus require extra humanization steps before any clinical applications, making the whole targeted drug delivery process even more complex.

We studied to employ DNA aptamers as targeting ligands for liposome-based drug delivery. Aptamers are single-stranded oligonucleotides selected through an in vitro selection process, termed System Evolution of Ligands by EXponential enrichment (SELEX), to bind specific target molecules.^[7] In many cases, aptamers have binding affinity and selectivity similar to those of antibodies, but they are produced by more straightforward chemical synthesis on automated synthesizers, which allows easy and site-specific modification and labeling on the aptamers for a variety of applications. Aptamer has been used for targeted drug delivery based on different drug carriers, mostly block copolymer nanoparticles and quantum dots (QDs).^[8] However, these studies are all limited to one RNA aptamer that targets the prostate-specific membrane antigen (PSMA) on the prostate tumor cells, and so far no investigation on aptamer directed liposomal drug delivery has been reported despite that liposomes are biocompatible, easy to prepare, highly efficient, and widely used as drug carriers. In addition, coupling of nucleic acids to liposomes is markedly easier than other drug carrying devices. Either antibody-functionalized liposomes or aptamer-linked nanoparticles/QDs require covalent

conjugation of the targeting ligands to the drug carriers. In comparison, aptamers can be labeled with a cholesterol moiety at the end during synthesis on an automated synthesizer. This cholesterol end group readily inserts into the lipid bilayer of the liposomes via hydrophobic interactions, thus placing the aptamer on the surface of the liposomes. With recent progress in the development of cell-specific aptamers,^[9] especially those based on DNA, cell targeting aptamers are becoming more available and economical for biomedical research and potentially real clinical applications. Wider application of aptamers as targeting ligands for different drug-carrying platforms is expected following these new developments. Here we demonstrate that aptamer-functionalized liposomes are able to deliver cisplatin into target cancer cells selectively without affecting control cells.

More importantly, we have explored, for the first time, the use of complementary DNA (cDNA) of the aptamer as an antidote to block, or reverse, aptamer-facilitated drug delivery. One unique feature of aptamers that is often overlooked is that aptamers' activity can be easily inhibited by their cDNAs because the strong base pairing between two complementary strands disrupts the aptamer's target-binding conformation. This feature is especially useful in therapeutic applications where drug overdose can have severe consequences and a good antidote or neutralizer is often hard to find. Nucleic acid based antidotes not only are easy to obtain, but also have predictable toxicity profiles, thus eliminating the safety issue associated with the antidotes. There have been reports applying cDNA as an effective inhibitor of the aptamer's therapeutic activity in blood plasma, in animals, and even in human body.^[10] However, using cDNA to inhibit aptamer's cell-targeting capability as a way to block delivery of other drugs has not been demonstrated. Considering drug carriers such as liposomes can carry many different drug molecules, in a sense, the cDNA of the targeting aptamer can serve as a "universal"

antidote to reduce the efficacy of all these drugs on the target cells. Our results show that cDNA of cell-targeting aptamer clearly lowers drug effect of cisplatin encapsulated in the liposomes. The clinical implication of our findings is that aptamer-functionalized liposomes not only provide simplicity, high selectivity and high efficiency for drug delivery, but also offer a practical strategy for convenient and effective drug dosage management.

2. Materials and Methods

2.1 Preparation of DNA functionalized liposomes.

Chemicals and reagents were from Sigma-Aldrich Corp. (St. Louis, MO) unless specified otherwise. The aptamer with sequence 5'-GGT GGT GGT GGT TGT GGT GGT GGT GGT TTT TTT TTT TT-3', a random DNA control, 5'-GAG AAC CTG AGT CAG TAT TGC GGA GAT TTT TTT TTT TT-3', and the cDNA of aptamer in 2'-O-Methyl RNA bases, 5'-CCA CCA CCA CCA CAA CCA CC-3', were obtained from Integrated DNA Technologies, Inc (Coralville, IA). Labels and modifications on the oligonucleotides were incorporated at the time of synthesis. HSPC, cholesterol, PEG2000-DSPE, and extruder were from Avanti Polar Lipids, Inc (Alabaster, AL). Buffer for liposome preparation contained 25 mM HEPES at pH 7.6, 150 mM NaCl, 5 mM KCl, 1 mM MgCl₂, and 1 mM CaCl₂. The elution buffer for column purification of liposomes was the same except containing 35 mM HEPES at pH 7.6.

HSPC, cholesterol, and PEG2000-DSPE in chloroform were mixed at a 2:1:0.16 molar ratio in a glass vial, with HSPC at 1.25 mg. This mixture was blown dry under N₂ and placed in a vacuum for at least 6 h. Following that, 100 µL of buffer containing 3 nmole of cholesterol-tagged DNA was added to hydrate the dry lipids. After at least 6 h

at 37 °C, 400 µL buffer containing cisplatin or Calcein was added. This solution was gently vortexed and placed at 37 °C for 3 h. Following that, the solution was vortexed, and quickly frozen and thawed for at least 5 cycles. The final solution was incubated at 37 °C overnight. The lipid mixture was then extruded to form liposomes in 200 nm diameter according to instructions from Avanti Polar Lipids, Inc. The liposomes were finally purified and separated from free cisplatin or Calcein on a column packed with Sephadex G-100 medium (Chalfont St. Giles, United Kingdom).

2.2 *Cell culture*

MCF-7 and LNCaP (ATCC, Manassas, VA, USA) used for in vitro studies were cultured in DMEM and Ham's F-12K according to the vendor's recommendation. The medium contained 10% FBS (Fetal Bovine Serum), 1000 units/mL aqueous Penicillin G and 100 µg/mL streptomycin.

2.3 *Confocal imaging*

MCF-7 and LNCaP cells were incubated in chamber slides in medium to allow 70% confluence in 12-24 hours. On the experiment day, cell medium was removed. Cells were washed with 100 µL/well prewarmed 1X PBS and incubated with prewarmed OptiMEM (phenol red reduced) for 30 min before the addition of liposome solution. Cells were further incubated for 5h or 10 hours at 37 °C. At certain time point, cells was washed with prewarmed PBS three times and fixed with 4% paraformaldehyde solution for 10 minutes. The cells were washed again with PBS and visualized by confocal fluorescent microscopy.

2.4 *Cell viability assay*

LNCaP and MCF-7 cell lines were grown in 96-well plates with recommended medium at concentrations allowing 70% confluence in 24 h. On the experiment day, cells were washed with PBS buffer and incubated with Opti-MEM medium for 30 min at 37 °C. After the addition of various formulations of liposomes, cells were incubated for 5 hours and then washed with 100 µL/well PBS twice. Cells were further incubated in prewarmed fresh growth medium for 48 h or 96 h. Cell viability was assessed colorimetrically with the MTT reagent (Sigma-Aldrich) following standard protocols provided by the manufacturer. The absorbance was read with a microplate reader at 570 nm. Each viability value was the average of readings from 3 wells of cells.

2.5 *Flow cytometry analysis*

MCF-7 and LNCaP cells were grown in 24 well plates at about 40,000/cm² density overnight. On the experiment day, the medium was replaced by OptiMEM and cells were incubated for 30 min before various liposome solutions were added into the wells. After 5 hours, cells were washed with 500 µL/well PBS buffer twice and treated with 0.25% trypsin with EDTA for 20 min. Cells were centrifuged at 1200 rpm for 5 min and trypsin solution was carefully removed by pipette. After washing with PBS twice, cells were further fixed by 4% formaldehyde solution for 10 min at room temperature. The formaldehyde solution was removed by centrifuge (1200 rpm, 5 min) and cells were further washed by PBS once. The resulted cells suspension was analyzed by flow cytometry in fluorescein channel. The analysis was gated at 10,000 events.

3. Results and Discussion

Nucleolin is a *bcl-2* mRNA-binding protein that is believed to be involved in cell proliferation.^[11] Nucleolin overexpression has been linked to some human cancer cells including breast cancer cells.^[12] Even though nucleolin is primarily located in cell nucleolus, it is also present on the plasma membrane as a surface receptor,^[11] which provides a possible target for cancer cell specific drug delivery. A 26-mer DNA aptamer, called AS1411, was discovered with high binding affinity to nucleolin.^[13] This G-rich aptamer forms special G-quadruplex structure under physiological conditions, which is resistant to nuclease degradation.^[14] AS1411 exhibited antiproliferation activity in a few cancer cell lines, presumably through binding to nucleolin.^[14] A recent study found that AS1411 bound to nucleolin and destabilized the *bcl-2* mRNA, which could lead to apoptosis in a few breast cancer cell lines including MCF-7 and MDA-MB-231.^[15] The same report showed that aptamer bound to the cell surface nucleolin could be effectively internalized into the cell cytoplasm via endocytosis. Based on these studies, we chose AS1411 and MCF-7 breast cancer cells as a model system to demonstrate aptamer-guided cisplatin delivery using liposomes.

The aptamer sequence used in current study (NuApt) is derived from AS1411, 5'-GGT GGT GGT GGT TGT GGT GGT GGT GGT TTT TTT TTT TT – Cholesterol -3'. The 12 extra T-bases at the 3' end make sure that the liposome surface is not too close to the aptamer as to affect its target binding capability. To confirm the internalization of the aptamer by MCF-7 cells, AS1411 was labeled with a TAMRA dye at the 5' end and incubated with MCF-7 cells at 37 °C for 10 hours. Similarly, a TAMRA-labeled random-sequence DNA underwent the same procedures. On a confocal microscope, the aptamer treated cells showed much stronger TAMRA fluorescence in the cytoplasm than the

control DNA treated cells (not shown). The fluorescence was seen predominantly in the MCF-7 cytoplasm instead of nucleus, in consistence with the endocytosis-based internalization mechanism.

3.1 Internalization of aptamer-functionalized liposomes (Apt-lipos)

The key to cell-specific drug delivery is the selective internalization of the devices carrying drug molecules. Endocytosis of the nucleolin aptamer by MCF-7 cells does not warrant that much larger liposomes can also be internalized successfully. To test the possibility of liposome endocytosis, we prepared aptamer-functionalized liposomes (Apt-lipos) with a 200 nm diameter. The formula of the liposome was derived from previous reports,^[5b, 16] and composed of hydrogenated soy phosphatidylcholine (HSPC) : cholesterol : methoxy poly(ethylene glycol) (*Mr* 2000)-derivatized distearoyl-phosphatidylethanolamine (mPEG2000-DSPE) at a 2:1:0.16 mol ratio. Due to a high transition temperature of the HSPC, this composition gives liposomes increased rigidity and decreased permeability.^[17] The inert and hydrophilic PEG polymer is commonly used on liposomes to increase the clearance time of the vesicles *in vivo* as well as reduce immune responses. We also observed decreased non-specific liposome internalization with increased PEG content, probably because hydrophilic surface PEG helped shield the lipid bilayer from fusing non-specifically with the cell membranes.

Apt-lipo was prepared by mixing the above liposomal reagents with the cholesterol-tagged NuApt in the hydration step of liposome preparation. To monitor the internalization of liposomes, the vesicles were encapsulated with 4 mM fluorescent dye Calcein. Calcein is a hydrophilic derivative of fluorescein that is often used to trace cell fusion and division because it is impermeable to hydrophobic membranes. MCF-7 cells

were incubated with Apt-lipo containing Calcein for 5 h, then washed and fixed with formaldehyde before being examined on a confocal microscope. As a comparison, a prostate cancer cell line LNCaP, not known for having nucleolin, was used as a control. Figure 7.1 shows clear fluorescence from Apt-lipo treated MCF-7 cells but notable absence of fluorescence from LNCaP cells. In the MCF-7 fluorescence image, the bright spots along the outline of the cells are likely intact liposomes bound to the cell surface, while the dimmer but more uniform patches of fluorescence are possibly from inside the cells.

To verify that Apt-lipo was indeed internalized and the fluorescence was not just due to the surface bound liposomes carrying Calcein, we conducted further tests using flow cytometry analysis. MCF-7 cells were similarly treated with Apt-lipo except that before formaldehyde fixing, 0.25% trypsin, a common protease, was added to cleave and break down any cell surface proteins. This step ensured that no membrane nucleolins were available to bind to Apt-lipo, therefore the fluorescence would only come from the Calcein dye delivered into the cells. Liposome treated and untreated cells were then analyzed in a flow cytometer to measure fluorescence intensity from each individual cell. LNCaP cells treated with Apt-lipo and MCF-7 cells treated with a random DNA attached liposomes were employed as the control. Figure 7.2 is the histograms showing numbers of cells exhibiting different fluorescence intensity. It can be seen that there is a solid shift to higher fluorescence on the MCF-7 cells treated with Apt-lipo compared to untreated MCF-7. Specifically, the median fluorescence of the treated cells is clearly higher than that of the untreated cells. In contrast, MCF-7 cells treated with the liposomes coated with a random DNA displayed little difference in fluorescence compared to the untreated ones. Although LNCaP cells incubated with Apt-lipo showed slightly increase in

numbers of cells with higher fluorescence compared to untreated LNCaP, the overall histogram peak did not shift significantly to higher fluorescence, evidenced by a just slightly increased median fluorescence. These findings have confirmed that the aptamer-functionalized liposomes can selectively bind to MCF-7 breast cancer cells and be readily internalized. By changing the encapsulated dye to chemotherapy drugs such as cisplatin, it would be possible to realize targeted drug delivery and reduced side effects.

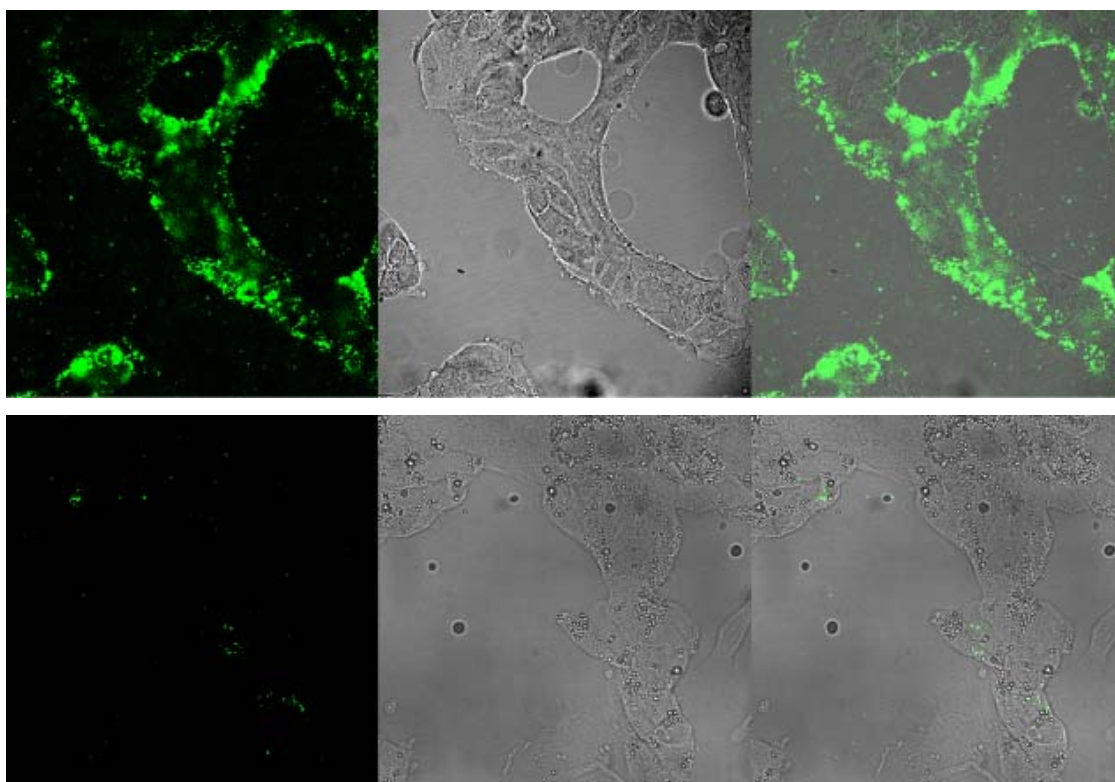


Figure 7.1 Confocal images of MCF-7 (top) and LNCaP (bottom) cells treated with aptamer-functionalized liposomes containing Calcein. From left to right: fluorescence image, transmission image, and overlay.

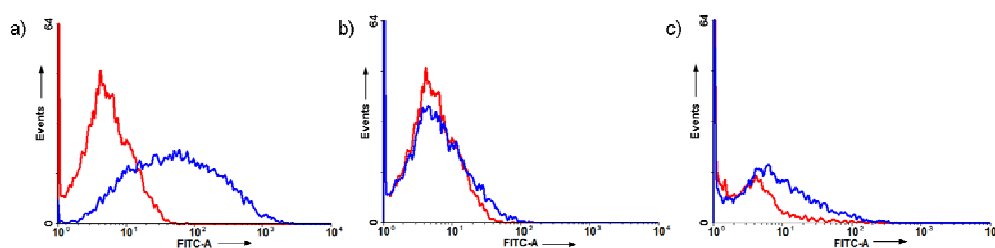


Figure 7.2 Flow cytometry analysis of untreated cells (red line) and cells treated with DNA-functionalized liposomes containing Calcein (blue line). From top to bottom: MCF-7 cells treated with aptamer-functionalized liposomes, MCF-7 cells treated with random DNA-functionalized liposomes, LNCaP cells treated with aptamer-functionalized liposomes.

3.2 *Cell toxicity study*

Apt-lipos were prepared to encapsulate approximately 4 mM cisplatin. The solubility of cisplatin in saline at room temperature is roughly 5 mM.^[18] Methods to increase cisplatin loading in liposomes have been investigated, which include preparing liposomes at elevated temperatures.^[18] However, cisplatin concentration is not a major focus of the current paper, therefore 4 mM cisplatin was used throughout the study.

For toxicity studies, cells were incubated with Apt-lipo loaded with cisplatin (Apt-lipo-cisPt) at 37 °C for 5 h. Following that, the cells were washed and cultured in fresh media. At the Day 2 and Day 4 time points of the culturing, cells were subject to standard MTT toxicity assay, which measures an enzymatic product produced by viable cells.^[19] The viability of the cells was obtained by comparing the MTT assay results from

treated and untreated cells and assuming the untreated cells had 100% viability. Besides MCF-7 cells treated with Apt-lipo-cisPt, we also tested MCF-7 treated with Apt-lipo without cisplatin or random DNA modified liposomes containing cisplatin (Ctrl-lipo-cisPt), and LNCaP cells treated with Apt-lipo-cisPt. Figure 7.3 shows the viability results from these tests. Only the Apt-lipo-cisPt treated MCF-7 cells displayed significant cell death, more than 20% at Day 2 and about 60% at Day 4. In comparison, the two control tests involving cisplatin still had 90% cell viability at Day 4. MCF-7 cells treated with Apt-lipos containing no cisplatin showed no noticeable cell death even at Day 4. Even though the AS1411 aptamer was reported to have cytotoxicity towards MCF-7 cells,^[15] the quantity of aptamer used in this paper was obviously not enough to cause any cell death. A side note here is that it is probably more economical to use aptamers as the targeting agents than therapeutic agents since the quantity needed is much lower and aptamers are usually more costly than small molecule drugs. Cytotoxicity of cisplatin toward MCF-7 and LNCaP cells has been previously evaluated and the IC₅₀ values of about 28 μ M and 5.95 μ M were reported for MCF-7 and LNCaP respectively.^[20] These numbers indicate that LNCaP cells are more prone to cisplatin induced cell death than MCF-7. However, by constraining cisplatin in liposomal vesicles and functionalizing the liposomes with cell-specific aptamers, much greater cell damage was observed for MCF-7 cells than for LNCaP. This finding demonstrates the successful implementation of combining cell-recognizing aptamers with liposomes to effectively deliver cisplatin to diseased cells to maximize its therapeutic efficacy and minimize its side effects.

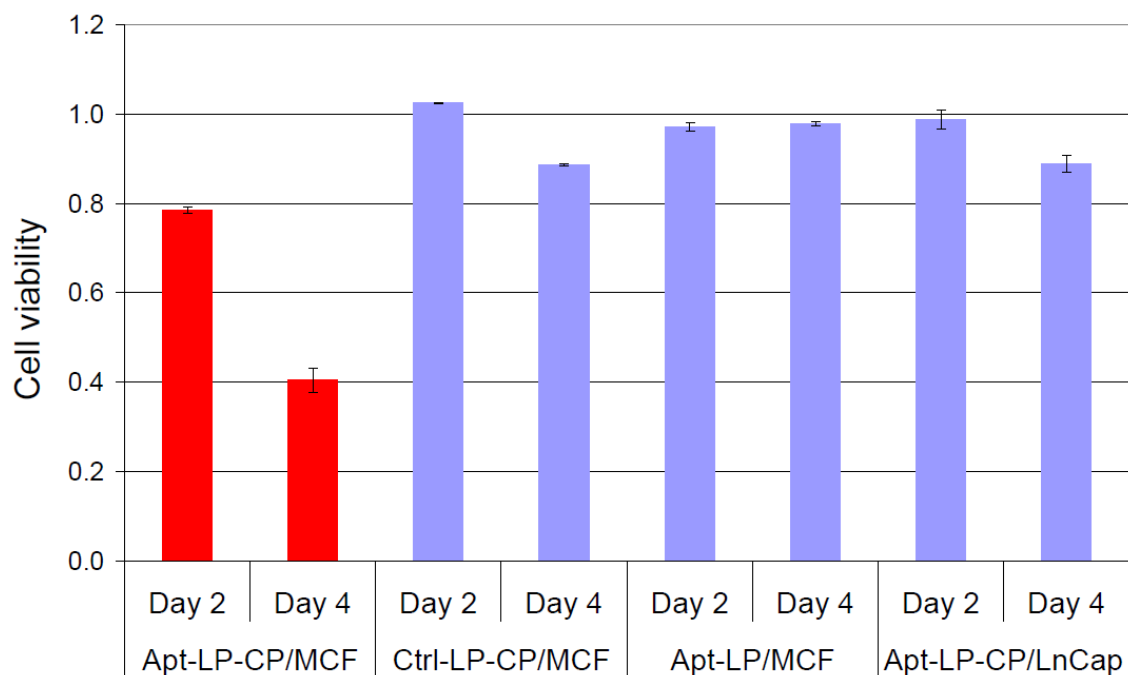


Figure 7.3 Cell viability assay of different liposome/cell combination. Viability measured at Day 2 and Day 4 of liposome/cell incubation.

3.3 *Reversed cisplatin delivery*

Following the cell toxicity study, the concept of using the cDNA of aptamer to block liposome-based cisplatin delivery was investigated. Our proposition was that by forming stable double strand with the aptamer, the cDNA could disrupt the G-quadruplex structure of the aptamer that is required for binding nucleolin, thus blocking the delivery of cisplatin. The cDNA we used had a 20-base sequence of 5'-CCA CCA CCA CCA CAA CCA CC-3', which was composed of all 2'-O-Methyl modified RNA bases in order to improve its resistance to nuclease degradation in cell culturing media. We first tested

concentration-dependent effect of the cDNA on cisplatin delivery and cell viability. Cell toxicity experiments using Apt-lipo-cisPt were carried out in the same way as mentioned earlier. At the beginning of the liposome/MCF-7 incubation, various amounts of cDNA were added to range roughly from 0 to 10 equivalents of the aptamer in the cell culture. Similarly, cell viability was measured by MTT assay at Day 2 and 4 time points of the cell culturing. Titration curves showing cDNA-dependent cell viability is presented in Figure 7.4. A clear ascending trend shows that excess cDNA effectively blocked cisplatin delivery into the cells and led to reduced cell death. With 10 equivalent of cDNA, the cell viability remained above 95% after 4 days. In contrast, absence of cDNA resulted in roughly 50% cell death in 4 days. The effect of cDNA on aptamer-based drug delivery is evident, which is potentially useful for dosage management in drug administration.

In the event of drug overdose or drug induced allergic reactions, it is critical to apply antidotes as early as possible. The effectiveness of antidotes usually drops as it moves further away from the time of drug administration. It is therefore of interest to investigate the time dependent antidote effect of the cDNA on aptamer-based drug delivery. We designed experiments to mimic the actual drug administration and application of antidote. Based on the toxicity test mentioned earlier, at different time point of the Apt-lipo-cisPt/MCF-7 incubation, the 20-mer cDNA at 10 equivalents of the aptamer was added to the cell culture. MTT assay was done at Day 2 and Day 4. The time-dependent effect is shown in Figure 7.5. Cells treated with cDNA at the same time of liposome addition remained mostly intact throughout the 4 day period, indicating no cisplatin was delivered to cells when the drug carrier was blocked from the beginning. The cDNA added after 1 h of liposome/cell incubation still showed strong inhibition of cisplatin toxicity, giving cell viability over 80% after 4 days. The cell death was likely

caused by fraction of drugs internalized in the first 1 h incubation. Later addition of cDNA showed further reduced antidote effect. The cDNA added at 5 h, the end of liposome/cell incubation, produced almost no effect, similar to the cells treated with no cDNA. This time-dependent study suggests that the cDNA of aptamer can be reasonably effective as antidote even 1 h after drug administration, thus giving plenty of time to reverse or modify the drug's therapeutic activity. It should be noted though, for drug delivery based on endocytosis of aptamers, the time frame in which the cDNA antidote can be effective is dependent on how fast the aptamers and drug carriers are internalized by the cells.

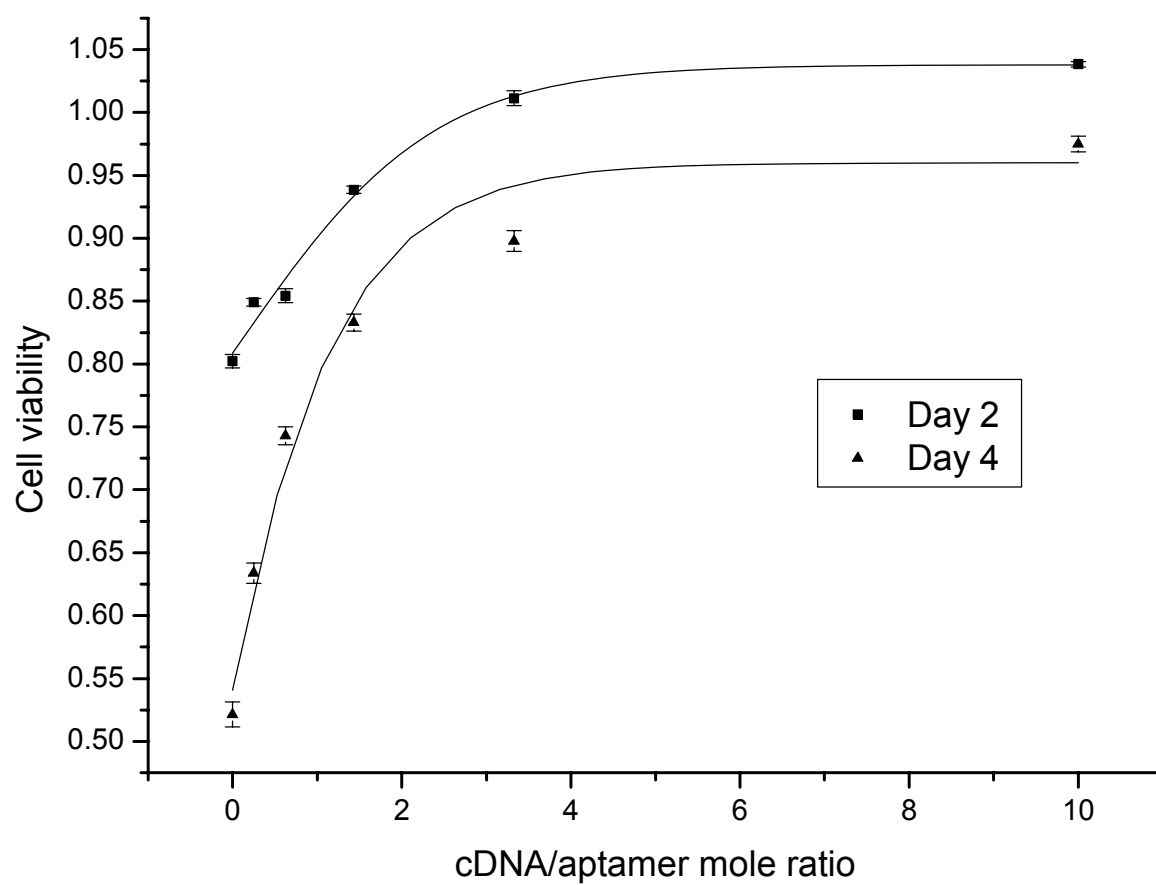


Figure 7.4 Effect of concentration of the cDNA of aptamer on viability of MCF-7 cells treated with Apt-lipo-cisPt. Titration curves are constructed using viability data from Day 2 and Day 4.

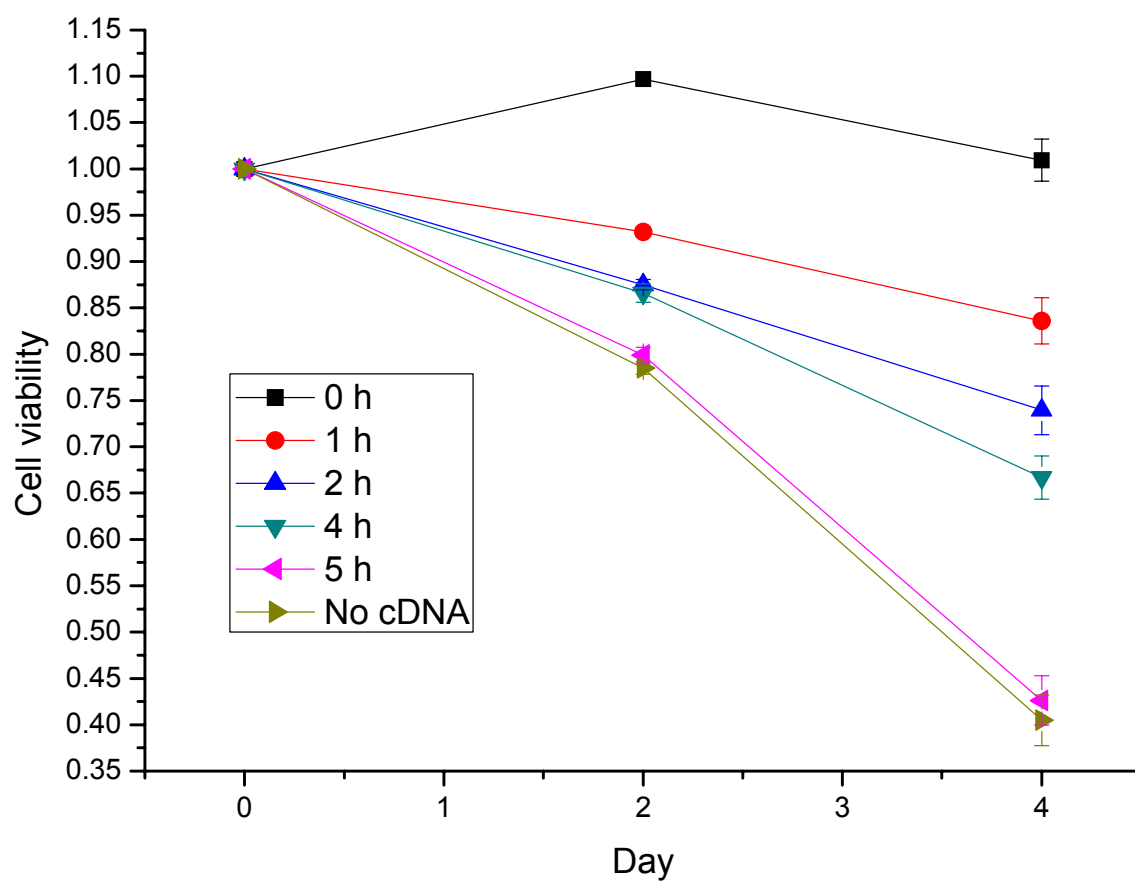


Figure 7.5 Time-dependent effect of cDNA on viability of MCF-7 cells treated with Apt-lipo-cisPt. The cDNA at 10 equivalents of the aptamer was added at different time point of the Apt-lipo-cisPt/MCF-7 incubation, and the cell viability was measured at Day 2 and Day 4.

4. Conclusions

Liposomes have been functionalized for the first time with cell-specific nucleic acid aptamers for selective delivery of cisplatin to diseased cells. The poor selectivity of cisplatin was largely overcome, evidenced by significant killing of target cancer cells but not control cancer cells. Aptamers possess some appealing features as targeting agents for liposome-based drug delivery. They are simple to make, can be produced in large quantity, and allow easy labeling and modification. Conjugation of aptamers to liposome carrier is especially easy compared to current strategies for targeted drug delivery. Furthermore, we explored the feasibility of using cDNA of the aptamer to block aptamer based drug delivery as a means to counteract drug overdose or drug-induced allergic reactions. Cisplatin encapsulated in aptamer-functionalized liposomes lost its cell killing activity in the presence of excess cDNA of aptamer, due to disruption of the binding between aptamer and its cellular membrane target. In summary, aptamer-functionalized liposomal drug carriers, combined with therapeutic potency of cisplatin, could provide a simple, powerful, versatile, and safe solution to the ever increasing needs for practical target-specific drug delivery.

5. References

- [1] (a) E. R. Jamieson, S. J. Lippard, *Chem Rev* **1999**, *99*, 2467; (b) L. Kelland, *Nat Rev Cancer* **2007**, *7*, 573.
- [2] A. D. Bangham, M. M. Standish, J. C. Watkins, *J Mol Biol* **1965**, *13*, 238.
- [3] (a) Y. Matsumura, H. Maeda, *Cancer Res* **1986**, *46*, 6387; (b) H. Maeda, J. Wu, T. Sawa, Y. Matsumura, K. Hori, *J Control Release* **2000**, *65*, 271.
- [4] (a) J. M. Meerum Terwogt, G. Groenewegen, D. Pluim, M. Maliepaard, M. M. Tibben, A. Huisman, W. W. ten Bokkel Huinink, M. Schot, H. Welbank, E. E. Voest, J. H. Beijnen, J. M. Schellens, *Cancer Chemother Pharmacol* **2002**, *49*, 201; (b) S. C. White, P. Lorigan, G. P. Margison, J. M. Margison, F. Martin, N. Thatcher, H. Anderson, M. Ranson, *Br J Cancer* **2006**, *95*, 822.
- [5] (a) J. W. Park, D. B. Kirpotin, K. Hong, R. Shalaby, Y. Shao, U. B. Nielsen, J. D. Marks, D. Papahadjopoulos, C. C. Benz, *J Control Release* **2001**, *74*, 95; (b) P. Sapra, T. M. Allen, *Cancer Res* **2002**, *62*, 7190; (c) T. A. Elbayoumi, V. P. Torchilin, *Eur J Pharm Sci* **2007**, *32*, 159.
- [6] P. Sapra, T. M. Allen, *Prog Lipid Res* **2003**, *42*, 439.
- [7] (a) C. Tuerk, L. Gold, *Science* **1990**, *249*, 505; (b) A. D. Ellington, J. W. Szostak, *Nature* **1990**, *346*, 818.
- [8] (a) O. C. Farokhzad, J. Cheng, B. A. Teply, I. Sherifi, S. Jon, P. W. Kantoff, J. P. Richie, R. Langer, *Proceedings of the National Academy of Sciences of the United States of America* **2006**, *103*, 6315; (b) J. Cheng, B. A. Teply, I. Sherifi, J. Sung, G. Luther, F. X. Gu, E. Levy-Nissenbaum, A. F. Radovic-Moreno, R. Langer, O. C. Farokhzad, *Biomaterials* **2007**, *28*, 869; (c) V. Bagalkot, L. Zhang, E. Levy-Nissenbaum, S. Jon, P. W. Kantoff, R. Langer, O. C. Farokhzad, *Nano Lett* **2007**, *7*, 3065; (d) F. Gu, L. Zhang, B. A. Teply, N. Mann, A. Wang, A. F. Radovic-Moreno, R. Langer, O. C. Farokhzad, *Proc Natl Acad Sci U S A* **2008**, *105*, 2586; (e) S. Dhar, F. X. Gu, R. Langer, O. C. Farokhzad, S. J. Lippard, *Proc Natl Acad Sci U S A* **2008**.
- [9] (a) M. Blank, T. Weinschenk, M. Priemer, H. Schluesener, *Journal of Biological Chemistry* **2001**, *276*, 16464; (b) C. Wang, M. Zhang, G. Yang, D. Zhang, H. Ding, H. Wang, M. Fan, B. Shen, N. Shao, *Journal of Biotechnology* **2003**, *102*, 15; (c) D. A. Daniels, H. Chen, B. J. Hicke, K. M. Swiderek, L. Gold, *Proc Natl Acad Sci U S A* **2003**, *100*, 15416; (d) L. Cerchia, F. Duconge, C. Pestourie, J. Boulay, Y. Aissouni, K. Gombert, B. Tavitian, V. de Franciscis, D. Libri, *PLoS Biol* **2005**, *3*, e123; (e) B. J. Hicke, C. Marion, Y. F. Chang, T. Gould, C. K. Lynott, D. Parma, P. G. Schmidt, S. Warren, *J*

- Biol Chem* **2001**, 276, 48644; (f) S. P. Ohuchi, T. Ohtsu, Y. Nakamura, *Biochimie* **2006**, 88, 897; (g) D. Shangguan, Y. Li, Z. Tang, Z. C. Cao, H. W. Chen, P. Mallikaratchy, K. Sefah, C. J. Yang, W. Tan, *Proceedings of the National Academy of Sciences of the United States of America* **2006**, 103, 11838; (h) K. T. Guo, R. SchAfer, A. Paul, A. Gerber, G. Ziemer, H. P. Wendel, *Stem Cells* **2006**, 24, 2220; (i) Z. Tang, D. Shangguan, K. Wang, H. Shi, K. Sefah, P. Mallikratchy, H. W. Chen, Y. Li, W. Tan, *Anal Chem* **2007**, 79, 4900; (j) D. Shangguan, L. Meng, Z. C. Cao, Z. Xiao, X. Fang, Y. Li, D. Cardona, R. P. Witek, C. Liu, W. Tan, *Anal Chem* **2008**, 80, 721; (k) H. W. Chen, C. D. Medley, K. Sefah, D. Shangguan, Z. Tang, L. Meng, J. E. Smith, W. Tan, *ChemMedChem* **2008**, 3, 991; (l) M. S. Raddatz, A. Dolf, E. Endl, P. Knolle, M. Famulok, G. Mayer, *Angew Chem Int Ed Engl* **2008**, 47, 5190.
- [10] (a) C. P. Rusconi, E. Scardino, J. Layzer, G. A. Pitoc, T. L. Ortel, D. Monroe, B. A. Sullenger, *Nature (London, United Kingdom)* **2002**, 419, 90; (b) C. P. Rusconi, J. D. Roberts, G. A. Pitoc, S. M. Nimjee, R. R. White, G. Quick, Jr., E. Scardino, W. P. Fay, B. A. Sullenger, *Nat Biotechnol* **2004**, 22, 1423; (c) C. K. Dyke, S. R. Steinhubl, N. S. Kleiman, R. O. Cannon, L. G. Aberle, M. Lin, S. K. Myles, C. Melloni, R. A. Harrington, J. H. Alexander, R. C. Becker, C. P. Rusconi, *Circulation* **2006**, 114, 2490.
- [11] M. Srivastava, H. B. Pollard, *Faseb J* **1999**, 13, 1911.
- [12] (a) M. Derenzini, V. Sirri, D. Trere, R. L. Ochs, *Lab Invest* **1995**, 73, 497; (b) Y. Otake, S. Soundararajan, T. K. Sengupta, E. A. Kio, J. C. Smith, M. Pineda-Roman, R. K. Stuart, E. K. Spicer, D. J. Fernandes, *Blood* **2007**, 109, 3069; (c) K. Xu, R. F. Luduena, *Cell Motil Cytoskeleton* **2002**, 53, 39.
- [13] P. J. Bates, J. B. Kahlon, S. D. Thomas, J. O. Trent, D. M. Miller, *J Biol Chem* **1999**, 274, 26369.
- [14] V. Dapic, P. J. Bates, J. O. Trent, A. Rodger, S. D. Thomas, D. M. Miller, *Biochemistry* **2002**, 41, 3676.
- [15] S. Soundararajan, W. Chen, E. K. Spicer, N. Courtenay-Luck, D. J. Fernandes, *Cancer Res* **2008**, 68, 2358.
- [16] (a) D. Kirpotin, J. W. Park, K. Hong, S. Zalipsky, W. L. Li, P. Carter, C. C. Benz, D. Papahadjopoulos, *Biochemistry* **1997**, 36, 66; (b) J. W. Park, K. Hong, P. Carter, H. Asgari, L. Y. Guo, G. A. Keller, C. Wirth, R. Shalaby, C. Kotts, W. I. Wood, et al., *Proc Natl Acad Sci U S A* **1995**, 92, 1327.

- [17] J. W. Park, K. Hong, D. B. Kirpotin, G. Colbern, R. Shalaby, J. Baselga, Y. Shao, U. B. Nielsen, J. D. Marks, D. Moore, D. Papahadjopoulos, C. C. Benz, *Clin Cancer Res* **2002**, 8, 1172.
- [18] J. Woo, G. N. Chiu, G. Karlsson, E. Wasan, L. Ickenstein, K. Edwards, M. B. Bally, *Int J Pharm* **2008**, 349, 38.
- [19] T. Mosmann, *J Immunol Methods* **1983**, 65, 55.
- [20] (a) A. Ghezzi, M. Aceto, C. Cassino, E. Gabano, D. Osella, *J Inorg Biochem* **2004**, 98, 73;
(b) D. R. Budman, A. Calabro, W. Kreis, *Anticancer Drugs* **2002**, 13, 1011.

CHAPTER 8

POLYMERIZATION OF *O*-CARBOXYANHYDRIDES

1. Introduction

It has recently witnessed economic and social issues associated with the depletion of fossil feedstocks and accumulation of conventional polyolefin plastics (e.g. polyethylene, polypropylene and polystyrene). Aliphatic biodegradable polyesters, such as poly (lactic acid) (PLA), poly (glycolic acid) (PGA) and poly (hydroxylalkynote) (PHA), have emerged as renewable resources materials with huge potential.^[1] Although concurrent PLA meets the requirement of a broad range of applications in industry, the manipulation of the polyester structure, especially in the functional group, is of high importance not only to substitute polyolefins with wide variety of mechanical properties but also to be applied in sophisticated biomedical fields such as tissue engineering implants. In 2002, Langer group synthesized a class of tough polyester by condensation of glycerol and sebacic acid.^[2] Baker group and Hennink group synthesized a various functionalized poly (α -hydroxyl acid)s with improved mechanical properties (varied T_g).^[3] In 2008, Hillmyer group reported the bifunctional lactide derivative to prepare toughening PLA derivatives.^[4] The multi-step synthesis of substitute lactide monomer might prevent the potential industrial scale production of functionalized polyesters; while uncontrolled poly-condensation reaction will raise the problems of repetitive properties of the materials. Natural amino acids exist as another large biorenewable resource for the preparation of biomaterials such as polypeptides.^[5] Here we present a scalable and concise synthetic strategy to prepare functionalized polyesters from amino acids through

controlled living polymerization. The strategy provides the polyester with mechanical toughening properties as potential substituent for polyolefins.

2. Materials and Methods

2.1 Polymerization methods

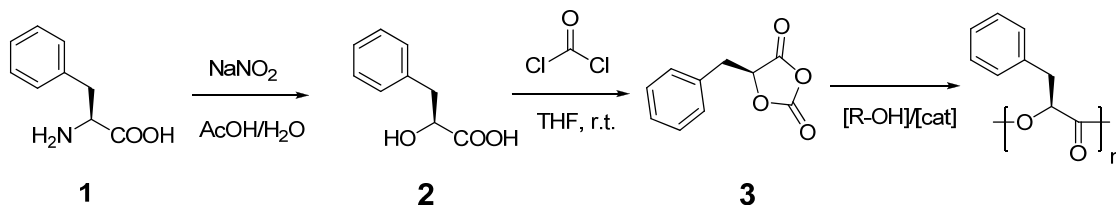
In a glove box, (BDI-1)ZnEt (3.8mg, 1 equiv) was mixed with Pyr-OH (1.7 mg, 1 equiv) in anhydrous THF (300 μ L). The mixture was stirred over 5-10 min. (solution A) PheOCA (142mg) was dissolved in anhydrous THF (1000 μ L) and mixed with a HMDS solution in THF (39mg/mL, 305 μ L) ([PheOCA]/[HMDS]=10/1, solution B). For [PheOCA]/[Zn]=100/1 reaction, solution B (184 μ L) was added into solution A under stirring (41.9 μ L, [PheOCA]=0.46M for the reaction solution) The conversion of LA was monitored by FTIR, by the disappearance of 1812 cm^{-1} anhydride band. The polymerization was completed after 6-8 hours. After diluting the concentration of poly(PheOCA) (PFOCA) to 20mg/mL using DMF, the solution was analyzed by GPC to obtain the molecular weight and distribution of PFOCA.

3. Results and Discussion

3.1 Synthesis of OCA monomer

It has been reported all nineteen protected α -amino acid can be converted to equivalent α -hydroxyl acid.^[6] L-Phenylalanine **1** was initially chosen considering its potential enhance of the mechanical property because of its phenyl structure. Diazotization of L-phenylalanine with sodium nitrite in acids efficiently provides optic pure 2-hydroxyl-3-phenylpropanoic acid **2** with satisfied yield (>75%). Condensation of

the resulted α -hydroxyl acid **2** with phosgene by reported procedures^[7] produced corresponding 1,3-dioxolane-2,4-diones, so-called *O*-carboxyanhydrides (PheOCA) **3**. The produced **3** is white crystal after recrystallization in glove box with reasonable yield (>50%). (Scheme 8.1)



Scheme 8.1 Synthetic scheme of PheOCA monomer and polymerization.

3.2 Screening metals for OCA polymerization

Bourissou group previously reported the ring opening polymerization (ROP) of AlaOCA (or LacOCA) by using DMAP and hydroxyl initiators.^[8] However, no polymerization proceeded when PheOCA was treated with similar condition using DMAP/pyrenemethanol as initiator in similar condition. Complete conversion of PheOCA was achieved in 12 hours at 60 °C; however the molecular weight distribution (MWD) was broader than expected ($M_w/M_n = 1.58$).

We then turned our attention to organometallic catalysts used for PLA polymerization (through insertion-coordination mechanism). In this context, we screened a variety of metal-amido complexes (Ca, Mg, Zn, Sn) with hydroxyl initiator for their capability to ROP of PheOCA.^[125] In contrast to the ROP of LA, the most active metal-amido complexes, $\text{Ca}[\text{N}(\text{TMS})_2]_2$, and $\text{Mg}[\text{N}(\text{TMS})_2]_2$, were not able to initiate PheOCA polymerization; $\text{Sn}[\text{N}(\text{TMS})_2]_2$ was also found less active to completely converted PheOCA for polymerization (Conv. <50%). $\text{Zn}[\text{N}(\text{TMS})_2]_2$ was eventually found as

promising initiator as near quantitative conversion of monomers was detected after 12 hours at room temperature (r.t.). (Table 8.1) In the control study of $\text{Zn}[\text{N}(\text{TMS})_2]_2$ without hydroxyl initiator, over 80% of PheOCA remains intact after reacting over 12 hours, suggesting the polymerization might go through Zn-alkoxide initiated polymerization. Other metal alkoxides ($\text{Al}(\text{OiPr})_3$, $\text{Y}(\text{OiPr})_3$) were examined and no polymerization happens over 12 hours.

Table 8.1 Polymerization of PheOCA.

entry ^a	R-OH	catalyst	Temp.	Time(h)	Conv (%) ^b	$M_n (\times 10^4 \text{g/mol})$	MWD (M_w/M_n) ^c
1	Pyr	DMAP	r.t.	24	0	--	--
2	Pyr	DMAP	70	18	>98	2.02	1.58
3	Pyr	$\text{Ca}[\text{N}(\text{TMS})_2]_2$	r.t.	12	0	--	--
4	Pyr	$\text{Mg}[\text{N}(\text{TMS})_2]_2$	r.t.	12	<50	--	--
5	Pyr	$\text{Sn}[\text{N}(\text{TMS})_2]_2$	r.t.	12	~50	--	--
6	Pyr	$\text{Zn}[\text{N}(\text{TMS})_2]_2$	r.t.	12	>98	1.67	1.71
7	Bn	$\text{Zn}[\text{N}(\text{TMS})_2]_2$	r.t.	12	>98	1.67	1.72
8	--	$\text{Zn}[\text{N}(\text{TMS})_2]_2$	r.t.	12	<20	--	--
9	Pyr	(BDI-1) $\text{ZnN}(\text{TMS})_2$	r.t.	12	>98	2.34	1.33
10	Bn	(BDI-2) $\text{ZnN}(\text{TMS})_2$	r.t.	12	>99	2.79	1.26
11	Bn	(BDI-3) $\text{ZnN}(\text{TMS})_2$	r.t.	12	>98	3.21	1.22
12	Bn	(BDI-4) $\text{ZnN}(\text{TMS})_2$	r.t.	12	>98	1.45	1.19

^a All reactions were performed in glove box with $[\text{PheOCA}] / [\text{R-OH}] / [\text{Catalyst}] = 100 / 1 / 1$ (molar ratio) in glove box at assigned conditions. Abbreviation: Temp.: temperature; Conv.%: conversion of monomer %; MWD: polydispersity index. ^bDetermined by FT-IR, monitoring the

disappearance of PheOCA anhydride peak at 1820-1800 cm^{-1} . ^cDetermined by gel permeation chromatography (GPC). Theoretical molecular weight was $1.49 \times 10^4 \text{ g/mol}$

3.3 *Selection of Single-site Zn catalysts*

In order to eliminate undesired transesterification and other side reaction, single site Zn catalyst, (BDI)ZnN(TMS)₂ was synthesized accordingly.^[9] Since it has been reported that subtle modification of BDI ligands structures would affect the centre Zn activity for polymerization,^[9c] a few of BDI-Zn variations were synthesized for testing their catalytic properties. The results indicated the nitrile group substituent (BDI-4) has significant effects on control the polymerization due in part to the electron withdrawing nature of the nitrile group as reported by Coates etc;^[9c] while steric effect of the aryl substituent of BDI was not noticeably significant. We attempted the polymerization of PheOCA with *in situ* mixed (BDI-4)ZnN(TMS)₂ / BnOH resulted in quantitative conversion of monomer with narrow MWD and predictable M_n . Leaving group seems important to the polymerization. Et/ NTMS₂ was found to successfully for the polymerization; while Zn-acetate cannot initiate polymerization. However, polymerization conducting with high monomer/catalyst ratio (>200/1) for all BDI-Zn derivative do not happen or at very low monomer conversion ratio.

Scheme 8.2 Various of BDI-Zn catalysts structures

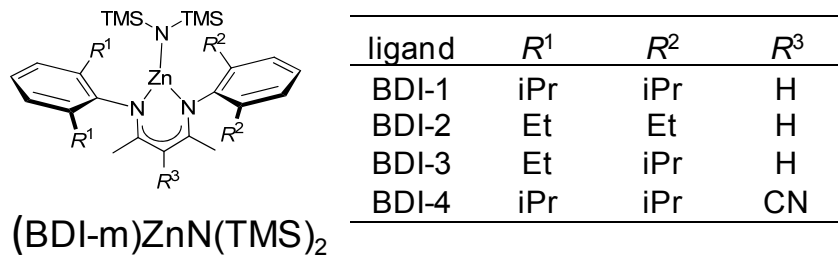


Table 8.2 Polymerization of PheOCA with various BDI-Zn catalyst.

entry ^a	R-OH	catalyst	Temp.	Time(h)	Conv _b (%)	$M_n (\times 10^4 \text{ g/mol})$ _c	MWD (M_w/M_n) _c
1	Pyr	(BDI-1)ZnEt	r.t.	12	>98	2.34	1.33
2	Pyr	(BDI-1)ZnEt	r.t.	12	>98	1.29	1.05
3	Pyr	(BDI-1)ZnEt	r.t.	12	<50	N.D.	N.D.
4	Pyr	(BDI-1)ZnEt	r.t.	12	<10	--	--
5	Pyr	(BDI-1)ZnEt	r.t.	12	<50	N.D.	N.D.
6	Pyr	(BDI-2)ZnN(TMS) ₂	r.t.	12	>99	2.79	1.26
7	--	(BDI-2)ZnOiPr	r.t.	12	<50	N.D.	N.D.
8	Bn	(BDI-3)ZnN(TMS) ₂	r.t.	12	>98	3.21	1.22
9	Bn	(BDI-4)ZnN(TMS) ₂	r.t.	12	>98	1.45	1.19
10	Bn	(BDI-5)ZnN(TMS) ₂	r.t.	12	<10	--	--

^a All reactions were performed in glove at assigned conditions. Abbreviation: Temp.: temperature; Conv.%: conversion of monomer %; MWD: polydispersity index. ^bDetermined by FT-IR, monitoring the disappearance of PheOCA anhydride peak at 1820-1800 cm⁻¹. ^cDetermined by gel permeation chromatography (GPC). dn/dc=0.63 based on the 100% mass recovery dn/dc program determination by GPC

3.4 *Cocatalyst: the investigation of HMDS*

It is surprisingly found the BDI-Zn alkoxide has no reactivity towards the polymerization. However both in-situ prepared (BDI)ZnN(TMS)₂ / alcohol mixture and (BDI) ZnEt / alcohol could initiate polymerization at the ratio of [PheOCA]/[Zn]=100/1. When the ratio of [PheOCA] / [Zn] was increased at 200/1 and 300/1, the conversion of monomer was dramatically dropped below 50% in 12 hours even for all available BDI ligand derivatives. In addition, raising the reaction temperature to 40-50 °C resulted in complicated phenomenon: for (BDI-1)ZnEt the conversion of PheOCA did not increase over 40 %; while for (BDI-3)ZnN(TMS)₂ the monomer was consumed in 12 hours at 50 °C, resulting in polymers with relative broad distribution. We hypothesized that the only difference for the reaction solution was the existence of HMDS in entry. Our group recently developed hexamethyldisilazane (HMDS)-mediated, controlled NCA polymerization. This polymerization proceeds *via* a unique, trimethylsilyl carbamate (TMS-CBM) propagating terminal group and involves the cleavage of the Si-N bond of HMDS during the initiation step. The resulting TMS-amine opens NCA ring at CO-5 to form a TMS-amide at the C-end while the TMS group is attached to the N-end to form a TMS-CBM, the chain propagating group. Polypeptide chains are propagated through the transfer of the TMS group from the terminal TMS-CBM to the incoming monomer to form a new TMS-CBM terminal propagating group. A mixture of BDIZnOiPr/ Pyr-OH and HMDS was tested and we surprisingly found to initiate polymerization with Mn and PDI. Similar base TEA was used at the same ratio and no polymerization happens. It is also found HMDS ratio is independent of BDI-Zn ratio; the increase of HMDS in the reaction mixture significantly promoted the control and reaction rate of the polymerization. Even HMDS was at the same equivalent of monomer, polymerization

proceeded smoothly with MW nearly identical to the expected MW. The detailed mechanism is currently under study. We preliminarily assumed that there is only one N-TMS group might regulate the polymerization, similar to the NCA reaction. The mixture of [PheOCA]/[allyl-NTMS]/[BDI-Zn-Pyr] (300/1/1) resulted in completely consumption of monomer, with broad distribution (PDI=1.36, M_n =15.4 kg/mol). Currently, detailed NMR and MS study was conducted to investigate the polymerization mechanism. Kinetic study is also planned to resolve the kinetic effect of the addition of HMDS.

Table 8.3 entries 12-14 showed the preliminary polymerization study of PheOCA using mPEG2k-OH as macroinitiator. The MW distribution is slightly broader and the MW are relatively identical to the expected MW. The study showed the potential using this synthetic strategy to prepare block copolymers of PEG and various OCA.

Table 8.3 Polymerization of PheOCA with cocatalyst combination of (BDI)Zn and HMDS.

entry ^a	R-OH	catalyst	[M]/[HMDS]/[Zn]	Temp.	Time(h)	Conv. (%) ^b	M_{cal} ($\times 10^4$ g/mol)	M_n ($\times 10^4$ g/mol) ^c	MWD (M_w/M_n) ^c
1	Pyr	(BDI-1)ZnEt	100/1/1	r.t	8	>98	1.51	2.69	1.19
2	Pyr	(BDI-1)ZnEt	200/1/1	r.t	8	>98	3.00	3.88	1.15
3	Pyr	(BDI-1)ZnEt	200/0/1	r.t	8	<20	--	--	--
4	--	(BDI-1)ZnOiPr	300/30/1	r.t	8	>98	4.49	3.32	1.11
5	Pyr	(BDI-1)ZnN(TMS) ₂	200/20/1	r.t	8	>98	3.00	3.71	1.27
6	Pyr	(BDI-1)ZnN(TMS) ₂	300/30/1	r.t	8	>98	4.49	4.78	1.21
7	Pyr	(BDI-1)ZnN(TMS) ₂	400/40/1	r.t	8	>98	5.98	5.78	1.17
8	Pyr	(BDI-1)ZnOAc	100/10/1	r.t	12	<30	--	--	--
9	Pyr	(BDI-3)ZnN(TMS) ₂	400/400/1	r.t	8	>98	5.98	5.87	1.17
10	Pyr	(BDI-3)ZnN(TMS) ₂	200/0/1	50	12	>98	3.00	3.69	1.47
11	Pyr	(BDI-3)ZnN(TMS) ₂	200/0/1	r.t	12	<20	--	--	--
12	mPEG2k-OH	(BDI-3)ZnN(TMS) ₂	100/10/1	r.t	12	>98	1.69	1.71	1.30
13	mPEG2k-OH	(BDI-3)ZnN(TMS) ₂	200/20/1	r.t	12	>98	3.18	3.82	1.20
14	mPEG2k-OH	(BDI-3)ZnN(TMS) ₂	300/30/1	r.t	12	>98	4.67	5.35	1.18

^a All reactions were performed in glove at assigned conditions. Abbreviation: Temp.: temperature; Conv.%: conversion of monomer %; MWD: polydispersity index. ^bDetermined by FT-IR, monitoring the disappearance of PheOCA anhydride peak at 1820-1800 cm⁻¹. ^cDetermined by gel permeation chromatography (GPC). dn/dc=0.63 based on the 100% mass recovery dn/dc program determination by GPC

Table 8.4 Polymerization of PheOCA by (BDI-3)ZnN(TMS)₂/HMDS.

entry ^a	R-OH	catalyst	[M]/[HMDS] /[Zn]	Temp.	Time (h)	Conv v (%) _b	M_{cal} ($\times 10^4$ g/ mol)	M_n ($\times 10^4$ g/mol) _c	MWD (M_w / M_n) _c
1	Pyr	(BDI-3)ZnN(TMS) ₂	50/5/1	r.t.	8	>98	0.77	0.97	1.13
2	Pyr	(BDI-3)ZnN(TMS) ₂	100/10/1	r.t.	8	>98	1.51	1.56	1.14
3	Pyr	(BDI-3)ZnN(TMS) ₂	200/20/1	r.t.	8	>98	3.00	3.17	1.11
4	Pyr	(BDI-3)ZnN(TMS) ₂	300/30/1	r.t.	8	>98	4.49	4.58	1.12
5	Pyr	(BDI-3)ZnN(TMS) ₂	400/40/1	r.t.	12	>98	5.98	5.78	1.19

^a All reactions were performed in glove at assigned conditions. Abbreviation: Temp.: temperature; Conv.%: conversion of monomer %; MWD: polydispersity index. ^bDetermined by FT-IR, monitoring the disappearance of PheOCA anhydride peak at 1820-1800 cm⁻¹. ^cDetermined by gel permeation chromatography (GPC). dn/dc=0.63 based on the 100% mass recovery dn/dc program determination by GPC

3.5 Copolymerization of OCA

It has been reported by Coates group that the ring opening polymerization can be achieved in isotactic stereo-control and living manner with the mediation of BDI-Zn-alkoxide. Since PheOCA can be also polymerized with the catalyst combination of in-situ prepared BDI-Zn-alkoxide/HMDS, it is hypothesized that we can achieved the copolymerization of LA (which representative of lactone) and PheOCA with the

mediation of BDI-Zn-alkoxide. It is found that the successive addition of PheOCA/HMDS (molar ratio 10/1) were consumed within 6 hours after PLA was polymerized by (BDI-1)ZnN(TMS)₂ / PyrOH; in contrast, for the reverse polymerization sequence, monomer LA was intact after addition to polymerized PheOCA solution. Although the detailed mechanism was still under investigation, it is likely the PheOCA chain end might not have the capability due to the structure reason to further initiator PLA polymerization; while BDI-Zn-alkoxide at PLA terminus remains high activity towards the addition of PheOCA. Table 8.5 showed the MW of various LA-co-PheOCA block copolymers by both GPC and NMR characterization, which were nearly identical to the calculated MW. This strategy potentially allowed the synthesis of various polyester copolymer beyond the current selection of cyclic lactones, further diversifying the library of polyesters and its copolymers for plastic engineering or biomedical applications.

Scheme 8.3 Proposed PheOCA polymerization mechanism by (BDI)ZnN(TMS)₂/HMDS

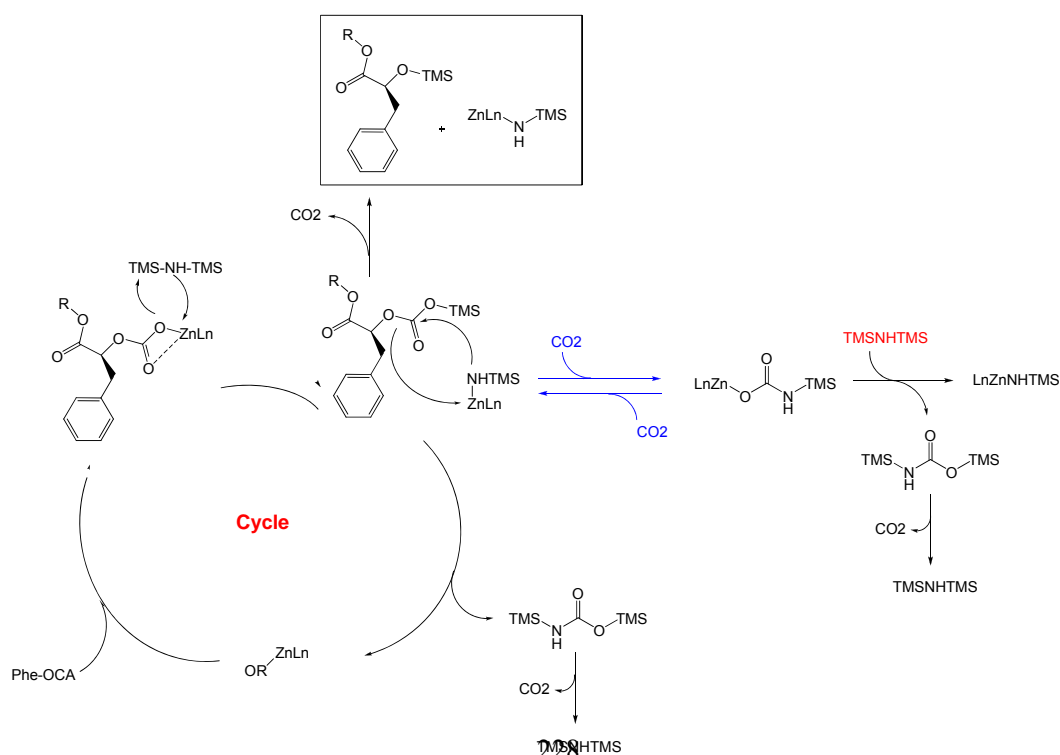


Table 8.5 Copolymerization of LA and PheOCA by HMDS/(BDI)-Zn catalyst

entry ^a	[LA]/[Zn] /[Pyr]	Zn catalyst	[PheOCA]/ [LA]/ [HMDS]	Temp.	Time (h) t _{LA} /t _{OCA}	Conv (%) ^b LA/O CA	M_{cal} ($\times 10^4$ g/mol)	M_n ($\times 10^4$ g/mol) ^c	MWD (M_w/M_n) ^c
1	100/1/1	(BDI-3)ZnN(TMS) ₂	100/100/10	r.t.	6/12	96/98	2.95	3.11	1.11
2	200/1/1	(BDI-3)ZnN(TMS) ₂	100/200/10	r.t.	6/12	95/98	4.39	4.52	1.07
3	300/1/1	(BDI-3)ZnN(TMS) ₂	100/300/10	r.t.	6/12	96/98	5.83	5.64	1.03
4	100/1/1	(BDI-1)ZnN(TMS) ₂	100/100/10	r.t.	8/12	98/98	2.95	3.94	1.02

^a All reactions were performed in glove at assigned conditions. Abbreviation: Temp.: temperature; Conv.%: conversion of monomer %; MWD: polydispersity index. ^bDetermined by FT-IR, monitoring the disappearance of PheOCA anhydride peak at 1820-1800 cm⁻¹. ^cDetermined by gel permeation chromatography (GPC). dn/dc=0.63 based on the 100% mass recovery dn/dc program determination by GPC

4. Conclusions

In conclusion, we set up the basis to develop a new polymerization technique to synthesize various poly α -hydroxyl esters. It is expected the resulted polymers will have potential application for both biomedical and plastic engineering use.

5. References

- [1] O. Dechy-Cabaret, B. Martin-Vaca, D. Bourissou, *Chem. Rev.* **2004**, *104*, 6147.
- [2] Y. D. Wang, G. A. Ameer, B. J. Sheppard, R. Langer, *Nat. Biotechnol.* **2002**, *20*, 602.
- [3] (a) F. Jing, M. R. Smith, G. L. Baker, *Macromolecules* **2007**, *40*, 9304; (b) T. Q. Liu, T. L. Simmons, D. A. Bohnsack, M. E. Mackay, M. R. Smith, G. L. Baker, *Macromolecules* **2007**, *40*, 6040; (c) X. Jiang, E. B. Vogel, M. R. Smith, G. L. Baker, *Macromolecules* **2008**, *41*, 1937; (d) X. W. Jiang, M. R. Smith, G. L. Baker, *Macromolecules* **2008**, *41*, 318; (e) M. Leemhuis, C. F. van Nostrum, J. A. W. Kruijtzter, Z. Y. Zhong, M. R. ten Breteleur, P. J. Dijkstra, J. Feijen, W. E. Hennink, *Macromolecules* **2006**, *39*, 3500.
- [4] F. Jing, M. A. Hillmyer, *J. Am. Chem. Soc.* **2008**, *130*, 13826.
- [5] (a) H. Lu, J. J. Cheng, *J. Am. Chem. Soc.* **2007**, *129*, 14114; (b) H. Lu, J. J. Cheng, *J. Am. Chem. Soc.* **2008**, *130*, 12562; (c) H. Lu, J. Wang, Y. Lin, J. J. Cheng, *J. Am. Chem. Soc.* **2009**, *131*, 13582.
- [6] S. Deechongkit, S. L. You, J. W. Kelly, *Org. Lett.* **2004**, *6*, 497.
- [7] L. Tang, L. Deng, *J. Am. Chem. Soc.* **2002**, *124*, 2870.
- [8] O. T. du Boullay, E. Marchal, B. Martin-Vaca, F. P. Cossio, D. Bourissou, *J Am Chem Soc* **2006**, *128*, 16442.
- [9] (a) M. Cheng, A. B. Attygalle, E. B. Lobkovsky, G. W. Coates, *J. Am. Chem. Soc.* **1999**, *121*, 11583; (b) B. M. Chamberlain, M. Cheng, D. R. Moore, T. M. Ovitt, E. B. Lobkovsky, G. W. Coates, *J. Am. Chem. Soc.* **2001**, *123*, 3229; (c) R. C. Jeske, A. M. DiCiccio, G. W. Coates, *J. Am. Chem. Soc.* **2007**, *129*, 11330.

CHAPTER 9

INITIAL EFFORTS FOR STEM CELL CULTIVATION

1. Introduction

1.1. Overview of induced pluripotent stem cells

Groundbreaking work demonstrated that ectopic expression of four transcription factors, *Oct4*, *Klf4*, *Sox2*, and *c-Myc*, could reprogram murine somatic cells to induced pluripotent stem cells (iPSCs), and human iPSCs were subsequently generated using similar genetic manipulation. To address the safety issues arose from harboring integrated exogenous sequences in the target cell genome, a number of modified genetic methods have been developed and produced iPSCs with potentially reduced. However, delivery of genes to hESCs is limited because there are safety concerns with viral approaches, and nonviral methods have low efficacy. For nonviral vectors, testing in the H9 hESC line showed that commonly used lipid- and polymer-based transfection agents including FuGENE, LipofectAMINE Plus, and ExGen 500 transfected less than 10% of the hESCs. In addition, many hESC gene transfer studies lack a reliable marker to separate transfected undifferentiated cells from differentiating, differentiated, and feeder cells. Among viral gene transfer approaches, adenovirus serotype 5 has been shown to transduce just 11% of undifferentiated H9 hESCs, and adeno-associated virus (serotypes 2, 4, and 5) has been shown to transduce only 0.01% at best. The most effective viral strategy to date has been lentiviral vectors, which have ~40% transduction efficiency in H1 and H9 hESCs. Although the transgene expression can be further enhanced by concentrated virus, appropriate promoters, and drug selection after transduction, the safety concerns associated with insertional mutagenesis after viral integration are difficult

to overcome. This issue limits their potential for human gene therapy. A safe and effective method for gene delivery to stem cells would be invaluable to the creation of new cell-based therapies.

One possible way to avoid introducing exogenous genetic modifications to target cells would be to deliver the reprogramming proteins directly into cells, rather than relying on the transcription from delivered genes. Previous studies have demonstrated that various proteins can be delivered into cells *in vitro* and *in vivo* by conjugating them with a short peptide that mediates protein transduction, such as HIV tat and poly-arginine. In addition, various solubilization and refolding techniques for processing inclusion body proteins expressed in *E. coli* to bioactive proteins have been developed to allow facile and large-scale production of therapeutic proteins. Ding and coworkers reported the generation of protein-induced pluripotent stem cells (piPSCs) from murine embryonic fibroblasts using recombinant cell-penetrating reprogramming proteins in 2009 and demonstrated that such piPSCs can long-term self-renew and are pluripotent *in vitro* and *in vivo*. For polymeric delivery system, protein delivery using micro- or nanoparicles has been well developed to enhance the absorption, bioavailability, and sustained therapeutic actions of proteins. Herein we proposed to use double emulsion method to delivery reprogramming proteins to mouse and human fibroblast cells in order to safely and efficiently generate iPS cells for potential regenerative medicine application.

1.2. Scaffolds for pluripotent stem cells cultivation

Hydrogels have attracted considerable attention. They are sometimes called smart materials^[1] because their physical and chemical properties are subject to change in response to external stimuli, such as pH, temperature, light, and electric fields^[2]. Such

stimuli-responsive hydrogels have been applied in a range of applications as controlled drug delivery vehicles, sensors, and energy-transducing devices ^[3]. In tissue engineering, hydrogel have been used as the scaffolds for cell adhesion and growing; it can also be used for delivering therapeutics or presenting other biological cues that are critical to the survival and/or differentiation of cells ^[4].

Several studies have explored the culture of hESCs in defined 3D settings by using a variety of natural and synthetic scaffolds for cell growth, differentiation, or lineage guidance. There has been a considerable effort to replace more biological but less controllable native materials with synthetic materials. Hyaluronic acid (HA), a nonsulfated linear polysaccharide of (1- β -4)d-glucuronic acid and (1- β -3)*N*-acetyl-d-glucosamine, have been demonstrated to support hESC growth *in vitro*, since it can co-regulate gene expression, signaling, proliferation, motility, adhesion, metastasis, and morphogenesis of hESCs. Besides its known role in embryogenesis, HA scaffolds have been reported for the cultivation of hESCs in 2007. HA-based hydrogels can maintain the undifferentiated state of hESCs in the presence of conditioned medium from MEFs until soluble factors are introduced to direct cell differentiation. The cultivation of hESCs in HA hydrogels maintained the state of cell self-renewal and enabled EB formation from released cells. However, the culture systems with cues simply added apparently cannot mimic the complex extracellular environments where growth factors and other biological cues are often secreted at controlled, optimal rates ^[4e, 5]. Numerous studies have demonstrated that the microenvironment and nano-structured hydrogel matrices plays significant roles to stem cell cultivation and self-renewal ^[6].

Direct ink writing (DIW) is a layer-by-layer assembly technique in which materials are patterned in both planar and 3D forms with lateral feature sizes that are at

least an order of magnitude smaller than those achieved by ink-jet printing and other rapid prototyping approaches, and nearly comparable in size to those produced by two-photon polymerization and interference holography. Central to this approach is the creation of concentrated inks that can be extruded through fine deposition nozzles in filamentary form, and then undergo rapid solidification to maintain their shape even as they span gaps in the underlying layers. We herein report the creation of hydrogel inks of HA that can be printed directly in air using DIW technique, where they undergo solidification via photopolymerization. Pluripotent human testicular embryonal carcinoma cell Ntera-2 can be cultivated in the resulted 1D and 3D hydrogel scaffolds without significant differentiation and the expression of *Oct4*, one of the key reprogramming proteins for pluripotency. Considering the tenability of the nanostructure using DIW, this technique for cultivation of human pluripotent stem cells is expected to have great potential for the tissue engineering and regenerative medicine.

2. Materials and Methods

2.1. Preparation of NPs encapsulating proteins by flow cytometry

Nanoparticles of various sizes were formulated according to the reference. Briefly, an aqueous protein solution (10% w/v) was emulsified in PLGA-mPEG (50 mg/mL) in DCM solution, using a probe sonicator for 1 min. The emulsion was poured into 1% PVA solution and sonicate over an ice bath for 3 min. The resulting emulsion was further dilute by 100 mL 0.5% PVA solution. The resulted solution was stirred in fume hood over 6 hours to evaporate DCM. The NPs solution was further centrifuged under 3000 rpm over 30 minutes, washed by DI water twice (50mL). NPs were finally concentrated

and collected by ultrafiltration (3000 rpm, Ultracel membrane with 10,000 NMWL, Millipore, Billerica, MA).

2.2. *Cell uptaking efficiency analysis by flow cytometry*

IMR 90 cells were grown in 24-well plates in DMEM medium (American Type Culture Collection), respectively, supplemented with 100 units/ml aqueous penicillin G, 100 µg/mL streptomycin, and 10% FBS at concentrations to allow 70% confluence in 24 h (i.e., 40,000 cells per cm²). On the day of experiments, cells were washed with prewarmed PBS and incubated with prewarmed phenol-red reduced OptiMEM media for 30 min before the addition of the PLGA-PEG/BSA-FITC (50 µg) NPs. The cells were incubated for 7 h at 37°C, washed with PBS (2× 500 µL per well) and subsequently treated with 0.25% trypsin with EDTA for 10 min. The cells were transferred to a 15-mL falcon centrifuge tube and centrifuged at 1200 rpm for 5 min followed by removal of the trypsin solution using a pipette. After the cells were washed with PBS (2× 500 µL/well), they were fixed with 4% formaldehyde for 10 min at room temperature, washed with PBS (1× 500 µL) and analyzed by FACS.

2.3. *Cell uptaking efficiency analysis by fluorescence microscope*

IMR 90 cells were grown in chamber slides in DMEM medium (American Type Culture Collection), respectively, supplemented with 100 units/ml aqueous penicillin G, 100 µg/mL streptomycin, and 10% FBS at concentrations to allow 70% confluence in 24 h (i.e., 40,000 cells per cm²). On the day of experiments, the medium was replaced with Opti-MEM medium (200 µL) containing PLGA-PEG NPs encapsulating FITC-BSA.

The cells and NPs were co-incubated for 7 h, after which the cells were washed with PBS ($3 \times 200 \mu\text{L}$), fixed with 4% formaldehyde, mounted and then analyzed on a Leica SP2 Laser Scanning Confocal Microscope at $10\times$ magnification.

2.4. *Synthesis of HA-MA*

Methacrylated hyaluronic acid (HA-MA) was synthesized by the addition of methacrylic anhydride (Sigma, ~20-fold excess) to a solution of 1 wt % HA (Lifecore, MW = 50, 350, and 1100 kDa) in deionized water adjusted to a pH of 8 with 5 M NaOH (Aldrich) and reacted on ice for 24 h. This synthesis was previously described, and the structure is shown in Figure 9.1. For purification, the macromer solution was dialyzed (MW cutoff 5–8 kDa) against deionized water for at least 48 h, and the final product was obtained by lyophilization.

2.5. *Ink preparation*

The ink was initially formed by mixing 1 mL deionized water (Milli-Q, Millipore), 5 g of glycerol (Sigma Aldrich), and. These constituents were magnetically stirred at room temperature until the acrylamide was fully dissolved.

2.6. *Direct-writing assembly of HA-MA hydrogel scaffolds*

Micropipette tips (World Precision Instruments) with diameters ranging from 1 to 10 mm were coated with a thin gold film (200 nm thick) to prevent photopolymerization of the ink prior to exiting the deposition nozzle. The micropipettes were mounted onto a rotating holder to ensure an even coverage, and coated inside a metal evaporator (Denton Vacuum DV-5024). Coverslip substrates were cleaned in piranha (sulfuric acid, hydrogen

peroxide) solution for 1 h, rinsed with deionized water, and dried with nitrogen. Coverslips were placed in a 98% toluene (Fisher Scientific), 2% 3-(trimethoxysilyl)-propyl methacrylate (Acros) solution for 18 h at 60 °C. The slides were removed just prior to drawing, rinsed with isopropanol, and dried. The ink was loaded into a syringe with an attached gold-coated tip in place. Once the substrate was leveled, ink flow was initiated by applying a pressure of 70–80 psi (1 psi = 6894.76 Pa). After the flow had begun, the pressure was reduced to 20–30 psi and the patterning was initiated. The printed scaffolds were defined by filament width, spacing between filaments, total patterned area, number of layers, and their geometry. We created both planar and 3D scaffolds with 1 to 5 mm filaments and a 5 to 20 mm spacing between filaments over 5mm² areas with 1–6 layers. A UV lamp (Omnicure S200; Exfo) with a 320–400 nm was used to expose the patterned structure to 5mW/cm² during the deposition process. Once patterning was complete, the scaffolds were exposed to a higher-intensity UV light source, 400mW/cm², for 20min to ensure a fully photocured structure. To drive off excess water and enhance scaffold rigidity, each scaffold was then heated to 60 °C for 18 h.

2.7. General cell culture

NTera-2 cells (pluripotent human embryonal carcinoma cells) were purchased from American Type Culture Collection (ATCC) and were cultured according to ATCC recommendations. BG01v-Oct4-GFP and NTera-2-Oct4-GFP cell lines were provided by Fei Wang lab and cultured in Fei Wang lab with instructed medium.

2.8. Scaffold imaging

The printed hydrogel scaffolds were soaked in deionized water for three days prior to cell culture to leach out glycerol and any unpolymerized acrylamide. Reflected-light optical microscopy (IX71; Olympus) was performed prior to cell plating to ensure structural integrity of the scaffolds. SEM images were obtained using a Philips XL30ESEM-FEG; structures were dried and sputter-coated with gold prior to imaging.

2.9. *NTera-2-Oct4-GFP cells cultivated in HA-MA scaffolds*

HA-MA scaffolds were first washed by PBS over 24 hours, and Opti-MEM over 24 hours before use. HA-MA scaffolds were sterilized prior to cell plating through UV-light exposure in the laminar flow hood for 20min. On the day of experiment, NTera-2 cells in culture medium (~5,000/mL) was gently pipetting onto the top of glass slides with HA-MA scaffolds. After 24 hours, the medium was removed. The medium was replaced everyday.

3. Results and Discussion

3.1. *Delivery of FITC-albumin to 3T3 and IMR-90 cells*

Various different sizes of NPs were prepared by double emulsion method to encapsulate BSA-FITC, which was used as a model protein molecule. We started to investigate the uptaking behavior of NPs/BSA-FITC in 3T3 fibroblast cells. Similar to the previous work, 160 nm sizes NPs was found to be uptaken by 3T3 cells with higher efficiency (47%) than 260 nm size NPs (29%) after 7 hours incubation, characterized by flow cytometry. Similar result was also observed through fluorescence microscope. 160

nm NPs/BSA-FITC was further tried in the human fibroblast cell line, IMR-90, which is the precursor cells used for the generation of iPSC. Satisfactory uptaking efficiency (37%) over 7 hours incubation was measured by flow cytometry (Figure 1), suggesting the potential of using protein delivery for the iPSC generation and culture.

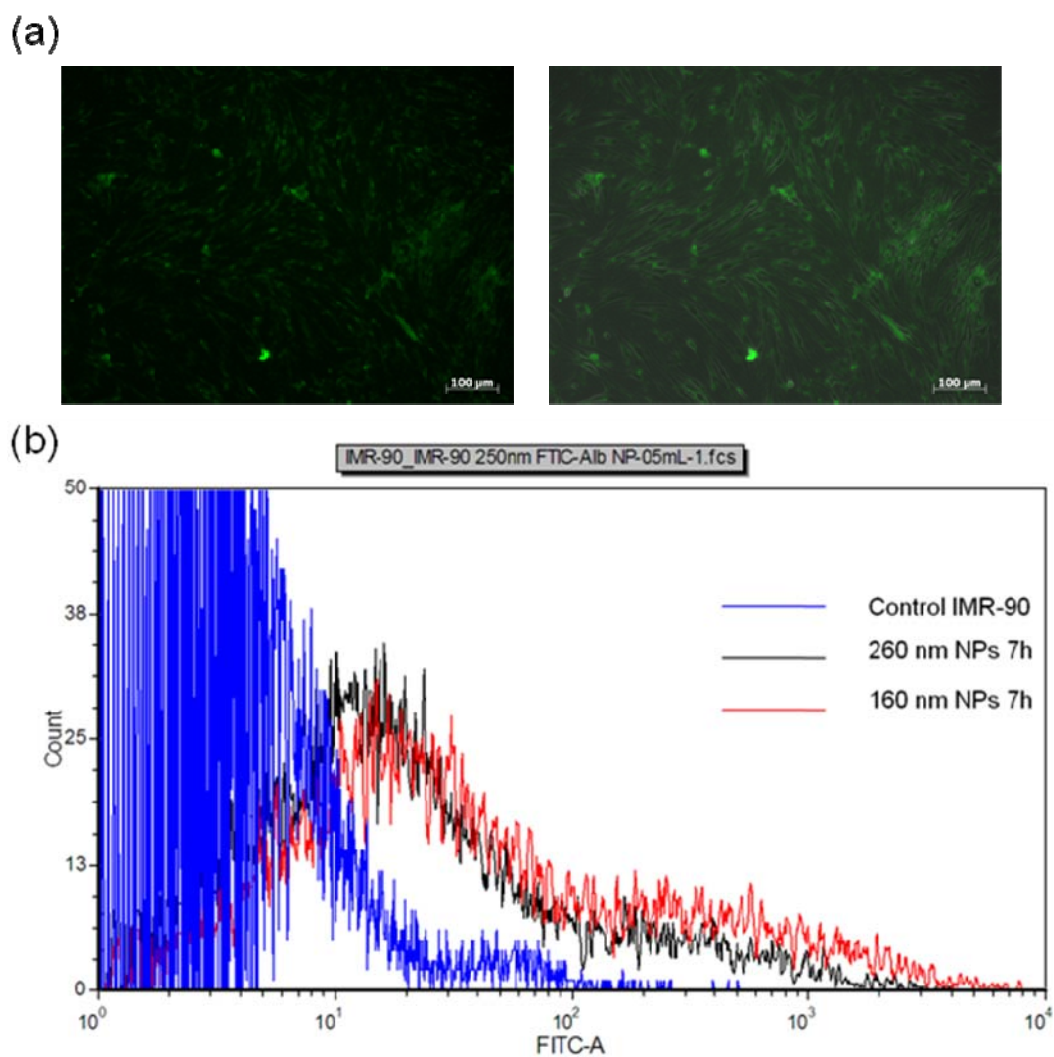


Figure 9.1 (a) fluorescence image of IMR-90 cell uptaking 1mg/mL PLGA-PEG/BSA-FITC after incubation for 7 hours. Left: fluorescence; right: overlay. (b) FACS analysis of IMR-90 cells uptaking different size NPs.

3.2. *Delivery of Sox2 to MEF cell line*

Sox2 protein was labeled with TAMRA dyes for the flow cytometry and fluorescence microscope. NPs encapsulating Sox2 was formulated using above double emulsion strategy to provide ~140 nm NPs. Reasonable uptaking efficiency (24%) was detected for MEF cells by flow cytometry after incubation over 16 hours. The colocalization of Sox2 with cell nucleus is under investigation (Figure 2).

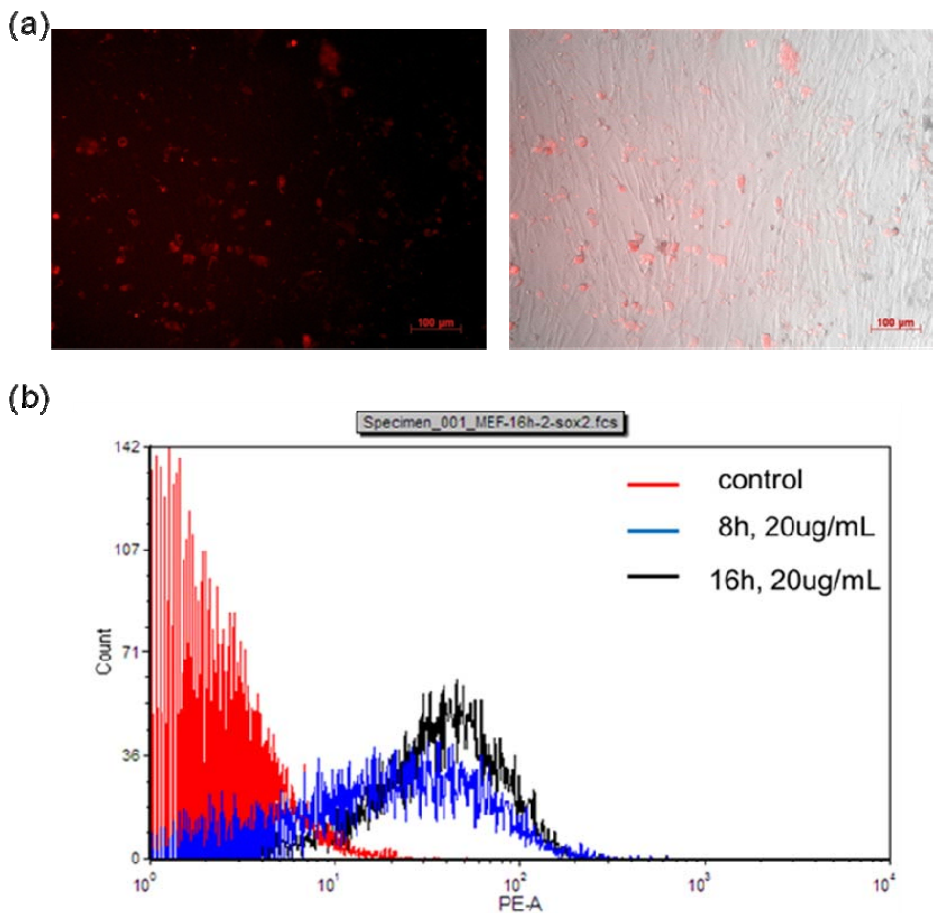


Figure 9.2 (a) fluorescence image of MEF cell uptaking 1mg/mL PLGA-PEG/Sox2-TAMRA after incubation for 16 hours. Left: fluorescence; right: overlay. (b) FACS analysis of MEF cells uptaking NPs for different time.

3.3. Preparation and characterization of ink for directed writing

The ink is prepared by first mixing methacrylate- hyaluronic acid (HA-MA), glycerol, water, polyethylene glycol-diacrylate (PEG-DA, MW=700Da) and photoinitiator I-2959 at the ratio of 8/50/50/8/0.1 (w/w). PEGDA was used as the crosslinking agents. The solution becomes homogeneous over 12 hours aging. The original ink was found occasionally stuck during the printing process. To optimize the ink condition, tween-20 was added into the ink with 0.1wt % ratio. The improved ink showed the improved mechanical properties. We also studied the PEG molecular weight effects different ratios on the stability of the HA hydrogels. Without low molecular weight PEG, the gel was not stable in DMEM cell medium. HA molecular weight is also critical to the mechanical behavior and stability of scaffolds in the cell medium.

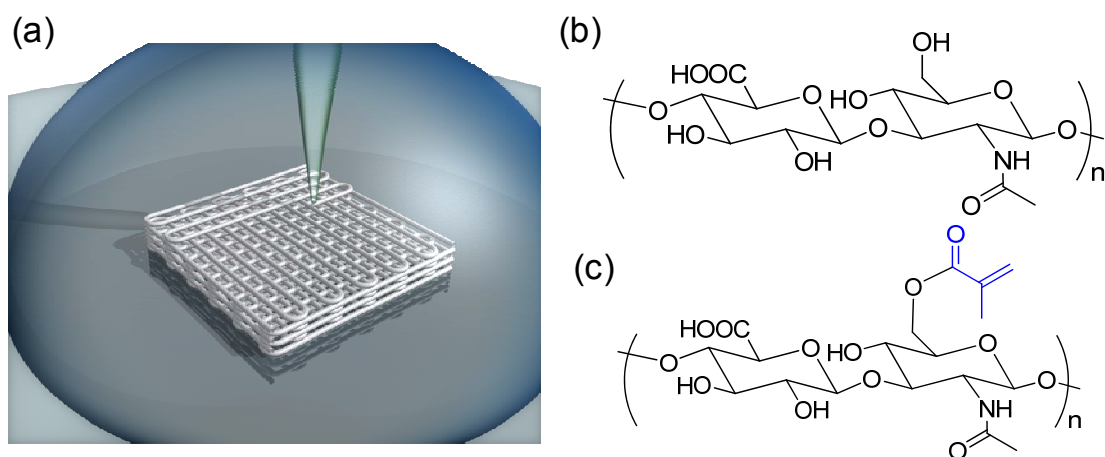


Figure 9.3 (a) Schematic illustration of direct-writing assembly through a silver-coated deposition micronozzle that is simultaneously photopolymerized via UV illumination; structure of (b) hyaluronic acid (HA) and (c) methacrylate hyaluronic acid (HA-MA). The acrylate group (blue) which is used for photopolymerization for crosslinking hydrogel

3.4. *Preparation of hyaluronic acid hydrogel scaffolds by DIW technology*

Using this modified DIW process, we pattern HA hydrogel scaffolds with precisely defined filament diameter, spacing, number of layers, and geometry. As a first example, we created hydrogel scaffolds composed of 5mm filaments with a 20mm spacing between filaments with 1–4 layers and a total area of 5mm² (Figure 9.4a and Figure 9.5b). To further demonstrate the capability of this novel approach, hydrogel scaffolds were printed with nominally 1 mm filaments with 5mm spacing between filaments with a total area of 1mm², as shown in Figure 9.4e.

3.5. *NTera-2 cells culture in 1D and 3D hyaluronic acid hydrogel scaffolds*

For this particular cell pluripotency study, it is important to note that some of these cells may be differentiated and others may be feeder cells. To avoid this, we made NTera-2-Oct4-GFP and hES BG01v-Oct4-GFP cells by introducing the hOct4-GFP-puro construct into hESCs. In this construct, the GFP reporter gene is expressed by the Oct4 promoter that is active when cells are in an undifferentiated state. Upon differentiation, the Oct4 promoter is gradually inactivated; therefore, the GFP reporter is downregulated. With these cells, pluripotent cells can be clearly distinguished from differentiated stem cells and feeder cells.

To determine their suitability for tissue-engineering applications, NTera-2 cells are first plated onto a flat glass substrate (control) as well as 1D and 3D micro periodic hydrogel scaffolds using HA-MA and HEMA. The cells plated on the control substrate display the typical flattened-out morphology shown in Figure 9.5(e). By contrast, cell interactions with the underlying glass substrate and patterned features result in their alignment along the patterning direction of the 1D microperiodic hydrogel scaffolds, as

shown in Figure 9.4(c-e). This type of elongated morphology is similar to that observed by us on 1D periodic patterned surface. We observed atypical fibroblast morphology in response to the 3D micro-periodic HA-MA hydrogel scaffolds (Fig. 5c and d), in which NTera-2 cells integrate themselves into the regions between interconnecting hydrogel filaments. It is found that the cells tend to sit in the square well created by interconnected filaments and then grow down into the scaffold towards the underlying glass substrate. Additionally, when the fibroblasts are in neighboring compartments, we observe interactions between the filaments of adjacent fibroblast cells (Figure 9.5d). In addition, for both 1D and 3D micro-periodic hydrogel scaffolds, green fluorescence was observed almost for every NTera-2 cells. The sustainable growth of NTera-2 cells was also noticeable shown in Figure 9.4(c-d) from 1 to 9 days. Some NTera-2 cells even expanded upon the periodic filaments (Figure 9.4d). These microscopy imaging study demonstrate the HA-MA scaffolds with well defined nanostructures have the capacity to support the growth and self-renewal of NTera-2 cells without disturbing the expression of Oct4. In contrast, synthetic pHEMA scaffolds lacked the biological capability for the plating and cultivation of Ntera-2 cells (Figure 9.5 e and f).

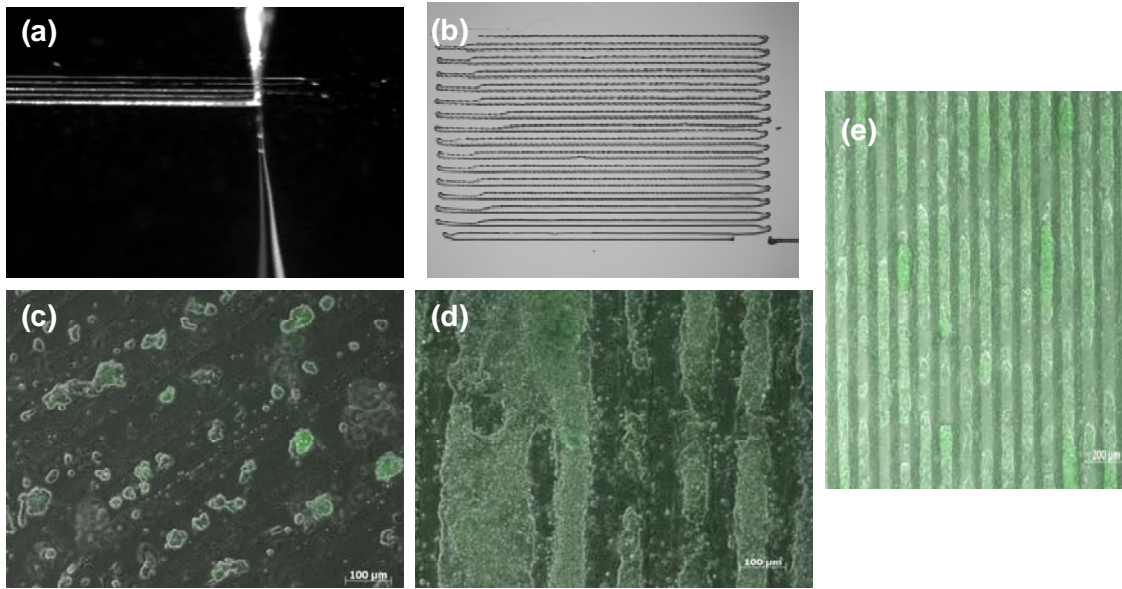


Figure 9.4 Optical image of a 1D hydrogel scaffold (a) during and (b) after using direct ink writing with the ink of HA-MA (350k) ; Overlay images (light and green fluorescence) of 1D HA-MA scaffolds plated with Ntera-2-Oct4-GFP cells over (c) 1 day and (d) 9 days; (e) Overlay images (light and green fluorescence) of 1D large area HA-MA scaffolds with Ntera-2-Oct4-GFP cells over 4 days. The color in the green fluorescence channel indicated the expression of OCT4.

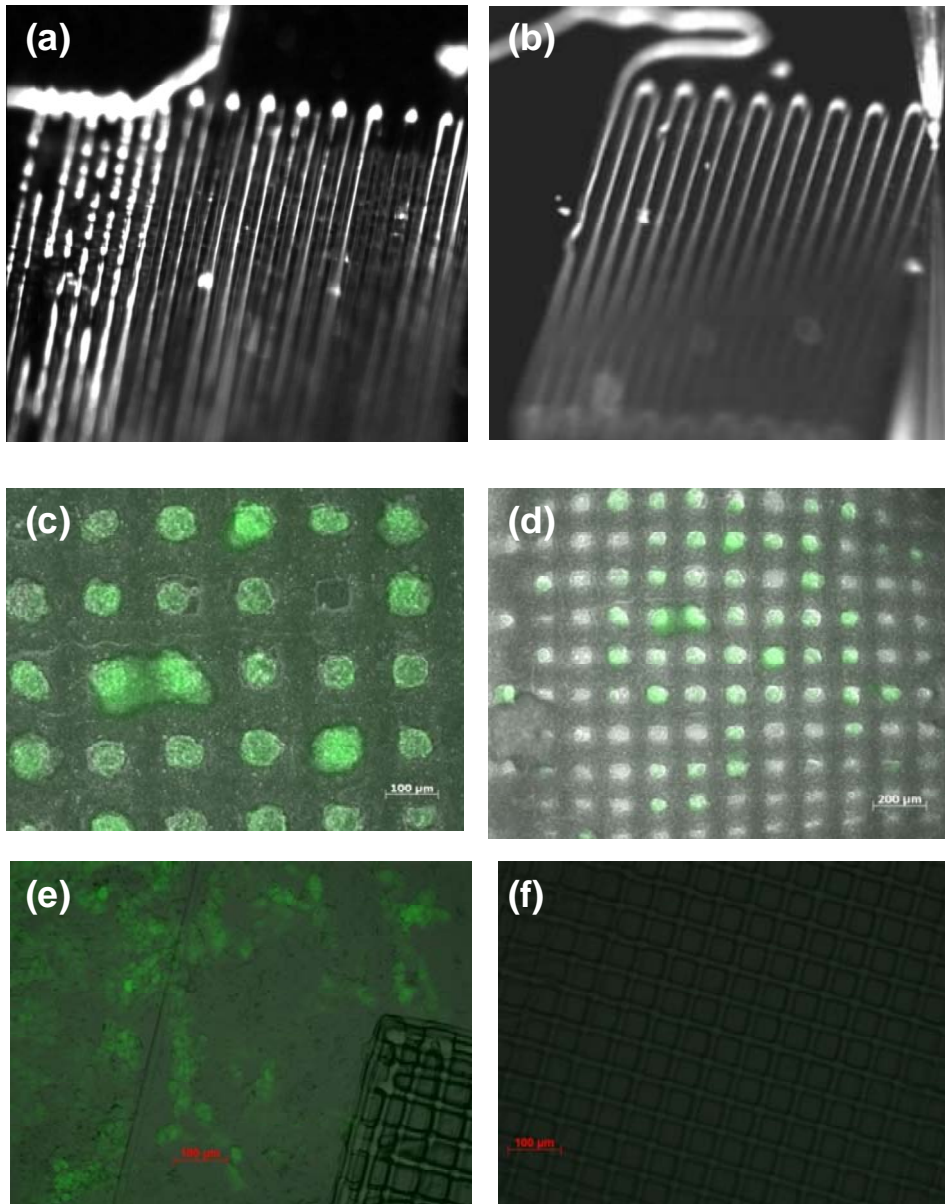


Figure 9.5 Optical image of a 3D hydrogel scaffold during direct ink writing using the ink of (a) HA-MA 50k and (b) HA-MA 350k (the composition and other components are the same); (c) and (d) Overlay images (light and green fluorescence) of 3D HA-MA scaffolds plated with Ntera-2-Oct4-GFP cells over 4 days; (e) and (f) Overlay images (light and green fluorescence) of 3D HEMA scaffolds plated with Ntera-2-Oct4-GFP cells over 4 days. The color in the green fluorescence channel indicated the expression of OCT4.

4. Conclusions

The initial study explored the possibility to use NPs delivering proteins to various fibroblast cells in order to generate iPSC. The combination of cell penetration peptide and nanotechnology for protein delivery would be expected to benefit the stem cell culturing and generation.

We present the development of constructing 3D HA scaffolds using DIW techniques. BG01 human embryonic stem cells are planned to be further plated on the scaffolds. This technique for cultivation of human pluripotent stem cells is expected to have control on the hESC self-renewal process and cell colony size. The exploration of 3D nanostructure parameter and ESC behavior will be investigated in the near future.

5. References

- [1] R. Langer, D. A. Tirrell, *Nature* **2004**, 428, 487.
- [2] (a) O. Kretschmann, S. W. Choi, M. Miyauchi, I. Tomatsu, A. Harada, H. Ritter, *Angew. Chem. Int. Ed.* **2006**, 45, 4361; (b) I. Berndt, J. S. Pedersen, W. Richtering, *Angew. Chem. Int. Ed.* **2006**, 45, 1737; (c) I. Berndt, C. Popescu, F. J. Wortmann, W. Richtering, *Angew. Chem. Int. Ed.* **2006**, 45, 1081; (d) A. Sidorenko, T. Krupenkin, A. Taylor, P. Fratzl, J. Aizenberg, *Science* **2007**, 315, 487; (e) W. A. Petka, J. L. Harden, K. P. McGrath, D. Wirtz, D. A. Tirrell, *Science* **1998**, 281, 389; (f) Y. Luo, M. S. Shoichet, *Nat. Mater.* **2004**, 3, 249; (g) M. R. Lutolf, F. E. Weber, H. G. Schmoekel, J. C. Schense, T. Kohler, R. Muller, J. A. Hubbell, *Nat. Biotechnol.* **2003**, 21, 513; (h) S. Nayak, L. A. Lyon, *Angew. Chem. Int. Ed.* **2005**, 44, 7686; (i) C. Wang, R. J. Stewart, J. Kopecek, *Nature* **1999**, 397, 417; (j) A. P. Nowak, V. Breedveld, L. Pakstis, B. Ozbas, D. J. Pine, D. Pochan, T. J. Deming, *Nature* **2002**, 417, 424.
- [3] (a) B. Pepin-Donat, A. Viallat, J. F. Blachot, C. Lombard, *Adv Mater* **2006**, 18, 1401; (b) T. Suzuki, S. Shinkai, K. Sada, *Adv Mater* **2006**, 18, 1043; (c) J. S. Mao, M. J. McShane, *Adv Mater* **2006**, 18, 2289.
- [4] (a) M. Tomita, E. Lavik, H. Klassen, T. Zahir, R. Langer, M. J. Young, *Stem Cells* **2005**, 23, 1579; (b) J. M. Karp, L. S. Ferreira, A. Khademhosseini, A. H. Kwon, J. Yeh, R. S. Langer, *Stem Cells* **2006**, 24, 835; (c) K. A. Davis, J. A. Burdick, K. S. Anseth, *Biomaterials* **2003**, 24, 2485; (d) M. J. Mahoney, K. S. Anseth, *Biomaterials* **2006**, 27, 2265; (e) S. Levenberg, N. F. Huang, E. Lavik, A. B. Rogers, J. Itskovitz-Eldor, R. Langer, *Proc. Natl. Acad. Sci. U. S. A.* **2003**, 100, 12741; (f) S. Levenberg, J. S. Golub, M. Amit, J. Itskovitz-Eldor, R. Langer, *Proc. Natl. Acad. Sci. U. S. A.* **2002**, 99, 4391.
- [5] M. C. Cushing, K. S. Anseth, *Science* **2007**, 316, 1133.
- [6] (a) N. A. Peppas, J. Z. Hilt, A. Khademhosseini, R. Langer, *Adv Mater* **2006**, 18, 1345; (b) M. P. Lutolf, J. A. Hubbell, *Nat. Biotechnol.* **2005**, 23, 47.